THE POTENTIAL OF NUTRACEUTICAL BASED COMPOUNDS IN TARGETING SENESCENT CELLS *IN VITRO*

Thesis submitted for the degree of

Doctor of Philosophy

By

Amanpreet Kaur (BSc)

Department of Respiratory Sciences

University Of Leicester

May 2021

Statement of Originality

This accompanying thesis submitted for the degree of PhD entitled “The Potential of Nutraceutical based compounds in targeting senescent cell *in vitro*” is based on work conducted by the author in the Department of Respiratory Sciences of the University of Leicester during the period between October 2017 and May 2021. All the work recorded in this thesis is original unless otherwise acknowledged in the text or by references. None of the work has been submitted for another degree in this or any other University.

Signed: Amanpreet Kaur

Date: 01.06.2021

COVID-19 Impact Statement

Due to the COVID-19 pandemic, the University of Leicester alongside the rest of the nation went into lockdown. This meant that lab facilities were not accessible for a period of **6 months**. Due to this loss my study endured a setback in the realisation of my experimental plans.

Due to the limited amount of time remaining, experiments had to be revised. Loss of expertise and facilities such as Jenny Hincks (FACS Facility manager) and the University's decision to not replace her meant there was very limited use of the facility. The disabling of machines such as Cryostat sectioning equipment and the loss of expertise to train and use alternatives meant I was unable to analyse prepared and archived biological material. The loss of six months due to lockdown meant I couldn't do *ex vivo* experiments I had planned to be included in the project. The changes in lab use such as limited number of occupancies meant working for fewer hours therefore, I was unable to carry out multiple repeats of experiments. Due to COVID-19 I was asked to move laboratories which meant time was spent moving materials and belongings.

Acknowledgements

First and foremost, I would like to thank my supervisor, Dr Cordula Stover, for collaborating on this project with me, for all the support, guidance and advice throughout which has been instrumental in completing this study. Also, for being caring, understanding and most of all encouraging during the good and bad times in these last few years.

I also cannot thank enough all the people that have been involved and contributed to this study: Dr Simon Byrne for all his invaluable technical expertise, support and guidance, Dr Ruth Saunders in the capacity of my secondary supervisor, your counsel has been most beneficial and significant particularly with data analysis. Thank you to Dr Emma Watson and Dr Alice Smith as well.

Thank you to Jenny Hincks of the FACS facility for her time and expertise on Flow cytometry and analysis. Also, Thank you to Natalie Allcock and Ania Straatman-Iwanowska (Electron Microscopy Facility) and Dr Kees Straatman (Advanced Imaging Facility) for support with cell imaging. I am also thankful to Dr Ravinder Chana (Tissue Culture Facility), Dr Karen Molyneux and Dr Izabella Pawluczyk (The Mayer IgA Nephropathy Lab) for the use of Nanostring Technologies. Thank you to Jasraj Bachu for all the guidance and advice regarding Nanostring and Dr Bryan Serrels for Nanostring analysis support. A special thank you to Dr Salvador Macip for all his valuable input into my project, collaborating on a Literature Review and making me part of his lab meetings.

A special thanks to my labmate Marwa Mohammed and all the BSc and MSc students that assisted with the study; Maria Papageorgiou (BSc), Justina Kailey (MSc) and Alicia Nicklin (MSc).

I am also very grateful to all the amazing friends I have made during my PhD who have supported me in many ways, Kate Robinson, Jez Brown, Tom O'Sullivan, Luke Baker, Emily Harper and Francesca Hodges. A huge thank you to my family who have supported and encouraged me to persevere with my studies.

The potential of nutraceutical-based compounds in targeting senescent cells *in vitro*

Amanpreet Kaur

Abstract

As a consequence of our cells preventing malignancy, cells become arrested in their cell cycle yet remain metabolically active, accumulating and causing tissue dysfunction contributing to poorer health quality in later life. This is known as cellular senescence. Certain nutraceuticals possess anti-inflammatory properties to combat the effects of cellular senescence. An *in vitro* senescence model through the artificial induction of senescence via DNA damage using irradiation in a mouse cell line was established. Thorough validation of the model for key markers of senescence was conducted of which include; lysosomal beta-galactosidase staining, protein detection for cell cycle inhibitors, proliferation assays, cell cycle analysis and imaging such as light microscopy, immunofluorescence imaging, scanning electron microscopy and transmission electron microscopy. The platform was then used to experimentally test nutraceutical compounds with the potential to prevent senescence (Senostatic) or induce apoptosis (Senolytic) of senescent cells. Nutraceuticals which were tested include Holy Basil, Allicin and Phytol. Apoptosis of senescent cells were measured through Cell counting, TUNEL assay, Annexin V-FITC detection, Bcl-2 detection by western blot. Senostatic properties were investigated through cell proliferation counts, p21 detection by Western blot, Cell cycle analysis by propidium iodide staining and Beta-galactosidase staining. Finally transcriptomic analysis of the platform when treated with the nutraceuticals was also performed using Nanostring. Annexin V-FITC and TUNEL assay analysis showed all three nutraceuticals to have senolytic properties and an increase in cell death was seen in Allicin treated cells as a result of senolytic effect. An increase in cell viability in Allicin and Phytol treated cells showed senostatic activity. Reduced Beta-Galactosidase analysis was seen in all treated cells and an increased percentage of cells in S phase of Holy Basil treated cells indicating senostatic potential. Nanostring analysis further confirmed the senescence model with upregulation of key genes associated with senescence.

Table of Contents

2 Development of a protocol to study SIPS (stress-induced premature senescence) in L929 mouse fibroblast cell line using irradiation

List of Figures

Figure 44: Traffic Light based diagram highlighting the effects of Holy Basil, Allicin and Phytol in SEN + treatment cells compared to SEN baseline

Figure 45: Genes identified that showed an increase or decrease in expression in CTRL and SEN + treatment cells compared to CTRL and SEN baseline when analysed using Nanostring.

List of Tables

Abbreviations

A, T, G, C Adenine, Thymine, Cytosine, Guanine
APS Ammonium persulfate
ARF Adenosine diphosphate-ribosylation factor
ATM Ataxia-telangiectasia mutated protein kinase
ATR Ataxia telangiectasia and Rad3-related protein kinase
BrdU Bromodeoyuridine
$CaCl_2$ Calcium Chloride
CHK1 Checkpoint kinase 1
CHK2 Checkpoint kinase 2
DAPI 4',6-diamidino-2-phenylindole
DNA Deoxyribose nucleic acid
DTT Dithiothreitol
ECL Electrochemiluminescence
EDTA Ethylenediaminetetraacetic acid
EdU 5-ethynyl-2'-deoxyuridine
FBS Fetal bovine serum
FITC Fluorescein isothiocyanate
HCl Hydrochloric acid
JAK Janus kinase
JNK c-Jun N terminal kinase
MAPK Mitogen activated protein kinase
MEM Minimum essential medium eagle
mRNA Messenger ribonucleic acid
MTT 3-(4,5-dimethylthiazol-2-yl)-2,5-diphenyltetrazolium bromide
NaCl Sodium Chloride
NAD+ Nicotinamide adenine dinucleotide
NADH reduced Nicotinamide adenine dinucleotide
NEMO NF-KB essential modulator
NF-KB Nuclear factor kappa-light-chain-enhancer of activated B cells
PBS Phosphate buffered saline
PI Propidium Iodide
PI3K Phosphoinositide 3-Kinase

RIG-1 Retinoic acid inducible gene I

RIPA Radioimmunoprecipitation assay

SDS-PAGE sodium dodecyl sulphate polyacrylamide gel electrophoresis

SEM Scanning electron microscopy

SIRT1 Sirtuin 1

STAT Signal transducer and activator of transcription protein

TEM Transmission electron microscopy

TEMED Tetramethylethylenediamine

$ZnCl_2$ Zinc Chloride

1 General Introduction

1.1 Cellular Senescence: A History

Over 50 years ago, Hayflick and Moorhead put forward the discovery of the phenomenon widely known as cellular senescence. Observing strains of diploid human cells *in vitro*, they put forth the Phase III phenomenon outlining the characteristics of senescence. They set out three key phases to describe the 'history of diploid cell strain'; phase I would involve cells to be harvested from their tissues and adhere to a surface, this was also known as the early growth phase which could last between 1-3 weeks. Phase II would begin with the formation of the first confluent sheet, where it would require 'subcultivation'. Phase II cells would undergo 'rapid cell multiplication and great acid production'. These cells would be further passaged twice a week when confluency had been achieved. The duration of phase II could last between 2-10 months. Phase III involves 'cell degeneration, reduced mitotic activity, debris formation and delayed confluency'. They also observed changes to nuclear shape and size of phase III cells in interphase. Hayflick and Moorhead articulated the involvement of the aging process and senescence in the event of phase III cells. (Hayflick & Moorhead, 1961).

Hayflick further followed up the phase III phenomenon in his 1965 article which focused in establishing a relation to senescence. He compared cell strains derived from fetal lung tissue and adult lung tissue, with results showing that adult cells reached phase III within fewer sub-cultivations compared to fetal cells, with an average difference of 30 passages, showing that 'passage potential is generally related to the age of the donor' (Hayflick, 1965).

Hayflick outlined and reinforced the existence of phase III cells, now commonly known as senescent cells. Whilst his work confirmed others' findings, the cause of the phenomenon remained unknown. Around 10 years later, Hayflick's work inspired the discovery of telomeres in cellular DNA and their association to aging. Elizabeth Blackburn, John Szostak and Carol Greider discovered a repetitive sequence of DNA on the end of chromosomes which became shortened in length with every cell division until a certain limit was reached and the cell would arrest

further replication. This decrease in telomeres correlated with Hayflick's limit. Greider extensively worked on isolating the enzyme telomerase which allowed for telomeres to maintain a consistent length and this was the case in immortalised cell lines where telomerase was abundantly expressed. The three scientists were awarded the Nobel prize in medicine and physiology in 2009 for their work on telomeres and telomerase (Varela & Blasco, 2010).

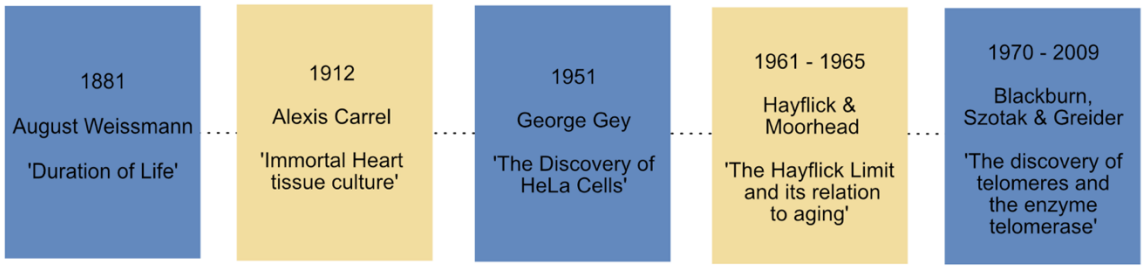

Figure 1: Timeline of key work in the field of Cellular Senescence. The diagram outlines key events in cellular senescence history, with Weissman hypothesizing that aging and death was a result of natural selection to make space for a younger, healthier generation. Carrel claimed to have produced chick heart cells that had infinite proliferative capabilities. Gey isolated cells which were characterized as HeLa cells, an immortal, supporting Carrels findings that cells were able to live *in vitro* forever. Hayflick and Moorhead refuted this through experiments of human lung cells that only lasted around 50 passages (known as the Hayflick limit). Based on Hayflicks work, Blackburn, Szotak & Greider further discovered the existence of Telomeres and telomerase in relation to aging.

Figure 1 depicts the timeline of key events in the history of senescence. From August Weissmanns' theory on death being a result of natural selection to make space for a new generation (Kirkwood & Cremer, 1982), Alexis Carrel claiming to have produced an infinitely replicating culture of chick heart cells (Carrel, 1912, Witkowski, 1980), the isolation of HeLa cells from Henrietta Lacks to provide one of the most commonly used immortalised cancer cell line (Callaway, 2013) to the works of Hayflick and Moorhead inspiring the research for telomeres and telomerase by Blackburn, Szostak and Greider (Blasco & Varela, 2010), the history of senescence is extensive and will continue to encourage further work in the field.

1.2 Cellular Senescence: A Definition

Gilbert (2000) describes aging as 'the time-related deterioration of the physiological functions necessary for survival and fertility' (Gilbert, 2000). It is a process conserved across species. On a cellular level aging is most commonly known as senescence. Senescence is characterised by irreversible cell cycle arrest in addition to a secretory phenotype known as SASP (van Deursen, 2014), however senescent cells remain metabolically active (Campisi & Wiley, 2016). They continue to accumulate in tissues and organs leading to functional deterioration as part of the process of aging (van Deursen, 2014). This results in a poorer quality of healthy life in the elderly.

With cellular senescence, key markers can be used to identify cells in this state with a cease in cell proliferation being fundamental. What makes senescent cells unique is attributed to the number of markers they display that have to be considered in conjunction to identify a cell as having undergone senescence. These markers include but are not limited to senescence-associated beta-galactosidase staining, cell cycle arrest, morphological and nuclear changes. Other cells also display cell cycle growth arrest such as terminally differentiated cells which include but are not limited to; Neurons, macrophages, muscle cells (Rodier & Campisi, 2011).

Quiescent cells are a set of cells that have become arrested in their cell cycle yet retain the ability to re-enter the growth cycle through re-activation when stimulated with growth signals. Quiescent cells are key to tissue regeneration and maintaining a constant state of balanced proliferation (Yao, 2014). In relation to cell cycle arrest, senescent cells are capable of expressing more p16 protein, a cell cyclin dependent kinase (CDK) inhibitor which prevents cell cycle progression, whereas this is not as highly expressed in quiescent cells (Stein et al., 1999). Furthermore, whereas senescent cells change morphology to become larger and flattened, quiescent cells maintain their original cell structure (Terzi et al., 2016).

The process of cellular senescence is one that remains not fully understood. With key roles in tumour suppression through p53 and pRB pathways, tumour promotion through the senescence associated secretory phenotype (SASP), overall contributing to aging and age-related diseases. Yet senescence remains a key defence mechanism against cancer and vital to tissue repair and regeneration. This geriatric related field remains complex and in need of further research (Rodier & Campisi, 2011).

1.3 Types of Cellular Senescence

Hayflick and Moorhead established replicative senescence; a form of senescence that manifests naturally in somatic cells in correlation with the physical aging of the body. Cells undergo multiple mitotic cell divisions, eventually reaching a limit at which their proliferative capabilities are lost. (Hayflick & Moorhead, 1961). Since then, other forms of senescence have been discovered, named aptly after their causes or methods of induction.

Senescence is mostly triggered through the DNA damage response (DDR). DNA damage induced senescence (DDIS) can have multiple stimuli. This includes the shortening of telomeres in replicative senescence. The change in DNA content following loss of telomeric length is recognised as DNA damage resulting in the initiation of the DNA damage response (Serrano & Munoz-Espin, 2014).
The DDR consists of key components which bring about the halt in cell cycle mechanics to stop further damage and replication of aberrant cells. These include ATM and ATR kinases which in turn activate cell cycle checkpoint proteins CHK1 and CHK2. These proteins regulate cyclin dependent kinases or CKDs, which become inhibited to arrest the cell cycle (Jackson & Bartek, 2009). In senescent cells, the main proteins involved in proliferative arrest are p21 and p16, described as cyclin-dependent kinase inhibitors (CDKIs). These are found to be overexpressed in senescent cells and are used as a marker for cell cycle arrest.

Additional stimuli exist which are considered telomere independent causes of senescence. These include oncogene-induced senescence which can be activated through the overexpression of tumour promoting oncogenes. A 1997

study conducted by Serrano et al., found that the overexpression of the *ras* oncogene in human and rodent cells exhibited a similar phenotype to cellular senescence. Cells were generated that would deliver an overexpression of *ras* through an activated *ras* allele (H-*ras* V12) and a replication-deficient retrovirus vector. An empty vector was used as a control. H-*ras* V12 incorporated human (IMR90) and rodent (MEFs & REF52) cells were found to be positive for senescence markers including lack of BrdU incorporation, cell counts indicated proliferative arrest, increase in p21, p16 and p53 proteins indicating cell cycle halt and increased expression of senescence associated Beta-galactosidase (Serrano et al., 1997). Other key oncogenic genes involved in this particular type of senescence include but are not limited to; Raf, c-Myc, Akt, E2F3 which become activated. Tumour suppressor genes can become activated or inactivated to induce senescence to counteract impending malignancy. Examples include PTEN, Hps72, Rb (Gorgoulis & Halazonetis, 2010).

Denham Harman introduced 'The free radical theory of aging' in the 1950s where aging was a result of an accumulation of oxidative damage (Harman, 1992) from reactive oxygen and nitrogen species (RONS). It is now recognised as the oxidative stress theory of aging. RONS are products of metabolism identified as 'reactive radical and non-radical derivatives of oxygen or nitrogen'. Examples of ROS (reactive oxygen species) include superoxide radical, hydroxyl radical and H_2O_2, all capable of compromising the integrity of cellular DNA. Sources of ROS in cells include by-products formed in the electron transport chain in mitochondria (Salmon et al., 2004). ROS 'readily react with DNA' causing damage to bases and DNA-protein cross-links ultimately causing DNA strand breaks', which would activate the DDR. Multiple senescence models have been established using oxidative stress with ionising radiation DNA-damage causing agents such as Hydrogen peroxide and bleomycin (Gonzalez-Hunt et al., 2018).

Mitochondrial dysfunction associated senescence (MiDAS) is associated with the accumulation of mitochondrial deterioration over age. The mechanism of MiDAS is not fully established. Possible causes include ROS produced by mitochondria or an elevation of NADH and in conjunction a decline in NAD+ to induce senescence within compromised mitochondria (Wiley et al., 2016). It has also

been documented that ‘NAD+ levels decrease in tissue with age’ (Wiley et al., 2016).

Epigenetically induced senescence involves the remodelling of chromatin structure within DNA to silence or activate particular genes to establish the aging phenotype. This configures with the senescence associated heterochromatin foci observed in senescent cell nuclei, representing denser and compact regions of chromatin no longer accessible for gene transcription such as genes needed for proliferation (Sidler et al., 2017). DNA hypomethylation (decrease in DNA methylation) is observed in senescent cells but not in immortalised cells (Wilson & Jones, 1983). Histone modifications can cause repression of certain genes, silencing those involved in cell cycle progression. Post-translational histone modifications such as ‘repressive H3K4Me3 and H3K27Me3 marks were found in replicative senescent mesenchymal stem cells and an active H3K4Me1 mark in hypomethylated areas’ (Franzen et al., 2016).

Paracrine senescence is mainly regulated by the senescence associated secretory phenotype or SASP, a collection of molecules secreted by senescent cells which include but are not limited to factors such as chemokines, cytokines, proteins and growth factors. The release of certain SASP factors is capable of altering the surrounding tissue microenvironment promoting further senescence of neighbouring cells (Tasdemir & Lowe, 2013).

1.4 Characteristics & Markers of Cellular Senescence

In order to define a cell having undergone senescence, it is key to determine the existence of multiple markers. There are many distinctive characteristics (Figure 2) displayed by senescent cells that have to considered in conjunction to define cellular senescence.

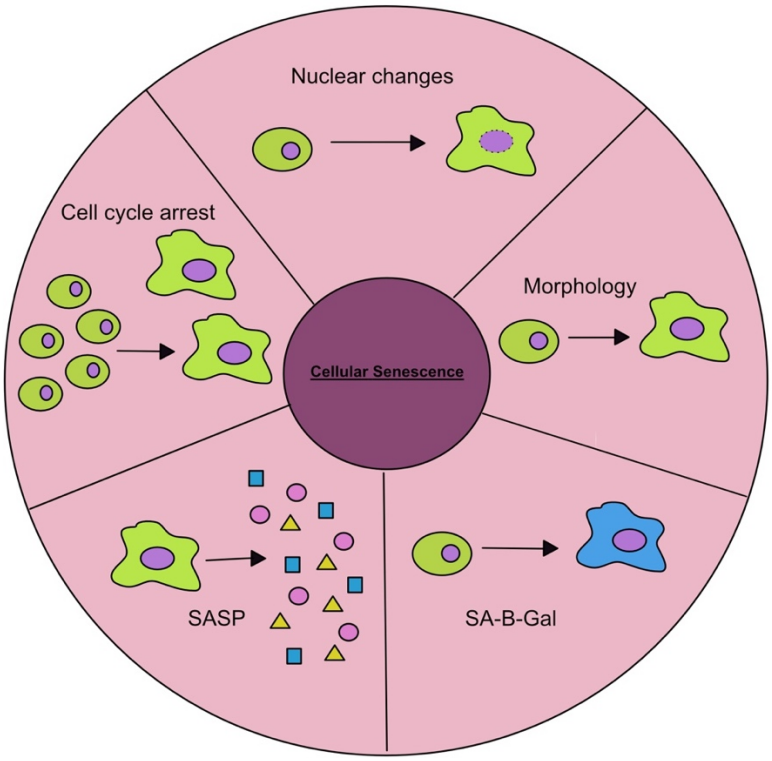

Figure 2: Illustration of the various markers and characteristics associated with cellular senescence. Changes in morphology, nuclear markers, positive for SA- β-Gal, Cell cycle arrest and SASP production are all characteristics exhibited by senescent cells.

1.4.1 Morphology

Senescent cells have a distinctive morphology that makes them different from normal proliferating cells. Cells become flatter and larger. The nucleus also becomes enlarged (Dimri, 2005).

1.4.2 SA- β-Gal activity & Lipofuscin

'Cytoplasmic content of senescent cells also changes with an increase in lysosomal senescence associated beta-galactosidase activity (SA-β-Gal). This enzyme is thought to exist in cell lysosomes, which are known to increase in size as cells age, therefore a high β-Gal activity would be expected in senescent cells'

(Kaur et al., 2020). However, β-Gal activity isn't considered to be specific to senescent cells as it can also be found in other cell types of non-senescent nature and in some cases may not establish itself in senescence. (Dimri et al., 1995, Lee et al., 2006, Rivera-Perez & Huang, 2014). Lipofuscin, known to some as age pigment, is an 'intralysosomal polymeric material consisting of oxidatively modified protein and lipid degradation residues' which form granules. These accumulate over time in non-proliferating or post-mitotic cells (Terman & Brunk, 2004). Lipofuscin granules exhibit a certain amount of detectable autofluorescence but can also be stained for using Sudan Black B for easier visualisation (Georgakopoulou et al., 2012).

1.4.3 Cell cycle arrest

For cell proliferation the progression of the cell cycle is key. As shown in figure 3 each phase of the cell cycle requires a protein complex consisting of a cyclin and a cyclin dependent kinase (CDK) such as Cyclin E/ CDK2 to progress from G1 to S phase. In senescent cells, this interaction between cyclins and CDKs is blocked by Cyclin dependent kinase inhibitors (CDKIs).

$P16^{INK4A}$ encodes p16 a protein which inhibits the Cyclin D/CDK4/6 complex by directly inhibiting the CDK (Jingwen et al., 2017) It is often used as a marker for senescent cells due to it increased levels of expression in cell cycle arrest. $P21^{CIP1}$ encodes p21, a protein also used as a senescence marker but is found to be involved in multiple pathways such as the DDR response (Hernandez-Segura et al., 2018). Therefore, it cannot be relied on solely to determine the senescence phenotype. Measurement of these markers can be carried out through Western blot.

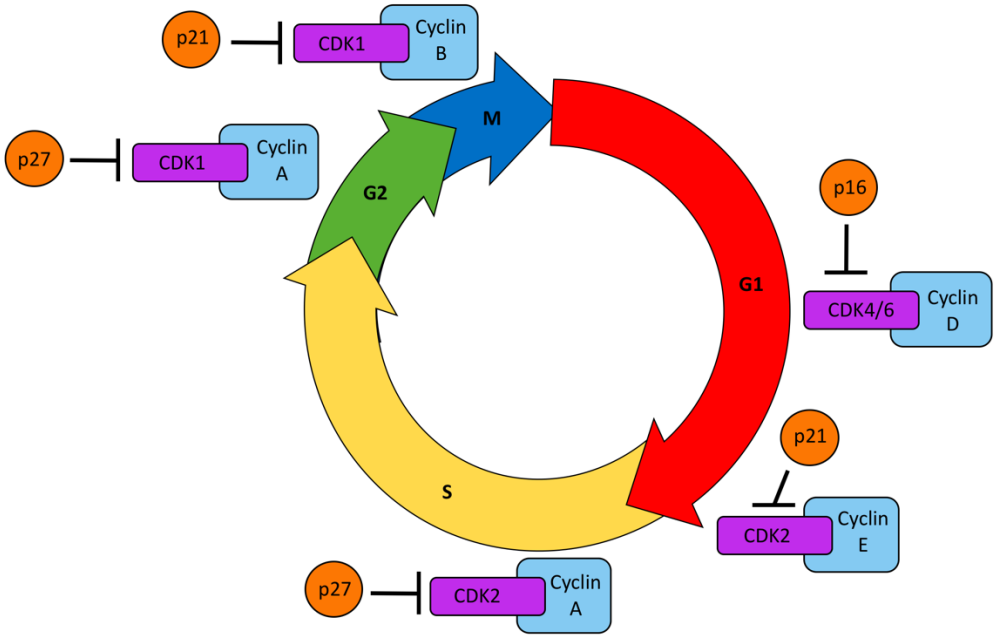

Figure 3: Mechanism of cell cycle arrest. The cell cycle has a number of checkpoints at which the cell has to go through in order to transition into the next phase of the cycle. Each checkpoint consists of CDK and cyclin in complex. If any DNA damage is detected, CDKIs will inhibit Checkpoint proteins from progressing the cell cycle. In senescent cells p21 and p16 are found to be upregulated in order to block further cell growth, DNA synthesis and cell proliferation.

1.4.4 Nuclear changes

The nucleus in senescent cells is distinctly affected: apart from an increase in size, the nuclear lamina, a structure relevant to mitotic division where it is constructed and deconstructed and ultimately key to nuclear stability (Freund et al., 2012), reacts with a decrease in Lamin B. Lamin proteins are type V intermediate filaments which form the nuclear lamina (Freund et al., 2012). Freund et al, found that a particular lamin protein, 'Lamin B1 was expressed differentially between pre-senescent and senescent cells' (Kaur et al., 2020). A decrease in Lamin B1 mRNA and protein expression was found in primary human fibroblast cell lines, indicating its potential use as a marker for senescence (Freund et al., 2012).

In addition, chromatin structure is also seen to be changed in senescence. Heterochromatin, transcriptionally inactive chromatin, increases in senescent cells along with the presence of senescence associated heterochromatin foci (SAHFs) (Aird & Zhang., 2012) possibly representing the now inaccessible genes of the DNA material needed for proliferation. These can be stained for and identified using DAPI. Epigenetic markers such as H3K9me3, H3K27me3 can be used to identify these SAHFs also (Parry & Narita., 2016).

1.4.5 SASP

The senescence associated secretory phenotype or SASP, is considered as a biomarker of senescence. The SASP is a mixture of components secreted by senescent cells altering their surrounding environment. These molecules include chemokines, cytokines, proteases and growth factors (Borodkina et a., 2018). The effect of SASP can be both beneficial and detrimental. Types of SASP factors include soluble signalling molecules which act through surface receptor binding of neighbouring cells. Examples include interleukins IL-6, IL-8 and IL-1a (Borodkina et al., 2018). These interleukins take part in activating signalling pathways such as Jak/STAT, PI3K, and MAPK (Kaur et al, 2020, Garbers et al., 2013). Other SASP factors include proteases such as matrix metalloproteases (MMPs) and serine proteases which are involved in the development and regeneration of the extracellular matrix (Kaur et al., 2020). The inhibitors of these proteins and signalling molecules are also secreted by senescent cells to 'regulate their functioning' (Borodkina et al., 2018).

The SASP works to promote tissue repair and regeneration through its secretory molecules and encourages immune surveillance, however it can also be detrimental to health through paracrine senescence (Kaur et al., 2020). The SASP can encourage surrounding cells to also become senescent, causing an accumulation of senescent cells which could lead to tissue dysfunction and age-related diseases.

1.5 Aging

As with cancer, aging has a set of characteristic hallmarks attributed to it. As mammals age, cells will acquire damage attributing to the aging phenotype. This damage can be the accumulation of numerous mutations eventually leading to aberrant cell replication, which is why the elderly are more at risk of developing cancer. Hallmarks such as genomic instability and telomere attrition are a form of DNA damage, resulting in cell cycle arrest. Mitochondrial function deteriorates with age, exhibiting changes in morphology and reductions in size and mitochondrial protein activity (Bratic & Larsson, 2013). Epigenetic alterations such as DNA methylation and Histone modification can silence or activate certain genes in association with the aging phenotype. It has been documented that aging cells from mice and other species of mammals encounter a decrease in global DNA methylation (Fraga & Esteller, 2007, Wilson and Jones, 1983).

Dysregulated proteostasis may also contribute to aging such as the impaired folding of protein structures which can be the case in the age-related disease Alzheimers. Other hallmarks include deregulated nutrient sensing, altered intracellular communication and stem cell exhaustion (Lopez-Otin et al., 2013).

Cells have telomeres which are closely related to the phenomenon of aging. Original research carried out by Blackburn et al, (Blasco & Varela, 2010), brought into the limelight the existence of telomeres and their characteristic changes in length with each cell division. Telomeres are ‘complexes composed of proteins and nucleotides of TTAGGG repeats at the ends of eukaryotic chromosomes.’ (Bernadotte et al., 2016). Considered as protective structures, when a cell divides, chromosomes are replicated and these telomeres shorten in length with each cell division. It is believed as part of telomere theory that aging is a result of the loss of telomeric length. The shortening of these telomeres can be observed in replicative senescence (Harley et al., 1990). The mechanism of telomere shortening during cell replication is illustrated in Figure 4.

The shortening of telomeres is recognised as DNA damage resulting in the persistent activation of the DNA damage response (DDR) in replicative senescence. This is supported by the work of Hewitt et al (2018), where DNA damage foci are located in the telomeres of cells in relation to stress-induced senescence and an increase in the presence of telomere associated foci is seen wit elderly mice (Hewitt et al., 2018).

The decrease in telomeric length with every cell division is attributed to the 'end-replication problem' (Muraki et al., 2012). DNA polymerase, responsible for DNA replication, is capable of replicating a DNA strand but only in one direction. This results in the formation of a leading and lagging strand. DNA polymerase acts on the leading strand to form a complete DNA strand whereas the lagging strand consist of Okazaki fragments which are single pieces of DNA which are later ligated by DNA ligase. When DNA polymerase detaches itself from the strands a few nucleotides worth of space is left. These nucleotides are not replicated, and the copied DNA strand is short of a few DNA fragments which is now the shortened telomere (Muraki et al., 2012)

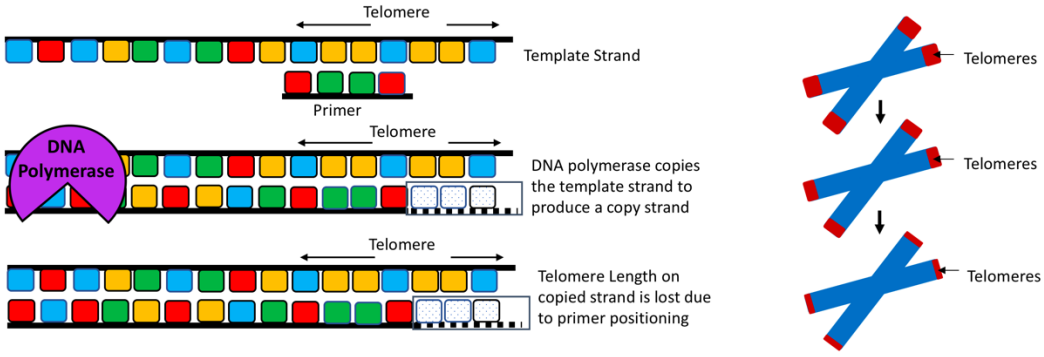

Figure 4: The shortening of telomeres during DNA replication and cell division. When the template strand is replicated during DNA synthesis, the primer misses a section of the telomere sequence and nucleotides are added to the copy strand upstream of the primer. This would result in a copy strand shorter than the template strand and missing the end of the telomere sequence. With every cell replication, the telomeres shorten in length as shown.

As telomeres become shorter and shorter with each cell division there will eventually be a major loss in telomeric DNA content, at this point the attrition is recognised as DNA damage and the DDR is initiated resulting in a halting of the cell cycle and therefore cell division – a key hallmark of cell senescence (Shammas, 2011).

Due to the characteristic shortening of telomeres, it has been suggested as the biomarker of choice in replicative senescence (Bernadotte et al., 2016). In the case of telomere-dependent induced senescence in normal aging and replicative senescence it could be considered as an additional biomarker however it would not prove useful in telomere independent based senescence such as oxidative stress induced or oncogene induced senescence, but these types of senescence are commonly investigated through *in vitro* methods. It must also be considered that other factors can also affect telomeric length, for example cancer, lifestyle choices such as smoking, diet, stress and exercise. (Shammas, 2011).

1.6 Cancer

It is now widely accepted that senescence is a tumour suppression mechanism, put into play when a cell approaches malignancy. Cancer cells exhibit uncontrolled cell proliferation and the counteractive mechanisms in place to stop the abnormal growth is apoptosis, quiescence or senescence (Dimri, 2005).

Growth arrest in senescent cells is maintained through the increased expression of tumour suppressive pathways. The particular pathway involved in preventing cancer depends on the stimuli involved to induce senescence and the species of interest. For example, mouse cells will senesce via the ARF-p53-p21-pRB pathway in response to non-telomeric signals and they do not undergo senescence through telomeric signals since their somatic cells possess a certain level of telomerase (Dimri, 2005). On the other hand, human cells undergo senescence through p53-p21-pRB pathway regardless of the type of stimuli, but some non-telomeric signals can also induce p16-pRB pathway related senescence (Dimri, 2005).

Multiple cancer research studies focus on the use of senescence as a therapy against cancer. By provoking cancerous cells to become senescent, a halt in the characteristic abberant proliferation in cancer could be achieved. Various drugs have been identified capable of achieving senescence in this state such as bleomycin, doxorubicin and cisplatin (Mikula-Pietrasik et al., 2019).

In order to induce cellular senescence in potentially malignant cells, the tumour suppressor pathways p53 and pRB/p16INK4a are crucial to cancer prevention (Rodier & Campisi, 2011) The relationship between cancer and senescence can be considered as what is known as antagonistic pleiotropy, this refers to the beneficial presence of a mechanism such as senescence at a younger age where it acts as tumour prevention but at an older age may encourage cancer initiation. Research shows that 'senescent cells have been identified in precancerous tissue, and hence cancer has to evade senescence to establish aberrant cell proliferation' (Fagagna & Giaimo, 2012).

At an older age, the senescence phenotype can serve as an aid in initiating cancer. The main hallmark of cancer associated with senescence is the changes in tissue microenviroment. Senescent cells may contribute to a more hostile tissue microenvironment through SASP and result in inflammation and promote tumorigenesis (Ruhland et al., 2016). Senescent cells can also contribute to tissue invasion and metastasis through the epithelial to mesenchymal transition (EMT). Through the SASP, certain chemokines, interleukins and proteins can promote cell migration and invasion of pre-metastatic cells (Laberge et al., 2011). Research carried out by Coppe et al, (2010) involved the co-culturing of X-radiation induced senescent mouse fibroblasts and pre-malignant mouse mammary epithelial cells which saw the stimulation of tumour formation (Coppe et al., 2010).

1.7 Immunology

The deterioration of the immune system with age is considered as 'immunosenescence' with literature focusing on dysfunction in the innate immune system in particular (Aw et al., 2007). This corroborates with the increased

likelihood of contracting infections at an older age. Literature suggests that there are differences in key components belonging to the innate and adaptive immune system between younger and older people. For example, Fulop et al., (2018) summarise that in the innate immune system increases in free radical, cytokine and myeloid cell number production are seen with aging whilst a reduction of phagocytosis, chemotaxis and free radical production is observed also. The adaptive immune system shows increased memory cell number, T cell number and B cell autoantibody production. Naïve cell number, T cell function, proliferation, IL-2 production, B cell number and function is reduced in the elderly (Fulop et al., 2018).

'Inflammaging' described as chronic low-grade inflammation, could be considered a result of the phenomenon of senescence (Pawelec, 2018). Chronic inflammation involves various inflammatory mediators such as cytokines for example IL-6 a which is a well-established marker for inflammation and SASP in various age-related diseases (Franceschi & Campisi., 2014). Thymic involution, the age-related decline in organ volume, is an obvious example of cellular senescence in immunology. With age, the replicative capacity of the bone marrow and lymphocyte diversity decline. T cells become oligoclonal and antibodies are of lower affinity. There is evidence of impaired antigen presentation and respiratory burst, indicating that senescence affects not only the adaptive but also the innate immune responses. Overall, the elderly individual is thought to become more susceptible to infectious disease and less protected in response to vaccines (Salam et al., 2013). Immune senescence is likely to have an impact on the normal immune surveillance of cancers, a homoeostatic mechanism by which the immune system patrols and eliminates cancerous outgrowth of self (Dunn et al., 2004). With immune health deteriorating with age, it becomes more difficult for senescent cell clearance generally mediated by Natural Killer (NK) cells and this accumulation can contribute to further tissue and organ dysfunction (Papismadov et al., 2017).

1.8 Key Pathways & Mechanisms involved in Cellular Senescence

1.8.1 p53/p21$^{WAF1/CIP1}$ Pathway and p16^{INK4A}/pRB Pathway

More commonly known as a tumour suppressor gene, p53 plays an important role in cellular senescence. p53 is a major transcription factor which is key to determining cell fate. In the event of stress induced DNA-damage it ultimately leads to cell cycle arrest halting cell growth allowing for DNA repair to take place, signal the initiation of apoptosis or prompt the cell to enter a state of senescence (Mijit et al., 2020). p21, encoded by the CDKN1A gene, is a cyclin-dependent kinase inhibitor protein which inhibits CDK2 and CDK4 complexes to stop G1 phase cell cycle progression. Yosef et al (2017) demonstrated the importance of p21 in maintaining senescent cell viability. In a p21 knockdown model, cells showed decreased survival as a result of the activation of JNK and caspase signalling mediated cell death. Additionally, reduced liver fibrosis as a result of senescent liver stellate cell elimination was seen in a p21 knockout mouse model (Krizhanovsky et al., 2008).

The DNA damage response (DDR) pathway is activated as a result of various stressors such as telomere loss, irradiation and oxidative stress. This provokes the activation of downstream signal transducers ATM (Ataxia-telangiectasia mutated protein) and ATR (Ataxia telangiectasia and Rad3 related protein) which further activate cell cycle checkpoint protein kinases CHK1 (Checkpoint kinase 1) and CHK2 (Checkpoint kinase 2) (Figure 5). These checkpoint proteins upregulate the expression of p53 through phosphorylation. p53 induces the activation of p21 which inhibits the cell cycle CDK2-Cyclin E complex which is key to driving G1 phase exit and S phase entry. Inhibition of the complex results in the RB protein (Retinoblastoma) not becoming phosphorylated keeping it bound to transcription factor E2F which cannot migrate to the nucleus to induce expression of target proliferative genes consequently halting cell cycle progression (Marechal & Zou, 2013, Bracken et al., 2011, Mijit et al., 2020).

$p16^{INK4A}$ induction is mediated by p38 mitogen-activated protein kinase (MAPK) pathway (Lin et al., 1998, Xiang et al., 2019). p16 interacts and binds to CDK4/CDK6 to inhibitsits activity, which also forms part of the G1/S phase checkpoint. This prevents RB becoming phosphorylated preventing E2F dissociation which mediates transcription of proliferative genes (Figure 5). p16 has been shown to increase with aging in replicative senescence of mammalian tissues and is therefore widely used as a biomarker (Krishnamurthy et al., 2004).

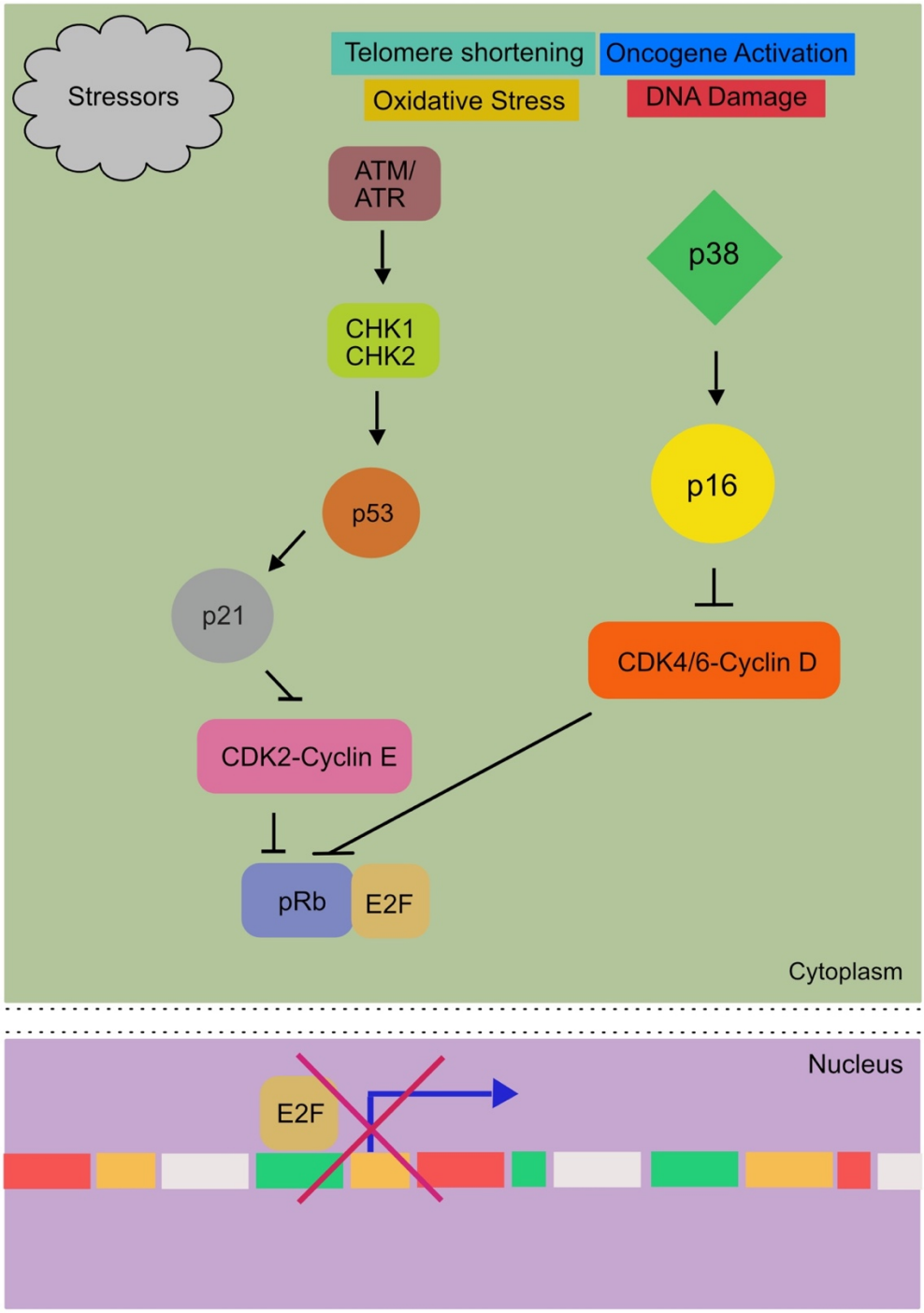

Figure 5: Illustrative diagram of p21-p53-pRb pathway and p16-pRb pathway in Cellular senescence. Stressors cause the activation of the DNA damage response or constitutive signalling of p38 which effect downstream targets p21 or p16 that inhibit cell cycle progression by sequestering E2F transcription through pRB binding.

1.8.2 NF-κB Signalling Pathway

The NF-κB pathway has been implicated in the initiation of SASP. Chien et al, (2011) identified NF-κB to be responsible for influencing the expression of SASP. Transcriptional profiling of oncogenic H-Ras^{V12} induced or replicative senescence in IMR-90 cells in which p65, a subunit of NF-κB, was suppressed. 406 genes were identified to be differentially expressed compared to control. These underwent enrichment for gene ontology (GO) terms which identified terms such as 'immune response' which highlighted genes such as IL-6 and IL-8 which are well recognised SASP components and 'positive regulation of NF-κB activity' (Chien et al., 2011). However, it is important to consider this suppression of p65 did not inhibit senescence as there are multiple pathways and components that allow for bypass. Research has also shown that cellular senescence and SASP are not mutually exclusive. Senescent cells may not always exhibit SASP (Stewart et al., 2019, Salminen et al., 2012).

In the induction of SASP in cellular senescence, NF-κB is stimulated through various pathways. These include the NEMO shuttle which is activated by DNA damage, p38MAPK in response to stress and RIG-1 which is induced by inflammasomes (Salminen et al., 2012). Similarly, Meyer et al (2017) found that SASP factors IL-6 and IL-8 were mediated through NF-κB in a DNA damage induced senescence murine fibroblast model. An *in-silico* knockout of NEMO (NF-κB essential modulator) showed inhibition of IL-6 and IL-8 reinforcing the concept of NF-κB regulating SASP (Meyer el al., 2017).

1.8.3 mTOR

mTOR (mammalian target of rapamycin) is a serine/threonine kinase protein which is evolutionarily conserved across species. It is known for its inhibitor, rapamycin. This inhibition has shown to extend lifespan and decelerate cellular senescence in various models (Demidenko et al., 2009). Harrison et al., (2009) showed that male and female mice fed rapamycin at late-stage life (beginning at 600 days) resulted in increased survival.

A study by Kucheryavenko et al (2019) showed that mTORC1, which in complex with mTORC2 forms mTOR, could be used as a target to eliminate senescent cells. Torin, an mTORC1 inhibitor was given to immunodeficient NSG mice that accumulate senescent hepatocyte cells at a faster rate compared to wild type mice. This resulted in reduced telomere associated DNA damage foci (TAFs) and yH2AX suggesting a selective apoptotic effect on senescent cells (Kucheryavenko et al., 2019). Furthermore, Rapamycin treated human cardiac progenitor cells attenuated replicative senescence and promoted cellular function (Park et al., 2020). Rapamycin is now being used in a clinical trial to evaluate its effect in longevity in humans. The study is currently recruiting for 1000 participants who will be subjected to various doses of rapamycin intermittently and assessed for visceral fat, bone density, lean body mass, liver and renal function, and a lipid and insulin profile (Clinicaltrials.gov, PEARL, 2021).

1.9 Nutraceuticals

1.9.1 Definition

Nutraceutical is defined as a ‘food, or food parts that provide medical or health benefits, including the prevention and treatment of disease’. These can include but are not limited to medical foods, phytochemicals, nutritional supplements, vitamins, minerals and herbal remedies (Kalra, 2003). Commonly found in dedicated health food stores not all are regulated and evidenced with clinical data to prove health benefits and safety from toxicity.

1.9.2 Senolytics

Compounds which can negate the effects of senescence recently have taken precedence in the field of aging research. The removal of senescent cells is beneficial in aging as the accumulation of these cells is ‘’associated with disease due to the SASP’’. The SASP is secreted by senescent cells in the form of pro-inflammatory and pro-tumoirigenic factors which can excaerbate chronic conditions or augment cancer. In additon to inducing other cells into senescence causing further damage. (Kobbe et al., 2019)). They have been known to

contribute to diseases such as parkinsons or Alzheimers, coronoary heart disease, Type 2 diabetes, cataracts and liver disease to name a few. By removing these cells and not allowing for their accumulation the onset of such diseases can be delayed or prevented to allow for improved quality of life and normal tissue and organ function. For example, the use of Nicotinamide Mononucleotide (NMN), a precursor of nicotinamide adenine dinucleotide (NAD+), which is an essential coenzyme needed for cellular functions such as DNA repair, metabolism and mitochondrial processes (Hong et al., 2020) Also, Navitoclax (ABT-263) an existing chemotherapeutic drug which has shown to cause apoptosis in senescent cells but has serious side effects to healthy cells (González-Gualda et al., 2020). These anti-senescence compounds are separated into two categories: senolytics and senostatics.

Senolytic drugs are agents that selectively induce apoptosis of senescent cells by targeting proteins such as Bcl-2, Bcl-XL, PI3K/AKT, p53 and p21, all of which facilitate cell death. They were first discovered by Zhu et al (2015). Their work identified that the pairing of quercetin and dasatinib successfully cleared senescent cells in mice leading to the combination becoming one of the most well-studied senolytics. Since then, multiple studies have shown that the duo of dasatinib, a previously established anti-cancer drug and quercetin, a plant flavonoid, caused selective apoptosis of senescent cells 'resulting in the improvement of physical function and increased survival in vivo' (Hickson et al., 2019, Xu et al., 2018, Zhu et al., 2015). Ogrodnik et al (2021) recently investigated the same combination in aged INK-ATTAC mice ($p16^{Ink4a}$ positive senescent cells are eliminated when subjected to treatment) to find 'significant attenuation of age associated cognitive dysfunction' (Ogrodnik et al., 2021). The combination of dasatinib and quercetin is also being investigated in clinical trials of patients with idiopathic pulmonary fibrosis, 'a cellular senescence driven disease', and has shown promise in alleviating cardiopulmonary dysfunction (Justice et al., 2018, Ellison Hughes., 2020). A separate clinical trial also studied the effect of dasatinib and quercetin in humans with diabetic kidney disease to find reduced markers of senescence including p16, p21, SA- β-Gal activity and decreased expression of SASP factors (Hickson et al., 2019). Other synthetic compounds with senolytic properties remain under investigation such as BCL

inhibitor ABT-737, HSP90 inhibitors or Panobinostat (Yosef et al., 2016, Fuhrmann-Stroissnigg et al., 2017, Samaraweera et al., 2017).

1.9.3 Senostatics

Drugs classed as senostatics interfere with the progression of cellular senescence and act by inhibiting paracrine signalling or by neutralising the SASP (Short et al., 2019). 'They can also prevent the emergence of senescent cells by blocking fundamental steps of the effector mechanisms of the phenotype, such as activation of the p53 pathway' (Althubiti et al., 2016, Kaur et al., 2020).
Rapamycin and metformin are examples of senostatics which have shown to be effective in previous studies (Short et al., 2019). Rapamycin is a naturally derived antibiotic with additional anti-fungal and immunosuppressant properties. The macrolide compound is an mTOR inhibitor and it delays the progression of senescence and improves health in animal models (Wang et al., 2017, Blenis et al., 2014). Wang et al, investigated its effects on mouse skin fibroblasts with a 24-hour treatment prior to senescence induction by oxidative stress using hydrogen peroxide. Its effects were shown to be a result of SASP inhibition. Park et al., (2020) shows how rapamycin is able to attenuate replicative senescence of human cardiac progenitor cells by inhibiting mTOR. Following on from these successful studies a clinical trial, PEARL (Participatory evaluation of Aging with Rapamycin for Longevity Study) has been set up to identify the long-term safety and efficacy profile of rapamycin use in decreasing aging measures such as visceral fat, bone density, blood count, liver and renal function, changes to insulin sensitivity and side effects in older adults (PEARL, Clinical Trials.gov, 2021).

Metformin, originally derived from the plant *Galega officinalis* more commonly referred to as Goat's Rue (Bailey, 2017), is a commonly prescribed anti-diabetic drug that, has been shown to be capable of inhibiting the SASP through the attenuation of the NFκB pathway (Moiseeva et al., 2013). It has been shown to extend the lifespan of *Caenorhabditis elegans* (Chen et al., 2017). C57BL/6 male mice treated with 0.1% w/w metformin showed increased life and health spans (Martin-Montalvo et al., 2013). Studies have led to the application of metformin in human clinical trials. TAME (Targeting aging with metformin) which is a six-year-

long trial consisting of approximately 3000 participants aged 65-80 years that will undertake a daily dose of metformin. It will aim to investigate the 'occurrence and progression of age-related diseases including heart disease, dementia and cancer' (AFAR.org, TAME Trial, 2021).

1.9.4 Established Nutraceutical in Senescence

For further information on established nutraceutical based senolytics and senostatics please see Appendix B, which consists of a literature review based on the use of nutraceutical based senolytics and senostatics in aging which was published in Frontiers in April 2020 authored by Amanpreet Kaur in collaboration with Dr Cordula Stover and Dr Salvador Macip (Head of Mechanisms of Cancer and Aging Lab at the University of Leicester). The publication focuses on the definition of plant-based compounds and how nutraceutical based senolytics and senostatics are being established in the field of senescence with some proving to be very effective; these included olive oil phenols, Green tea catechins, Fisetin and Resveratrol.

1.10 Holy Basil

Holy Basil, technically known as *Ocimum sanctum* or *Ocimum tenuiflorum,* is commonly referred to as an ayurvedic herb with various medicinal properties. Traditionally it has been used to treat a slew of ailments such cough, cold, headache, respiratory and gastric disorders, fevers such as typhoid and even as antidotes for poisons from snakes and scorpions (Singh & Chaudhuri., 2018).

Studies have shown Holy Basil extracts to exhibit anti-oxidant, anti-cancer, anti-inflammatory, anti-microbial, anti-diabetic, anti-hyperlipidemic and other beneficial properties (Chaudhary et al., 2020, Mohan Kumar et al., 2020, Manaharan et al., 2014, Yamani et al., 2016, Parasuraman, 2015). It is also considered an 'adaptogenic' herb, which helps to restore physical and chemical imbalances to negate the effects of stressors on the body (Cohen, 2014).

Holy Basil has also shown promising radioprotective effects. In cell line and mouse models exhibiting tumorigenic attributes, *Ocimum sanctum* has shown to protect against 'tumoricidal effects of radiation in normal tissue and cells' (Baliga et al., 2014, Subramanian et al., 2005). A systematic review by Jamshidi & Cohen (2017) highlighted the safety and clinical efficacy of Holy basil use in humans when used as a therapeutic with various studies indicating effectiveness with no major adverse side effects (Jamshidi & Cohen, 2017).

There are no studies pertaining to the use of whole Holy Basil to determine its effectiveness in senescence or aging based experiments. However, there are a few limited studies using the main phenolic component of Holy Basil, Rosmarinic Acid (RA). RA is a caffeic acid ester and is found to be naturally occurring in plants of the *Lamiaeceae* family (Nadeem et al., 2019). It has been shown to have some anti-aging effects with studies in *Caenorhabditis elegans* showing RA to significantly extend lifespan (Wang et al., 2011).

Hahn et al (2017) investigated the effect of RA in hydrogen peroxide induced cellular senescence in human dermal fibroblasts. Application of RA prior to senescence inductions resulted in a reduction in cellular senescence measured using SA-β-Gal activity. However, this was the only marker for senescence that was analysed. RA was also investigated in a replicative senescence model using human skin fibroblasts applied as a long-term dose. Cells underwent serial passaging until cessation of cell proliferation was reached and 90% of cells were SA-β-Gal positive and were treated with RA throughout passaging. Results showed that RA did not have a significant effect on the replicative lifespan of cells compared to control, but telomere length analysis showed that RA treated cells had a slower loss of telomere restriction fragments (Sodagam et al., 2019).

Further research of Holy Basil and its components is warranted to discover underlying mechanisms of action and if this all-encompassing plant is capable of anti-senescence action.

1.11 Allicin

The main bioactive compound found in garlic (*Allium Sativum L*.) is Allicin (allyl 2-propenethiosulfinate or diallyl thiosulfinate). It is an 'organosulfur containing volatile compound and is culpable for the strong smell and taste attributed to garlic' (Nadeem et al., 2019). The cutting and exposure of whole garlic cloves results in the production of alliin and alliinase enzyme which when combined form Allicin. As a compound Allicin is 'poorly stable and short lived however it is capable of rapidly infiltrating cell membranes and interacting with free thiol groups for further metabolism' (Nadeem et al., 2019, Bayan et al., 2014). Allicin has shown to have anti-microbial, anti-oxidant, anti-inflammatory, anti-cancer and cardioprotective properties. (Ankri & Mirelman, 1999, Nakamoto et al., 2020, Chung, 2006, Prasad et al., 1995, Arreola et al., 2015, Schafer & Kaschula, 2014, Zhang & Yang, 2018, Chen et al., 2018, Chen et al., 2019).

There remains a limited number of studies regarding the use of allicin as a senescence therapy. Research has shown that allicin may possess anti-aging properties. Chen et al (2019) concluded that Allicin ameliorated hematopoietic stem cell aging induced by lead exposure. Allicin was also found to inhibit senescence of human umbilical endothelial cells induced by hydrogen peroxide (Lin et al., 2017). A recent study by Rosas-Gonzalez et al (2020) investigated the effects of Allicin on apoptosis and senescence in MCF-7 and HCC-70 cells, which are breast cancer cell lines. Senescence was induced using doxorubicin and cell viability measures showed a significant reduction in live senescent cells following Allicin application (Rosas-Gonzalez et al., 2020).

Allicin bioavailability has been found to be complicated. Alliinase becomes quickly deactivated through heat or acid. Lawson & Hunsaker investigated the Allicin bioavailability and bioequiavelnce (ABB) of enteric, non-enteric garlic supplements and garlic foods. Following consumption, analysis of breath metabolites of allicin, non-enteric supplements showed high ABB (80-111%) with Kwai black garlic powder showing 80% (Lawson & Hunsaker., 2018). With few studies investigating the use of Allicin in cellular senescence further research which would focus on aging models*, in vitro* and *in vivo*, would allow for a

conclusion to be reached on the anti-senescence properties of the garlic derivative.

1.12 Phytol

Phytol is an isoprenoid commonly found in chlorophyll. The acyclic monounsaturated diterpene alcohol is a compound that can be found in Vitamin E and K (de Moraes et al., 2014). Phytol is widely used in fragrance and cosmetic therapies. The plant-based derivative has shown to have antibacterial, antimicrobial, antioxidant, anti-inflammatory, antinociceptive and anticancer properties (Lee at al., 2016, Islam et al., 2018, Santos et al., 2013, Silva et al., 2013, de Alencar et al., 2018). Phytol is well absorbed with 30-66% of a dose being ingested successfully (de Moraes et al., 2014).

The investigation of phytol in senescence has only been carried out in a singular study by Jeong (2018). HaCaT keratinocytes were subjected to phytol treatment for a 24-hour period prior to senescence induction by oxidative stress using hydrogen peroxide. Results indicated reduced inflammatory markers such as TNF-a, IL-6, IL-8 and COX2. Cell cycle analysis showed a reversion of cells into the G0/G1 phase with the dose dependent addition of phytol.
CASP3 activity analysis through a colorimetric assay showed inhibition of the component indicating reduced apoptosis with phytol treatment. This suggests at the investigated concentrations (1,5 and 10 uM) phytol has protective effects. SA-β-Gal activity showed a reduction in positively stained cells in a dose dependent manner indicating suppression of cellular senescence and showing that phytol has senostatic properties (Jeong, 2018).

However, this paper only studies senescence with the use of SA-β-Gal activity which is known to be a key marker in senescence. It cannot be solely relied upon to reach a conclusion regarding the effects of senescence. Cell cycle analysis can support the suppression of senescence with an increased number of cells being present in the G0/G1 phase of the cell cycle, the reduction of SASP factors following phytol treatment in addition to reduced expression of downstream p53 targets such as Cyclin B and 14-3-3 sigma which are known G2 cell cycle arrest

inducing genes. The outcome of the study suggests that phytol has senoprotective capabilities and would warrant further investigation of the compound.

2 Development of a protocol to study SIPS (stress-induced premature senescence) in L929 mouse fibroblast cell line using irradiation

2.1 Introduction

The original senescence model for *in vitro* work would be the human replicative senescence model discovered by Hayflick and Moorhead in 1951 (Hayflick and Moorhead, 1961). However, it is not the most practical of models with final senescent cell numbers being finite and the extensive time it takes to finally reach senescence through 50 passages. In comparison mouse models for replicative senescence are more achievable because primary cells attain a senescent state within 5-6 passages (Khan & Gasser, 2013). This is due to their different regulation of telomere lengths and telomerase activities (Calado & Dumitriu, 2013). Despite this, artificially induced senescence models also exist. Through DNA damage, cells can undergo an accelerated form of aging in response to various stimuli. These are commonly referred to as SIPS (stress induced premature senescence) models (Touissant et al., 2002).

DNA single and double strand breaks (induced by exposure to radiation, prolonged oxidative stress, etc.) result in the activation of the DDR and can eventually lead to stress-induced premature senescence (SIPS), which is independent of telomere length (Boothman & Suzuki, 2008). *In vitro* SIPS models have been established using oxidative stress, ionizing radiation or DNA damage causing agents such as the anti-neoplastic drug bleomycin which causes a release of free radicals (González-Hunt et al., 2018). Overexpression of the *ras* oncogene in primary human and rodent cells was found to elicit a phenotype similar to cellular senescence. The activation of oncogenes such as Raf, c-Myc, Akt and E2F3 have been found associated with development of senescence in normal cells (Serrano et al., 1997, Ko et al., 2018, Astle et al., 2011).

Aims and Objectives

The aim was of the chapter was:

- to create a routinely applicable and reproducible model using L929 mouse fibroblast cell line using irradiation to minimise time spent in harvesting primary mouse fibroblasts and passaging to reach senescence.
- to extensively characterise for multiple markers of senescence to assure the attainment of the phenotype. These include measuring a halt in proliferation, changes in morphology and the presence of SASP.
- to have developed and characterized a model of senescence that is suitable for testing the senostatic and senolytic properties of various nutraceuticals.

2.2 Material and Methods

2.2.1 Cell line

The L929 cell line is derived from normal subcutaneous areolar and adipose tissue of a 100-day old male C3H/An mouse and was acquired from ECACC (Cat No: 85011425). Cells were maintained in culture medium consisting of MEM (Gibco), 5% 2mM L-Glutamine, 5% Penicillin/Streptomycin, 10% FBS (Gibco) and 5% Non-essential amino acids at 37^{o}C and 5% CO_2 in a humidified atmosphere. Sub-confluent cultures were split 1:4 using 0.25% Trypsin-EDTA and centrifuged at 300rcf for 5 minutes.

2.2.2 Cell seeding

Cells were trypsinised as above and assessed for viability using the trypan blue exclusion method and counted. Cells of >90% viability were seeded in 35mm sterile cell culture grade dishes at a density of 100,000 cells per dish. Cells were left overnight for 24 hours to allow for adherence.

2.2.3 Serum Starvation

Cells underwent serum starvation for 24 hours in medium consisting of MEM (Gibco), 5% Non-essential amino acids, 5% Penicillin/Streptomycin and 5% 2mM L-Glutamine.

2.2.4 Irradiation

Media was removed from cells and replaced with PBS without Ca^{2+} and Mg^{2+} for the X-Ray irradiation procedure. Dishes were transported to the University of Leicester Irradiation facility. Using the X-Strahl RS320 X-Ray irradiator cells were subjected to a dose of 15Gy at 195kV at 10mA with a copper filter for 9 minutes and 28 seconds. Control cells were not subjected to any X-Ray irradiation, but were kept in PBS and at room temperature during the irradiation procedure. PBS was removed from cells and replaced with cell culture media for 72 hours.

2.2.5 Splitting

Cells were split 1:3 and maintained for a further 7 days with regular cell culture media changes.

2.2.6 Senescence model achieved on Day 10

7 days after the 1:3 split, cells were harvested for further analysis. Figure 6 illustrates the full protocol for achieving SIPS in the L929 mouse fibroblast cell line using irradiation.

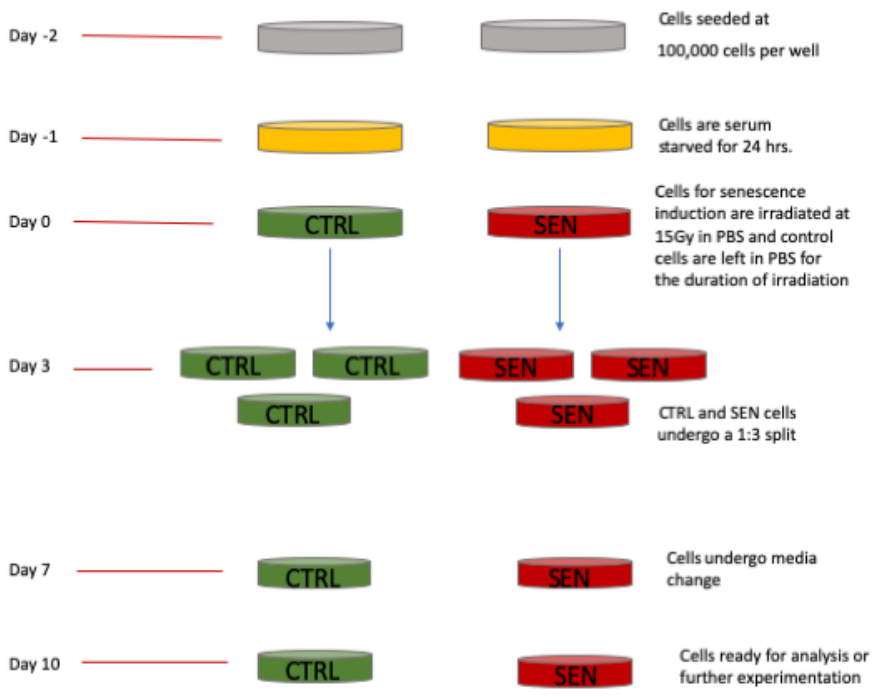

Figure 6: Protocol to induce SIPS in L929 cell line using irradiation. L929 cells undergo stress-induced pre-mature senescence by seeding at a low cell-density, 24-hour serum starvation, irradiation at 15Gy, 1:3 split 72 hours following irradiation and maintenance of cells until day 10 of protocol when senescence is achieved.

2.2.7 Measuring cell proliferation

Cell proliferation was measured using 0.4% Trypan-Blue (Sigma, T6146) and a Neubauer haemocytometer at specified time points. Cells were harvested through gentle cell scraping and centrifuged at 300rcf for 5 minutes. Cell pellet was resuspended in 1ml of cell culture media. 15µl of this suspension was mixed with equal amount of 0.4% Trypan Blue and deposited into the glass haemocytometer. The cells were counted using a light microscope at 100x magnification. Each cell suspension was counted twice after resuspension, counts took into account the dilution factor and were averaged.

2.2.8 Cell cycle analysis using propidium iodide

For cell cycle analysis using propidium iodide, cells were scraped and harvested using centrifugation at 300rcf for 5 minutes. Cells were washed once with PBS and fixed in cold 70% ethanol overnight at 4^{o}C. Cells were centrifuged at 300rcf for 5 minutes to remove the ethanol and washed twice in cold PBS. Cell pellets were re-suspended in 50µl of RNAse (100µg/ml) and left on ice for 20 minutes. 200µl of Propidium iodide (100µg/ml) was added to the cell suspension and covered in foil for 10 minutes. Cell were immediately analysed on the flow cytometer Cytoflex (Beckman and Coulter). Cell cycle stages and gating were determined with assistance of Jennifer Hincks (FACS Facility manager).

2.2.9 Senescence associated Beta-Galactosidase (SA-β-Gal) staining

Staining for SA-β-Gal was carried out according to protocol for senescence detection kit (abcam) (ab14085). Senescent cells express an increased level of lysosomal beta-galactosidase which can be stained for using the substrate X-Gal (5-bromo-4-chloro-3-indolyl-β-D-galactopyranoside) to obtain a blue colour of cells to indicate senescence. Stained samples were incubated overnight for at least 12 hours and then visualised under light microscope.

2.2.9.a Statistical Analysis

For the characterisation of CTRL and SEN cells when tested for SA- β -Gal, a statistical unpaired t-test was performed using a 5% significance level to determine a significant difference. For the identification of cell cycle phase of CTRL and SEN a statistical t-test was performed using a 5% significance level to determine a significant difference. This was performed following an F-test to determine equal or unequal variance between CTRL and SEN cell cycle phases.

2.2.10 Western Blot

2.2.10.1 Gel Preparation

The 10% SDS-PAGE gel was prepared in a BioRad 1.0mm Glass plate system using the components listed in Table 1. The resolving gel was made and poured in between the glass plates, butan-1-ol was used on top to prevent drying and assist with levelling. The gel was left to polymerise for 20 minutes at room temperature. The stacking gel was prepared according to table 1, the butan-1-ol was removed and the stacking gel was poured on top of the resolving gel and left to polymerise for 15 minutes at room temperature. The gel was either used immediately or stored overnight in a cold room at 4^{o}C, wrapped in cling film to prevent drying.

Components	Resolving Gel	Stacking Gel
40% acrylamide (containing methylenebisacrylamide)	2.5ml	0.5ml
1.5M Tris pH 8.8 (containing 0.4% SDS)	2.5ml	-
1.0M Tris pH 6.8 (containing 0.4% SDS)	-	630µl
H_2O	4.9ml	3.82ml
10% (w/v) Ammonium persulphate sol	100µl	50µl
Tetramethylethylenediamine (TEMED)	4µl	5µl

Table 1: Components used to prepare 10% SDS-PAGE gel for Western blot. The reagents and amounts used to make the SDS-PAGE gel for Western blot.

2.2.10.2 Cell lysate preparation

Cells were scraped and lysed in RIPA lysis buffer (150mM NaCl, 1% Nonidet P-40, 0.5% Sodium deoxycholate, 0.1% SDS, 50mM Tris (pH 7.4), and ddH_2O) and

incubated on ice for 30 minutes. The cell suspension was centrifuged at 13,000xg for 3 minutes and the supernatant was collected and cell pellet discarded. The cell lysate was stored at -20°C.

2.2.10.3 Protein quantification

The total protein concentration was quantified using Pierce™ 660nm assay reagent (Thermofisher Scientific, Cat. No 22660) and Pierce™ Bovine Serum Albumin Standard Pre-diluted Set (Thermofisher Scientific, Cat No. 23208). The quantification was set up in a 96 well plate as illustrated in Figure 7. The optical density was measured on Labtech LT4500 Plate reader using compliant software from Labtech.

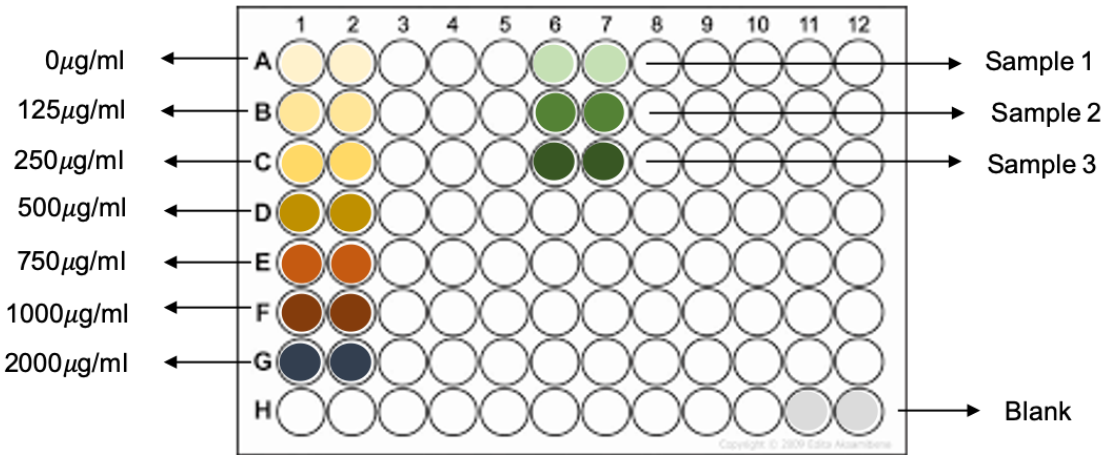

Figure 7: Schematic of plate set up for Pierce assay for protein quantification. The plate was set up with Bovine Serum Albumin (BSA) standards from 0-2000μg/ml, blank (RIPA lysis buffer) and the samples of unknown concentration in duplicates.

The optical density values were averaged across each standard to create a standard curve of known protein concentration versus optical density using Prism 7 software. The values for the unknown protein concentrations for samples were calculated by interpolating from the standard curve. Values could then be normalised to the samples with the least amount of protein available per μl and diluted to obtain equivalent protein content for gel loading.

2.2.10.4 Loading Sample preparation

5µl of SDS-PAGE Sample buffer (0.25M TrisCl, pH 6.8, 50% (v/v) glycerol, 5% (w/v) SDS, 0.25M DTT, 1% (w/v) bromophenol blue) to each sample of 25µl of cell lysate normalised for equal protein content. Samples were heated for 10-15 minutes at 55^{o}C on a heated block to denature proteins prior to running.

2.2.10.5 Performing the Western blot

A molecular weight marker (ThermoScientific^{TM} Page Prestained protein ladder) and the samples were loaded into the wells of the prepared gel and ran in running buffer (25mM Tris, 190mM Glycine, 0.1% (w/v) SDS, pH 8.3) for 30 minutes at 90V and 120V for another 45 minutes. The proteins were transferred to a nitrocellulose membrane (Biotrace^{TM} NT) using BioRad's mini Trans-Blot Cell system at 250mA for 50 minutes in transfer buffer (50mM Tris, 40mM glycine, 10% methanol).

2.2.10.7 Blocking and Application of Antibodies

The membrane was blocked in Blocking solution (see Table 2 for all solution preparation) for 1 hour at room temperature, followed by the application of the primary antibody overnight at 4^{o}C. The following day the membrane is washed in washing solution for 45 minutes changing the solution every 15 minutes. The membrane was then blocked in the secondary antibody for 1 hour at room temperature. The membrane was then washed as above.

Solution	Preparation
Blocking Solution	5% (w/v) skimmed milk in PBS
Antibody Solution	5% (w/v) skimmed milk in PBS
Primary Antibody	Anti-p21 polyclonal Antibody (St. John's Laboratory, Cat No STJ97470

	Dilution: 1:3000 in antibody solution
Secondary Antibody	DAKO Polyclonal Swine Anti-Rabbit Immunoglobulins HRP Cat No: P021702 Dilution: 1:3000 in antibody solution
Washing Solution	0.05% Tween 20 (Sigma-Aldrich) in PBS
ECL kit	Invitrogen Novex ECL HRP Chemiluminescence Substrate Reagent Kit
X-Ray film	Hyperfilm (Amersham Sciences)

Table 2: Solutions and their preparation instruction for blocking, application of antibodies, application of chemiluminescence substrate and developing of blot.

2.2.10.7 Application of ECL and developing of blot

The proteins were visualised using an ECL kit as in Table 2 and developed using Hyperfilm in a dark room. Following appropriate exposure, the film was submerged in developing solution for 2-3 minutes, washed in water for 1 minute and finally fixed in fixative solution for 2 minutes in the dark.

2.2.11 Gelatin Zymography

2.2.11.1 Sample preparation

Following the last media change on Day 7, cells were supplemented with no serum media to eliminate any pre-existing MMPs present in the MEM component of cell culture media. Cells were incubated for 3 days and conditioned media was collected on Day 10, centrifuged at 300rcf for 5 mins and stored at 4^{o}C. Prior to loading, equal amounts of sample from each condition were taken and 5X non-

reducing sample buffer (4% (w/v) SDS, 20% (v/v) Glycerol, 0.01% (w/v) bromophenol blue and 125mM Tris-HCl, pH 6.8) were added to samples.

2.2.11.2 Gel preparation and running of zymogram

The gel was prepared according to instructions in Table 3.

Component	Separating Gel (7.5% acrylamide)	Stacking gel
1.5M Tris pH 8.8	2 mL	-
0.5M Tris pH 6.8	-	1.25 mL
30% (v/v) acrylamide	2 mL	0.670 mL
H_2O	2 mL	3.075 mL
Gelatin (4mg/mL)	2 mL	-
10% (w/v) SDS	80µL	50µL
10% (w/v) APS	80µL	50µL
TEMED	10µL	10µL

Table 3: Preparation of gelatin zymography gel.

Samples were loaded into wells along with a protein ladder and ran in running buffer (see 2.2.10.5 for recipe) at 90V for 1.5 hours or until good separation of molecular weight ladder.

2.2.11.3 Washing and Incubation of zymogram

The gel was washed in washing buffer (2.5% Triton-X 100, 50mM Tris-HCl, pH 7.5, 5mM $CaCl_2$, 1µM $ZnCl_2$) for 30 minutes and the buffer was changed after 15 minutes. The gel was rinsed in incubation buffer (Triton-X 100, 50mM Tris-HCl, pH 7.5, 5mM $CaCl_2$, 1µM $ZnCl_2$) for 10 mins at room temperature with agitation.

The gel was then incubated with fresh incubation buffer for 24 hours at 37°C, with agitation.

2.2.11.4 Staining and destaining of zymogram

The following day the incubation buffer was removed and the gel was stained with staining solution (see Table 4) at room temperature on shaker for 1 hour. The gel was rinsed in water and incubated with destaining solution (see Table 4) for 15 minutes at room temperature or until white/clear bands could be seen against the dark blue stained background of the gel.

Staining Solution (100mL)	Destaining Solution (250mL)
Methanol – 40mL	Methanol – 100mL
Acetic Acid – 10mL	Acetic acid – 25mL
H_2O – 50mL	H_2O – 125mL
Coomassie Blue – 0.5g	

Table 4: Staining and destaining solutions for Gelatin zymography.

2.2.12 Light Microscopy

Cells were imaged at regular intervals during the senescence induction protocol specifically at Day 3 and Day 10 at 10X magnification using a light microscope.

2.2.13 Immunofluorescence Microscopy

Cells were seeded on coverslips on Day 3 of the senescence induction protocol. On Day 10, cells were fixed onto the coverslip using 2% paraformaldehyde for 10 minutes at room temperature. Cells were then stained with DAPI (Sigma-Aldrich) for 2 minutes at room temperature. The coverslip was mounted on to a glass slide using 40% glycerol and sealed using nail polish. The slide was imaged using the Nikon microscope 3 (LED) with an Andor iXonEM+ EMCCD DU 885 camera and

NIS elements viewing software. DAPI filter used: DAPI - Ex: 340-380nm; Dichroic: DM400; Em: 435-485nm

2.2.14 Electron Microscopy

2.2.14.1 Transmission Electron Microscopy (TEM)

Cells were seeded onto coverslips on Day 3 and kept in media until Day 10 and processed by the EM facility at the University of Leicester using the following protocol.

1. Growth media was immediately replaced with 2.5% glutaraldehyde / 0.1M sodium cacodylate pH7.3 and fixed for 1 hour
2. Washed in 0.1M sodium cacodylate for 2x within 45mins
3. Secondary fixation in 1% Osmium tetroxide / 1.5% potassium ferricyanide / 0.1M sodium cacodylate buffer for 60 minutes
4. Washed in 0.1M sodium cacodylate 3x within 45 minutes
5. Stained in 1% tannic acid in 0.05M sodium cacodylate in the dark (RT) for 1hour
6. Washed in 1% sodium sulfate in 0.05M cacodylate for 5 minutes
7. Washed in distilled de-ionised water 2x 10mins
8. Dehydrated through 30%, 50% & 70% ethanol series for 10min each
9. 70% ethanol overnight
10. Dehydrated through ethanol 90% & 100% 30 mins each
11. Dehydrated through analytical grade ethanol for 2 x 30mins
12. Transferred through 2 x propylene oxide 2 x 5 mins
13. Infiltrated with propylene oxide : modified Spurr's resin hard mix

    3:1 for 60min

    1:1 for 60 min

    1:3 for 90 min

14. 100% Spurr's resin for 30 minutes
15. 100% Spurr's resin overnight

16. Fresh Spurr's resin 1 x 8 hours
17. Flat embed and polymerise for 16hours at 60°C

Samples were sectioned to a thickness of 70nm using a Reichert Ultracut E ultramicrotome, collected onto copper mesh grids and stained 5 minutes in Reynold's lead citrate.

Samples were viewed on a JEOL JEM-1400 TEM with an accelerating voltage of 100kV. Digital images were collected with a EMSIS Xarosa digital camera with Radius software.

2.2.14.2 Scanning Electron Microscopy (SEM)

Cells were seeded onto coverslips on Day 3 and kept in media until Day 10 and processed by the EM facility at the University of Leicester using the following protocol.

1. Growth media was immediately replaced with 2.5% glutaraldehyde / 0.1M sodium cacodylate pH 7.3 and fixed for 1 hour
2. Washed in 0.1M sodium cacodylate buffer 2 x within 1h
3. Coverslips were transferred into 12 well plates with 0.1M sodium cacodylate buffer and processed for TEM. The original dishes were processed further for SEM
4. Washed in dd water 3x within 70min
5. Dehydration in Ethanol series: 30% - 25min, 50% - 20min, 70% - 1h, then overnight at 4°C,
6. Then dehydrated in ethanol at 90% - 30min, 100% - 20min
7. Anhydrous analytical ethanol 2x25min
8. Mix Analytical Ethanol : HMDS (Hexamethyldisilazane)

   3:1 - 25min

   1:1 - 25min

   1:3 - 30min

9. Pure HMDS 1x25min, 1x 25min

10. Left overnight in fumehood
11. Dried samples were mounted onto aluminium stubs using carbon sticky tabs, and coated with gold/palladium in a Quorum Q150 TES coating unit.
12. Samples were viewed on a Hitachi S3000H Scanning Electron Microscope with an accelerating voltage of 10kV.

2.3 Results

With the aim of developing a senescence model, drawing on literature allowed for the setting up of the model according to key criteria that had to be fulfilled. Key characteristics were chosen to ensure senescence had been achieved. In addition to a successful model, reproducibility was also a necessity. By opting for an irradiation model instead of using hydrogen peroxide, which is known to be an unstable compound, we could ensure technical steps would be kept the same. Various inducers of senescence were investigated in a preliminary study to establish the model (Figure 9). Use of a fibroblast cell line would mean that further experimentation with nutraceuticals could be compared to an *in vivo* mouse model using fibroblasts extracted from skin tissue. Use of a cell line would also provide an unlimited source of cells for the senescence model compared to use of primary cells from mice which proved to be very time consuming and rate-limiting in obtaining the number of cells needed for appropriate experiments. In addition to this, senescence related behaviour of primary cells from mice can be influenced by their age and weight (List et al., 2016).

Senescence characteristics were measured through analysis of cell proliferative capabilities, expression of SA- β-Gal, cell cycle analysis using propidium iodide (PI) staining, monitoring cell morphology and determining expression of cell cycle arrest proteins and matrix metalloproteinases. As there is no single marker that uniquely characterises senescence, monitoring multiple attributes is key to produce a senescence cell model.

2.3.1 Loss of cell proliferative capabilities

Loss of proliferative capabilities is a key marker of the senescence phenotype, therefore, to assess proliferation, two groups of cells were analysed in parallel. The experiment was set up as 2 CTRL dishes and 4 SEN dishes, each a biological repeat, and cells were counted at seeding, before serum starvation, before irradiation treatment, on day 3 whilst carrying out the 1:3 split, on day 6 and finally on day 10.

All cells follow the pattern of proliferation up until irradiation, after which SEN cells decline in number and CTRL cells continue to replicate (Figure 8). From day 3 to day 10, CTRL cells continue to increase in number whereas SEN cells plateau to a constant number of cells as would be expected for a senescent cell model to indicate a halt in cell cycle progression.

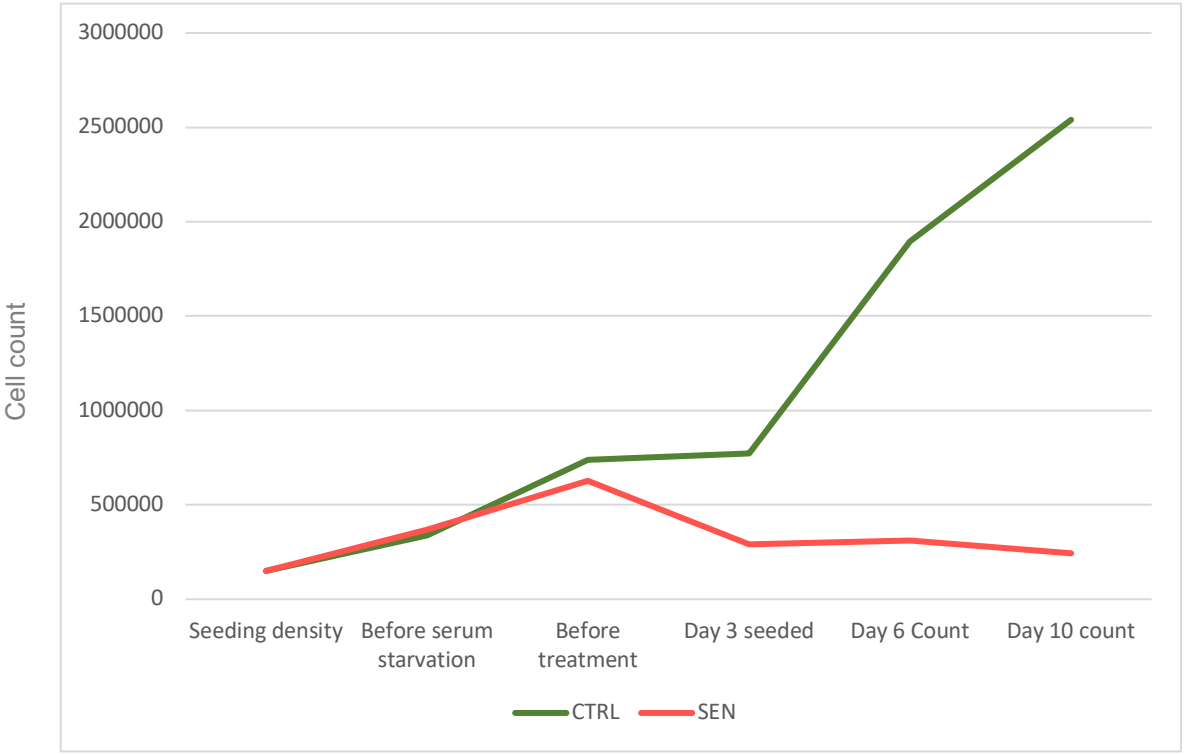

Figure 8: Comparison of cell proliferative capabilities between Control and Senescent cells. CTRL = Control, SEN = Senescent. CTRL cells continue to increase in cell number over the 10 days, whereas the SEN (irradiated at 15Gy)

cells start to plateau from Day 3 onwards indicating halt in cell proliferation. Note that cell numbers in SEN cultures at the end of the experimental duration are similar to the seeding densities to show no overall cell death (please see appendix for Mean ± standard deviation values) (CTRL N=2, SEN N=4).

A pilot study consisting of single biological experiments was conducted using multiple inducers of senescence and the most promising method would be taken forward to base the senescence model on. Methods tested included hydrogen peroxide treatments at 300 and 600μM. In addition to, irradiation at 10Gy, 15Gy and 10Gy x2 in which cells were irradiated twice over the 10-day protocol course. Irradiation levels were chosen using pre-existing data carried out in the field (Ye et al., 2013, Alexander et al., 2013, Imaizumi et al., 2010, Chen et al., 2007). CTRL cells showed an increase in cell number over a 10-day course in comparison to treated cells which had a much lower rate of replication (Figure 9). Since cells remained attached to the cell culture dishes in SEN and did not take up the trypan blue for counting it can be said with confidence that SEN cells were metabolically active. With H_2O_2 already an established method of senescence induction in various forms of fibroblasts all of which used different doses and treatment periods (Chen & Ames, 1994, Chen et al., 2007, Kiyoshima et al., 2012, Wang et al., 2013), the focus was on an irradiation senescent phenotype. Using this, the 15Gy dose was finalised in setting up and further characterising the model.

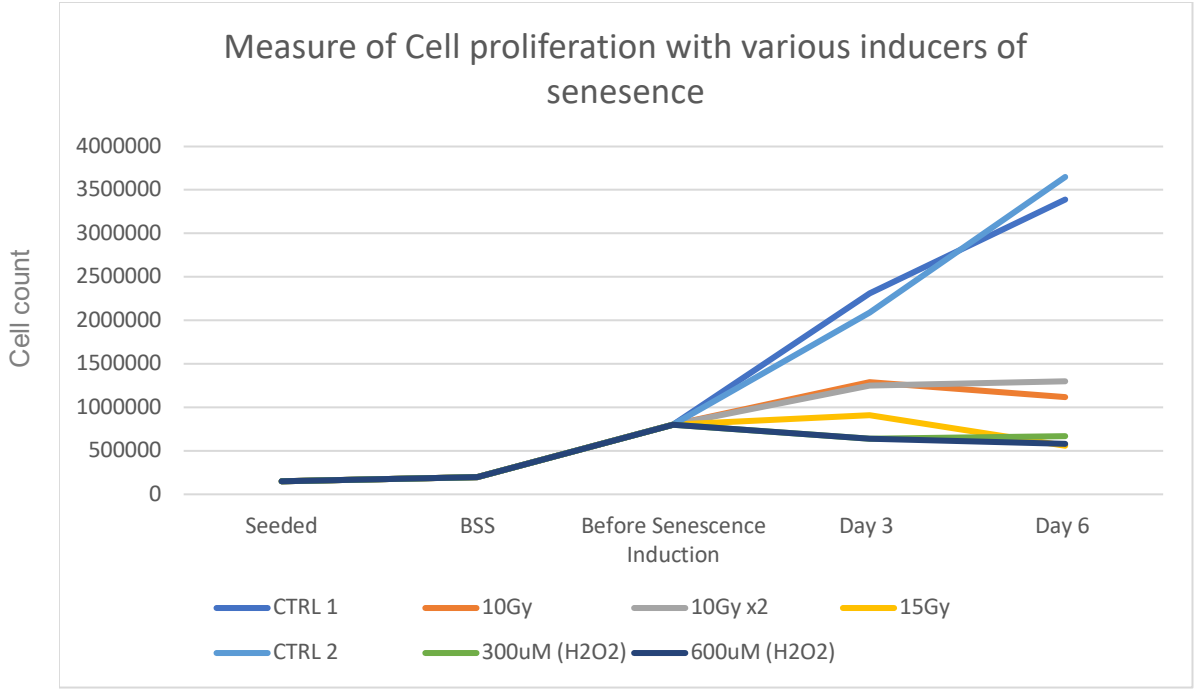

Figure 9: Measure of Cell proliferation for various senescence inducers. Irradiation at levels of 10Gy, 10Gy double dose and 15Gy were used to create a senescent phenotype by measuring cell proliferation in comparison to Controls and H_2O_2 treated (at 300uM and 600uM) cells for a baseline of cell proliferation halt. BSS = Before serum starvation. N=1 for each treatment sample. Cell proliferation was measure over a 6 day period

2.3.2 Increased expression of SA-β-Gal

SA- β-Gal staining of CTRL and SEN cells were carried out on the final day of the senescence induction protocol. Three biological repeats were carried out to ensure reliability and reproducibility. As with cell proliferation, density and confluency of cells was important, a highly confluent sample would result in higher levels of SA- β-Gal activity. It was important to ensure a single monolayer of cells was established prior to irradiation and senescence induction. Images were taken of cells following the SA- β-Gal blue staining and then cells were stained with Nuclear Fast Red stain to image the outline of individual cells which gave a qualitative indication of cell size and shape and to provide ease of counting for a quantitative measure (Figure 10). SEN cells show a clear increase

in cell and nuclear size compared to CTRL cells distinctive of the senescent phenotype. The number of cells, stained vs unstained, was counted and used to calculate percentage of β-Gal cells to provide a quantitative value (Figure 11). Statistical analysis in the form of a paired T-Test (following an F-test which confirmed unequal variance between samples) was calculated to attain a P-value of 0.039 at a 5% significance level (full analyses can be found in Appendix A) indicating there is a significant difference between percentage of SA- β-Gal positive stained cells in SEN compared to CTRL.

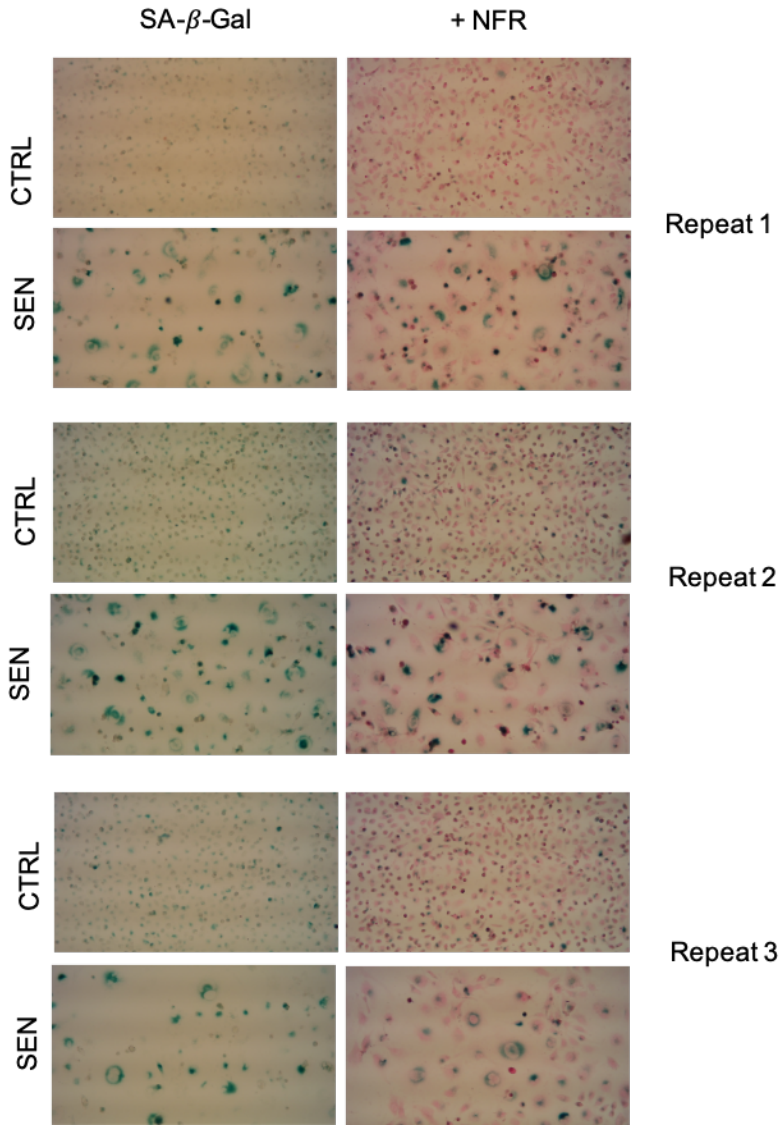

Figure 10: SA- β-Gal staining of CTRL and SEN cells. All images taken at 100x magnification. Changes in cell morphology is distinctly clear between CTRL and SEN cells with SEN cells showing a larger phenotype along with an increased Blue staining for SA- β -Gal. Nuclear Fast Red (NFR) stain provides a pink coloring to the cytoplasm of an individual cell. All cells were counted double blind, by hand. Images were not enhanced and were as the original taken on the microscope camera. N=3 for each sample group.

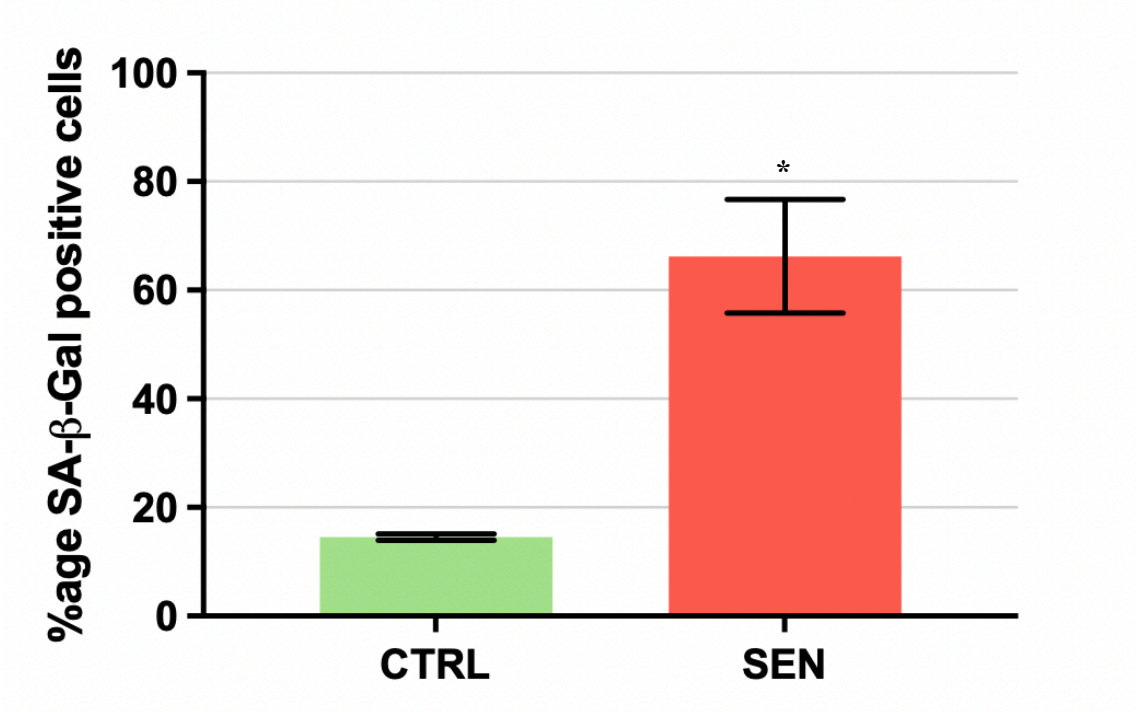

Figure 11: Percentage of SA- β -Gal positive cells for the characterisation of CTRL and SEN cells following irradiation induced senescence. SA- β – Gal positive cells were counted against the total number of cells in both CTRL and SEN samples to provide a quantitative measure of Beta-galactosidase activity. A total of 1070 CTRL and 307 SEN cells were counted across three repeats to obtain the percentages displayed, smaller bars represent standard error of mean. * represents a p-value (0.039) obtained that was less than 0.05 (5% significance level) indicating a significant difference between CTRL and SEN SA- β-Gal staining. N=3 for each sample group.

2.3.3 Cell cycle analysis using PI

Cell cycle analysis was carried out using Flow cytometry in order to obtain an assessment of the distribution of cell size and cell cycle status. Following serum starvation of cells prior to senescence induction it was expected for majority of CTRL cells to be in the same cell cycle phase (See Appendix A). Day 10 CTRL

cell cycle analysis shows 83% of cells in G1 phase, whereas SEN cell cycle analysis shows a shift towards G2 phase and sub-G1. (Figure 12A & 12B) Cell size and granularity can be determined observing the forward-side scatter plot (Figure 12C & 12D) which indicate SEN cells to be larger and more complex compared to CTRL cells. Biological repeats were conducted using 3 samples for each condition (please see appendix A for additional repeat data). Figure 13 shows the shift in numbers of cells from the different phases of the cell cycle between CTRL and SEN cells. A loss of cells in G1 is seen in SEN cells which are driven into G2 and Sub-G1.

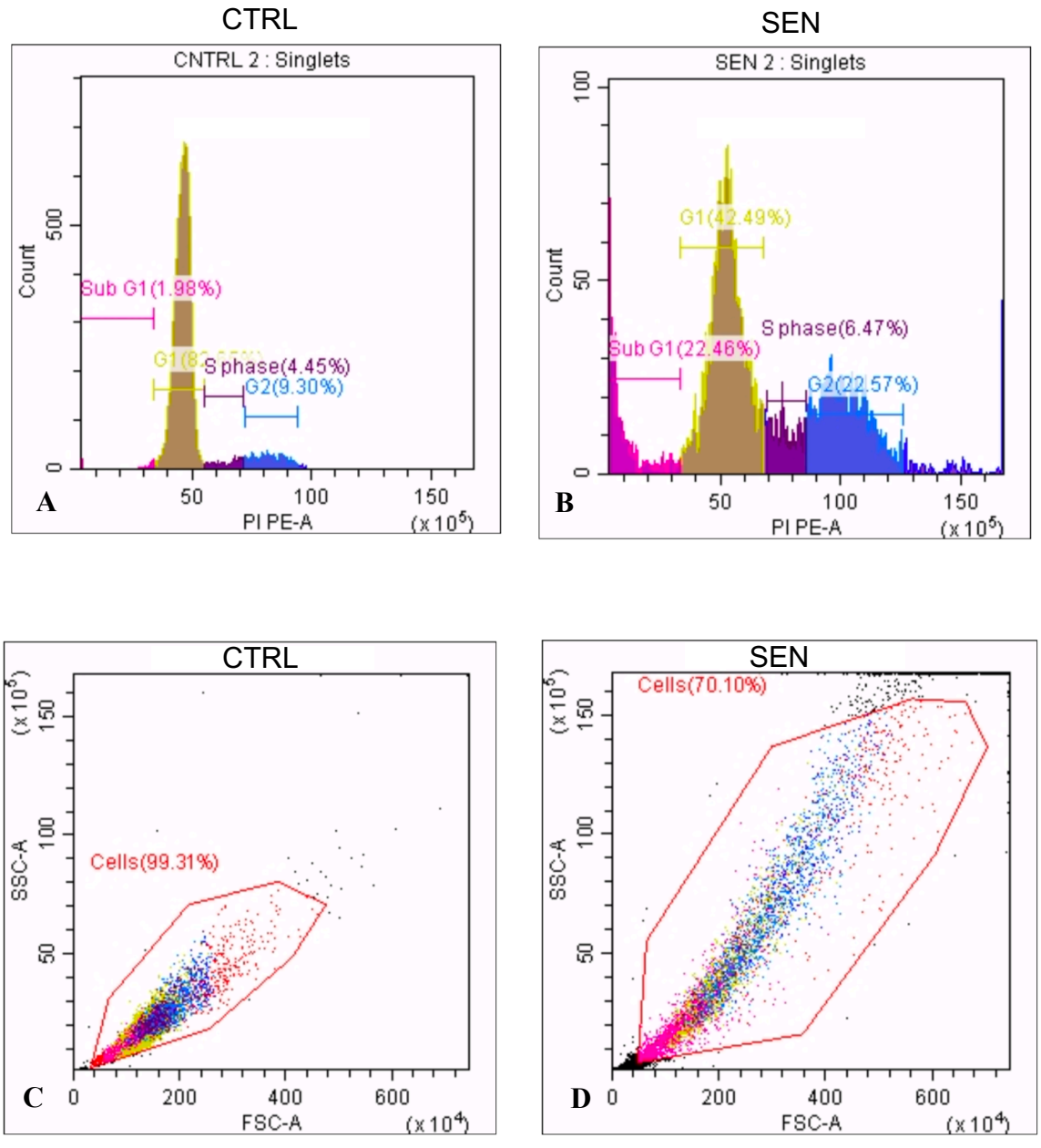

Figure 12: Propidium Iodide staining of CTRL and SEN cells for cell cycle analysis. (A) CTRL cell cycle analysis. (B) SEN cell cycle analysis (C) CTRL forward-side scatter plot shows the size of cells (D) SEN forward-side scatter plot. Experiments were replicated three times with biological and technical repeats. 10,000 cells were analysed for each sample and condition.

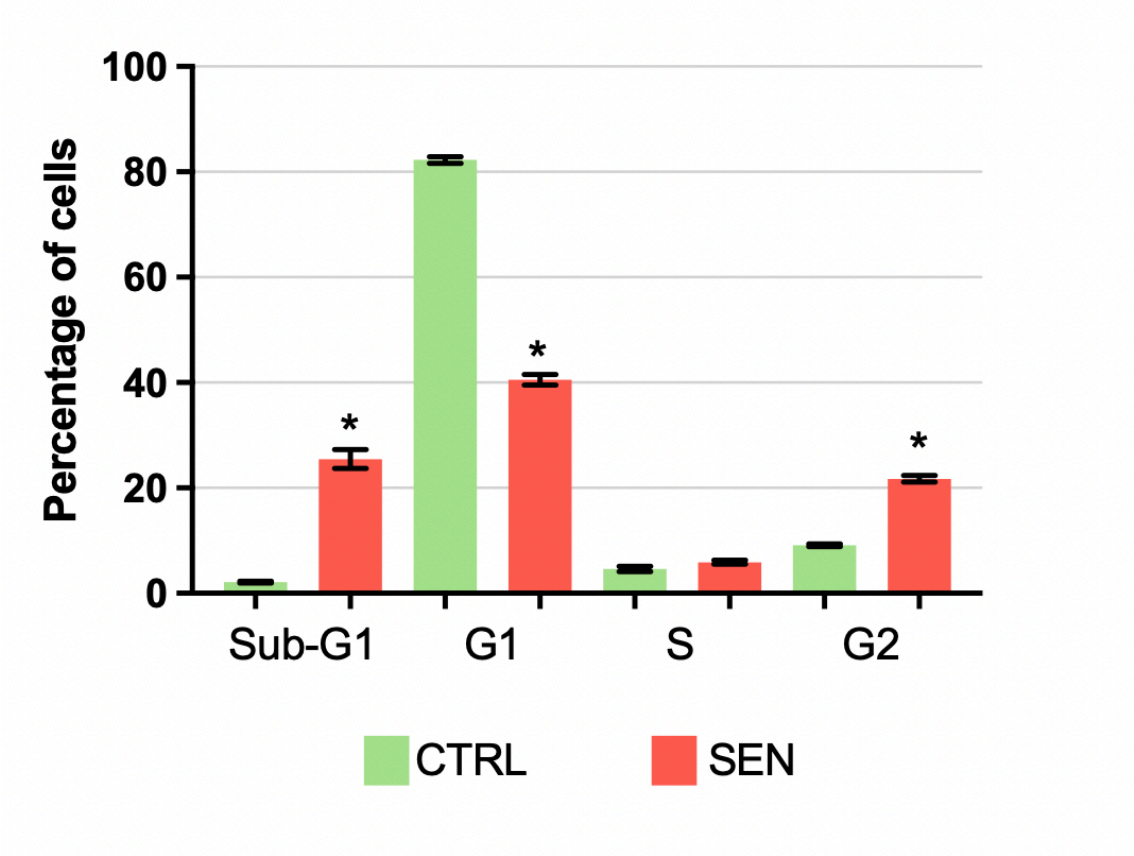

Figure 13: Graph to show the percentage of cells in each phase of the cell cycle in CTRL and SEN cells. These values were taken by averaging three repeats. Smaller bars represent standard errors of mean. T-test statistical analysis: * represents p-values less than 0.05 indicating a significant difference between CTRL and SEN (full analyses can be found in Appendix A).

2.3.4 Increased expression of p21

Cell cycle arrest was determined by the increase of cell cycle arrest proteins, specifically p21 (Figure 14). Loading was normalized to equal amounts of protein using Pierce assay or to the equal number of cells lysed in the protein extraction step for both conditions. 940,000 cells for each condition were lysed and

analysed for the presence of p21. Both blots show an increase in p21 expression in SEN cells compared to CTRL in keeping with an increase in cell cycle arrest.

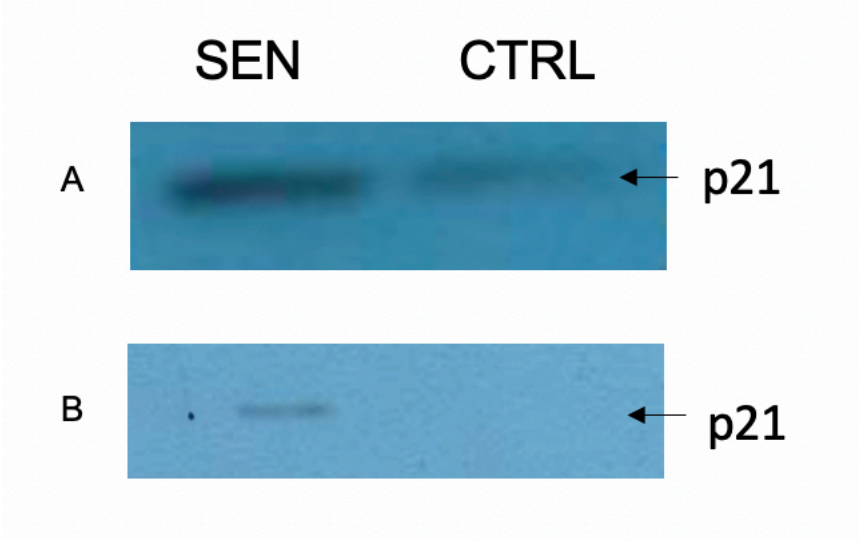

Figure 14: Western Blot for the identification of p21 protein measured at ~21kDa in CTRL and SEN cells. (A) Loading normalized to equal amounts of protein using Pierce assay. (B) Loading normalized to equal number of cells (940,000) lysed in protein extraction step. SEN cells were treated with 15Gy irradiation and cultured over a 10 day period. CTRL cells were not subjected to irradiation but were kept in the same conditions and cultured over a 10 day period. CTRL, N=2. SEN, N=2. Signal was not quantified due to a visually recognized difference in the presence of p21 in samples in both blots. The experiment was carried out twice, once with loading being normalized to equal protein amounts and again with protein harvested from 940,000 cells.

2.3.5 Increased expression of Matrix Metalloproteinase activities

Gelatin zymography was carried out to pursue the hypothesis that establishment of a senescence model would result in the presence of the SASP. The SASP contains matrix metalloproteinases which can be detected using this technique. The SDS-PAGE Gel contains gelatin, which in the presence of metalloproteinases will become digested through gelatinase of the metalloproteinases, resulting in a clear/white band against the blue stained background. CTRL and SEN cell culture media was collected and analysed

through gelatin zymography for SASP activity (Figure 15). An increased level of metalloproteinase activities is expected in senescent cells and is clearly observed with the digestion band for SEN at around 65kDa being visually thicker than CTRL, indicating a greater amount of MMP activity. This sized band correlates with the size of an isoform of the mouse MMP-2 protein at 65kDa (UniProt MMP-2, 2020). This particular metalloproteinase has been shown to stimulate cell motility when secreted in the SASP (Coppe et al., 2010).

Figure 15: Gelatin Zymography. CTRL and SEN cell culture media was tested for the expression of MMPs through gelatin zymography. SEN cells show a heavily digested band compared to CTRL indicating the presence of SASP in senescent cells. CTRL, N=1. SEN, N=1. Unable to carry out repetition due to lab closures as part of COVID-19 Lockdown. The output desired from the gelatin zymography was a binary answer in terms of if one sample shows greater MMP signal than the other therefore signal quantification was not considered as result was clear. If repetitions had been carried out, zymograms would have undergone signal quantification through densitometry for total data analysis.

2.3.6 Changes in Cell morphology

So far, the experiments have shown typical features of senescence in the irradiation induced condition. With the senescent phenotypes most distinctive

features being changes in morphology, experiments were set up to investigate changes in cell size and shape.

2.3.6.1 Light microscopy imaging

Over the course of the 10-day protocol, light microscopy images were taken on Day 3 and Day 10 to document changes to cell size, shape and confluency of fibroblasts. CTRL cells were seen to become fully confluent by day 10 maintaining original size and shape whereas SEN cells by Day 10 had little change in proliferation and showed a larger increase in size and a distinct flatness compared to CTRL cells (Figure 16).

CTRL: Day 3 CTRL: Day 10

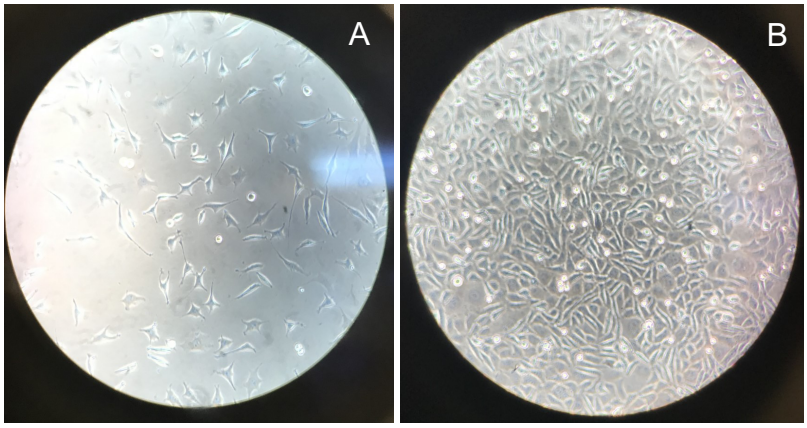

SEN: Day 3 SEN: Day 10

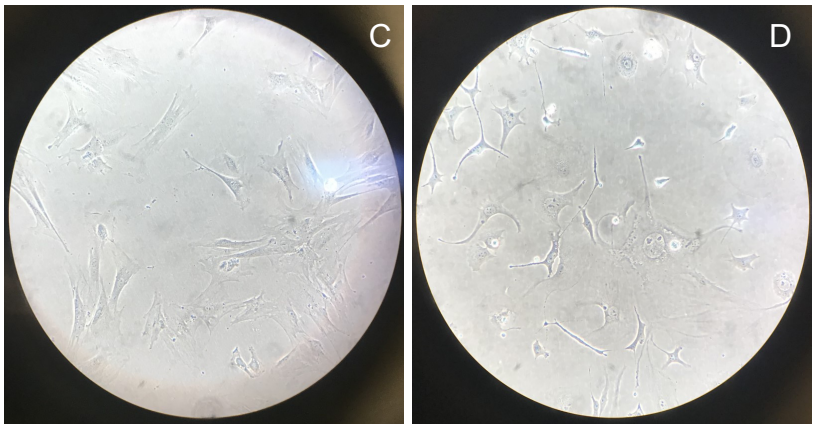

Figure 16: Light microscopy imaging of CTRL and SEN cells. (A) CTRL cells on Day 3 of the senescence induction protocol, show the original cellular morphology of fibroblasts. (B) CTRL cells on Day 10 show an increase in cell number and confluency. This is in contrast to (C) SEN on Day 3 and (D) SEN on Day 10 which shows fewer cells but with a larger, flatter morphology distinctive of the senescent phenotype. Images were taken at 10X magnification.

2.3.6.2 Immunofluorescence microscopy imaging

Immunofluorescence imaging of the nucleus of CTRL and SEN cells using DAPI (Figure 17) allowed for clear visualisation of nuclear shape and size. With the same magnification it can be clearly seen that SEN cell nuclei were much bigger in size along with more intense areas of staining which may represent senescence associated heterochromatin foci (SAHFs) distinctive to senescent cells.

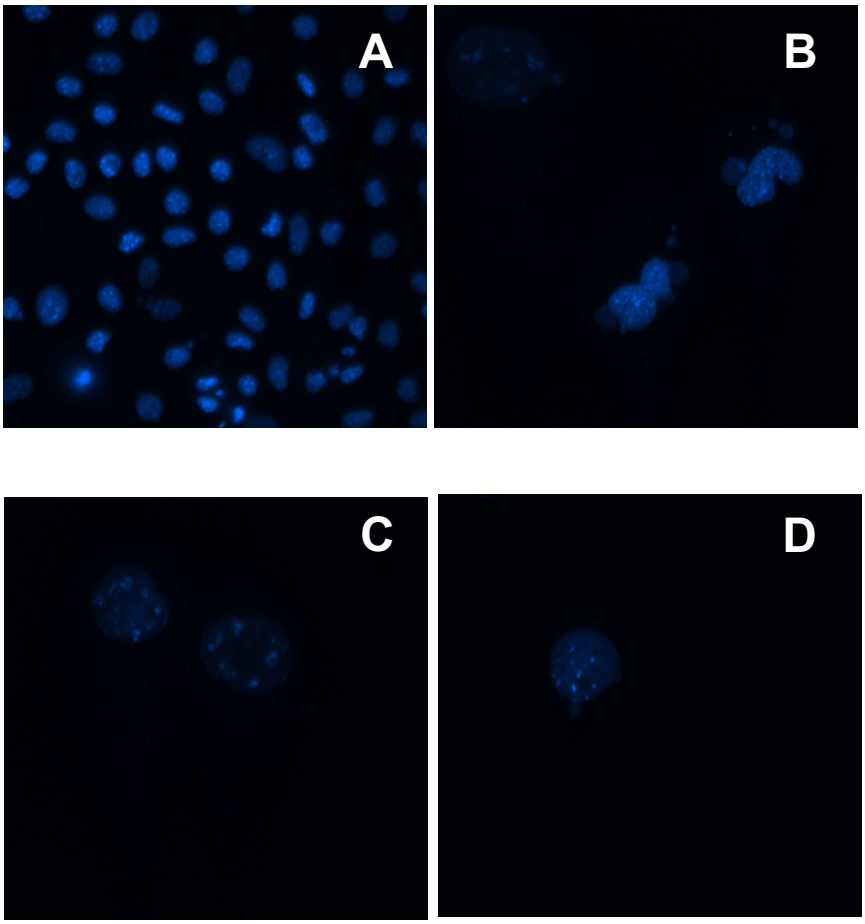

Figure 17: Immunofluorescence imaging of CTRL and SEN cells. (A) shows DAPI staining of CTRL cells, (B, C, D) show DAPI staining of SEN cells. SEN show an increase in nucleus size. All images taken at the same magnification at 40X.

2.3.7 SEM and TEM analysis

2.3.7.1 Scanning electron microscopy analysis

Surface imaging of CTRL and SEN cells using SEM analysis allowed for the visualisation of the size and shape. All magnifications show clear differences in size with CTRL cells being smaller, raised and confluent in sample images. Whereas SEN cells exhibit a much flatter morphology and an evidently large increase in size (Figure 18).

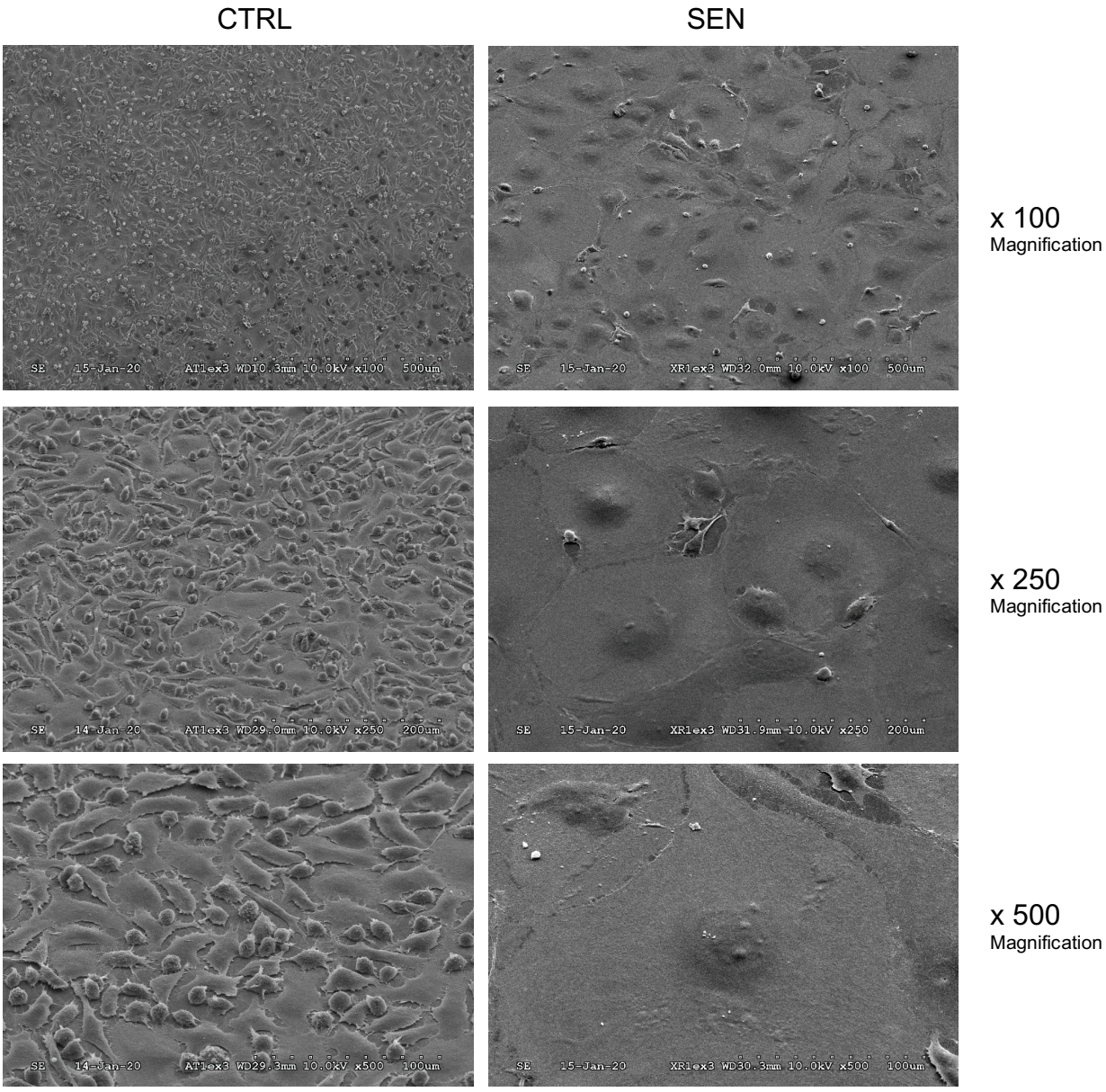

Figure 18: Panel of images of CTRL and SEN cell of SEM analysis.
Images indicate changes in morphology specifically in cell size and shape. Magnifications at which images were taken include x100, x 250, x500. CTRL, N=1. SEN, N=1.

2.3.7.2 Transmission electron microscopy analysis

TEM analysis of CTRL and SEN cells (Figure 19) highlighted key differences between the internal structures of the two phenotypes. These differences include a change in nuclear membrane integrity. CTRL cells show a complete nuclear membrane whereas SEN cells show blebbing indicating a loss of Lamin proteins (Figure 19- (1) & 19- (2)). The equal dispersion of heterochromatin and euchromatin is evident in the CTRL cells, whereas SEN cells show exclusively heterochromatin (Figure 19- (3)). Mitochondria can be seen in both conditions (Figure 19- (4) & 19- (5), Figure 19- (10) & 19- (11)), with changes in density and cristae formation evident. The changes in cell shape can be seen with SEN cells showing a flatter cross-section compared to the CTRL, (Figure 19- (6) & 19- (7)). Lysosomal SA- β-Gal activity is known to be increased in senescence, in line with this an increase in circular structures (Figure 19- (8) & 19- (9)) can be seen in SEN cells which may represent an increase in senescence associated lysosomes.

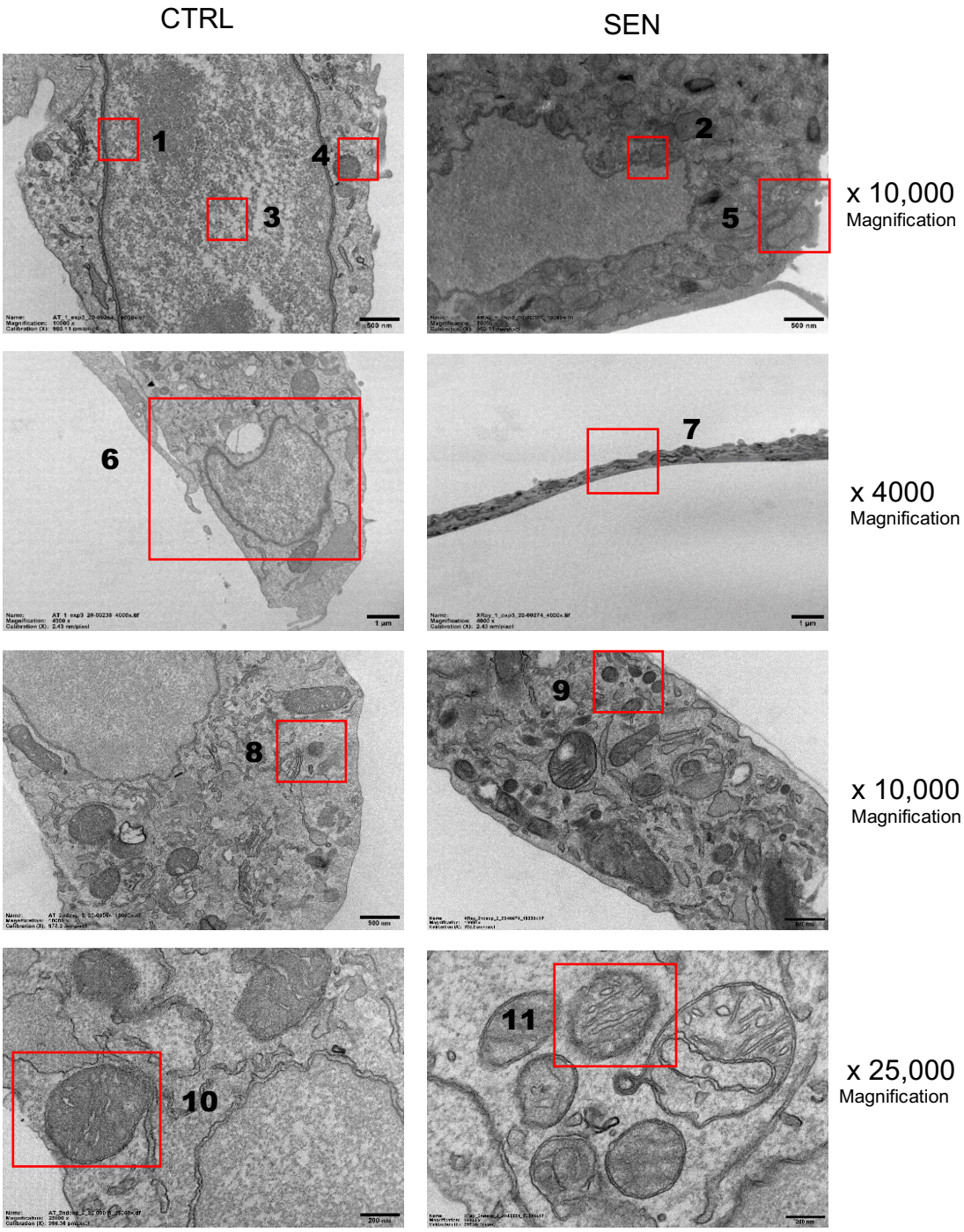

Figure 19: Panel of images of CTRL and SEN cells of TEM analysis. Areas outlined in red boxes highlight the following feature: (1) Intact nuclear membrane of CTRL cells. (2) Nuclear membrane blebbing in SEN cells. (3) Area of heterochromatin in CTRL cells. (4) Mitochondria in a CTRL cell. (5) Mitochondria in a SEN cell. (6) Cross-sectional depth of a CTRL cell. (7) Cross-sectional depth of a SEN cell. (8) CTRL cell lysosome. (9) SEN cell lysosomes. (10) Mitochondria in CTRL cell. (11) Mitochondria in SEN cell. Images were taken from one experiment. N=1 for CTRL and SEN. Repeats were planned however due to

COVID-19 lockdown and facilities being closed repeats were unable to be performed.

2.4 Discussion

The model devised using irradiation as an inducer of senescence in the L929 mouse fibroblast cell line met multiple criteria outlined in order to be classed as a senescence model. Evidence has been presented for cell cycle arrest using cell counts, measurement of p21 and cell cycle analysis, changes in cellular and nuclear morphology and a marker for the presence of SASP. Whilst devising this model it was important to ensure that it was capable of reproducibility, this was achieved by adhering to the same protocol include cell seeding density which had to be optimised, to ensure each experiment started with a sparse monolayer of cells and not an overconfluent sample which could adversely affect assessment of proliferation, morphology and SA-β-Gal analysis (Yang & Hu, 2005). Cells had to be managed regularly through passaging keeping media composition, temperature and CO_2 levels consistent.

Having critically analysed existing research in the literature regarding use of a control, it was found that most studies would seed a control, a certain amount of days before the end of the senescence induction protocol to achieve an almost confluent layer of control cells for comparison in analysis. This would mean that any effects of media, conditions, confluency and duration of experiment on cells would not be taken into account. Thus, for this study it was decided that experiments would include a true control (CTRL) which would be kept in the exact same conditions as SEN cells.

Due to the extensive morphological changes in SEN cells an increase in cytoplasmic content meant it became increasingly difficult to determine an accurate and appropriate housekeeping protein to use for normalisation during Western blot analysis. Using commonly available housekeeping proteins as controls such as alpha or beta-tubulin, Beta-2-microglobulin were excluded, largely due to the fact that changes in cell size may inadvertently affect the levels of these proteins leading to cell cytoplasm dilution (Neurohr et al., 2019) It was

concluded that protein content of lysed cells would be measured and normalised so that each Western blot sample would contain equal amounts of total protein and in equal cell numbers in order to determine a true proportion of p21 present in cells.

2.4.1 Cease of cell proliferation

A key characteristic of the senescent phenotype is the loss of cell proliferative capabilities. Cell counting in Figure 8 shows the difference in the replication of cells between CTRL and SEN. After the split on Day 3, the SEN cells show a plateau in cell number whereas CTRL cells continue to replicate. It was important to monitor the cell number over the full senescent cell model protocol to ensure that a halt in cell cycle arrest was being established. Using a cell counting technique has proven to be the best way to measure cell proliferation from its use by Leonard Hayflick in the original paper detailing the discovery of senescence (Hayflick and Moorhead, 1951). Since then, other forms of measuring cell proliferation have come into existence such as colorimetric based proliferation assays based on MTT activity, however this assay can be affected by changes to metabolic related mitochondrial activity in senescence (Mirzayans et al., 2017), therefore it is not a suitable assay for measuring proliferation in this setting or EdU staining (Salic & Mitchinson, 2008) to investigate DNA synthesis during replication, which has clear advantages over BrdU staining in terms of sensitivity, time and sample preservation and could be used to confirm cell count data in future.

Proteins that directly affect cell proliferation through cell cycle mechanics are also used to investigate cell cycle arrest. Cyclin dependent kinase inhibitors such as p21, a key cell cycle regulator, are known to be upregulated in senescence. This is illustrated in the SEN model in this study where Western blot analysis of p21 expression is increased in SEN compared to CTRL (Figure 14). Other models have also incorporated the investigation of p21 and other cell cycle arrest proteins such as p16, p53 by studies that generated hydrogen peroxide induced senescence in mouse gingival fibroblasts to find an increase in p21 and p53 in senescent cell samples (Kiyoshima et al 2012).

Cell cycle analysis was also investigated. With little evidence existing as to the cell cycle phases of senescent cells particularly in the model used, the results collected would set a baseline for future experiments. Cells were first synchronised through a 24-hour serum starvation period to encourage cells to enter the cell cycle in the same phase (Chen et al., 2012). The analysis shows that compared to control cells where the majority of cells are in the G1 phase, the majority of senescent cells shift into a G2 phase as a result of induction of SIPS following X-ray irradiation, this is supported by existing literature (Mao et al., 2012, Gire & Dulic, 2015). There is also an increase in a Sub-G1 population in the SEN cells. According to Studencka & Schaber (Studencka & Schaber, 2017) irradiation induced senescence results in a controlled cleavage of DNA pushing cells into deep senescence, accompanied by an increased SA-β-Gal activity which may account for some cells in SEN showing an intense blue colour compared to others in the sample (Figure 10).

2.4.2 Changes in cell morphology

The senescent phenotype is characterised by the distinctive change in morphology specifically the enlargement and flattening of the cell. Light microscopy, SEM and TEM analysis of SEN cells shows that the cell senescence model exhibited an increase in size and flattening. These characteristics are supported by existing literature (Herranz & Gill, 2018) detailing the evident changes in size and shape of senescent cells.

Flow cytometry analysis of the cells allowed for a measure of the size and complexity of the cells in the SEN model in comparison to CTRL cells. The forward and side scatter plots show an increase in cell size and granularity for SEN cells in relation to the plots for CTRL cells, supporting the evident morphological changes observed in the senescent phenotype.

With these changes in morphology being pertinent to characterising the model, using a number of different techniques all showing the same results to the shape and size change highlights the reproducibility and robustness of the model.

2.4.3 Nuclear changes

Immunofluorescence staining and TEM analysis highlighted changes in nuclear morphology. Not only is the size of the nucleus affected with enlargement but SEM images show nuclear membrane blebbing. This is commonly observed in the senescent phenotype (Shimi et al, 2011) and accredited to the loss of Lamin B1 in senescent cells. This finding could further be confirmed in this model by assessing Lamin B1 expression using western blotting techniques. Senescence associated heterochromatin markers can also be identified as described by Aird & Zhang, in which a greater number of SAHFs can be seen in an oncogenic *Ras* induced senescent model using immunostaining (Aird & Zhang, 2013). Additionally, the equal dispersion of heterochromatin and euchromatin is evident in the CTRL cells, whereas SEN cells show exclusively heterochromatin.

2.4.4 Expression of SASP

One of the features of SASP is increased MMP activity. This was analysed through a Gelatin Zymography technique to show an increase in MMP activity in the conditioned media collected from SEN cells in comparison to CTRL cells.. This particular technique identifies the presence of matrix metalloproteinases known to be increased in the senescent phenotype. Several MMPs have been shown to be upregulated in the SASP. Therefore MMP detection using gelatin zymography was selected as it was a cheap and quick method to use as an indicator for presence of SASP for optimisation of experimental conditions, as opposed to measurement of different cytokines which would require a number of different more expensive ELISA kits. Instead Nanostring analysis in Chapter 4 included measurement of gene expression of a number of different SASP associated cytokines; and identified upregulation of CXCL1, IL-6, IL7, IL15, CCL2, CCL7, CCL20 and CXCL1, which could be confirmed with targeted ELISAs in future work. MMP-2 and MMP-9 have previously been shown to increase in rat achilles tenocytes with aging (Yu et al., 2013). Other components of SASP can also be identified using multiple techniques such as focusing on specific components like IL-6, a cytokine shown to be increased in cell culture medium of

senescent cells. Various screening methods exist to identify these cytokines such as Enzyme-linked immunosorbent assays (ELISA) (Di et al., 2014) or cell-based biosensors (Rolt et al., 2019), which could be used to investigate the model further in future work. Via secretion of cytokines such as Il-6 or chemokines such as IL-8 the expression of SASP may stimulate epithelial to mesenchymal transition of premalignant cells *in vitro* (Ortiz-Montero et al., 2017), a characteristic of invasive tumours. This could present a potential avenue of research to further understand the mechanistic of the relationship between cancer and senescence which are closely intertwined in the theorised antagonistic pleiotropy effect.

2.4.5 Conclusion

With the aim of establishing a platform to test the effects of nutraceuticals, a reproducible irradiation induced senescent fibroblast model was produced. This model was characterised using a combination of different markers to ensure the reactive phenotype was achieved and sustained for a duration of 10 days. This model was then used in further experiments to determine the effects of plant-based compounds on senescent cells and the progression of senescence in a series of senostatic and senolytic experiments.

3 The investigation of Holy Basil, Allicin and Phytol as senolytic and senostatic therapies for aging in a SIPS (stress-induced premature senescence) L929 mouse fibroblast cell line model

3.1 Introduction

Plants and plant-based compounds have been used in medicine since ancient times. Some have led to mainstay as an inotrope (digitalis), to relieve cancer pain (morphine), as an antitussive (Codeine), an antispasmodic (atropine), an exfoliator (salicylic acid) and many more. Looking for drugs in nature could provide a source of compounds useful in treating and curing senescence associated conditions and illnesses.

Synthetic compounds with senolytic or senostatic properties can be effective, however, they are not specific, and systemic side effects can be severe and deleterious to healthy cells (Malavolta et al., 2018). Hence, a movement toward the research of natural based compounds (nutraceuticals) with potential anti-senescence properties has begun. Nutraceuticals are bioactive compounds derived from food, including plant material, with physiological benefits in the prevention or treatment of disease (Rafieian-Kopaei et al., 2014). The aim remains to find potential anti-aging therapies that are effective but exhibit minimal side effects, and some natural plant-based compounds could fit this criterion.

For the purpose of this research, nutraceuticals were chosen based on their novel use in a senescence induced model where research was previously limited or non-existent. Full background and details on each of the nutraceuticals investigated can be found in General Introduction.

Aims and Objectives

The aims of this chapter were:

- To determine the appropriate dosage of nutraceuticals to apply to cells using cytotoxicity assays on healthy L929 mouse fibroblasts cells.
- To utilise the senescent model developed and characterised in L929 mouse fibroblasts in the previous chapter to assess the effects of various nutraceuticals in a **senostatic** capacity by assessing key markers of senescence; including SA-β-Gal activity, PI FACS analysis, Western blotting for p21 expression and cell proliferation.
- To utilise the senescent model developed and characterised in L929 mouse fibroblasts in the previous chapter to assess the effects of various nutraceuticals in a **senolytic** capacity through measurement of levels of apoptosis by assessment of Bcl-2 expression, use of the TUNEL assay and Annexin V-FITC FACS analysis and cell death.

Senolytic Application of Nutraceuticals

3.2 Materials and Methods

3.2.1 Cell proliferation assay to determine Nutraceutical dose for application

Cell proliferation assay was carried according to protocol using WST-1 cell proliferation reagent (ready to use, ab155902, Abcam). Healthy L929 Fibroblasts were seeded in 96-well plates at a density of 5000 per well and incubated for 24 hours. Cells were then treated with various doses of the different nutraceuticals for 24 hours. The WST-1 proliferation reagent was added to each well using a multi-channel pipette at 10µl per well. Cells were returned to incubation for 4 hours and the optical density of the resultant formazan dye measured by assessing the absorbance at 450 nm using LT400 Plate reader. Each condition was performed in triplicate. Triplicates were averaged, the culture medium background was subtracted to give the amount of absorbance which was proportional to cell number. A threshold for a loss of 15% of viable cells was accepted as the maximum strength of nutraceutical applied for senolytic experiments.

3.2.2 Preparing the model for nutraceutical application

Control and Senescent cells were prepared as described in Chapter 2. Cells were treated with doses of each nutraceutical determined through cytotoxicity experiments. Nutraceuticals were applied for 24 hours, removed and replaced with cell media for 24 hours to allow for any recovery and analysed for various markers of apoptosis and cell death. Nutraceuticals were commercially sourced, and one batch used for all experiments. Holy Basil (Sigma-Aldrich Product Code: CAS 91845-35-1), Allicin, (Santa Cruz Biotechnology Product Code: CAS 539-86-6), Phytol (Sigma-Aldrich, Product No: W502200).

All nutraceuticals were diluted in autoclaved distilled water, all solubilised well to leave a clear colourless solution apart from Holy Basil which produced a clear dark brown coloured stock solution. When diluted in media the colour dissipated. Stock solutions were stored as below and working solutions were made up fresh with every treatement application. Control cells were subjected to media containing an equal amount of distllied water as per the working solutions for nutraceutical media.

	Solubility	Stability	Toxicity	Purity
Holy Basil	No data available	Stable under recommended storage conditions Stored at -18^{o}c	No data available	Pharmaceutical primary standard grade
Allicin	No data available	Stable under recommended storage conditions Stored at -80^{o}c	Toxic when in contact with skin, inhaled or swallowed	≥ 98%
Phytol	No data available	Stable under recommended storage conditions Stored at 4^{o}c	Toxic when in contact with skin	≥ 97%

Table X1: Solubility, stability, storage, toxicity and purity information for Holy Basil, Allicin and Phytol according to product safety data sheet.

3.2.3 Cell Counts

Cell counts were carried out using Trypan Blue solution. For all cell counts, the media was taken off and saved (for the presence of any detached dead cells). Cells were trypsinised, centrifuged at 300rpm for 5 minutes. And resuspended in 1ml of previously saved media. 20µl of the cell suspension was mixed in equal parts with trypan blue. This mixture was loaded on to a cell haemocytometer and viewed under the microscope for counting. Counts were performed for live and dead cells present in the haemocytometer grid.

3.2.4 Annexin V - FITC detection

Cells were scraped with a plastic cell scraper and centrifuged. Cells were re-suspended in binding buffer and Annexin V-FITC and propidium iodide. Protocol was followed according the Annexin V-FITC apoptosis detection kit (ab14085) (abcam). Annexin V-FITC binding was analysed using flow cytometry (Ex = 488nm; Em = 530nm) using FITC signal detector and PI staining by the PE (phycoerythrin emission) signal detector. 2 repeats of the experiment were carried out and averaged for data presentation.

3.2.5 TUNEL Assay

Cells were analysed using the TUNEL Assay Kit – HRP-DAB (ab206386) (abcam). Slides were prepared using single cell suspensions.

1. Cells were fixed in 4% formaldehyde and 80% ethanol, immobilised on to glass slides and allowed to air dry
2. Slides were rehydrated using 1x TBS
3. Specimen was permeabilised using Proteinase K in 10mM Tris pH 8
4. Specimens were quenched to inactivate endogenous peroxidases using hydrogen peroxide in methanol. Slides were rehydrated in 1X TBS
5. Specimens were subjected to equilibration using tdT Equilibration buffer to prepare for labelling

6. Working TdT labelling reaction mix (TdT Enzyme + TdT Labelling Reaction Mix) was prepared and blotted onto specimens and incubated for 1.5 hours in a humidified chamber at room temperature.
7. Labelling reaction was terminated using stop buffer following 1x TBS slide immersion
8. Specimens were incubated with blocking buffer
9. Conjugate solution was prepared and applied to each of the specimens, incubated in a humidified chamber for 30 mins at room temperature
10. Specimens were incubated with DAB solution, incubated at room temperature for 15 minutes and then rinsed with water
11. Specimens were counterstained with Methyl green counterstain for 1-3 minutes at room temperature, immersed in 100% ethanol repeatedly.
12. Slides were immersed in 100% xylene repeatedly.
13. Glass coverslips were mounted using DPX over the specimen and viewed under light microscope.
14. Cells were scored according to Figure 22, by 2 independent scorers.

3.2.6 Western Blotting for Bcl-2

Western blot was performed as in Chapter 2 Section 2.2.10.

Antibody	Dilution	Provider
Primary Antibody	1:1000	Anti Bcl-2 (St Johns Laboratory)
Secondary Antibody	1:3000	Swine Anti Rabbit HRP Conjugated (DAKO)

Table 5: List of Antibodies used for Western blotting.

3.3 Results

3.3.1 Determining doses for Nutraceutical application

In order to assess the effect of these nutraceuticals in a senolytic capacity it was important to determine an appropriate dose that would not cause substantial death of healthy cells i.e less than 15% threshold outlined in the methods. A dose response assay was set up using the WST-1 assay to measure the percentage of viable cells following nutraceutical application. The assay was carried out in triplicates and averaged and repeated over 2 different biological duplicates (Table 6).

Phytol		Holy Basil		Allicin	
Concentration (µM)	Percentage of viable cells	Concentration (µg/ml)	Percentage of viable cells	Concentration (µM)	Percentage of viable cells
0	100	0	100	0	100
1	99.9	12.5	111.2	5	87.7
5	88.6	25	98.9	10	74.5
10	87.7	50	101.3	15	64.7
20	95.6	100	91.4	30	35.6
Concentration (µM)	Percentage of viable cells	Concentration (µg/ml)	Percentage of viable cells		
0	100	0	100	Concentration (µM)	Percentage of viable cells
1	102.9	50	114.4	0	100
5	88.7	75	102.9	5	86.3
10	79.4	100	89.1	10	61.0

Table 6: WST-1 assay measuring percentage of viable cells following Holy Basil, Allicin, Phytol application. Assay was performed in two biological repeats, each does was tested in triplicates and averaged. Doses and results highlighted in colours (purple – phytol, green – Holy Basil, Blue – allicin) shows the final suitable doses chosen for application.

Nutraceutical	**Percentage viable cells (Mean ± Standard Deviation)**
Holy Basil	88.7 ± 0.1
Allicin	90.3 ± 1.6
Phytol	87.0 ± 1.0

Table 7: Mean ± Standard deviation of final doses chosen for application.

Phytol was applied to the L929 fibroblast cells at concentrations between 0-20μM based on concentrations used in investigations in human keratinocytes (Jeong, 2018). The optimal dose for application was considered to be 5 μM with which there was an 11.3 ± 0.1 % loss of viable cells (mean ± standard deviation). For Holy Basil the optimal dose for application was considered to be 100 μg/ml with which there was a 9.7 ± 1.6% loss of viable cells (mean ± standard deviation). For Allicin the optimal dose for application was considered to be 5 μM with which there was a 13.0 ± 1 % loss of viable cells (mean ± standard deviation).

3.3.2 Effect of nutraceuticals on cell counts

Cell counts were assessed in SEN versus CTRL cells to determine the amount of cell loss that occurred following application of nutraceutical treatment in a senolytic capacity. Compounds were added to cell culture media on Day 10 for 24 hours, removed and replaced with fresh culture media without treatment on Day 11 and allowed for recovery for 24 hours. Cell counts were taken at each stage as shown in Table 8. Changes in live and dead cell numbers are illustrated in Figure 20.

	Day 3	Day 10 (Senolytic added)		Day 11 (Senolytic removed)		Day 12 (recovered)	
	Seeded	Live	Dead	Live	Dead	Live	Dead
CTRL	250000	660000	0	800000	0	2090000	0
CTRL + HB	250000	660000	0	1100000	70000	2070000	40000
CTRL + ALL	250000	760000	0	1140000	20000	2600000	20000
CTRL + PHY	250000	850000	0	1090000	0	2910000	0
SEN	10000	20000	0	50000	30000	30000	20000
SEN + HB	10000	30000	0	90000	50000	20000	20000
SEN +ALL	10000	30000	0	40000	30000	30000	20000
SEN + PHY	10000	30000	0	50000	0	20000	0

Table 8: Cell counts for Senolytic application of nutraceuticals over an 11-day period. Cell counts were performed on Day 3, 10, 11 & 12 with the potential senolytic treatments (1 day treatment of cells using Holy basil (100ug/ml), Allicin (5uM) and Phytol (5uM)) being applied on Day 10 and removed on Day 11. Each count was taken in replicates and averaged.

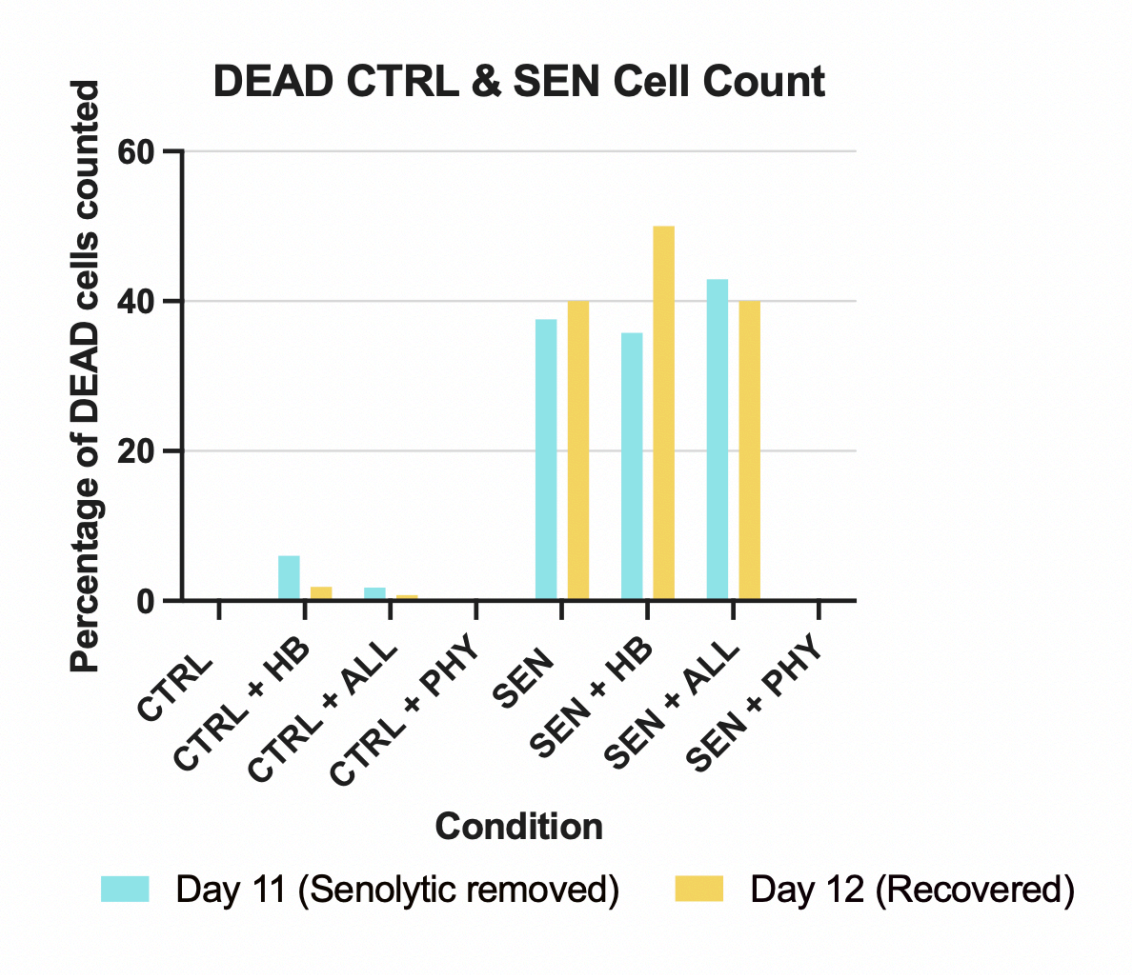

Figure 20: Percentage of DEAD CTRL and SEN Cells out of Total cells counted following senolytic application of nutraceuticals. Counts were performed on Days 10, 11, 12 when the senolytic treatments (Holy Basil - HB, Allicin - ALL and Phytol - PHY) were added, removed and cells allowed to recover over a 24-hour period.

As shown in Figure 20, with the addition of Holy Basil (6.0%) and Allicin (1.7%) the percentage of dead cells counted in the CTRL condition increased compared to baseline CTRL (0%) in line with the cytotoxicity seen when determining the doses of nutraceuticals to use. However, phytol treatment (0%) shows no dead CTRL cells. In support of the data in chapter 2, as expected in the senescence model there was an increase in the proportion of dead cells (37.5%) in untreated SEN cells compared to CTRL cells. The addition of HB to SEN cells shows a slight decrease (35.7%) in percentage of dead cells whereas Allicin (42.9%) treatment shows an increase in percentage of dead cells compared to baseline SEN (37.5%). With Phytol (0%) treatment no DEAD SEN cells are identified. This could be due to cells being at a more advanced stage of apoptosis, such that they have disintegrated and are thus undetectable. This is supported by there being a slight increase in apoptotic cells detected by the more sensitive Annexin-V FITC assay in the phytol treated SEN cells compared to SEN cells (see Figure 21C). This could be further assessed using Lactate Dehydrogenase (LDH) assay to detect LDH levels in the cell supernatants.

After 24-hour recovery

The removal of HB (50%) shows an increase in percentage of DEAD SEN cells compared to baseline SEN (40%), suggesting it may still have continued senolytic effect. There was no change in percentage of DEAD SEN cells following the removal of Allicin treatment (40%). There was no cell death in phytol added CTRL cells. The removal of treatment from SEN showed no change in percentage of dead cells for Allicin suggesting the treatment is only effective during application. Phytol removal has no effect on the number of dead cells detected, subject to the same limitations outlined above.

3.3.3 Annexin V-FITC detection

Annexin V-FITC detection through flow cytometry analysis shows minimal cell death in all CTRL samples (Figure 21) with a slight increase in apoptotic cells treated with Allicin indicating cell sensitivity. This can be attributed to the loss of cells due to toxicity of nutraceuticals treatments as established when determining dosage amounts.

Treatment of SEN cells (Figure 21) show an increase in the percentage of apoptotic cells compared to CTRL. Using SEN cells with no treatment as a baseline, a slight increase in apoptotic cells is seen in all three treatments. SEN + Phytol shows the greatest increase compared to SEN. All treatments according to Annexin V-FITC detection show a senolytic effect with SEN + HB showing an increase to 13.8 ± 4.9, SEN + Allicin showing an increase to 13.9 ± 8.03, SEN + Phytol showing an increase to 14.0 ± 6.12 compared to SEN with no treatment showing a mean percentage of apoptotic cells at 8.3 ± 1.3 (data presented as mean ± standard deviation).

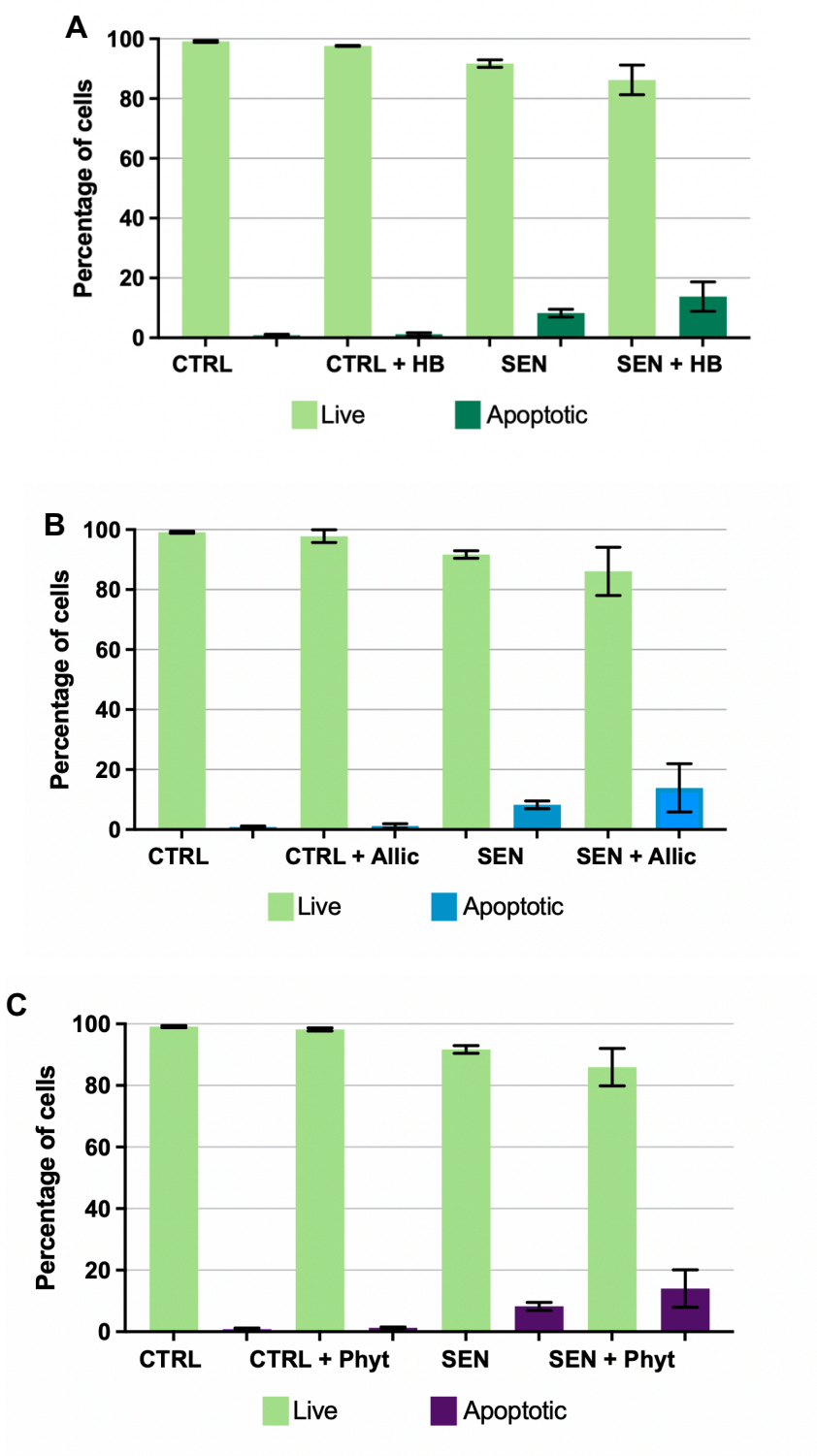

Figure 21: Flow cytometry analysis of Annexin V-FITC detection for CTRL and SEN cells. (A) CTRL and SEN cells + Holy Basil. (B) CTRL and SEN cells + Allicin. (C) CTRL and SEN cells + Phytol. Results shown are means averaged over 2 replicates and smaller bars represent standard deviation. Each experiment had a no treatment control for both CTRL and SEN cells. 1 day treatment of cells using Holy basil (100ug/ml), Allicin (5uM) and Phytol (5uM).

	Live	Apoptotic
Condition	Mean ± SD	Mean ± SD
CTRL	99.1 ± 0.33	0.9 ± 0.33
CTRL + HB	97.6 ± 0.18	2.4 ± 0.17
CTRL + Allic	97.8 ± 2.14	2.2 ± 2.14
CTRL + Phyt	98.2 ± 0.5	1.8 ± 0.49
SEN	91.7 ± 1.3	8.3 ± 1.3
SEN + HB	86.2 ± 4.9	13.8 ± 4.9
SEN + Allic	86.1 ± 8.0	13.9 ± 8.03
SEN + Phyt	86.0 ± 6.1	14.0 ± 6.12

Table 9: Mean ± SD for Live and Apoptotic cells detected using Annexin V-FITC. Mean ± standard deviation shown averaged over 2 repeats.

3.3.4 TUNEL Assay

TUNEL Assay of samples was used to compare cells with a brown deposit which labels free DNA ends, indicative of apoptosis. Apoptotic and normal cells were assessed in duplicate, counted by two independent scorers using images in Figure 22 as a baseline and averaged to give values as shown in Figure 23.

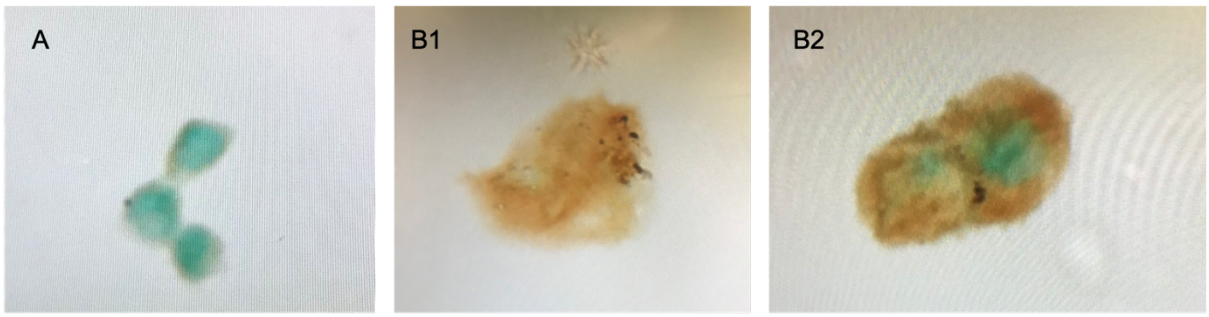

Figure 22: Baseline images of CTRL and Apoptotic cells used for scoring. (A) Shows healthy CTRL cells, exclusively blue in colour, showing no indication of apoptosis. (B1, B2) shows examples of SEN cells scored as apoptotic due to distinctive brown staining using the TUNEL assay. (All images were taken under x40 magnification using an oil immersion objective).

Compared to CTRL cells, CTRL + Allicin and CTRL + Phytol show a decrease in apoptotic cells, with CTRL + HB showing an increase in apoptotic cells. As expected, unstimulated SEN cells show an increase in apoptosis, with 18.25% of cells identified as apoptotic, compared to CTRL cells with 8.75% apoptotic. All three treatments show an increase in apoptotic cells (57.35 % apoptotic cells treated with Holy Basil, 41.55% apoptotic cells treated with Allicin, and 47.85% apoptotic cells treated with Phytol) in agreement with the Annexin V-FITC data, with the HB treatment resulting in the greatest apoptotic cell count. This indicates that according to TUNEL assay analysis HB has greater senolytic properties compared to Allicin and Phytol which show senoptosis but to a lesser extent. Results indicate that all three nutraceutical applications resulted in senolytic cell death of treated groups compared to their non-treated controls.

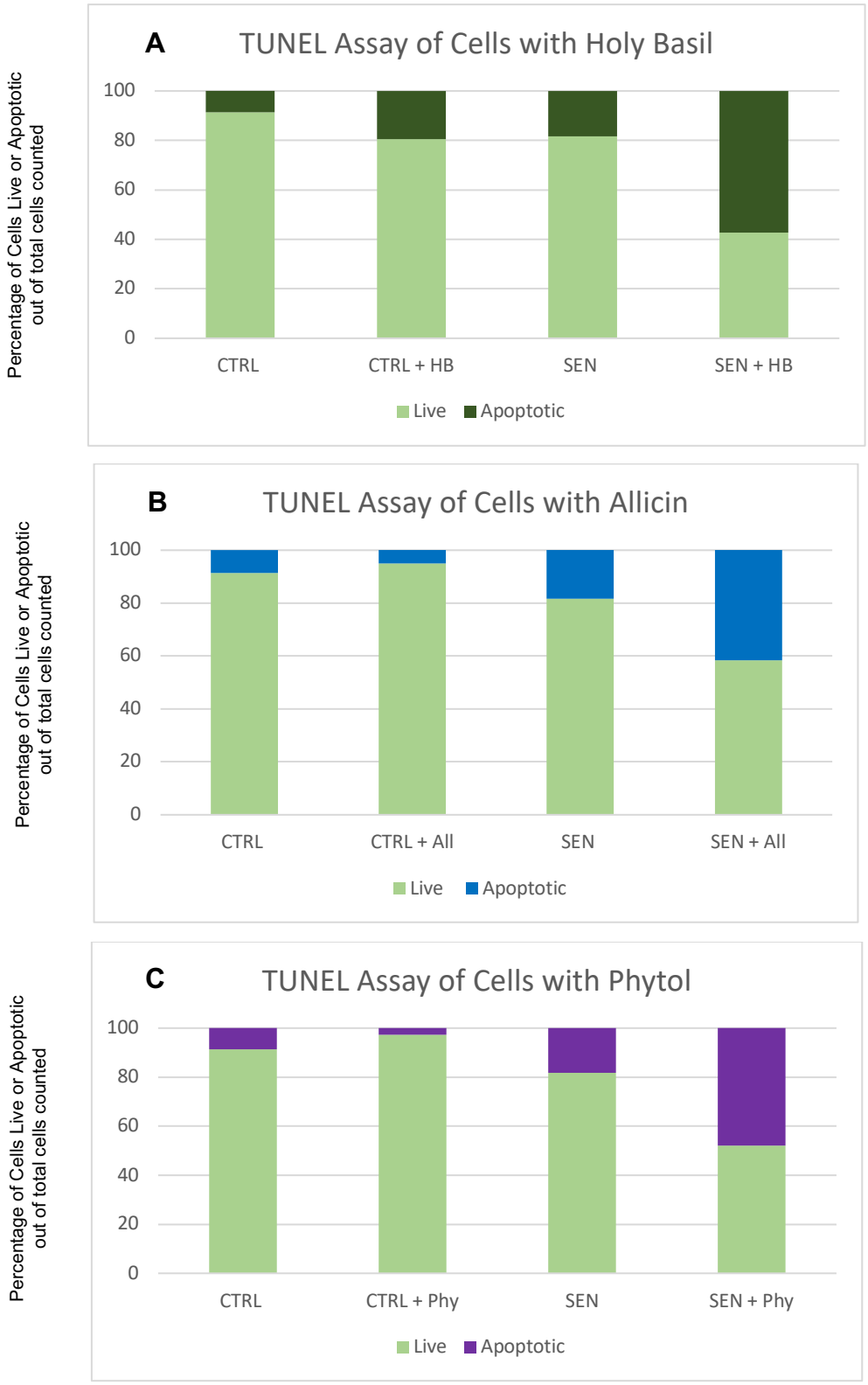

Figure 23: TUNEL Assay analysis of CTRL and SEN cells treated with various nutraceuticals. (A) CTRL and SEN + HB, (B) CTRL and SEN + Allicin, (C) CTRL and SEN + Phytol. Graphs show the percentage of cells that were counted as normal vs apoptotic. Experiments consisted of 2 repetitions, assessed by two independent scorers and averaged to calculate mean and standard deviation. 1 day treatment of cells using Holy basil (100ug/ml), Allicin (5uM) and Phytol (5uM)

	Mean ± SD	Mean ± SD
	Live	Apoptotic
CTRL	91.3 ± 0.28	8.75 ± 0.35
SEN	77.25 ± 7.57	22.75 ± 7.57
CTRL +HB	80.45 ± 6.01	19.55 ± 6.01
SEN +HB	42.65 ± 0.92	57.35 ± 0.92
CTRL +All	95.05 ± 2.33	4.95 ± 2.33
SEN+All	58.45 ± 12.94	41.55 ± 12.9
CTRL+PHY	95.8 ± 3.54	4.2 ± 3.54
SEN+PHY	52.2 ± 1.13	47.85 ± 1.13

Table 10: Mean and Standard Deviation for all samples assessed with the TUNEL assay. Experiments consisted of 2 repetitions, were assessed by two independent scorers and averaged to calculate mean and standard deviation

3.3.5 Western Blotting for Bcl-2

Western Blot analysis (Figure 24) for Bcl-2 shows levels of protein in CTRL and SEN as baseline with Bcl-2 exhibiting a stronger signal in CTRL compared to SEN indicating a lower occurrence of apoptotic activity in CTRL cells. This is evident in other studies that use Bcl-2 as an anti-apoptosis marker but these studies were carried out in cancer cells which characteristically over express Bcl-2 (Sun et al, 2015, Naseri et al., 2015). This is why it is important to take into account the CTRL cell model and how it was nurtured alongside the SEN cell model for 10 days and exhibited to the same stresses minus the treatments.

The detection of BCL-2 via Western blot in response to nutraceutical treatments shows a less abundant band for Bcl-2 with a CTRL + HB compared to CTRL with no treatment suggesting some apoptotic activity which could be attributed to the general loss of cells as a result of HB toxicity similar to when dosages of treatments were being determined using the WST-1 assay. There is a clear increase of Bcl-2 in SEN + Allicin and SEN + Phytol in comparison to SEN. However, the addition of HB to SEN cells showed no visible change in protein amount in comparison to its SEN baseline control indicating no change in apoptotic activity.

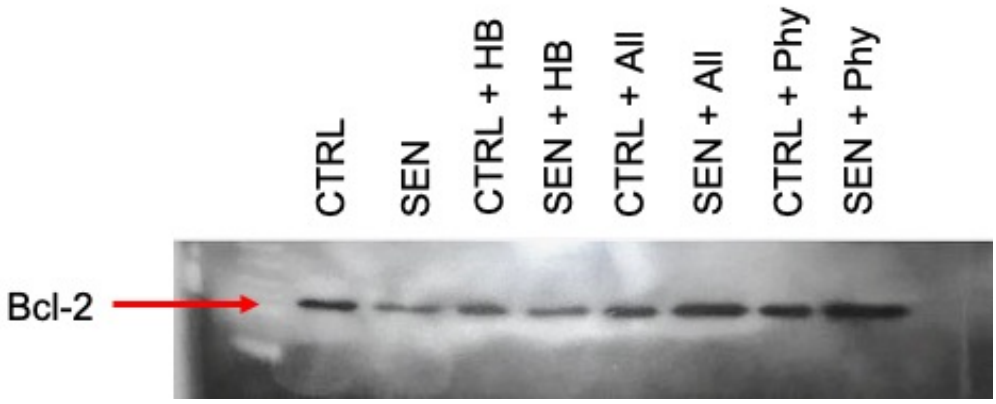

Figure 24: Western Blot analysis for Bcl-2 in mouse L929 fibroblast cell line treated with Holy Basil, Allicin and Phytol. A consistent signal is seen at a protein molecular weight of approximately ~25kDa which conforms to mouse Bcl-2 size. All samples were quantified and normalised to allow for equal loading of protein amount across all lanes. CTRL (no irradiation treatment), SEN (senescence induction with irradiation), CTRL + HB (no irradiation treatment, 24 hour Holy Basil application), SEN + HB (senescence induction with irradiation, 24 hour Holy Basil application), CTRL + All (no irradiation treatment, 24 hour Allicin application), SEN + All (senescence induction with irradiation, 24 hour Allicin application), CTRL + Phy (no irradiation treatment, 24 hour Phytol application), SEN + Phy (senescence induction with irradiation, 24 hour Phytol application). 1 day treatment of cells using Holy basil (100ug/ml), Allicin (5uM) and Phytol (5uM). N=1 for each sample.

3.4 Discussion

3.4.1 Determining an appropriate dose for treatment and associated problems

Determining an appropriate dose for senolytic application was carried out to ensure that application of the nutraceutical wouldn't cause excessive harm to normal healthy cells which were not senescent. Dose response assays were set up. The most appropriate dose was chosen according to two criteria being fulfilled. One being that approximately 15% of viable cells would be lost; the second being the percentage of viable cells remaining for chosen dose must be similar across the biological repeats. Jeong (2018) also used WST-1 assay to

determine various phytol concentrations to use in investigating the compound in cellular senescence of HaCaT keratinocytes. Determining doses for treatments can be complicated, not only is it vital to ascertain a dosage that causes minimal toxicity to cells, but exposure times also have to be taken into account. Our results only account for an exposure of 24 hours. A shorter exposure may also have an effect on the toxicity levels recorded through the WST-1 assay. Additionally, the assay required incubation for up to 4 hours following the addition of the WST-1 reactive agent which may have had an effect on proliferation results by interfering with the assay and diluting the nutraceutical concentration. Other methods of studying cell proliferation could be carried out in further studies to validate doses through simple cell counting with Trypan blue dye. Perhaps markers that indicate loss of cell membrane integrity such as components that would leak out of the cell that are contained in the cytoplasm such as Lactate dehydrogenase (LDH), which is involved in converting pyruvate to lactate (Riss et al., 2019) which can be measured through fluorescent imaging. Recently, novel methods of high throughput content screening analysis provide a combination of methods that can provide astringent results in regard to cell toxicity at different concentrations of multiple compounds. For example, Boncler et al (2017) measured three different cellular functions as part of their high content screening assay which included analysis of mitochondrial membrane potential, cell membrane integrity and nuclear membrane (Boncler et al., 2017).

3.4.2 Measuring Cell Death to determine senolytic activity of nutraceuticals

As seen in Results, various methods of measuring senolytic activity were used to ensure a nutraceutical possessed apoptosis inducing capabilities. The results highlighted that when investigating the same marker, cell death, not all assays give the same pattern of results, which is why it is essential to perform more than one technique to assess the senolytic activity of the nutraceuticals and to discuss the limitations of the methods used and potential alternatives.

3.4.2.1 Cell Counting to measure number of dead cells

Counting live and dead cells has been a method of determining cell proliferation and cell death for decades. Dyes such as Trypan blue can be used to stain for cells that have compromised cell membranes to allow for visualisation, to assess the number of dead cells present. This counting can be done manually through the use of a haemocytometer or using automated cell counter machines. This method usually provides an accurate representation of the entire sample but may not be as reliable when measuring samples with few cells. It also can be subjective of human sampling errors such as mis-counting specific cell types. This is why it was important to measure cell death using various methods of identification.

3.4.2.2 TUNEL Assay

The TUNEL assay works by labelling the free 3'-hydroxyl terminus of DNA strand breaks which can present in early and late apoptosis. Even though it is a method that is widely accessible and relatively easy to use it is a subjective method and relies on the assumption that human bias sampling be kept low for accurate and reproducible results (Mirzayans & Murray, 2020). To combat this, counts were assessed by two independent scorers, where cell type criteria was pre-determined and used as a baseline for identification. In relation to using it for apoptosis, it's important to understand the process of senescent cell death. Senoptosis, is known as uncomplete or stalled apoptosis and presents in cells that enter 'deep senescence' which exhibit reduced DNA content, and absence of SASP (Studencka & Schaber, 2017). Mirzayans & Murray (2020) highlight the importance of developing improved methods of identifying better biomarkers for apoptosis due to the prospect of anastasis which is the recovery of cells from late-stage apoptosis. This could also be the case in senescent cells which already show a resistance to apoptosis (Mirzayans & Murray, 2020). Nevertheless, it remains a widely used method of apoptosis detection in senescence research (Wang et al., 2016, Hinkal et al., 2009).

3.4.2.3 Bcl-2 Western blot

Western blot analysis for Bcl-2 showed a high intensity band in CTRL compared to SEN indicating a level of apoptosis occurring in SEN cells. This may be due to it not being in complex with other apoptotic proteins to initiate or induce the process as apoptosis doesn't occur to a great extent in healthy control cells. This is supported by existing literature that shows a subset of senescent cells undergo apoptosis (Ohshima, 2006). The Western blot shows a clear increase of Bcl-2 in SEN + Allicin and SEN + Phytol in comparison to SEN. However, the addition of HB to SEN cells showed no visible change in protein amount in comparison to its SEN baseline control indicating no change in apoptotic activity. This data does not support the Annexin V-FITC and TUNEL assays that suggest that the addition of these treatments can have a small senolytic affect. We would expect a lower level of Bcl-2 in the conditions treated with the nutraceuticals to support their potential senolytic activity. This is because Bcl-2 protein is known as an anti-apoptotic protein and acts as a cell death inhibitor. Increased expression of Bcl-2 inhibits cytochrome c release by lowering the mitochondrial membrane permeability (Makpol et al., 2012, Tzifi et al., 2012). Therefore, in the event of apoptosis we would expect lowered levels of Bcl-2 protein.

However, in relation to apoptotic markers, literature shows Bcl-2 is phosphorylated to regulate anti-apoptotic function, therefore it may have been more informative to look at the phosphorylated form (Agostinis, 2003). Bcl-2 has also been known to act as part of a mechanism with anti-oxidant properties and may be acting as part of a mechanism that is working to prevent apoptosis (Hockenbery et al., 1993, Cox & Hampton, 2007) and may be working to prevent nutraceutical induced cell death.

In addition, a reduction in Bcl-2 levels in senescence is not consistent across existing literature. Tombor et al (2003) showed that Bcl-2 was found to be increased in senescent primary fibroblast cells induced through *Ras* overexpression and Hydrogen peroxide induction (Tombor et al., 2003). Cells for Western blot analysis underwent RIPA buffer lysis, which preferentially captures

cell membrane proteins and can disrupt weak protein-protein interactions therefore any functional association of Bcl-2 to have an anti-apoptotic effect may be lost (Kale et al., 2017).

In addition, Birch & Gil (2020) recently found that the BCL-2 family inhibitor ABT-737 reduced levels of p21 in adult mice that underwent partial hepatectomy which results in a 'transient increase in p21 in a sub-population of hepatocytes' indicating the use of ABT-737 as a senostatic compound and its mechanism of action is through BCL-2 inhibition (Birch & Gil., 2020) highlighting its important in senescence.

Thus, further experiments are required to both confirm this data and to further explore the relationship between BCL-2 expression and apoptosis in the senescent cells, for example blocking BCL-2 activity in the presence of the nutraceuticals and seeing if there is any difference in levels of apoptosis or analysis of other markers of apoptosis such as BAX or Caspase-3 to assess senolytic potential of the nutraceuticals tested.

3.4.3 The senolytic potential of the nutraceuticals tested

3.4.3.1 Holy Basil

Annexin-V FITC and TUNEL assay analysis showed cell death as a result of Holy Basil application in SEN cells. Cell counts for dead cells also showed an increase in HB treated samples. Although Western blot analysis of SEN + HB shows an increased expression of Bcl-2 compared to SEN baseline, suggesting less apoptotic activity there are a number of limitations with the interpretation of this data as described earlier. Overall, the data suggests that Holy Basil could have some senolytic activity.

In support of a potential role of Holy Basil (*Ocimum sanctum*) as an anti-aging nutraceutical, Holy Basil has well-established anti-oxidant properties and it is widely marketed as an additive to cosmetic based products that boast of anti-aging effects. Studies such as Chaiyana et al (2019) investigated *Ocimum*

sanctum extracts on 3T3 fibroblast cells to find reduced inhibition of collagen and hyaluronic acid degradation, both of which play major roles in aging of the skin. They also found reduced NF-κB expression and IL-6 secretion (Chaiyana et al., 2019). This study only used the 3T3 mouse cell model to investigate protein levels such as MMP-1, 2,3 and 9 through Western blot analysis and was not specifically investigating cellular senescence. It concluded that Rosmarinic acid was found in highest of quantities in *O. sanctum* extracts and responsible for the anti-aging effects. Pandey et al (2013) investigated the effects of *O. sanctum* in *Caenorhabditis elegans*. They found that at a concentration of 1mg/mL *O. sanctum* increased the life span of *C. elegans* and exhibits thermo-protective and antioxidant properties (Pandey et al., 2013).

Considering the outcome of the senolytic experiments, further investigation of the plant-based compound is necessary across multiple senescent models at various doses and durations to ascertain its full potential as a senescence therapy.

3.4.3.2 Allicin

When applied to the SEN model for 24 hours, there was a small increase in the percentage of dead cells between SEN and SEN + Allicin indicating the treatment had a small senolytic effect. In agreement with this the Annexin V- FITC and TUNEL assay showed increased cell death on SEN samples with treatment. In agreement with Holy Basil Western blot analysis showed increased expression of Bcl-2 in response to Allicin, which is subject to the same limitations in interpretation. Thus overall, the data suggests that Allicin could potentially have modest senolytic properties. This is supported by recent studies investigating the anti-aging properties of Allicin and other garlic derivatives. Lui et al (2019) showed how Allicin attenuates frailty related to osteoporosis. F344 rats were subjected to various doses of Allicin and Vitamin D as a control that were administered intragastrically once a day for 8 months. Frailty index (FI) was assessed to find a lowered FI in the group treated with Allicin compared to the age-matched control group. Bone strength analysis showed high dose Allicin treated femurs had a significantly higher elastic and maximum load indicating greater bone strength in comparison to an age-matched control group (Lui et al., 2019).

Rosas-Gonzalez et al (2020) studied the effects of Allicin in breast cancer, specifically of cell death, senescence and senolytic activity. MCF-7 (luminal A positive) and HCC-70 (triple negative) breast cancer cells were subjected to 72-hour treatment of Allicin at 45μM and 20μM respectively. Cells were then stained for beta-galactosidase activity. Neither concentration of Allicin induced senescence in the cell types. The senolytic effect of allicin was investigated by treating senescent breast cancer cells that underwent senescence through doxorubicin (1μM) induction. These cells were then treated with 20uM and 45μM of allicin for 24 hours and assessed for cell viability using WST-1. Results showed a significant decrease in cell viability of senescent MCF-7 and HCC-70 cells treated with Allicin compared to CTRL (Rosas-Gonzalez et al., 2020).

Considering the outcome of the senolytic experiments, further investigation Allicin is necessary to determine its full senolytic properties. This would be best done across multiple cellular senescence models.

3.4.3.3 Phytol

Following phytol application there were no dead cells counted in CTRL or SEN cells. In contrast in the annexin V-FITC and TUNEL assays there was an increase in apoptotic cells in SEN cells treated with phytol compared to SEN with no treatment. Bcl-2 Western blot analysis showed increased expression of the protein suggesting lower levels of apoptosis compared to SEN with no phytol treatment. The cell count and Bcl-2 data is subject to the limitations described above. Thus, it is difficult to interpret the potential use of phytol as a senolytic. Indeed, there are very limited research studies on Phytol in relation to senescence to support this. The few that exist are focused on skin related aging. Jeong (2018) investigated the effect of Phytol on HaCaT keratinocytes prior to senescence induction. This would indicate Phytol may act in a senostatic capacity rather than senolytic. Since Jeong (2018) no further studies on Phytol have been carried out. This could be as a result of Phytol having poor solubility and low bioavailability (Sathya et al., 2017) and therefore not being suitable as a potential senescence therapy.

3.5 Conclusion

Parallel analyses of methods in this study showed that Holy Basil, Allicin and Phytol have senolytic capabilities dependent on measure of apoptosis. A definitive status for each cannot be concluded because a single measure can't be given precedence over another. As each comes with its advantages and limitations it is crucial to look at multiple markers. These markers however do not confer the same result. Therefore, further investigation into these potential senolytic compounds would be necessary to ascertain their calibre as a senescence therapy. Other factors would also need to be considered such as duration of dose, application of treatment prior or post senescence induction and if removal of application diminishes senolytic capabilities. This would require the testing of various doses in multiple senescence cell models and cell lines, ultimately if proven to be beneficial against aging be committed to in vivo mouse models to gather information on toxicity and side effects.

Senostatic Application of Nutraceuticals

3.6 Materials & Methods

Control and Senescent cells were prepared as per chapter 2.

3.6.1 Nutraceutical application

Nutraceuticals were prepared as below and applied following irradiation. Media with nutraceuticals were added from Day 1 until Day 10, with 2 media changes during the 10-day period. To minimise toxicity due to prolonged application of plant-based compounds, concentrations from the senolytic experiments were halved.

Nutraceutical	Dose
Holy Basil	50µg/ml
Allicin	2.5µM
Phytol	2.5µM

3.6.2 Measuring Cell proliferation

Cell proliferation was measured using 0.4% Trypan-Blue (Sigma, T6146) and a Neubauer haemocytometer at specified time points. Cells were harvested through gentle cell scraping and centrifuged at 300rcf for 5 minutes. Cell pellet was resuspended in 1ml of cell culture media. 15µl of this suspension was mixed with equal amount of 0.4% Trypan Blue and deposited into the glass haemocytometer. The cells were counted using a light microscope at 100x magnification. Each cell suspension was counted twice after resuspension, counts took into account the dilution factor and were averaged.

3.6.3 Senescence associated Beta-Galactosidase staining

Staining for SA-β-Gal was carried out according to protocol for senescence detection kit (abcam) (ab14085). Senescent cells express an increased level of lysosomal beta-galactosidase which can be stained for using the substrate X-Gal (5-bromo-4-chloro-3-indolyl-β-D-galactopyranoside) to obtain a blue colour of cells to indicate senescence. Stained samples were incubated overnight for at least 12 hours and then visualised under light microscope.

3.6.4 Propidium iodide analysis using Flow cytometry

For cell cycle analysis using propidium iodide, cells were scraped and harvested using centrifugation at 300 rcf for 5 minutes. Cells were washed once with PBS and fixed in cold 70% ethanol overnight at 4^{o}C. Cells were centrifuged at 600rcf for 5 minutes to remove the ethanol and washed twice in cold PBS. Cell pellets were re-suspended in 50µl of RNAse (100µg/ml) and left on ice for 20 minutes. 200µl of Propidium iodide (100µg/ml) was added to the cell suspension and

covered in foil for 10 minutes. Cell were immediately analysed on the flow cytometer Cytoflex (Beckman and Coulter).

3.6.5 Western Blotting for p21

Western blot analysis was carried out as described in Chapter 2 Section 2.2.10.

3.7 Results

3.7.1 Cell counts

CTRL and SEN cells were seeded at equal numbers of 33,333 cells per condition and cell counts were carried out following senostatic treatment (Table 11). Counts were performed on Day 10, when treatment was removed and on Day 11 following a 24-hour recovery period. Even though all cells were seeded in the same capacity the number of live and dead cells accounted for on day 10 and day 11 varied greatly (Figure 25).

	Day 0	Day 10 (Removal of Treatment)		Day 11 (Recovery)	
	Seeded	Live	Dead	Live	Dead
CTRL	33,333	1,990,000	30,000	2,410,000	50,000
CTRL+HB	33,333	1,480,000	40,000	1,820,000	70,000
CTRL+ALL	33,333	1,740,000	60,000	2,040,000	100,000
CTRL+PHY	33,333	3,080,000	50,000	3,210,000	60,000
SEN	33,333	40,000	40,000	50,000	20,000
SEN+HB	33,333	20,000	30,000	90,000	40,000
SEN+ALL	33,333	100,000	20,000	60,000	40,000
SEN+PHY	33,333	100,000	30,000	50,000	40,000

Table 11: Cell counts for all conditions during senostatic application of Holy Basil, Allicin and Phytol. Nutraceuticals were applied for 10 days, removed on the 10th day and cells were counted for live and dead components.

10-day treatment of cells using Holy basil (50ug/ml), Allicin (2.5uM) and Phytol (2.5uM). Cells were also allowed to recover for 24 hours and counted to ascertain residual effects of compounds if any. Each count was taken in replicates and averaged.

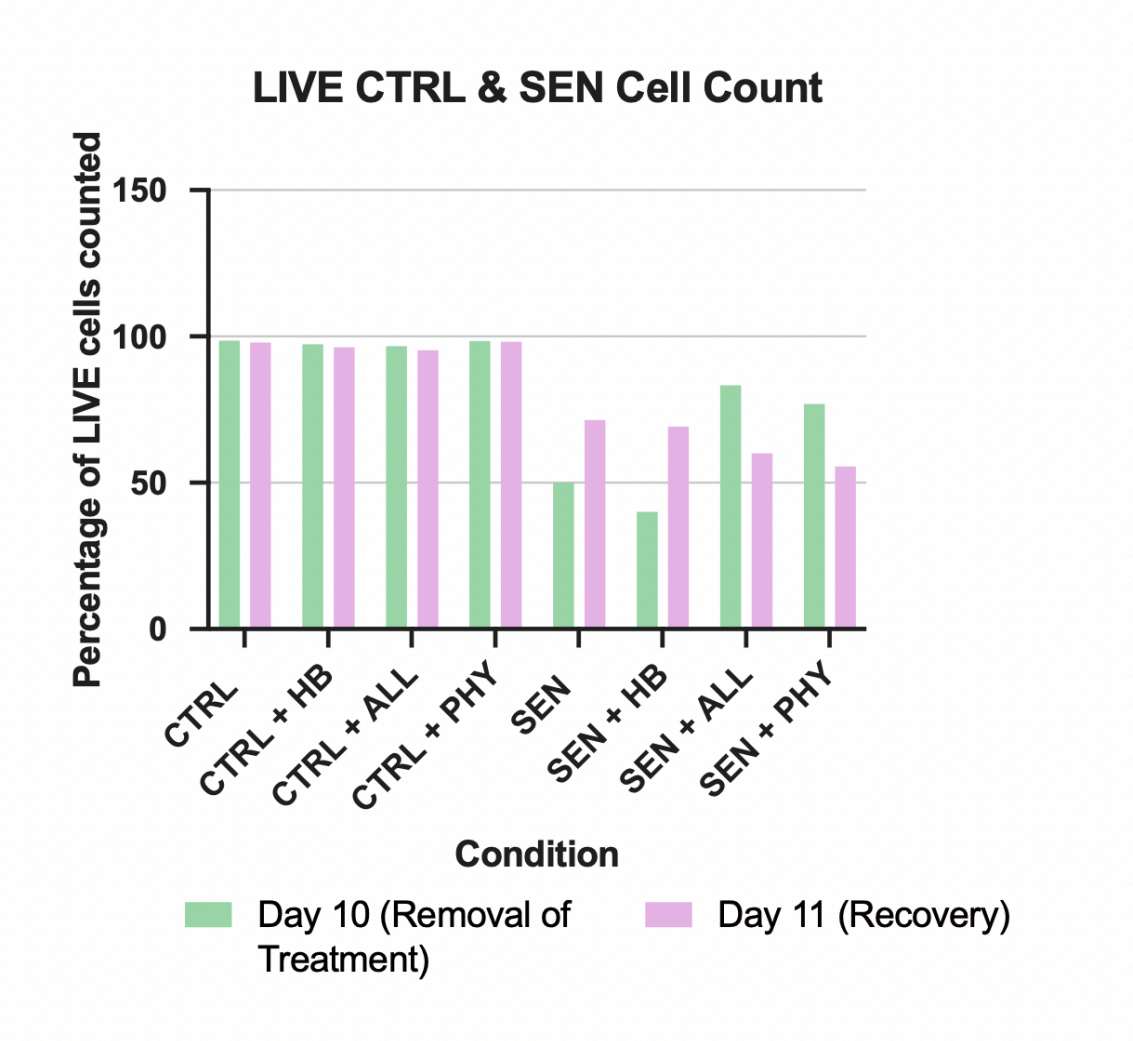

Figure 25: Percentage of Live cells of total cells counted for CTRL and SEN cells following senostatic treatment. Percentage of Live cells were calculated for CTRL and SEN cells under all treatment conditions as in Table 11.

Compared to baseline CTRL (98.5 %) the addition of Holy Basil and Allicin resulted in a lower percentage of live cells (97.4% and 96.7% respectively) whereas phytol (98.4%) treatment showed no change in percentage of LIVE CTRL cells (Figure 25A), suggesting Holy Basil and Allicin slowed cell proliferation whereas phytol showed no effect on cell proliferation.

SEN cells showed an increase in percentage of LIVE cells with the addition of Allicin (83.3%) and Phytol (76.9%) and a decrease in percentage of live cells with addition of Holy Basil (40%) between the start of the senostatic application and Day 10 at which it was removed (Figure 25B) compared to baseline SEN (50%). This suggests that Allicin and Phytol may have potential senostatic properties.

After 24-hour recovery

Compared to CTRL baseline (97.6%), when HB and Allicin treatment was removed the percentage of LIVE CTRL cells was seen to be reduced (96.2%, 95.3%) whereas Phytol removal resulted in a slight increase in LIVE CTRL cells (98.2%). Removal of treatments from SEN cells shows varied results. The absence of Holy Basil causes proliferation of LIVE SEN cells on Day 11 (69.2%) compared to Day 10 (40%), suggesting anti-proliferative capabilities. Allicin also shows a decrease (60%) in comparison to baseline SEN on Day 11 and SEN + Allicin on Day 10. However, removal of phytol also shows a decrease in percentage of LIVE SEN cells (55.5%) compared to baseline SEN. Varied results are also seen with the percentage of dead cells, with no effect seen in HB, but an increase seen with Allicin and Phytol in the SEN cells, which makes it hard to interpret the senostatic potential of the nutraceuticals.

3.7.2 SA-β-Gal staining

SA-β-Gal staining shows clearly the changes in morphology between CTRL and SEN cells (Figure 26) as described in Chapter 2. Before and after SS (Serum starvation) shows the original confluency, shape and presence of SA-β-Gal prior to senescence induction and treatment. All CTRL samples with and without treatment show similar confluency, shape, size and weaker SA-β-Gal staining. Following induction of senescence, the cells display a larger phenotype and stronger SA-β-Gal staining compared to control cells, validating results presented in the previous chapter. SEN sample shows strong SA-β-Gal staining, SEN + HB shows a reduction in the number of cells exhibiting blue staining as does SEN + Phy. SEN + Allicin shows the presence of a cluster of normal, L929 fibroblast cells suggesting that the nutraceutical may have a senostatic effect on the progression of senescence. However, it is also important to consider that the

cluster of cells may belong to an early cell or cells that may have escaped senescence and contributed to a heterogenous senescent cell population (Kirschner et al., 2020). This could account for the difference in SA-β-Gal blue staining intensities across the SEN conditions, where not all SEN cells show the distinctive blue staining. This data suggests that the nutraceuticals are reducing SA-β-Gal staining and may therefore have senostatic properties however further work is required to confirm this.

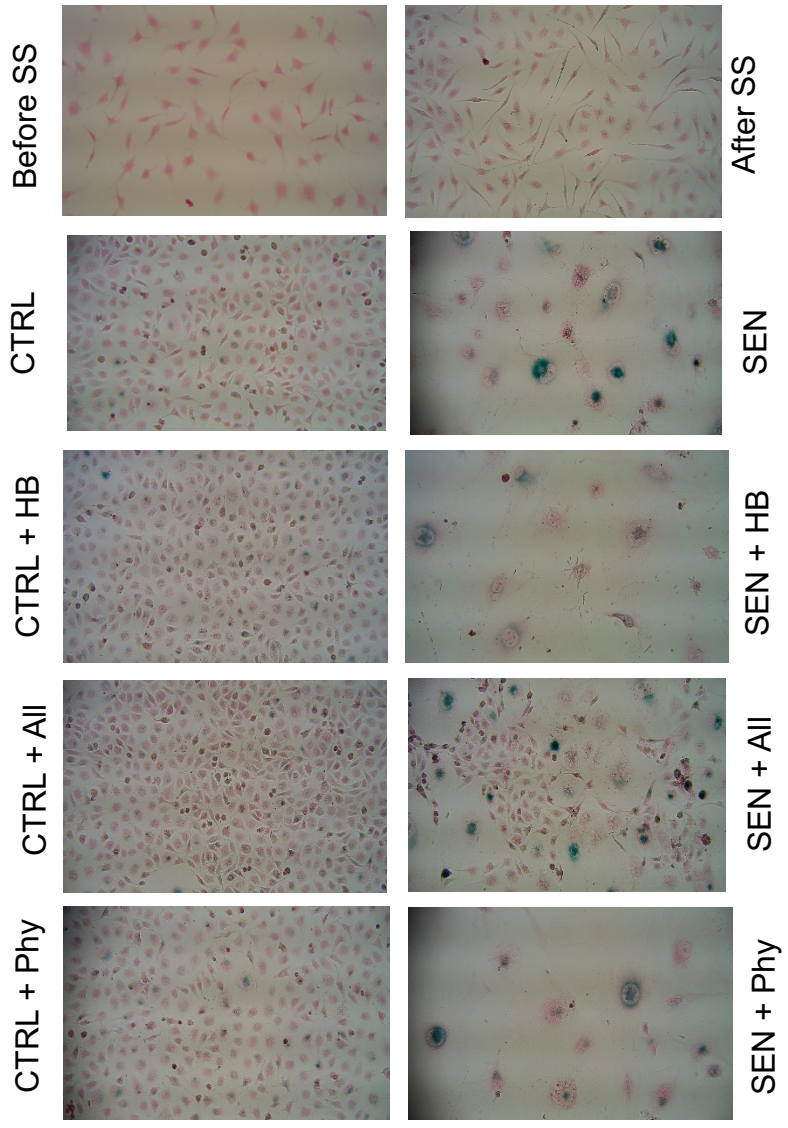

Figure 26: Light Microscopy imaging of SA-β-Gal stained CTRL and SEN treated cells. Imaging of CTRL and SEN cells treated with Holy Basil (HB), All (Allicin) and Phy (Phytol). 10-day treatment of cells using Holy basil (50ug/ml), Allicin (2.5uM) and Phytol (2.5uM). SS = Serum starvation. All images were taken with the same magnification at x100.

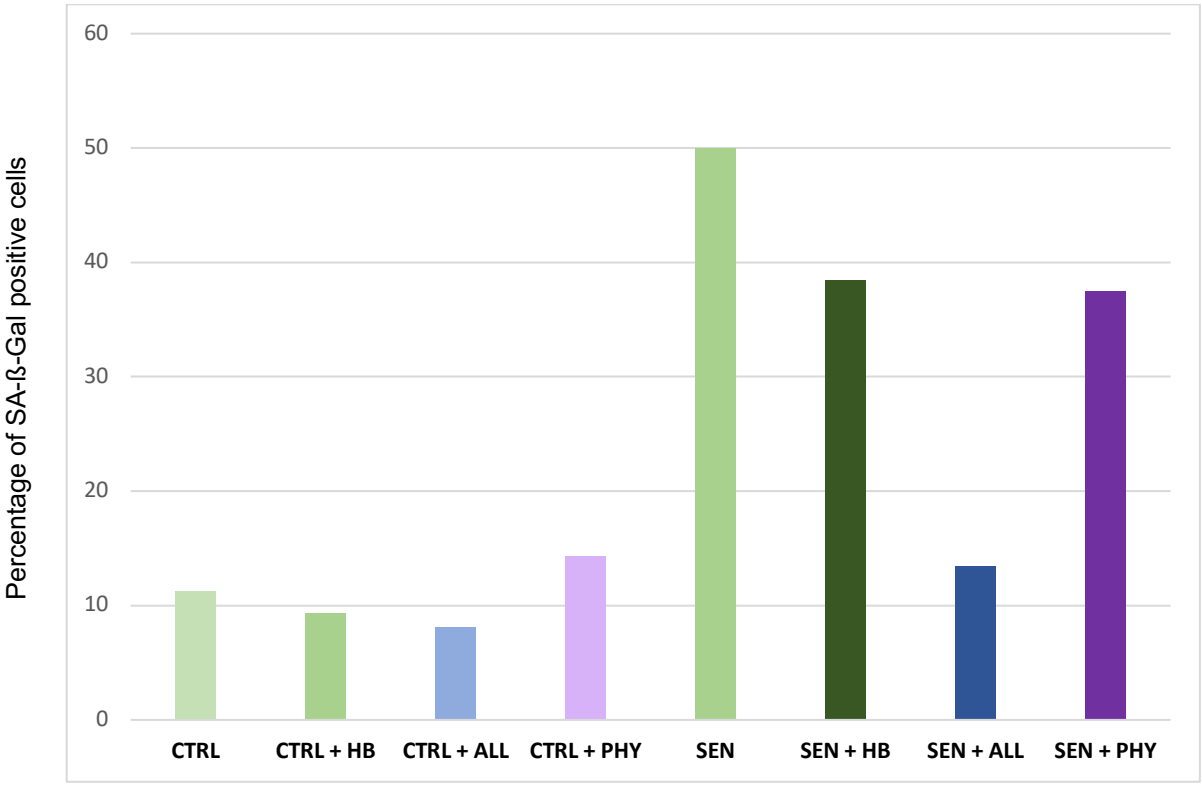

Figure 27: Percentage of Cells SA-β -Gal positive in CTRL, CTRL + Nutraceutical, SEN and SEN + Nutraceutical samples. Graph shows percentage of SA-β-Gal positive cells in SEN. SEN + HB, SEN + All and SEN + Phy. 10-day treatment of cells using Holy basil (50ug/ml), Allicin (2.5uM) and Phytol (2.5uM). All samples treated with a plant-based compound showed a lower percentage of positively stained cells compared to SEN baseline. This measure of cells only takes into account blue stained cells. (N=1, for all individual controls and treatment samples).

In SEN cells, results showed all three plant-based compounds (Figure 27) (HB – 38.5%, Allicin – 13.4% and Phytol – 37.5 %) exhibit a lower percentage of positively stained cells compared to SEN baseline (50%). This measure only takes into account cells that were stained blue. There were SEN cells in all samples that showed senescence morphology but did not stain blue. This applies particularly to SEN + All (Figure 26) which showed a collection of cells that mimicked normal fibroblasts as they appear smaller in size similar to CTRL cells. It would be difficult to discern whether this is due to the effect of allicin or due to the heterogenous senescent population of cells, where a cell may have escaped senescence and continued to proliferate.

3.7.3 Propidium iodide analysis using Flow cytometry

Propidium iodide (PI) analysis of CTRL and SEN samples set a baseline for cell cycle mechanics and changes exhibited following senescence induction. In agreement with the previous chapter there is a decrease in cells in the G1 stage and an increase in cells in the Sub-G1 stage of the cell cycle in SEN v CTRL cells. Treatment of CTRL cells with HB, Allicin and Phytol show no changes to cell cycle phases (Figure 28 & 29). SEN + Allicin also shows no evidence of phase change compared to SEN with no treatment. Following Phytol treatment analysis of the data with one-way ANOVA shows that the SEN cells have a significantly reduced S phase and increased Sub-G1 phase compared to untreated SEN cells, indicating an increase in dead cells as the cells are not able to take up the PI (Figure 28, for p values see Table 12). This suggests that Phytol is having a senolytic effect. This may also explain why senolytic results are not as convincing with phytol as the cells may be further through the cell death process and therefore not detected in the assays used. In addition, following HB treatment analysis of the data with one-way ANOVA showed a significantly reduced sub-G1 phase and increased S phase compared to untreated SEN cells (Figure 28, for p values see Table 12), which could be indicative of a regression of senescence, suggesting a potential senostatic role for HB. Full PI Flow cytometry analysis results can be found in the appendix for duplicates and additional controls.

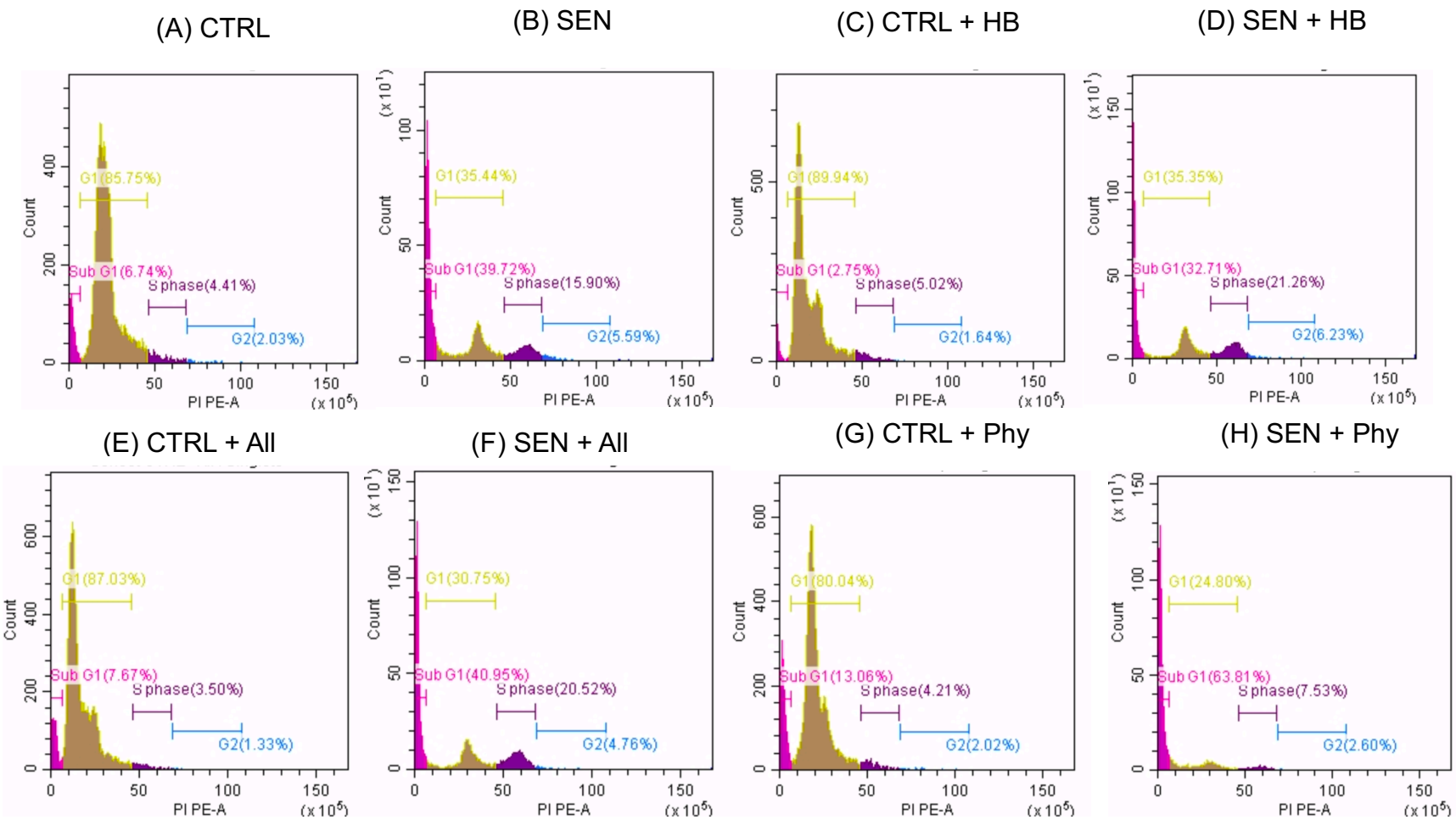

Figure 28: Cell cycle analysis of CTRL and SEN cell treated with nutraceuticals. 10-day treatment of cells using Holy basil (50ug/ml), Allicin (2.5uM) and Phytol (2.5uM). Using propidium iodide cell cycle analysis was carried of the various cell types. (A) CTRL, (B) SEN, (C) CTRL + HB, (D) SEN + HB, (E) CTRL + All, (F) SEN + All, (G) CTRL + Phy, (H) SEN + Phy.

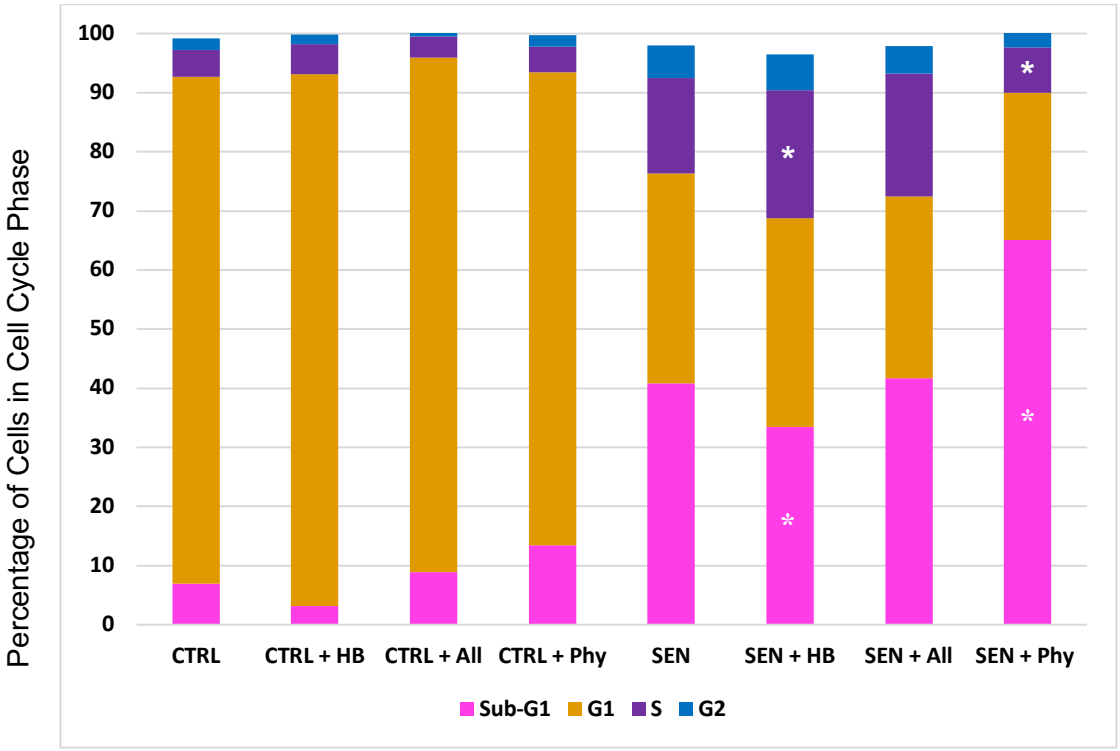

Figure 29: Bar graph to show changes to individual cell cycle phases between different CTRL and SEN samples with and without nutraceutical treatment. CTRL, SEN, CTRL + HB, SEN + HB, CTRL + All, SEN + All, CTRL + Phy, SEN + Phy. 10-day treatment of cells using Holy basil (50ug/ml), Allicin (2.5uM) and Phytol (2.5uM). An increase percentage of cells in sub-G1 and decrease in percentage of cells in S Phase is seen in SEN + Phy compared to SEN. A decrease in percentage of cells in sub-g1 and increase in S phase is seen in SEN + HB. * indicates p-values calculated showed a significant difference between group and its condition control.

Sample	Cell Cycle Phase	SEN Baseline (Mean ± SD)	SEN + Nutraceutical (Mean ± SD)	P-Value
SEN + HB	S	16.20 ± 0.42	21.62 ± 0.51	0.007
SEN + HB	Sub-G1	40.88 ± 1.64	33.42 ± 1.00	0.031
SEN + Phy	S	16.20 ± 0.42	7.69 ± 0.22	0.002
SEN + Phy	Sub-G1	40.88 ± 1.64	65.13 ± 1.87	0.005

Table 12: One way ANOVA to determine a significant difference between SEN and SEN + Phy (S phase) and (Sub-G1 phase). Statistical analysis shows a p-values calculated in comparison to SEN baseline control. A p-value threshold of 0.05 was used. SEN baseline, SEN + HB and SEN + Phy Means and Standard deviation error means were also calculated. Statistical analysis was performed on 2 replicates.

3.7.4 Western blotting for p21

Western blot analysis for p21 (Figure 30) shows an increase in SEN compared to CTRL as would be expected. The addition of HB to SEN shows no visibly detectable change in protein levels and therefore has no effect on p21 related actions of senescence in the form of senostatic application over a period of 10 days. However, an increase in p21 is seen with the addition of Allicin and Phytol in SEN cells compared to SEN with no treatment. A more abundant band for p21 is seen across all CTRLs treated with HB, Allicin and Phytol compared to CTRL with no treatment.

If the nutraceuticals were acting in a senostatic capacity, it would be expected that the p21 levels would be reduced following treatment in the SEN cells. However, a recent study by Hsu et al (2019) using human colon cancer and human lung cancer cell lines show how the dynamics of p21 expression in response to anti-cancer treatments which aim to induce senescence are more complex than this. Single cell analysis showed that there were three distinct patterns of p21 dynamics resulting in either a senescent or proliferative cell fate. Senescent fated cells either expressed low or high levels of p21 at early stages of the cellular senescence process with intermediate levels of p21 expression resulting in the emergence of

proliferative cancer cells following chemotherapy treatment (Hsu et al., 2019). Thus it is difficult to interpret the downstream effects of the increased p21 expression seen with allicin and phytol in the context of the senostatic model.

In addition, the BCL-2 family inhibitor ABT-737 has been shown to reduce p21 expression resulting in enhanced liver regeneration in a mouse model following partial hepatectomy (Birch and Gil, 2020). This suggests that increased BCL-2 expression could be linked to increased p21 expression. Interestingly the increase in BCL-2 expression following treatment with allicin and phytol that was described earlier in the chapter, is mirrored by an increase in p21, which could have implications for cell fate. The role of p21 in determining cell fate has also been shown to be dependent on exposure to cell stressors, with p21 switching from being anti-apoptotic to pro-apoptotic following UVB exposure (Chen et al, 2015).

Further work is required to investigate the downstream effects of the increased p21 following treatment with allicin and phytol on cell fate in the senescent model.

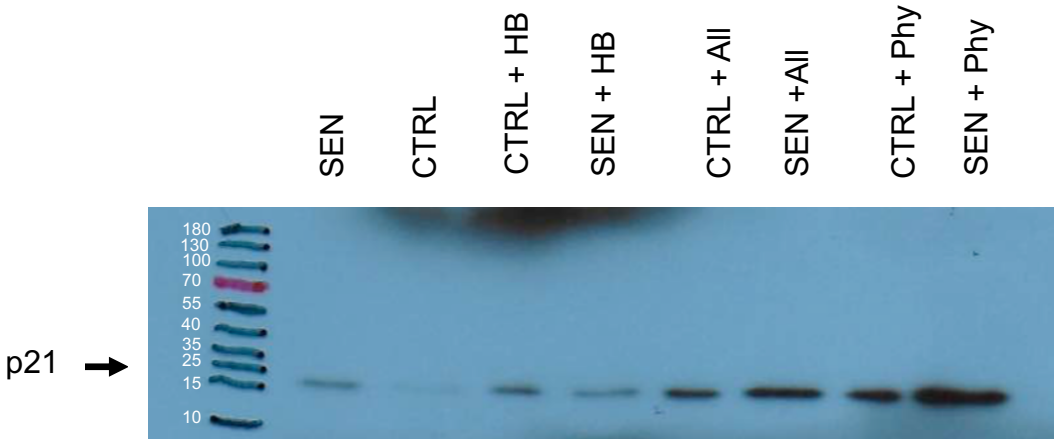

Figure 30: Western Blot identifying the presence of p21 in various treated samples. CTRL, SEN, CTRL + HB, SEN + HB, CTRL + All, SEN + All, CTRL + Phy, SEN + Phy. Arrow shows bands at molecular weight of ~21. CTRL (no irradiation treatment), SEN (senescence induction with irradiation), CTRL + HB (no irradiation treatment, 10 day Holy Basil application), SEN + HB (senescence induction with irradiation, 10 day Holy Basil application), CTRL + All (no irradiation treatment, 10 day Allicin application), SEN + All (senescence induction with irradiation, 10 day Allicin application), CTRL + Phy (no irradiation treatment, 10 day Phytol application), SEN + Phy (senescence induction with irradiation, 10 day Phytol application). Blot shows increased levels of p21 in SEN compared to CTRL as expected. A visibly increased level of p21 in CTRL + HB, CTRL + All, CTRL + Phy, SEN + All and SEN + Phy compared to their controls. SEN + HB shows similar levels of p21 compared to SEN indicating very little change in protein expression following treatment. Protein levels in each sample were normalised and loaded equally into each lane. N=1 for each sample.

3.8 Discussion

3.8.1 SA-β-Gal staining

The change in morphology of cells cannot be ignored in Figure 26 but the utilisation of SA-β-Gal staining comes with its advantages and limitations. Almost all senescence related research studies use this assay to augment their models or

findings and is therefore universally used as a marker for senescence. However, it can't be solely relied on due to its lack of specificity. Yang & Hu (2005) showed that various factors such as serum starvation, confluence of cell culture, cell age can cause an increase in SA-β-Gal activity. The model used in this project underwent serum starvation prior to senescence induction by irradiation and the CTRL culture was highly confluent at the time of assessment with SA-β-Gal staining. Yang & Hu (2005) also showed that SA-β-Gal activity 'induced by these two factors were reversible'. Nevertheless, these conditions were part of the model created in this study.

Regardless of its limitations SA-β-Gal staining remains a highly valuable marker, Cai et al (2020) were able to use it in a targeted approach for the application of prodrug SSK1 to eliminate senescent cells in order to alleviate inflammation and restore physical function (Cai et al., 2020). However, it is highly recommended that this staining be used in conjunction with other markers for senescence.

3.8.2 Propidium Iodide Cell Cycle Analysis

Cell cycle analysis of SEN cells and the addition of treatments showed Holy Basil and Phytol had an effect on Sub-G1 and S phases, albeit in opposing ways. Holy Basil application resulted in a reduced Sub-G1 phase and increased S phase compared to baseline SEN whereas Phytol resulted in an increased Sub-G1 phase and reduced S phase when compared to baseline SEN. Results indicate that Phytol may have toxic effects and caused cell death resulting in the increase in Sub-G1 phase. Holy Basil may have senescence-protective effects and work to regress the process by increasing cells in S Phase. However, there could be multiple factors causing these results.

Existing literature cannot conclude in what phase of the cell cycle senescence cells are in when induced; G1, G2 (Mao et al., 2012, Mombach et al., 2014, Feringa et al., 2018, Li et al., 2018) or some sub-G1 populations representing deeply senescent

cells (Studencka & Schaber., 2017). In spite of this, sub-G1 populations are widely considered apoptotic cells (Plesca et al., 2008). This would suggest Phytol had a senolytic effect and Holy Basil resulted in a regression of senescence according to cell cycle analysis results.

3.8.3 p21 detection

Hsu et al (2019) show how p21 is affected by certain treatments with the involvement of senescence. Human colon cancer and human lung cancer cell lines were treated with anti-cancer treatments to induce senescence and investigated using single cell analysis. They found that there were three distinct patterns of p21 dynamics to achieve certain cell fates, these cell fates being either senescent or proliferative. Results showed that senescent fated cells expressed low p21 at early stages of the cellular senescence process and the emergence of proliferative cancer cells following chemotherapy treatment (Hsu et al., 2019). This could be the case for the model used in the senostatic experiments.

With the exception of SEN + HB, all other samples showed a more abundant band for p21. The expected result would have been for the reduced expression of p21 in SEN cells treated with the potential nutraceuticals. Yosef et al (2017) showed how p21 is necessary to maintain the viability of DNA-damage induced senescent cells in a caspase and JNK dependent manner (Yosef et al., 2017). Therefore, it is uncertain if the action of p21 and the nutraceuticals act in opposing ways. For example, the plant-based compounds may be working to stop or slow down the progression of senescence but across most samples an increase in p21 is seen indicating a potential cellular battle to keep cells in their senescent state.

3.8.4 Exploring the Senostatic capabilities of Holy Basil, Allicin and Phytol

3.8.4.1 Holy Basil

The various methods used in this study to assess senostatic capabilities of potential nutraceuticals were carried out with the aim to provide results that conferred with each other. In regard to Holy Basil, SA-β-Gal cell cycle analysis suggest that it may have some senostatic capabilities, whereas outcomes for p21 protein analysis showed no change in comparison to baseline senescent control. Cell proliferation results showed a decrease in percentage of live proliferating cells suggesting an apoptotic effect. This could be supported by the fact that once Holy Basil was removed, cell proliferation increased.

Very few studies have assessed Holy Basil over a prolonged period of time, none of which relate to cellular senescence. Ponnusam et al (2015) orally administered Holy Basil to Adult Wistar male rats subjected to carbon tetrachloride-based liver injury, to find enhanced antioxidant activity (Ponnusam et al., 2015), however the publishing journal 'Ayurvedic' is not well recognised and has no associated impact factor.

3.8.4.2 Allicin

Results for Allicin application to SEN cells showed increased p21 expression and higher live cell proliferation, reduced SA-β-Gal activity but no change in cell cycle compared to baseline senescence controls. Further work is required to establish wether Allicin has senostatic potential.

Garlic and its extracts have been widely studied in senescence (Nishiyama et al., 1997, Rahman, 2003) and have been shown to have therapeutic effects in age related diseases such as Arthritis, Diabetes and Alzheimer's disease (Chung, 2019). Kim (2016) investigated the effect of powdered garlic at a concentration of 50ug/mL on UVB induced senescent human keratinocytes (HaCaTs). Results showed reduced SA-β-Gal activity, SIRT1 activity and reduced IL-6 and IL-1B production

(Kim, 2016). These cells were treated with garlic prior to senescence induction. Thus, it may be more informative to investigate Allicin application in the SEN model prior to irradiation.

Additionally, Lin et al (2017) studied the effect of Allicin on a Hydrogen peroxide induced HUVECs (Human umbilical vein endothelial cells) aging model. This model pre-treated cells with 5ng/mL of Allicin prior to senescence induction. Results showed reduced ROS production, increased activation of SIRT1, increased cell viability and reduced SA-B-Gal activity. The study concluded Allicin had anti-aging effects on the oxidative stress induced senescence-based model and acted through SIRT1 activation (Lin et al., 2017).

3.8.4.3 Phytol

Results for phytol support a potential senostatic role of Phytol, in addition to providing further support for a potential senolytic role of Phytol, based on the cell cycle analysis. The only study carried out using Phytol in a senescent cell model pertains to the research carried out by Jeong (2018). This study applied Phytol at various doses to Human keratinocytes for 24 hours, 6 hours prior to senescence induction via hydrogen peroxide. Parameters such as inflammatory markers, SA-β-Gal activity, Caspase-3 analysis and cell cycle analysis were investigated. Results showed reduced expression of inflammatory markers such as TNF-a, IL-6, IL-8 and COX2. Reduced expression of CASP-3 was found indicating less apoptosis compared to control. Propidium Iodide Flow cytometry analysis showed Phytol was able to reverse the suppressive effect of hydrogen peroxide on cell cycle progression. SA-β-Gal activity was also reduced in a Phytol concentration dependent manner compared to control (Jeong, 2018). This study showed promise for Phytol in inhibiting oxidative stress induced senescence. This PhD project investigated the effect of Phytol in a DNA-damage induced senescence model and therefore may not provide similar outcomes to pre-existing studies. In addition to Phytol being added as a pre-treatment whereas in the project phytol was used over

a period of 10 days after senescence induction. It would be beneficial to investigate the effect of Phytol prior to senescence induction in the SEN model in future work.

3.9 Conclusion

In the SIPS model studies, Holy Basil, Allicin and Phytol have senostatic effects based on SA-β-Gal staining carried out. Holy Basil and Phytol application produce cell cycle changes and Allicin and Phytol result in increased live cell proliferation during treatment. However, overall measures of senescence carried out do not confer with each other in order to conclude definitive senostatic capabilities.

Therefore, further investigation into these potential senostatic compounds would be necessary to ascertain their calibre as a senescence therapy. Other factors would also need to be considered such as duration of dose, application of treatment prior or post senescence induction and if removal of application diminishes senostatic capabilities. This would require the testing of various doses in multiple senescence cell models and cell lines, ultimately if proven to be beneficial against aging be committed to *in vivo* mouse models to gather information on toxicity and side effects.

4 The Transcriptomic analysis of cells exposed to Holy Basil, Allicin and Phytol as senostatic interventions in an L929 irradiation induced senescence model

4.1 Introduction

Investigating changes in gene expression across conditions can prove useful to obtain global information in relation to cellular processes, metabolism pathways and immune based responses. Gene expression studies continue to inform regarding key pathways involved in cellular senescence and similar factors that are implicated across different types of senescence. Even though the human body mostly experiences replicative senescence in relation to telomere shortening RNA-seq studies have shown that the presence of SASP factors are conserved across senescence models achieved with varying stimuli. Purcell et al, (2014) performed gene expression profiling of replicative, H_2O_2-induced, adriamycin-induced and 5-aza-2-deoxycytidine induced senescence in fibroblasts. Their data highlighted 48 senescence related genes across the 4 types of senescence, related to innate immune function, interferon pathways and inflammation (Purcell et al., 2014). By exploring mRNA levels of inflammation related genes through gene sequencing, further information can be gathered regarding the effects of conditions and treatments on cell models.

4.2 Aims & Objectives

Morphological, chemical and physiological changes induced by the application of the nutraceuticals have been investigated in Chapter 2. However, some variables that have been measured have their limitations. Therefore, the aims of this chapter were to analyse differences in gene expression between CTRL and SEN cells, as well as the effect on gene expression in nutraceutical treated versus untreated cells. This was to provide further information on key pathways involved in cellular senescence using the specific model created in Chapter 1 and following treatment with three nutraceuticals to be able to inform future work. Chronic inflammation is known to be

strongly involved in the process of aging, also termed inflammaging, therefore RNA samples from CTRL and SEN cells in the presence and absence of nutraceuticals were assessed specifically for genes related to inflammation to identify changes in expression of key genes. This was done by testing mRNA levels using Nanostring Technology in the form of the Nanostring Sprint Profiler with an Inflammation Mouse specific panel that would investigate the expression of 254 targets – a full list of the genes is provided in the appendix.

4.3 How Nanostring Works

The nCounter Analysis Sprint Profiler system is capable of detecting and analysing a vast number of genes in a single reaction that comprises hybridisation, electrophoresis and immobilisation. It does this by directly profiling individual molecules through assigned fluorescently labelled probes to target genes using 70 to 100 bp of complementarity. Nanostring allows for a vast number of genes to be investigated from a very small amount of a single sample without prior amplification or cloning.

There are multiple but simple steps involved in the process of Nanostring analysis which counts individual mRNA transcripts (Figure 31). During the process of hybridisation, the capture probe and reporter probe identify and hybridise to the complementary target mRNA. This is done through the gene specific sequences provided dependent on the target sequences of interest within the panel. The 3’ and 5’ end repeat sequences are used to purify the so-called tripartite complex by extracting excess reporter and capture probes. A slide coated in streptavidin with biotinylated capture probes are used to attach the complexes before an electric current is applied to stretch and align the complex using biotinylated anti-5’ oligonucleotides to the slide to become fixed. The reporters in the complex are imaged with a fluorescence microscope and counted.

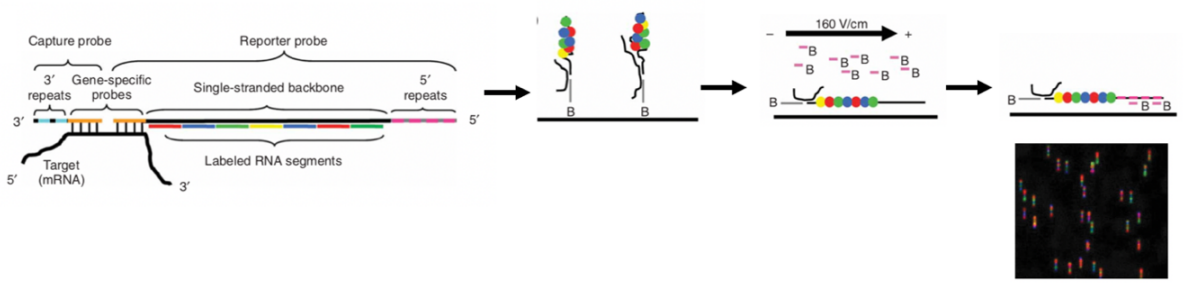

Figure 31: Diagrammatic overview of Nanostring nCounter Analysis technology. The illustration highlights the key steps involved in the sequencing process from capture and reporter probe hybridisation, purification of target-probe complex, attachment through streptavidin-biotin interaction, application of voltage to stretch the complex, imaging and counting reporter probes (Taken directly and adapted from Geiss et al., 2008).

Whereas traditional methods of RNA sequencing require multiple steps which can introduce variability, bias and therefore irreproducibility, Nanostring nCounter analysis was chosen as an alternative in order to obtain robust reproducible data that could be done in fewer, simpler steps to minimise margin of error in a quicker timeframe.

Various research groups have successfully used Nanostring technologies in senescence related studies. Rahman et al (2018) were able to identify ‘significant upregulation of pro-senescence targets’ in young and old mice that had been subjected to 6 months’ exposure of cigarette smoke to assess if it worsens lung associated diseases such as COPD and emphysema dependent on aging.

Schwab et al (2019) studied senescence and DNA repair in professional contact sport athletes that had mild traumatic brain injury. Nanostring gene expression profiling, in the form of a custom panel with 169 genes relating to DDR and cellular senescence was used to compare between donated brains with and without trauma. Results showed downregulation of DNA repair genes and ‘increased susceptibility to cellular senescence’ following trauma compared to without trauma (Schwab et al., 2019). Nanostring analysis has shown to achieve ‘high reproducibility, sensitivity and

robustness'. It has been compared to Next Generation Sequencing in relation to transcriptome profiling (Bondar et al., 2020).

4.4 Materials & Methods

4.4.1 Senostatic Application of Nutraceuticals

Control and Senescent cells were prepared as described in Chapter 1. Cells were treated with doses of each nutraceutical determined through cytotoxicity experiments. Nutraceuticals were applied for a total of 10 days from the application of Irradiation on Day 0 till removal of nutraceutical media on day 10. New media with nutraceutical was replenished on day 3 and day 6.

4.4.2 Harvesting of cells

Cell media was removed from and the cell culture dishes with adherent cells were frozen. Cells were harvested using Qiagen Buffer RLT and scraped using cell scrapers.

4.4.3 RNA extraction

RNA from cells was extracted using the RNeasy Mini Kit (QIAGEN Product Code: 74104).

1. Added 300µl of Buffer RLT to cell culture dishes and scraped cells.
2. Added 300µl of 70% ethanol to the lysate and mixed well.
3. Transferred cell lysate to a RNeasy mini spin column with a collection tube
4. Centrifuged for 15s at >8000 x g. Discarded the flowthrough
5. Added 700µl of Buffer RW1 to the RNeasy spin column. Centrifuged for 15s at >8000 x g. Discarded the flowthrough

6. Added 500ul of Buffer RPE to the RNeasy spin column. Centrifuged for 15s at >8000 x g. Discarded the flowthrough.
7. Added 500ul of Buffer RPE to the RNeasy spin column.

Centrifuged for 2 min at >8000 x g.

8. Place the RNeasy spin column in a new collection tube. Added 30µl of RNAse free water to the spin column membrane. Centrifuged for 1 min at > 8000 x g to collect RNA.

4.4.4 RNA quantification

RNA content of samples was quantified using the Nanodrop One (Thermoscientific). The Nanodrop one was blanked using RNAse free water and 1ul of sample was applied for measuring RNA.

4.4.5 RNA Normalisation prior to hybridisation

RNA content was equalised across all samples to contain 200ng per sample of 30µl. RNA was diluted in RNAse free water.

4.4.6 nCounter analysis using Nanostring

4.4.6.1 RNA hybridisation using Reporter and Capture CodeSets for Mouse Inflammation Panel

RNA hybridisation was carried out according the nCounter XT CodeSet Gene Expression Assay protocol (Nanostring).

1. Thermal cycler was pre-heated to 65^{o}C.
2. All components for hybridisation, the Reporter and Capture codeset were allowed to thaw at room temperature

3. A master mix was created by adding 70µl of hybridisation buffer to the reporter codeset and mixed by inverting and spun down in a microfuge.
4. Sample tubes were labelled and 8µl of the master mix was transferred into each tube.
5. 5µl of RNA sample was added to each tube.
6. 2µl of Capture probeset was added to sample tube. Samples were inverted to mix and spun down in a microfuge
7. Samples were placed in the thermal cycler and incubated for 20hrs total.

4.4.6.2 Loading and Running samples on the SPRINT profile cartridge

1. Cartridge was removed from -20^{o}C and allowed to equilibrate to room temperature for 15 mins
2. Hybridised samples were removed from the thermal cycler taking care to not let the samples remain at room temperature for longer than 15 mins. Initialising the run had to be done within the 15 mins.
3. The samples were spun down in a microfuge.
4. Sample volume was brought to 30µl using RNAse free water.
5. 30 µl of each sample was injected into the cartridge as shown in Figure 32.
6. Empty lanes were loaded with water.
7. The sample loading ports were sealed and cartridge was placed into the Nanostring instrument as shown in Figure 32.
8. Run was initialised.

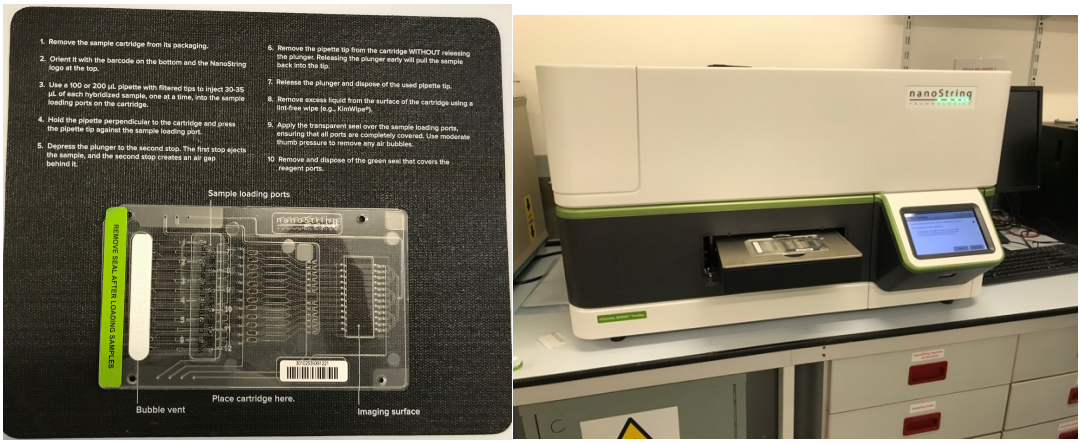

Figure 32: Sprint Profiler Cartridge for Nanostring Analysis. All samples and water (for empty lanes) were loaded in the sample loading ports ensuring the entire sample was pushed through channel. Prior to loading the cartridge into the Nanostring Profiler the loading ports were sealed with tape and the tape (green) covering the reagent ports was removed. The cartridge was placed in the instrument and the run was initiated until completed.

4.4.7 nSolver Data analysis

nSolver data analysis was aided by the assistance of Dr Bryan Serrels, a Field Applications scientist from Nanostring. Over video meetings Dr Serrels guided in the analysis of data obtained from the experiment. nSolver Analysis Software is a Nanostring provided analysis platform allowing for custom normalisation of nCounter data. The RCC files from the Nanostring cloud database for the gene expression assay were obtained and uploaded into the Software. The Software was used to create normalisation counts taking into account positive and negative controls. Background was calculated by averaging the negative control counts + 2*Standard Deviation of the negative control counts. Counts were normalised taking into account the background. Signal to noise ratio was calculated by using the formula Signal:Noise Ratio = Count/Background. Genes with a signal:noise ratio of greater than 5 were considered as robust counts indicating a signal above background.

These genes were compiled into a list and their counts used to calculate fold change and Log2 Values for further data visualisation.

4.4.8 Functional Annotation analysis using DAVID

The Database for Annotation, Visualisation and Integrated Discovery (DAVID) was used to retrieve functional annotation information regarding the final gene list. This database was used to identify enriched biological themes and GO (Gene Ontology) terms.

4.5 Results

4.5.1 RNA Quantification and normalisation

RNA content of all cell types was quantified using the Nanodrop One (Thermoscientific). Each sample showed a varied amount of RNA concentration in ng/µl (Table 13). The A260/A280 ratio indicates the quality of the RNA with values being close to 2 showing high quality, uncompromised RNA. Using these quantifications, RNA content was equalised across all samples using RNAse free water for dilution to obtain 200ng RNA per sample for a concentration of 20ng/µl. The quantities allowed for the normalisation of RNA content in loading of samples for Nanostring nCounter gene expression analysis.

Cell Type	RNA ng/µl	A260/A280
CTRL	56.5	1.94
CTRL + HB	206.95	2.05
CTRL + All	507.75	2.08
CTRL + Phy	455.85	2.08
SEN	110.65	2.05
SEN + HB	55.05	2.05
SEN + All	131.35	2.06
SEN + Phy	91.0	2.06

Table 13: RNA quantification using the Nanodrop One. The RNA concentration (ng/µl) of each sample and the A260/A280 ratio is shown**.** RNA quantities were measured in each sample twice and averaged.

4.5.2 Analysis of Mouse Inflammation Panel using nSolver by Nanostring

4.5.2.1 Expression of Positive Controls

Positive Controls also known as housekeeping genes were analysed to show that all followed the same pattern of expression across all samples (Figure 33) and were expressed with counts of 1000 or more indicating positive expression.

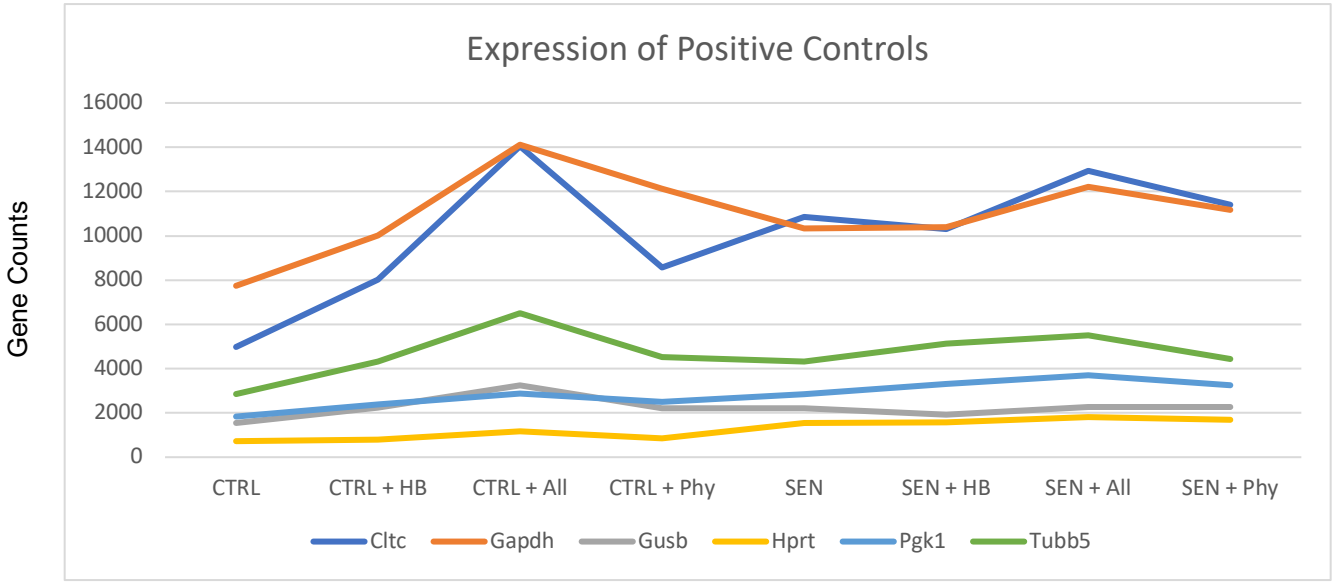

Figure 33: Counts for Positive Controls across all samples. Expression of positive controls across all samples show a similar trend indicating relative stability. Housekeeping genes investigated include Cltc (Clathrin Heavy Chain 1), Gapdh (Gylceraldehyde-3-Phosphate Dehydrogenase), Gusb (Glucoronidase Beta), Hprt (Hypoxanthine-Guanine Phosphoribosyltransferase), Pgk1 (Phosphoglycerate kinase 1) and Tubb5 (Tubulin beta 5).

4.5.2.2 Normalised counts

Normalised counts were extracted from nSolver following processing of RCC files and negative controls were used to calculate background. Background was subtracted from counts and ordered according to highest to lowest counts. A total of 254 target genes were analysed. A full list of gene expression count data can be found in the appendix.

4.5.2.3 Signal to noise ratio

Next, the signal to noise ratio was calculated (Figure 34) to determine expression of genes. A high signal to noise ratio indicates the strong signal or expression of target gene. This ratio was used to compile a list of 116 target genes that expressed a signal that was robustly above background indicating the presence of a high-count number in a particular sample. Figure 34 only shows a sample extract, a full list can be found in the appendix.

	CTRL + All	CTRL + HB	CTRL + Phy	CTRL	SEN + All	SEN + HB	SEN + Phy	SEN
Atf2	41.25	33.88	45.57	42.72	77.87	50.60	63.08	62.85
Bcl2l1	16.31	12.94	17.82	15.56	29.25	20.50	25.20	25.54
Birc2	16.87	13.90	19.84	16.65	21.95	15.12	17.51	18.10
C1ra	11.15	9.66	15.56	9.17	7.88	4.57	6.57	6.26
C1s	60.21	32.04	91.74	42.32	63.35	25.36	51.24	52.94
C2	20.29	14.69	24.79	19.28	23.66	12.07	18.00	17.64
Ccl2	98.25	88.90	40.68	111.19	797.58	555.11	837.03	638.93
Ccl7	15.94	16.19	11.59	17.58	93.44	65.34	87.65	76.33
Cd40	6.83	7.38	10.14	7.80	27.46	17.06	24.17	19.23
Cdc42	414.84	408.12	460.03	412.86	548.30	395.71	468.70	447.46
Cebpb	197.79	210.63	249.65	226.21	163.74	104.61	122.74	129.39
Cfl1	518.98	454.68	502.53	446.12	711.04	569.36	587.34	574.29
Csf1	998.57	610.21	899.35	514.38	2621.14	2165.82	2313.14	2307.13
Cxcl1	8.17	7.83	6.90	6.87	110.25	66.55	117.68	94.50
Daxx	6.29	4.75	6.43	5.86	8.96	6.80	6.46	6.29
Ddit3	147.93	139.67	189.00	140.04	326.30	181.61	287.08	270.90
Fos	33.60	16.33	27.78	35.69	7.93	3.82	4.80	4.08
Gnaq	42.23	24.05	38.86	20.81	72.20	48.66	56.72	62.49
Gnas	649.56	587.32	693.11	588.91	825.22	578.22	694.27	704.19
Gnb1	179.85	131.25	171.22	139.72	240.42	199.01	201.11	211.14
Grb2	24.56	17.55	26.34	22.27	39.82	28.60	33.03	34.48
Hc	10.60	5.09	9.09	6.26	6.77	5.44	5.39	6.50
Hdac4	9.10	4.18	7.71	5.42	15.55	10.74	12.66	13.61
Hif1a	207.74	156.66	208.19	155.97	248.28	157.70	195.35	201.54
Hmgb1	127.18	138.35	150.87	117.41	127.64	83.99	100.15	101.18
Hmgn1	212.91	207.27	221.19	229.85	224.59	195.26	183.23	194.76
Ifit2	5.58	5.37	5.76	3.68	17.05	11.86	13.87	15.10
Igp1	16.02	39.31	43.54	15.92	50.15	28.53	37.37	30.68
Il10rb	11.65	11.36	14.89	11.64	20.79	16.67	18.30	19.15
Il1r1	35.04	28.74	35.93	27.12	48.70	25.99	34.50	36.87
Il1rap	12.46	8.51	12.49	8.25	19.39	13.19	16.39	16.38
Il23a	2.46	2.23	3.20	2.75	3.77	2.93	3.12	3.21
Il6	2.08	4.78	4.51	3.07	21.08	11.30	18.49	15.12

Figure 34: Signal to noise ratio of normalised counts for expression analysis of Nanostring Inflammation Panel. An sample extract of the genes with high signal to noise ratio are shown with those highlighted in green, which represent S:N ratio above threshold, (green representing above 5, yellow shows between 3 and 5 and white indicates below 3) indicating robust data and results to provide a list of 116 genes that were further analysed for fold change.

4.5.2.4 Fold Change

Fold change was calculated for all 116 genes against their baseline sample i.e CTRL/SEN, CTRL/CTRL+HB, CTRL/CTRL+ALL, CTRL/CTRL+Phy, SEN/SEN+HB, SEN/SEN+All and SEN/SEN+Phy. The fold change values underwent Log2 (Log2(FC)) transformation and genes with values above +1 and below -1 were filtered to determine upregulated and downregulated genes respectively (Figure 35). The aim was to assess responses that discriminate between CTRL and SEN conditions 10 days after the initiation of the experiment and interrogate the effect of treatments on the matched conditions.

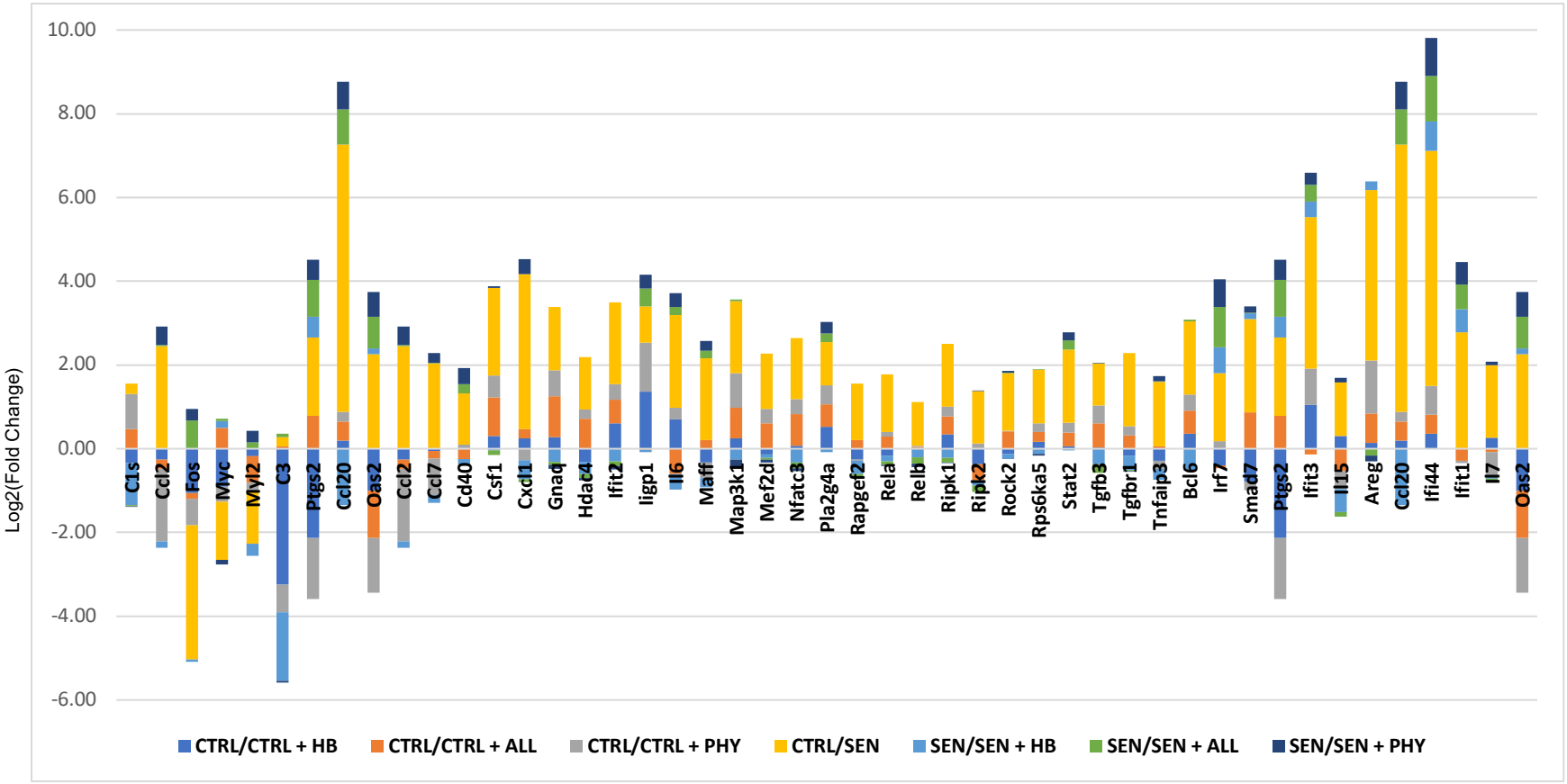

Figure 35: Log2(Fold change) across genes that were upregulated or downregulated in comparison to their baseline controls. Log2 of Fold change was calculated over the treatment applied and its control condition as CTRL + HB/ CTRL, CTRL + Allicin/CTRL, CTRL + Phytol/CTRL, CTRL/SEN, SEN + HB/SEN, SEN + Allicin/SEN and SEN + Phytol/SEN. The graph shows genes with a log2(FC) value above +1 or below -1 to represent upregulated or downregulated genes.

4.5.2.5 Upregulated Genes

Table 14 shows the genes with a positive Log2(FC) of 1 or more across the samples. A total of 38 genes were found to be upregulated, the majority being upregulated in SEN compared to CTRL, including Ccl2, Ccl7, Cxcl1, Ifit3, Il6, Smad7, Areg, Ccl20, Ifi44, Il7 and Oas2. These were found to have a log2(FC) value of above 1. Iigp1 was found to be upregulated in CTRL + HB and CTRL + PHY in comparison to CTRL. Areg is also found to have increased expression in CTRL + PHY. SEN + ALL showed an increase in Ifi44 compared to SEN baseline expression. Figure 36 shows the tabulated information in heatmap form with red representing upregulated genes in the samples.

	CTRL/CTRL + HB	CTRL/CTRL + ALL	CTRL/CTRL + PHY	CTRL/SEN	SEN/SEN + HB	SEN/SEN + ALL	SEN/SEN + PHY
Ccl2	-0.26	-0.22	-1.73	2.44	-0.15	0.04	0.43
Ccl7	-0.06	-0.18	-0.88	2.04	-0.18	0.01	0.24
Cd40	-0.02	-0.23	0.10	1.22	-0.12	0.23	0.37
Csf1	0.31	0.92	0.52	2.09	-0.04	-0.10	0.05
Cxcl1	0.25	0.21	-0.28	3.70	-0.46	-0.06	0.36
Gnaq	0.27	0.98	0.62	1.51	-0.31	-0.08	-0.10
Hdac4	-0.31	0.71	0.23	1.25	-0.29	-0.09	-0.06
Ifit2	0.61	0.56	0.36	1.96	-0.30	-0.11	-0.08
Iigp1	1.37	-0.03	1.17	0.87	-0.06	0.42	0.33
Il6	0.70	-0.60	0.27	2.22	-0.37	0.20	0.33
Maff	-0.33	0.21	-0.36	1.95	-0.23	0.19	0.23
Map3k1	0.25	0.73	0.84	1.72	-0.26	0.04	-0.20
Mef2d	-0.14	0.60	0.34	1.33	-0.08	-0.04	-0.07
Nfatc3	0.07	0.76	0.35	1.45	-0.33	-0.14	-0.07
Pla2g4a	0.53	0.53	0.45	1.03	-0.09	0.20	0.27
Rapgef2	-0.26	0.20	-0.03	1.35	-0.32	-0.08	0.00
Rela	-0.17	0.29	0.12	1.37	-0.13	-0.09	-0.03
Relb	0.02	0.03	0.03	1.04	-0.21	-0.15	-0.08
Ripk1	0.35	0.43	0.23	1.50	-0.22	-0.11	-0.01
Ripk2	-0.36	-0.39	0.12	1.25	-0.13	-0.15	0.02
Rock2	-0.12	0.42	0.02	1.37	-0.13	0.02	0.04
Rps6ka5	0.17	0.23	0.21	1.28	-0.13	0.00	-0.04
Stat2	0.06	0.32	0.24	1.75	-0.04	0.22	0.19
Tgfb3	0.03	0.58	0.42	1.01	-0.37	-0.21	0.01
Tgfbr1	-0.17	0.32	0.21	1.75	-0.34	-0.03	-0.01
Tnfaip3	-0.29	0.05	-0.19	1.54	-0.26	0.02	0.12
Bcl6	0.35	0.55	0.39	1.74	-0.49	0.05	-0.03
Irf7	-0.39	-0.07	0.18	1.63	0.61	0.96	0.66
Smad7	-0.78	0.87	-0.21	2.23	0.13	0.01	0.16
Ptgs2	-2.13	0.78	-1.46	1.88	0.49	0.89	0.48
Ifit3	1.04	-0.13	0.88	3.61	0.37	0.41	0.29
Il15	0.30	-0.54	-0.43	1.28	-0.55	-0.11	0.11
Areg	0.13	0.71	1.26	4.08	0.21	-0.16	-0.15
Ccl20	0.20	0.45	0.23	6.39	-1.35	0.83	0.66
Ifi44	0.35	0.47	0.69	5.60	0.70	1.09	0.91
Ifit1	-0.02	-0.27	-0.05	2.78	0.55	0.58	0.54
Il7	0.27	-0.08	-0.59	1.73	-0.05	-0.06	0.08
Oas2	-1.01	-1.13	-1.30	2.25	0.15	0.75	0.59

Table 14: Upregulated genes and conditions obtained from Nanostring Inflammation Panel analysis. The table shows 38 genes that were found to be upregulated in at least 1 condition. The Log2(FC) pertaining to the upregulated gene is highlighted in blue. Any genes that showed a Log2(FC) of 1 or more were regarded as upregulated in the condition compared to its relative control (Control/Condition).

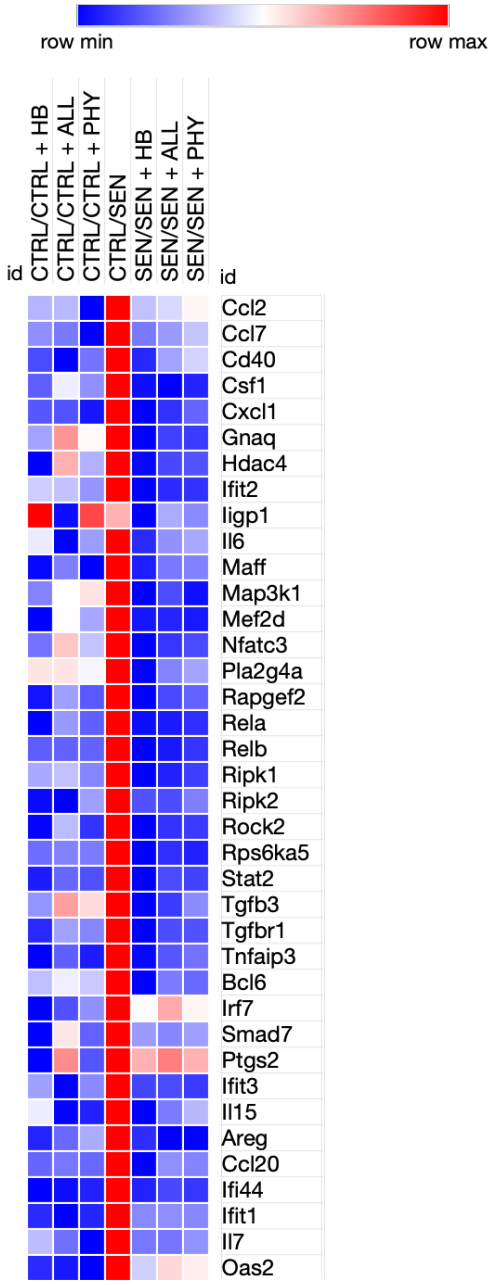

Figure 36: Heatmap of upregulated genes obtained from Nanostring Inflammation Panel Analysis. The heatmap illustrates the relative expression of listed genes that were identified to be upregulated in a certain condition subjected to treatment compared to its relative control (Heatmaps were created using MORPHEUS software).

4.5.2.6 Downregulated Genes

Table 15 shows the genes with a negative Log2(FC) of 1 or less across the samples. A total of 9 genes were found to be downregulated. Fos, Myc and Myl2 were found to be downregulated in SEN compared to CTRL. C1s, C3, Ccl20 showed reduced expression in SEN + HB compared to baseline SEN. Ccl20 and Ptgs2 were downregulated in CTRL + PHY compared to CTRL. Fos, C3, and Ptgs2 were also downregulated in CTRL + HB and Oas2 showed reduced expression in all CTRL samples treated with a nutraceutical in comparison to baseline CTRL. Figure 37 shows the tabulated information in heatmap form with blue representing downregulated genes in the samples.

	CTRL/CTRL + HB	CTRL/CTRL + ALL	CTRL/CTRL + PHY	CTRL/SEN	SEN/SEN + HB	SEN/SEN + ALL	SEN/SEN + PHY
C1s	-0.34	0.47	0.83	0.24	-1.01	-0.03	0.00
Ccl2	-0.26	-0.22	-1.73	2.44	-0.15	0.04	0.43
Fos	-1.06	-0.12	-0.64	-3.21	-0.05	0.67	0.28
Myc	-0.91	0.49	-0.36	-1.38	0.17	0.05	-0.11
Myl2	-0.18	-0.64	-0.19	-1.27	-0.29	0.16	0.27
C3	-3.25	0.06	-0.66	0.22	-1.64	0.09	-0.05
Ptgs2	-2.13	0.78	-1.46	1.88	0.49	0.89	0.48
Ccl20	0.20	0.45	0.23	6.39	-1.35	0.83	0.66
Oas2	-1.01	-1.13	-1.30	2.25	0.15	0.75	0.59

Table 15: Downregulated genes and conditions obtained from Nanostring Inflammation Panel analysis. The table shows 9 genes that were found to be downregulated in at least 1 condition. The Log2(fold change) (Log2(FC)) pertaining to the downregulated gene is highlighted in orange. Any genes that showed a Log2(FC) of -1 or below were regarded as downregulated in the condition compared to its relative control (Control/Condition).

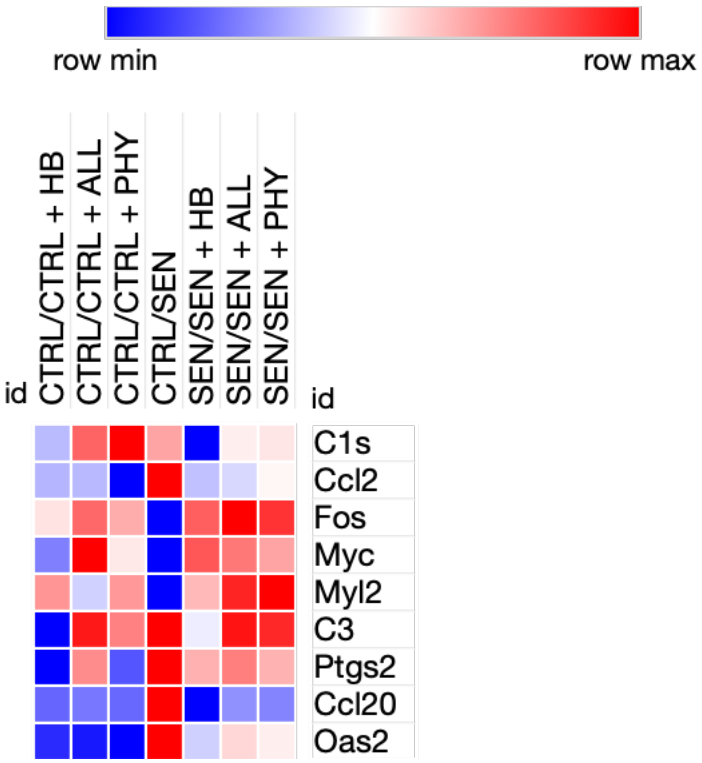

Figure 37: Heatmap of downregulated genes obtained from Nanostring Inflammation Panel Analysis. The heatmap illustrates the relative expression of listed genes that were identified to be downregulated (represented by the blue) in a certain condition subjected to treatment compared to its relative control (Heatmaps were created using MORPHEUS software).

4.5.3 DAVID Functional Annotation Analysis

The list of 47 genes found to be up and/or downregulated across the treatments in relation to their controls was further analysed by DAVID, a publicly available database and tool to assign information relating to gene ontology, biological processes and related pathways (Huang et al., 2009). The list of genes was submitted to the DAVID functional annotation tool, specifying the identifier in the form of the genes 'official gene symbol' and the species to which the list related to was specified to *Mus musculus*.

4.5.3.1 Functional Annotation Clustering based on Gene Ontology

The strategy to analyse the data was based on the following premise. Clustering by gene ontology (GO) specifically in relation to biological processes (BP), cellular component (CC) and molecular function (MF) can provide information on groups of genes that are represented in certain categories relating to BP, CC and MF. Clusters are classified into functional groups and assigned an enrichment score. Each cluster includes a list of terms that have 'similar biological meaning as a result of sharing similar gene members' (Huang et al., 2009). The enrichment score signifies the importance of the cluster to the input list of genes and the higher the core the more enriched the cluster. This enrichment score 'ranks the biological significance of the clusters based on the EASE scores of all enriched annotation terms' (Huang et al., 2009). The EASE score is a modified Fisher Exact P-Value and the smaller the P-value the more enriched the cluster (Huang et al., 2009).

Exploring the 3 functional categories separately, BP, CC and MF (Figure 38, 39 and 40 respectively) can make it easier to identify key GO terms in relation. Clustering data according to enrichment score identifies groups of GO terms for which gene counts are high highlighting the importance and potential relevance of these terms in the context of the project or experiment.

4.5.3.2 Biological Processes

In terms of Biological Processes, 5 clusters were identified (Figure 38). The cluster with the highest enrichment score (Cluster 1) includes the GO terms 'positive regulation of transcription', Cluster 2 contains groups of genes related to 'aging', 'cytokine-mediated signalling pathway' and 'cellular response to TNF'. These processes highlight the relation to senescence such as changes in gene expression as a result of regulation of transcription and TNF involvement which has been well-documented in relation to senescence (Khandaya-Pillai et al., 2017, Beyne-Rauzy et al., 2004, Li et al., 2017). This is supported by the TNF signalling pathway being identified using the KEGG function of DAVID as the pathway with the highest number of genes affected.

4.5.3.3 Cellular Components

Cellular Components analysis (Figure 39) identified components in which the input genes pertained to. These include as expected cytoplasm, protein complex, nucleus, extracellular space with the highest number of genes in relation. As is well documented and demonstrated in the model of senescence described in chapter 1, senescent cells undergo harsh morphological changes such as an increase in cell size and flattening. Wallis et al (2020) highlight the role of extracellular vesicles (EVs) in senescence and evidence the increased levels of EVs in senescent cells as part of the complex processes involved in the SASP. It was also suggested that this increase in EV production may be linked to the changes seen in lysosomal content of senescent cells as part of Beta-Galactosidase activity (Wallis et al., 2020). Such changes in lysosomal content were also observed in the SEN model described in chapter 2.

4.5.3.4 Molecular Function

Molecular function analysis identifies 2 clusters (Figure 40) drawing out GO terms such as Protein kinase activity, transferase activity, transcription factor activity, DNA binding and chromatin binding across the 2 clusters with DNA binding and Kinase binding have the greatest gene counts. DNA binding and Kinase binding are broad GO terms and transcriptional and translational changes are involved in many processes including regular cell functioning and induction or suppression of cellular senescence. For example, Kinase activity can pertain to the activation and succession of key pathways such as MAPK Kinase signalling.

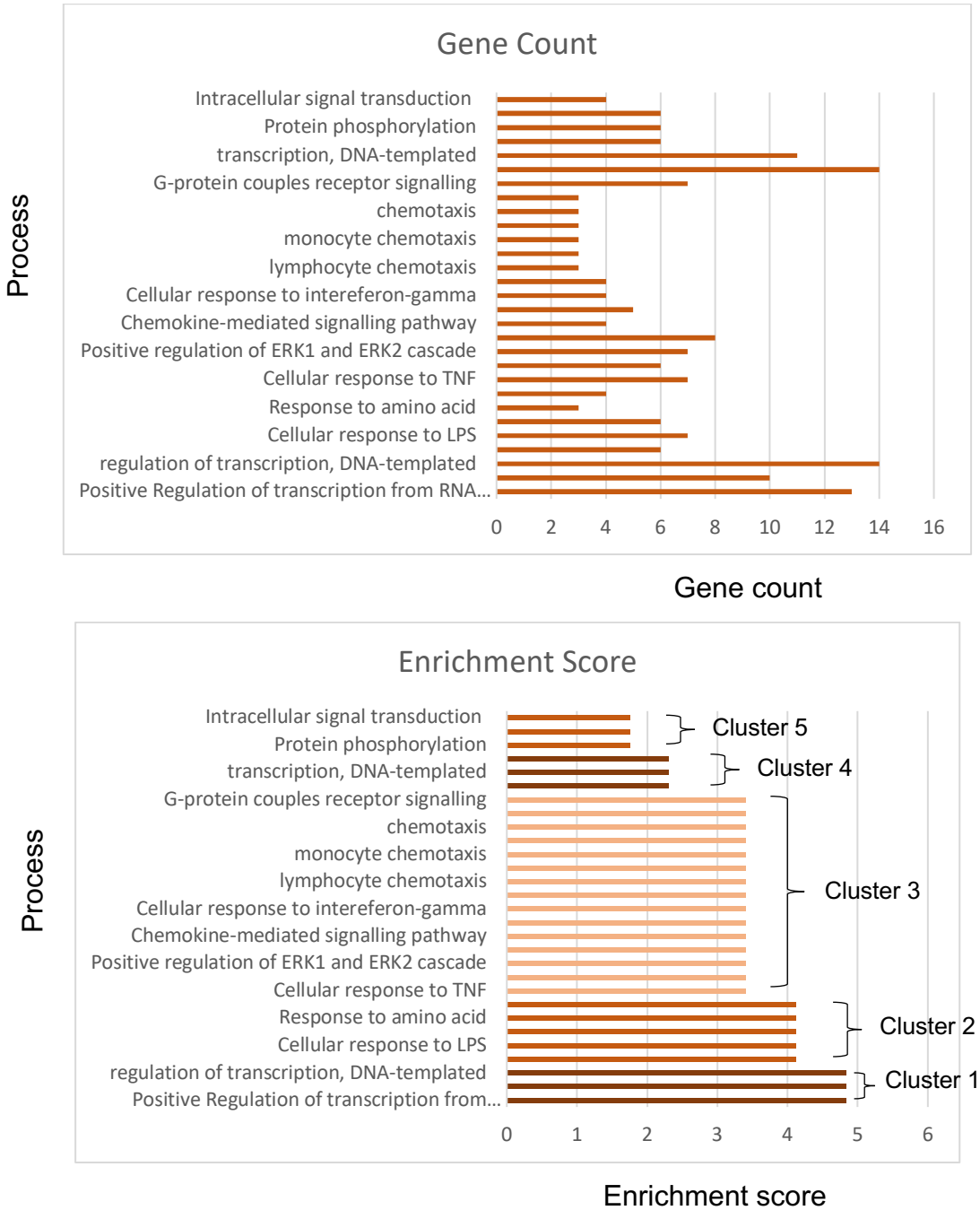

Figure 38: Biological Processes GO terms vs Gene Count and Enrichment score. Functional annotation clustering identified 5 clusters with varying scores of enrichments. The gene count shows the GO terms with the highest and lowest number of genes identified from the list provided that are affected in the biological processes.

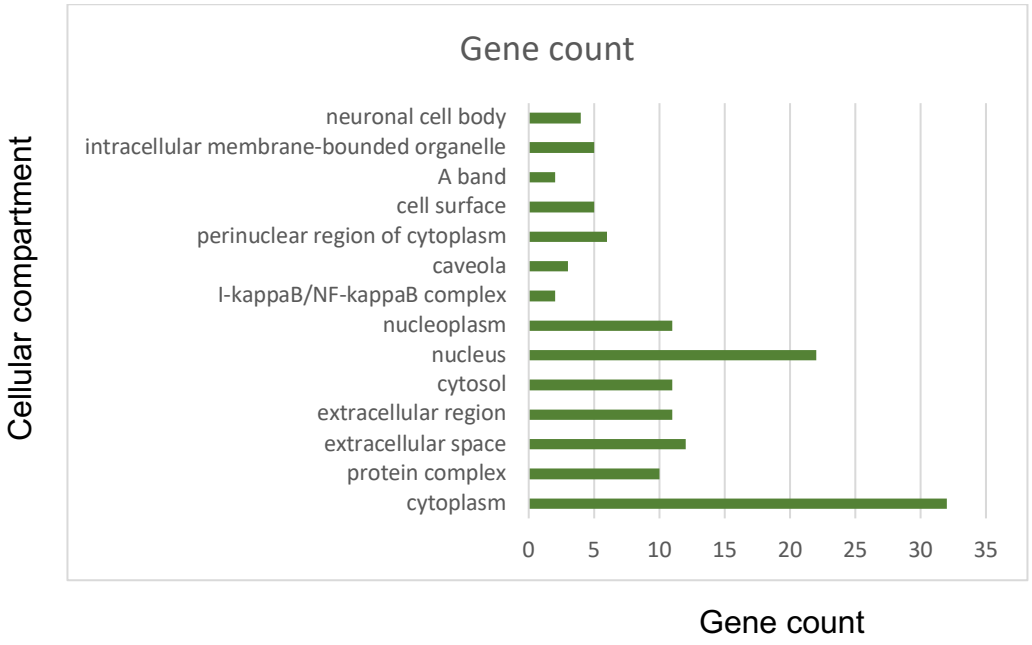

Figure 39: Cellular Compartments GO terms vs Gene Count and Enrichment score. Functional annotation clustering identified 2 clusters with varying scores of enrichments. The gene count shows the GO terms with the highest and lowest number of genes identified from the list provided that are affected in relation to cellular components.

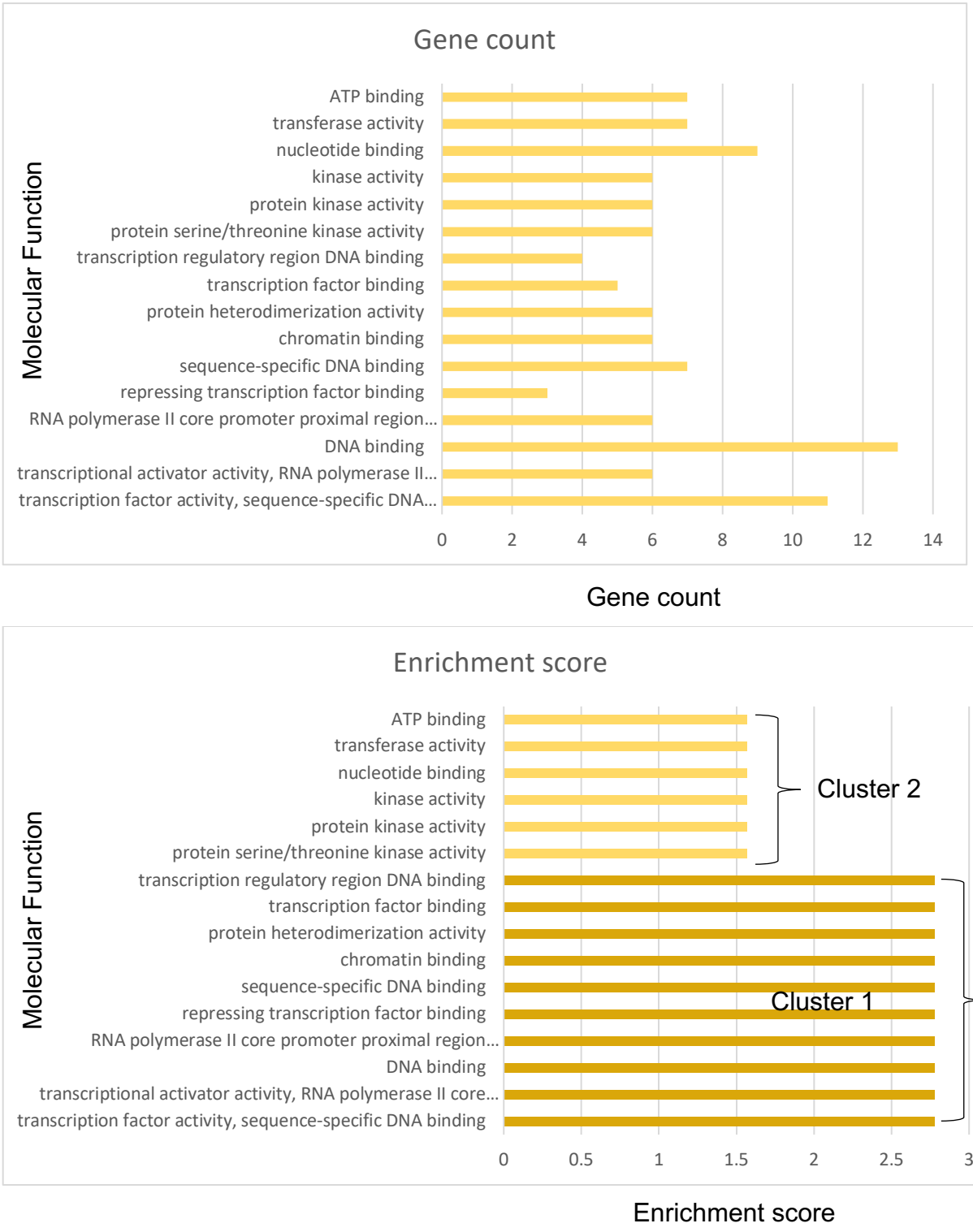

Figure 40: Molecular Function GO terms vs Gene Count and Enrichment score. Functional annotation clustering identified 5 clusters with varying scores of enrichments. The gene count shows the GO terms with the highest and lowest number of genes identified from the list provided that are affected in Molecular Function.

4.5.3.5 KEGG Pathway Function

Using the KEGG pathway function, key pathways pertinent to the list of genes input for DAVID analysis were identified. Pathway mapping may aid in identifying and developing potential therapeutic targets. With a focus on signalling pathways (Figure 41), TNF signalling and MAPK signalling pathways were identified as the two categories which included the greatest number of genes from the input list, with 12 and 11 respectively.

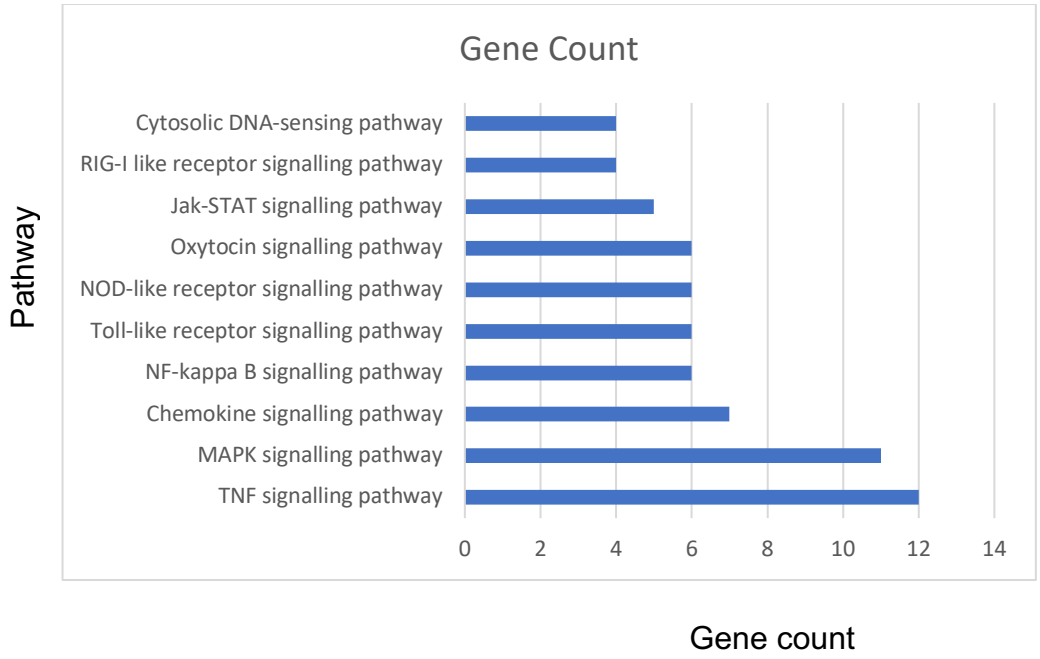

Figure 41: Signalling pathways identified by DAVID. Signalling Pathways with the highest gene counts include TNF, MAPK, NF-kappa B, chemokine signalling and Toll-like receptor.

4.6 Discussion

4.6.1 Upregulated Genes

A total of 38 genes were found to be upregulated across the samples and their controls. All genes in the treatment conditions and genes with a Log2(FC) value of 2 and above are discussed hereafter. Genes that showed the greatest Log2(FC) difference or were implicated in a treatment condition were further researched to identify their existing role and function along with any association to senescence. Any genes with a Log2(FC) +2 or above between CTRL and SEN and +1 and above in any nutraceutical treated samples were discussed for their relevance to senescence. These included Ccl7, Ccl2, Ccl20, Cxcl1, Csf1, Ifit1, Ifit3, Ifi44, Il-6, Areg, Smad7 and Oas2, and Iigp1 respectively.

4.6.1.1 CCL7

CCL7 Is a chemokine, also known as MCP3, is involved in the innate immune response and recruits' cells such as monocytes, neutrophils, eosinophils and basophils to inflammatory sites (Ford et al., 2019). CCL7 also plays a role in promoting tumour formation and metastasis (Liu et al., 2018).

CCL7 was found to be upregulated in SEN cells compared to CTRL. This is supported by current literature (Coppe et al, 2010) which dictates that CCL7 is upregulated in senescent liver stellate cells and is found to be overexpressed in prostate and skin fibroblasts. It must be taken into account that the references provided for this statement do not contain evidence of the same. There is limited concrete evidence around the presence and role of CCL7 in senescence but has been researched in aging. Valentine et al., 2017, found that CCL7 was overexpressed in type II alveolar epithelial cells harvested from young (8 weeks) vs old (20 months) mice (Valentine et al., 2017). The evidence further supports the SEN model established in this project and could be further validated using qPCR and chemokine detection techniques.

4.6.1.2 CCL2

CCL2, also known as MCP-1 (monocyte chemoattractant protein-1) is 'involved in the regulation of monocyte and macrophage migration and infiltration' (Deshmane et al., 2009), in order to aid during immune defence. CCL2 has been extensively researched in connection with senescence and aging. Its role in senescence is a part of the SASP. Ogho et al., 2015 found that CCL2 was upregulated in senescent human dermal fibroblasts and it plays a part in enhancing stem cell migration. Additionally, oncogene-induced senescent hepatic cells secrete CCL2 (Eggert et al., 2016). CCL2 as a component of SASP mediates paracrine senescence (Acosta et al., 2013). Gene and protein analysis showed increased expression of CCL2 in aged aortic vascular smooth muscle cells compared to young (Song et al., 2012). In Nanostring analysis CCL2 was found to be upregulated in SEN compared to CTRL cells. It is important to consider the limited number of replicates in the experiment therefore validation would be necessary in different model types to confirm.

4.6.1.3 CCL20

CCL20 (CC-Chemokine cysteine motif chemokine ligand 20) is a chemokine that solely binds to the receptor known as CCR6, to initiate 7-transmembrane-domain G-Protein coupled receptors (GPCRs). This sole relationship between CCL20 and CCR6 indicates their responsibility for 'tightly regulated functional roles' (Frick et al., 2016). Also known as MIP-3a (macrophage inflammatory protein 3 alpha), CCL20 is expressed in various organs and tissues such as skin, colon, prostate, cervix, lung and liver and may play a role in certain diseases such as HIV and Rheumatoid arthritis in relation to its receptor CCR6 (Osuala and Sloane, 2021).

CCL20 is known as a component of SASP that contributes to paracrine senescence. Acosta et al (2013) identified CCL20 as a SASP factor that mediated paracrine senescence through proteomic analysis of human and mouse OIS models (Acosta et al., 2013) and is generally considered to be upregulated in senescent cells (Davalos et al., 2010). This supports the gene expression

analysis results of CCL20 which was found to be upregulated in SEN cells compared to CTRL. CCL20 was found to be downregulated in SEN + HB compared to SEN, suggesting it may have anti-SASP effects. Holy basil may work by neutralising and interfering with the CCL20 mechanism of action.

4.6.1.4 CXCL1

CXCL1 is also a chemokine that plays a role in 'recruiting and activating neutrophils to combat microbial infection' (Sawant et al., 2016). It does this by 'activating a release of proteases and reactive oxygen species to neutralise the pathogen'. It carries out its function by binding to glycosaminoglycans and the CXCR2 receptor (Sawant et al., 2016). CXCL1, also known as GRO-a (Growth regulated protein alpha) is an inflammatory cytokine which 'promotes chronic inflammation in senescence as part of SASP' (Yamane et al., 2020). It has been documented that senescence can be induced through the CXCL1. Kim et al (2018) found that CXCL1 was capable of progressing the transformation of normal fibroblasts into senescent cancer associated fibroblasts in oral squamous cell carcinoma measured through cytokine array applications (Kim et al., 2018). Similarly de- activation of CXCL1/CXCR2, its receptor complex, was found to prevent oncogene-induced senescence in Kras mice and exacerbated tumour growth through proliferation in pancreatic ductal adenocarcinoma (Lesina et al., 2016).

Cai et al (2020) investigated the levels of CXCL1 along with other SASP related genes in three separate senescence induced mouse embryonic fibroblast models and aged models following SSK1 drug treatment, a new senolytic. Activity of CXCL1 was found to be downregulated in the treated group when measured in serum through ELISA and Total RNA sequencing (Cai et al., 2020) suggesting CXCL1 plays an important role in senescence. Our data shows that CXCL1 was upregulated in SEN compared to CTRL which further confirms findings by other studies and the successful establishment of the model. Literature shows that CXCL1 plays an important role in senescence, particularly in the progression of cancer and could potentially be used as a therapeutic target.

4.6.1.5 Iigp

Iigp (interferon inducible GTPase 1) also known as Igra6, is an interferon which is capable of anti-viral defense and inhibiting tumour cell proliferation (Cheng et al., 1991). Very limited research pertaining to its association to senescence exists and any information on Iigp would need to be considered as part of the IFN inducible defense response. Research by Kaiser et al (2003) showed that Iigp plays a role in Cis-Golgi organisation (Kaiser et al., 2003). It is regulated by IFN-y and plays a role in innate immunity and 'IFN-induced intracellular membrane trafficking' (Zerrahn et al., 2002). Qui et al (2018) showed that Gbp1 (from the same family of GTPase proteins) was found to be significantly reduced in the white adipose tissue of aged mice. They also found that Gbp1 knockdown macrophages underwent senescence and therefore may be important to macrophage activity in the process of aging (Qui et al., 2018). Our analysis showed that Iigp was upregulated in CTRL + HB cells and CTRL + PHY compared to CTRL cells but showed no changes in expression in SEN compared to CTRL or in SEN cells that were treated with Holy Basil and Phytol.

4.6.1.6 Ifit3

Ifit3 is part of the IFIT (Interferon-induced protein with tetratricopeptide repeats) gene family. It is expressed in minimal amounts under basal conditions but when faced with 'viral infection, PAMPs (pathogen-associated molecular patterns) and interferon they are found to be upregulated. They may also play a role in cell proliferation and migration' (Pidugu et al., 2019).

Our Nanostring analysis showed Ifit3 to be upregulated in SEN cells compared to CTRL cells. This is supported by existing literature. Colombo et al. (2018) found that Ifit3 to be upregulated in three different models of artificially induced senescence through transposable element analysis using RNA-sequencing (Colombo et al., 2018). Ifit3 has also been shown to be upregulated in TNF-a driven senescence in HUVECs compared to control (Khandaya-Pillai et al., 2017). Yamagami et al (2018) showed that fibroblasts, in the form of a replicative senescence model, from a Werner's syndrome patient expressed a higher level

of Ifit3. Werner's syndrome causes the appearance of premature aging in young people due to a mutation on the WRN gene. However, this study was only conducted with a single patient and a larger sample size would be needed to validate findings. Also, Werners is a genetic mutation on the WRN gene and has impairment in the aging process so a comparison cannot be easily made to an artificially induced senescent model (Yamagami et al., 2018).

Similar to Ifit3, Ifit1 belongs to the same family and is induced by interferon. Ifit1 was found to be upregulated in SEN cells compared to CTRL cells by a Log2(FC) value of 2.78. Recently, Park & Kim (2021) carried out an extensive transcriptomic analysis on senescent endothelial cells which also showed an upregulation of Ifit1 over a Log2(FC) value of 2.3, further supporting the SEN model (Park & Kim., 2021).

4.6.1.7 Ifi44

Ifi44 (Interferon induced protein 44) has been implicated in regulating antiviral response and immune response to autoimmune diseases. It has also been shown to play a role in antigen presenting and in NFKB signalling pathways (Pan et al., 2020). Ifi44 was found to be upregulated in SEN + Allicin cells compared to SEN cells. There is no existing literature that suggests Ifi44 specifically is affected by Allicin. However, Feng et al (2012) showed increased survival of allicin treated Balc/c mice infected with a parasite had increased levels of interferon-gamma (IFN-y). Furthermore, Human cytomegalovirus (HMVC) infected glioma cells treated with Allicin showed decreased levels of IL-6, a well-established SASP component and Interferon-B (IFN-B) ultimately showing reduced proliferation of cells (Yang et al., 2020).

Nanostring analysis also showed increased expression of Ifi44 in SEN cells compared to CTRL by a Log2(FC) value of 5.6. Gluck et al (2017) showed that Ifi44 was found to be upregulated in WI-38 senescent cells which also showed loss of lamin B1 when investigating cyclic GMP-AMP synthase (cGAS) and how the process of DNA sensing regulated cellular aging through cytosolic chromatin fragments recognition (Gluck et al., 2017).

Khandaya-Pillai et al (2017) studied the senescence driven by TNFa in human umbilical vein endothelial cells (HUVECs). Senescence was induced through repeated exposure to recombinant human TNF-alpha. When measuring interferon signature along with other interferon related genes through gene expression profiling by microarray analysis they also found Ifi44 to be upregulated in senescent cells compared to control. Even though there is limited research into Ifi44 and senescence in particular, there is research evidencing an association between interferons and cellular aging (Kim et al., 2009, Yu et al., 2015, Frisch & MacFawn, 2020).

4.6.1.8 Areg

Areg, also known as Amphiregulin, is a ligand of the EGFR (epithelial growth factor receptor. Its been found to be important in functions and responses such as infection, the immune system, inflammation and tissue repair (Ziass et al., 2015). Studies have shown Areg to be implicated in senescence. Pommer et al (2021) showed that Areg was induced in a OIS model of BRAF V600E transduced melanocytes. Deletion of Areg in the same model showed reduced senescent characteristics.

Nanostring analysis showed increased Areg expression in SEN cells compared to CTRL. It was also found to be upregulated in CTRL + PHY but had no effect in SEN treated cells. Recently Areg has been investigated in relation to senescence in the field of cancer but there is limited information on it in regard to aging (Xu et al., 2019, Jiang et al., 2019). Further investigation in replicative senescence models and artificially induced models would be required to ascertain its presence and role in the process of senescence.

4.6.1.9 Oas2

To combat viruses, the immune system is capable of producing antiviral cytokines, the most powerful of which is Interferon (IFN) which in turn induces IFN induced genes to further progress the antiviral response. OAS2 is a protein stimulated by IFN (Choi et al., 2015). Oas2, fully known as 2'-5'-Oligoadenylate

Synthetase 2, is an immune activated antiviral enzyme. It is involved in the synthesis of 2'-5'-Oligoadenylate for Rnase L activation and inhibition of viral replication through viral RNA degradation (Gu et al., 2016, Choi et al., 2015).

The OAS family of genes can be used to identify certain diseases in which they can be found to be upregulated. This is usually found in autoimmune diseases and chronic infection which accompany higher levels of inflammation. Existing literature highlights that Oas2 is upregulated in senescent cells. Mullani et al., (2019) showed the increased expression of Oas2 in senescent WI38 cells (Mullani et al., 2019). Oas2 is also shown to be upregulated in TNFa-driven senescent cells (Khandaya-Pillai et al., 2017) and is suggested to impact senescence through the OAS.RNASEL pathway.

Results showed that Oas2 was upregulated in SEN compared to CTRL. However, it was also found to be downregulated in CTRL + HB, ALL and PHY in comparison to baseline. Contrastingly no changes in expression were observed in SEN cells that were treated with the same compounds.

4.6.1.10 Smad7

Smad7 is an inhibitory protein that negatively regulates TGF-B (transforming growth factor B), involved in inhibiting the TGF-B/activin signalling and BMP signalling, its key to processes such as 'embryonic development, fibrosis, cell differentiation, regulation of immune response, tumorigenesis, inflammation and metabolic activity' (Chen et al., 2011). TGF-B signalling has been shown to be 'associated with age-related diseases and cellular senescence' (Tominga & Suzuki., 2019).

Our gene expression data showed an upregulation of Smad7 by a log2(FC) of 2.23 in SEN cells compared to CTRL cells. Recent data supports this, where Smad7 has been found to be upregulated in passaged normal human dermal fibroblasts (Kim et al., 2019). These studies were carried out using western blot experiments and corroboration would be needed in terms of levels of mRNA transcribed in the same model and conditions.

4.6.2.11 IL-6

IL-6 (Interleukin-6) is a cytokine that is a well-established component of the SASP and as a result is found to be upregulated in senescence (Kuilman et al., 2008, Rodier et al., 2009). Its predominantly known to play a key role in the actions of the immune system, with roles in both innate and adaptive immunity and supporting immunocompetence (Rose-John et al., 2017). Additionally, IL-6 also regulates cellular functions such as survival, proliferation and differentiation. IL-6 is known to increase with age as it 'exists in non-detectable amounts in the absence of inflammation' (Ershler, 1993, Puzianowska-Kuźnicka et al., 2016). Essentially it is regulated by NF-KB. Bonda et al (2018) evaluated the expression of p53 in an IL-6 mouse knockout model. p53 is known to be upregulated in aging and it was found to be reduced in knockout heart tissue compared to wildtype when measured with western blotting and mRNA analysis using qPCR, suggesting its high relevance to aging by diminishing the accumulation of p53 (Bonda et al., 2018).

Nanostring analysis showed an upregulation of IL-6 in SEN by a Log2(FC) value of 2.22 as would be expected in a senescence model. Studies suggest that IL-6 works through the activation of its downstream targets JAK/STAT3 to regulate senescence. IL-6 is also part of the paracrine response of senescence in provoking neighbouring cells to enter the same state (Vassilieva et al., 2020).

4.6.2.12 Csf1

Csf1 (Colony stimulating factor 1) also known as M-CSF is a cytokine involved in regulating macrophage differentiation from hematopoietic stem cells. It is a well-established component of SASP which aids in immune cell recruitment (Rihnn et al., 2019). It is commonly found upregulated in senescence. For example, Storer et al (2013) found an increased expression of Csf1 in embryo development in which senescence is a developmental mechanism (Storer et al., 2013). A study by Moon et al (2019) saw an increase in senescence markers in UV-irradiated nerve cells with the addition of GM-CSF (granulocyte macrophage colony stimulating factor), which included MMP-9, NF-κB1, and IL-1B (Moon et al.,

2019). In senescence accelerated mice (SAMP8) derived macrophages from bone marrow, the exposure to GM-CSF resulted in impaired proliferation compared to controls from senescent resistant (SAMR1) mice (Espia et al., 2008).

4.6.2 Downregulated Genes

Nanostring analysis identified 9 genes that were found to be downregulated as a result of condition or treatment to CTRL and SEN cells either with no treatment, or Holy Basil, Allicin or Phytol application. Genes that showed a negative Log2(FC) value of -1 and below or were implicated in a nutraceutical treatment condition were further researched to identify their existing role and function along with any association to senescence. These included C1s, Ccl2, Ccl20, C3, Fos, Myc, Myl2, Ptgs2 and Oas2.

4.6.2.1 C1s

C1s is a serine protease that forms the C1 complex by binding to another serine proetase called C1r. The C1 complex is key component of the complement system, specifically the activation of the classical pathway (Garnier et al., 2003). The complement system is largely a part of the innate immune system serving as a protective mechanism against infection. The activation of the classical pathway ultimately leads to the generation of C3 convertase, which is cleaved to produce C3a, an inflammatory mediator and C3b which attach to the surface of pathogens (Janeway et al., 2001) and act as opsonins, which aid in identifying foreign bodies for the process of phagocytosis (Winklestein, 1973).

Nanostring data analysis showed a downregulation of C1s in SEN + HB compared to baseline SEN cells by 1 Log2(FC). Literature on HB is extremely limited and further studies on the compound and its properties in different biological models is required to ascertain its effectiveness as a treatment. Perez-Roses et al (2017) showed that an active constituent of Holy Basil known as eugenol does show to induce senescence in human adipose derived stem cells. Telomere length was found to be decreased over a 48-hour study post treatment

(Perez-Roses et al., 2017). Even though the downregulation is exclusive to the comparison of HB treated SEN cells to SEN cells, it's important to consider the relationship between aging and the complement system to hypothesise potential mechanisms of action of Holy Basil. It would also be important to carry out further studies on Holy Basil in various models of aging and how it affects inflammatory markers in some age-related diseases.

A previous study by Medeiros Tavares Marques et al (2017) showed that C1s was found to be upregulated in senescent vs young human mesenchymal stem cells as part of an expression profiling analysis (Medeiros Tavares Marques et al., 2017). A large population study investigating complement activity based on age and sex revealed increased levels of C1 inhibitor, C5, C8 and C9 with age. A decrease in factor D and C3 was also found (Gaya de Costa et al., 2018). Since a contributing factor to age-related diseases is chronic inflammation also known as 'inflammaging' which is characterised by increased levels of inflammatory markers (Ferrucci & Fabbri., 2018), Cedzynski et al (2019) suggests that the complement system plays a role in preventing chronic inflammation (Cedzynski et al., 2019). However, our projects senescence model does not exhibit any changes in C1s expression compared to CTRL, this could be a result of the type of model and further investigation is warranted to determine the role of C1s in senescence.

4.6.2.2 C3

C3 mRNA expression was found to be downregulated by a Log2(FC) value of 3.3 in the conditions of CTRL+HB compared to CTRL and of 1.64 in SEN + HB compared to SEN. C3 levels show no change when subjected to other treatments or in the SEN cells when compared to CTRL cells. Similar to C1s, this indicates that HB may have an effect on the Classical pathway of complement. The downregulation of C1s would also result in the decreased production of C3 downstream as they are part of the same pathway.

Previous age-related studies in relation to Complement component C3 suggest it may play an important role in the process of senescence. These studies mostly

focus on its role related to retinal health. Shi et al (2015) found that in C3 deficient mice (Gene Knockout) compared to an age, strain and gender matched wildtype control synapse loss in the hippocampus of the brain is affected. Older control mice showed loss of synpases compared to C3 KO mice which exhibited better performance on memory and learning tests highlighting the adverse effects of C3 in aging of the brain (Shi et al., 2015).

Roginska et al (2017) carried out studies on C3 deficient mice which showed increased expression of genes related to neural retinal physiology maintenance, improved autophagic activity, reduced 4-hydroxynonenal (4-HNE) (oxidative stress marker) and caspase 3 expression, slowed deterioration of retinal thickness and bioelectrical function (Roginska et al., 2017). A study by Wan et al (2020) investigated C3 deficiency in kidney aging. They found increased expression of C3 in aged wildtype mice. However, in C3 deficient mice, 'levels of inflammation and fibrosis were decreased' (Wu et al., 2020). Various studies show that complement C3 may play an important role in the aging process would be worth further investigation in multiple models of aging and senescence in order to determine potential targets for age-related disease therapies.

4.6.2.3 Fos

Fos is a proto-oncogene, which when downregulated can encourage 'oncogenic progression'. It is a gene involved in cell proliferation and differentiation. (Velazquez et al., 2015). It forms a heterodimer with Jun to form transcription factor activator protein 1 or AP-1. (Garces de los Fayos Alonso et al., 2018) AP-1 is able to bind to DNA through its leucine-zipper domain to control cell proliferation and apoptosis through cell cycle regulation. (Garces de los Fayos Alonso et al., 2018)

Nanostring analysis shows that mRNA expression of Fos was downregulated by a Log2(FC) value of 3.21 in SEN cells compared to CTRL. It was also downregulated by 1.06 Log2(FC) in CTRL+HB cells compared to untreated CTRL. Fos is usually found to be upregulated in models of senescence according

to existing literature. However older studies originally exhibited the opposite in which Fos was found to be downregulated.

The role of Fos in senescence has been widely known for many decades. With early studies of the protein in senescent human fetal lung fibroblasts basal levels of c-fos mRNA were found to be decreased (Seshadri and Campisi, 1990). However more recent publications suggest it can be upregulated dependent on cell type or model. Rivard et al (2000) demonstrated that expression of c-fos was found to be increased in old (4-5 years) vascular smooth muscle cells extracted from New Zealand Rabbits compared to young (6-8 month old) (Rivard, Andres and Principe, 2000). Debacq-Chainiaux et al (2005) found that human skin fibroblasts induced into senescence by UVB exposure were found to have elevated levels of c-fos mRNA when analysed using real-time RT-PCR (Debacq-Chainiaux et al., 2005). The mixed results for Fos expression across literature highlights the need to consider the effect, the type of model and senescence induction can have on gene expression.

4.6.2.4 Myc

MYC is a proto-oncogene and is a key regulator of cell cycle entry and proliferation. Whilst it functions as a transcription factor, if de-regulated it can lead to uncontrolled cell replication and promote tumorigenesis. Nanostring analysis showed Myc is downregulated in SEN cells in comparison to normal CTRL cells which is somewhat contradictory to existing research.

In relation to existing literature Hofmann et al., (2015) were able to show that Myc haploinsufficient ($Myc^{(+/-)}$) mice exhibited an increased lifespan along with resistances to numerous age-related diseases such as osteoporosis, cardiac fibrosis and immunoscenescence. Particularly affected were metabolic pathways that regulate aging. These mice were found to have a higher metabolic rate compared to $Myc^{(+/+)}$. It is widely known that metabolic activity depletes with age (Hofmann et al., 2015). An abundance of Myc can lead to activation of tumour suppressor mechanisms in the form of apoptosis and senescence (Hydbring & Larsson, 2010).

Originally considered as a key player in halting senescence c-Myc activation is now also known to promote oncogene-induced senescence, by increased p14ARF transcription which has downstream affects on p53 which in turn accelerates cellular aging (Ko et al., 2018). Myc clearly plays an important role in senescence, however none of the nutraceutical treatments seemed to have an effect on Myc expression.

4.6.2.5 Myl2

Myl2 or Myosin light chain 2 is an EF-hand calcium binding protein and a form part of the sarcomeric component of striated muscle of the heart muscle (Sheikh et al., 2015).Myl2 was found to be downregulated in SEN cells compared to CTRL cells in Nanostring gene expression data by a Log2(FC) value of 1.27.

Previously Myl2 has been shown to be upregulated in adult hearts compared to fetal hearts (Acun et al., 2018). Lin et al (2018) showed in a recent study increased expression of Myl2 in the skeletal muscle of 24 month old mice compared to 3-month old mice from transcriptomic analysis by high throughput RNA sequencing experiments (Lin et al, 2018). Otherwise there is limited information on how Myl2 expression is affected in specific senescence based models and there is focus on aged heart studies. Further information on senescence and Myl2 is needed in various models however since it is a protein pertaining to heart formation and function it would be worth investigating in various heart/muscle cell based senescence models.

4.6.2.6 Ptgs2

Ptgs2, Prostaglandin-endoperoxide synthase 2, also known as COX-2 (cyclooxygenase- 2) is an isoenzyme of Ptgs. Ptgs is vital to prostaglandin biosynthesis (GeneCards, 2021). Prostaglandins are ‘lipid autacoids derived from arachidonic acid’ (Ricotti and Fitzgerald, 2011). They are required in the normal functioning of processes such as immune function, reproductive biology and gastrointestinal health (Williams et al., 1999). PTGS1, the other isoform is found

to be constitutively expressed in cells whereas PTGS2 is induced in the event of an inflammatory response (Ricotti and Fitzgerald, 2011), known mostly as a pro-inflammatory gene.

Our gene expression data shows that Ptgs2 mRNA was downregulated in the presence of HB when applied to CTRL cells however it was upregulated in SEN cells compared to CTRL. Further sample repeats would be required to ascertain the effect of HB in relation to Ptgs2 and the activity of cyclooxygenases in general. To support Nanostring results, Ptgs2 or COX-2 is generally found to be upregulated in senescence models. For example, it was found to be increased in senescent human dermal fibroblasts and when blocked by a COX-2 inhibitor called NS398, markers of senescence in cell growth, morphology and SA-B-Gal studies were 'partially inhibited'. These results were also consistent in NF-KB and H_2O_2 induced senescence models (Zdanov et al., 2007). However other COX-2 inhibitors such as Celecoxib and Nimesulide had the opposite effect and contributed to the progression of senescence, studied on a translational level (Kim et al., 2007). Previous literature shows that COX-2 may play an important role in the progression of senescence and further studied in multiple models would be essential to discovering potential therapies.

4.6.3 Functional Annotation analysis using DAVID

4.6.3.1 Pathways identified by KEGG function

KEGG function analysis identified multiple pathways implicated from the input gene list. Out of the many signalling pathways, a focus on TNF and MAPK signalling pathways are discussed below. These 2 pathways showed the highest enrichment scores.

4.6.3.1.1 TNF Signalling Pathway

TNF (Tumour necrosis factor) is a major pro-inflammatory cytokine, mostly produced by monocytes and macrophages, and is known to be involved in and affect numerous signalling pathways (Holbrook et al., 2019). It exists in the form

of a 26kDa transmembrane protein located on cell surfaces ready for cleavage. TNF has two receptors, TNFR1 and TNFR2. As shown in Figure 42, the downstream effects of TNF activation through TNFR1 are capable of recruiting TRADD, tumour necrosis factor receptor type 1 associated DEATH domain protein. TRADD sets in motion programmed cell death eventually leading to apoptosis (Holbrook et al., 2019). The pathway through different downstream targets which involve MAPK and NFKB also promotes cell survival, inflammation and induction of immune cell proliferation.

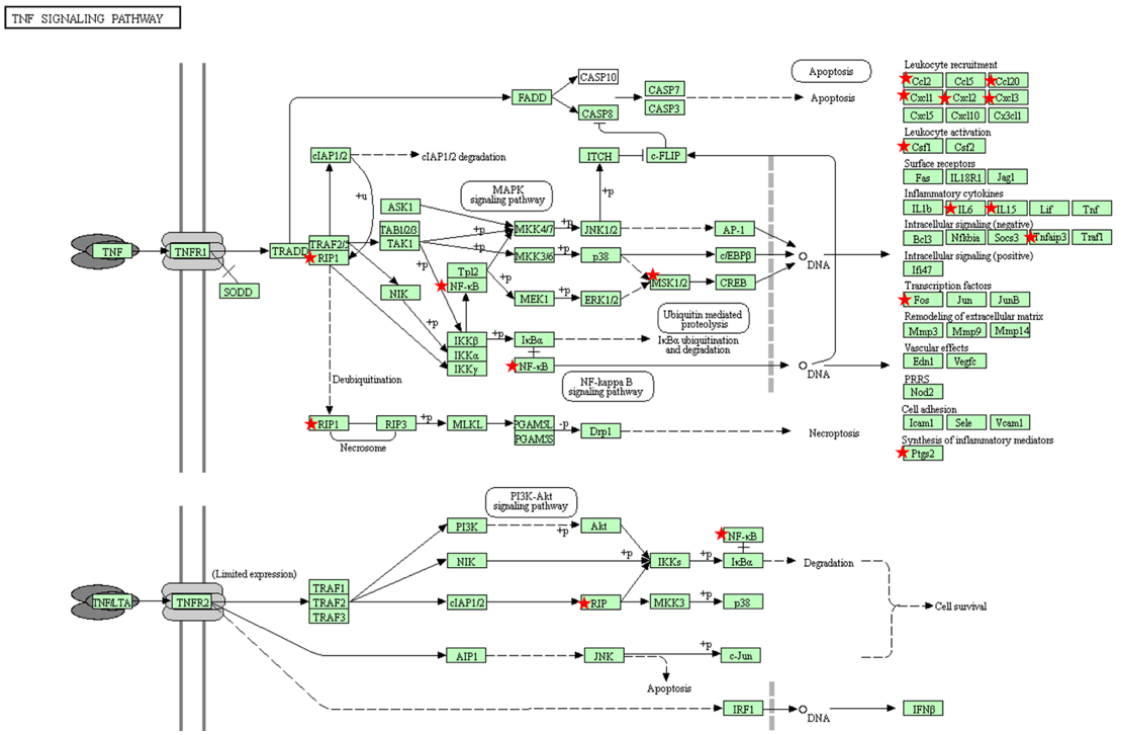

Figure 42: TNF signalling pathway. The red stars show the genes which were identified to be differentially expressed with Nanostring analysis (Taken directly from Huang et al., 2009)

Previous data has shown that TNF, particularly TNF-a is capable of inducing senescence. Li et al (2017) showed the cytokine promoted premature senescence of rat nucleus pulposus (spinal cord) cells. In addition, when the PI3K/Akt pathway was inhibited TNF-a induced senescence did not occur. (Li et al, 2017). However, a study conducted by Green et al (2016) contradicts this in which transmembrane TNF-a removal on endothelial colony forming cells induced senescence but 'expression of transmembrane TNF-a on ECFCs selects for higher proliferative potential' (Green et al., 2016).

DAVID analysis of the Nanostring gene list in relation to TNF signalling illustrated in figure 42, shows upregulation of Rip1, a downstream target of TNF. RIP1 is a kinase involved in initiating various branches of the TNF signalling pathway through complex formation with TRADD and decides whether a cell survives or dies (Christofferson et al., 2014).
With further downstream targets such as NFkB and MSK1/2 also known as Rps6ka5, a ribosomal protein kinase involved in inflammatory gene regulation by suppressing RELA and downregulating expression of inflammatory genes (Gene Cards, 2021). Even further downstream targets are shown to be affected such as Ptgs2, IL6 and various leukocytes.

4.6.3.1.2 MAPK Signalling Pathway

MAPK or Mitogen-activated protein kinase signalling pathway plays a key role in various cellular processes. These include but are not limited to proliferation, differentiation, immune defence and cell death (Soares-Silva et al., 2016).

MAPK signalling works through three different ‘modules’ which are initiated through ERK1/2, JNK1/2/3 and p38 kinase. The ERK Pathway is initiated in response to ‘growth factors, hormones and proinflammatory stimuli’. The ligand binds to receptor tyrosine kinase (RTK) to activate a G protein called Ras. In turn activates Raf, which phosphorylates MEK to then induce ERK1/2 activity (Soares-Silva et al., 2016). ERK1/2 then allows for transcriptional regulation of key genes. In the case of the DAVID analysis carried out NFKB, cPLA2, Myc and Fos were differentially expressed (Figure 43), all of which have been shown to effected in senescence (Jing and Lee, 2014, Debacq-Chainiaux et al, 2005, Hydbring & Larsson., 2010, Gentili., 2004).

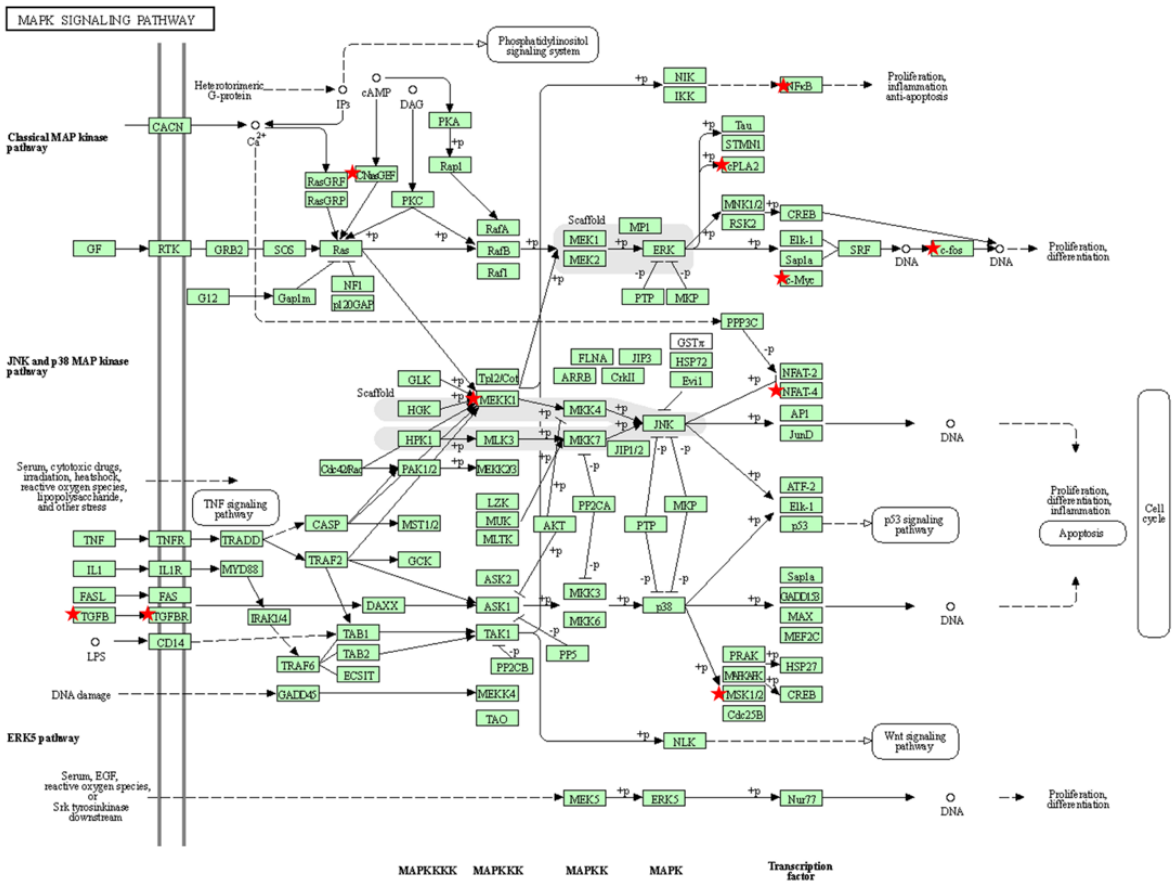

Figure 43: MAPK signalling pathway. The red stars show the genes which were identified to be differentially expressed with Nanostring analysis (Taken directly from Huang et al., 2009).

The DAVID Analysis allows for in depth knowledge of key genes, processes, and pathways involved in the input gene list. By discovering which processes and pathways are affected by the differential expression of the input genes it can provide further information to continue investigation. For example, with the above information, further analysis of TNF and MAPK signalling pathways could be carried out through profiling panels. Custom made panels of pathways consisting of key genes pertaining to it can be used to see which proteins are phosphorylated or genes are overexpressed. Further validation would allow for the identification of key targets or understanding of mechanisms involved in senescence and the effects of potential senolytics and senostatics.

4.7 Conclusion

As seen in the Nanostring analysis the majority of differential gene expression was identified in SEN vs CTRL cells and could identify processes and pathways related to senescence. A minimal number of genes were affected by nutraceutical treatments therefore, we were unable to determine any key processes or pathways that may have been affected by the treatments. Genes with the most differential expression were described and discussed and how their expression relates to senescence and the effect the treatment has on the expression of the gene. For future consideration, the Nanostring analysis should be performed in a number of repeats to ensure consistency of data, as it was only carried out with one replicate only (due to restrictions associated with COVID Lockdown). In addition, it must also be taken into account that these inflammatory based genes provided within the panel may not be suitable candidates for regulation by nutraceutical treatment, therefore other panels should be assessed for their suitability. However, although the Nanostring analysis has not enabled the derivation of concrete conclusions in regard to the effect of treatments, the data presented clearly shows that it is a valuable pilot study to assess the suitability of the technique for such investigations and to gather preliminary data to inform further investigations.

Nanostring analysis provided a substantial amount of varied data on gene expression in SEN vs CTRL cells and following nutraceutical treatments. Due to Holy Basil, Allicin and Phytol having limited existing research in relation to senescence definitive conclusions cannot be reached but data discussed warrants further investigation of nutraceuticals.

4.7.1 The Model

The Nanostring analysis of inflammation related genes in Control and Senescent cells treated with various nutraceutical compounds was able to provide information on the effects of these treatments on inflammation related gene expression. Majority of upregulated and downregulated genes shown in the analysis are supported in data seen in existing literature in regard to senescence.

It has been established that replicative senescence acts through telomere dependency, which shorten with every cell cycle replication, specifically through the $p21^{CIP}$ pathway. Whereas, models induced through stress, which work in a telomere independent manner activate senescence through $p16^{INK4A}$ (de Jesus & Blasco, 2012). Therefore, it is difficult to make assumptions about the transferability of research across models particularly in a field such as senescence.

It also important to consider that the SEN cell cultures may not be homogenous and in fact include a mixture of cells that may have avoided or escaped senescence or may have undergone apoptosis during marker analysis. Markers of senescence investigated during this study are not definitive characteristics of cellular aging which is why multiple markers were assessed to ensure a reliable model.

4.7.2 Further Validation

Various genes, whose role in senescence is supported existing research and published studies, are differentially expressed in the SEN vs CTRL cells and following treatment, such as; Interferon related genes, SASP related factors would need to be further validated through mRNA expression using qPCR or further Nanostring analysis using a custom panel at a transcriptional level and through protein detection methods such as western blotting to measure at translational level. The genes that were affected by Nutraceutical treatment such as Oas2, C3, Ccl20, C1s, Fos, Ptgs2, Iigp, Ifit3 and Ifi44 could be further investigated by applying Holy Basil, Allicin and Phytol using other methods and in different senescence models starting with a replicative senescence model and measuring telomere markers to identify mechanism of action.

5 Final Discussion

5.1 Statement of Novelty

The model established in Chapter 2 is a novel model in regard to the method of induction used in this particular cell line. Other studies have induced senescence in L929 using Pseudolaric Acid B (PAB) (Yu et al., 2013), Hydrogen peroxide when investigating oxidative stress and damage (Park et al., 1992, Tsai et al., 2012, Jose et al., 2019 Tsai et al., 2020) and recently irradiation by UVA (Ribeiro et al., 2020). In accordance with existing literature researched by authors of this study this is the sole model to use X-Ray based irradiation in L929 murine fibroblasts.

The purpose of this study was to identify a potentially novel plant-based compound that could be used as an anti-senescence treatment. According to existing literature Holy Basil has not been researched on as a therapy for cellular senescence or tested in a senescence model. It has been alluded to as potentially having anti-aging effects when its antioxidant properties were being investigated. This was particularly noted in the study of its effects in cognitive function decline in relation to age-induced diseases such as Alzheimer's (Cohen, 2014).

Allicin has been investigated in a few limited senescence or aging related studies such as in an oxidative stress cell model (Lin et al., 2017), in vivo regarding osteoporosis related frailty (Yang et al., 2020) and in the effects of allicin on the cancer cell lines MCF-7 and HCC-70 treated with doxorubicin to induce senescence (Rosas-Gonzalez et al., 2020). From the review of existing literature allicin has not been investigated in a DNA-damage induced senescence model.
The sole study which investigated phytol in a senescence model was carried out with the use of hydrogen peroxide (Jeong, 2018). This PhD study attempted to research if the effects of phytol could be replicated and if the compound had the same effect in a DNA-damage induced senescence model.

5.2 Establishing a model

A mouse cell line was selected for development of the irradiation induced senescence model. A mouse fibroblast cell line was used with the aim being to use an induced model rather than a replicative model to optimise measurement of senescence markers and effects of nutraceuticals more quickly in comparison to setting up a replicative senescence model particularly when numerous markers are required to establish senescence as there is no universal characteristic. The plan was then to confirm and validate results in an ex-vivo model where harvested mouse fibroblasts can reach senescence in 5-6 passages. However due to the events of the COVID-19 pandemic, the harvesting and culturing of mouse cells was not possible. The disadvantages of using a mouse fibroblast cell line is that they are an immortalised cell line and continue to divide indefinitely this is not usual of *in vivo* cells, they may also express different genes to normal cells and would be more resistant to the induction of senescence. Due to this disadvantage the aim was to use an *ex vivo* mouse tail fibroblast model was set up to test the nutraceuticals on as a form of validation of transferable effects. The purpose of establishing an in-house model would provide me with a method to produce senescent cells infinitely. Using senescent cell lines can come with their own drawbacks. These would be cell lines that display oncogene-induced senescence i.e overexpression of genes such as *Ras.* The process of aging is largely attributed to the shortening of telomeres which eventually is recognised as DNA damage. It is only fitting to test a model that mimics the same response pathway – the DNA damage response pathway. This is different to the process of oxidative stress which is generally recognised as an imbalance between ROS production and accumulation and antioxidant defences which can ultimately lead to DNA, cellular and tissue damage (Pizzino et al., 2017, Betteridge, 2000). Therefore, a DNA-damage induced senescence model using irradiation would allow for a better likeness to replicative senescence without the requirement to carry out multiple passages. Irradiation is a commonly used stimulus for inducing senescence, alongside replicative and drug induced senescence. Use of exogenous drugs to induce sensescence carries a source of error between different batches/lot numbers used across the study. By using the irradiation protocol and keeping the identical settings on the X-Strahl machine for every

induction this source of error was mitigated. Additionally, using the radiation was a more cost effective method, due to having access to our in house radiation facility, and also a safer method, with both bleomycin and doxorubicin having a number of health hazards associated with them, should accidental exposure occur. Further into the study, the nutraceuticals could be tested on a replicative senescence model by harvesting primary mouse fibroblasts and passaging until senescence which would take up to 5 or more passages as opposed to human primary cells requiring serial cultivation upwards of 50 passages to achieve replicative senescence (Appendix A). This study allowed for a convenient, time-efficient and relatively cheap model to be produced which would provide plentiful cells for preliminary experiments, the results of which could then be confirmed in the more time consuming and cell number limited primary cell replicative senescence model.

5.3 The need for a universal standard

Senescence research is carried out in different models across the globe. These differences in models highlight the fact that comparisons for therapies cannot be made if research groups use separate, contrasting platforms for experimental work. The need for a universal standard is critical. Ideally the most suitable model for research would be a human based replicative senescence model. This would allow researchers to compare results and draw outcomes in the form of large meta-analyses. This would allow scientists to make more accurate assumptions when transitioning to *in vivo* models and ultimately clinical trials.

5.4 Heterogenous populations: *in vitro* and *in vivo*

Another issue affecting senescence research but is not exclusive to it is the occurrence of heterogenous populations. A recent paper by Kirschner et al (2020) highlights that the emergence of senescence heterogeneity is fuelled by cell type and stimulus. When different cell types undergo senescence induction, they may all present with different markers and characteristics. The paper also outlines how even different oncogenes can result in opposing markers. For example, ‘Ras induced senescence in human dermal fibroblasts show the typical increase in cell

and nuclear size whereas overexpression of Raf in the same cell type does not' (Kirschner et al., 2020). Other examples pertaining to the different effects of the same senolytic in different senescence models, such as 'Fisetin being capable of having senolytic effects in HUVECs but not in IMR90s (human lung fibroblasts).' This adds to the weighting not all senescence therapies will work the same for all models. The senolytic or senostatic effects of compounds may be positive in a particular cell model compared to another, defending the necessity for a universal cellular senescence model. This heterogeneity in senescence cell cultures could potentially be overcome with marker specific cell sorting through flow cytometry in research as explored by Hewitt et al (2013) or marker targeted drug delivery as investigated by Cai et al, using ß-Galactosidase (Cai et al., 2020). This heterogeneity, while prevalent in tissue, is a confounding factor when standardising an *in vitro* model.

Kirschner et al (2020) also refers to evidence of primary senescence (replicative senescence, DNA damage induced, oncogene induced, oxidative stress induced) and secondary senescence (paracrine senescence and recently juxtacrine notch signalling) having different transcriptional signatures (Teo et al., 2019). This could explain the contrasting regulation of certain genes investigated in the previous chapter with the transcriptomic analysis of SEN models. The discrepancies between characteristics and markers of different models as referenced above also translates to how important it is to standardise a model and factor this heterogeneity when researching senescence.

This heterogeneity not only effects markers of senescence but also how senescence therapies work across different models. It is important to reiterate that not just the compounds investigated in this study, but all potential senolytic and senostatic drugs should be tested across various, researcher-agreed platforms to ensure results and responses are consistent and therefore likely to be transferable into human models and trials.

5.5 Procurement and preparation of Plant based compounds

The preparation of plant-based compounds or extracts can have an effect on their potency, bioavailability and quantity. The solvent used, temperature and duration of extraction can all affect the quality of the final product and with numerous methods of extraction as described by Zhang et al (2018). This highlights the need for extraction, fractionation, isolation and storage procedures to be optimised and regulated across studies (Abubaker & Haque., 2020) alongside an international research community effort to issue specific information by companies regarding products, as is the case for some *in vivo* modelling.

5.6 Defining Holy Basil, Allicin and Phytol as Senescence Therapies

Based on existing literature, Holy Basil, Allicin and Phytol have shown to exhibit properties that may potentially be useful as senescence therapies. They have already been shown to have certain properties such as antioxidant and anti-inflammatory properties and therefore could potentially have the capability of negating the effects of senescence. Having not been assessed thoroughly in a senescence based model these three compounds were chosen to discover potential novel therapies for use. Holy basil and Allicin were primarily chosen for their high phenolic content (Panchal & Parvez., 2019, Gajula et al., 2009) which has shown to contribute towards anti-senescence in compounds such as olive phenols and senescence in flowers has been associated with decreased phenolic content (Ahmad & Tahir, 2016). Phytol had shown promising results in a previous study (Jeong, 2018). With compounds showing different effects in different models, Phytol was selected in this capacity to see if its senostatic potential could translate across cell types and to further confirm and validate its use as an anti-senescence therapy. Natural or plant based senolytics may be better than synthetic drugs due to fewer or lesser side effects, reduced toxicity and are more amenable to a dietary lifestyle. For example, some types of diet have been associated with the prolonging of lifespan such as the Mediterranean diet (Capurso et al., 2019). Diet induced weight loss was also found to reduce senescent cell number in weight cycled mice compared to obese mice (List et al.,

2016). This study indicates that these nutraceuticals may also have senolytic and senostatic properties (Figure 44) and resulted in changes in gene expression (Figure 45). In order to confirm this, they would need to be tested across multiple senescence platforms with varying cell types and stimuli for induction of senescence. Also, it is important to consider that Holy Basil has been shown to have extensive radioprotective effects according to multiple cancer studies when treated prior to radiotherapy (Baliga et al., 2016). Therefore, Holy Basil would need to be investigated in models with no irradiation involvement. It also suggests that Holy Basil may have better senotherapeutic effects prior to senescence induction. In order to fully assess the effects of these plant- based compounds it would be of utmost importance to repeat experiments to ensure efficacy of treatments. Key factors to consider in future work that would need to be evaluated is duration of doses, application of treatment prior or post induction of senescence, if application of treatment needs to be continuous to be effective and type of model.

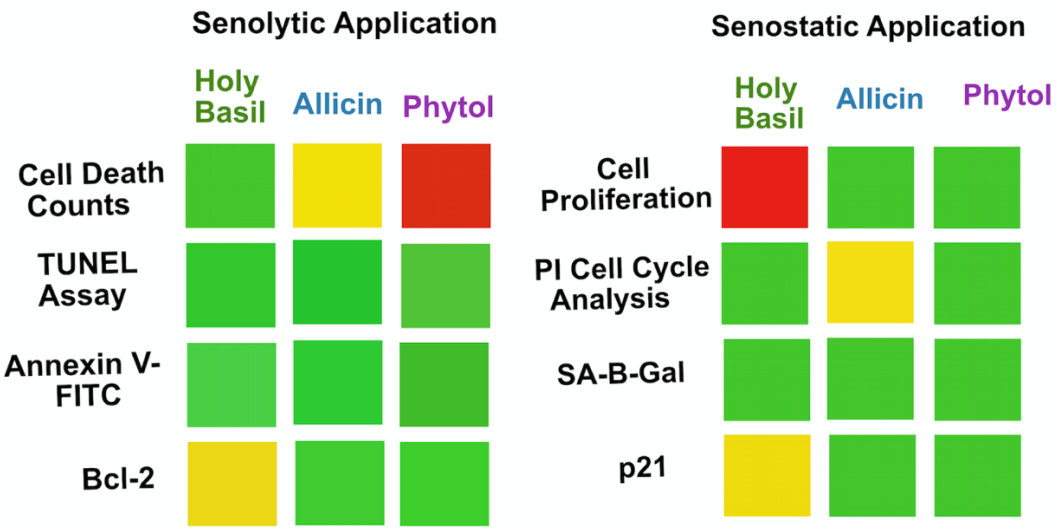

Figure 44: Traffic Light based diagram highlighting the effects of Holy Basil, Allicin and Phytol in SEN + treatment cells compared to SEN baseline. Green = Positive effect/Increased result, Yellow = no change, Red = Negative effect/decreased result. Outcomes of analyses is varied across treatments.

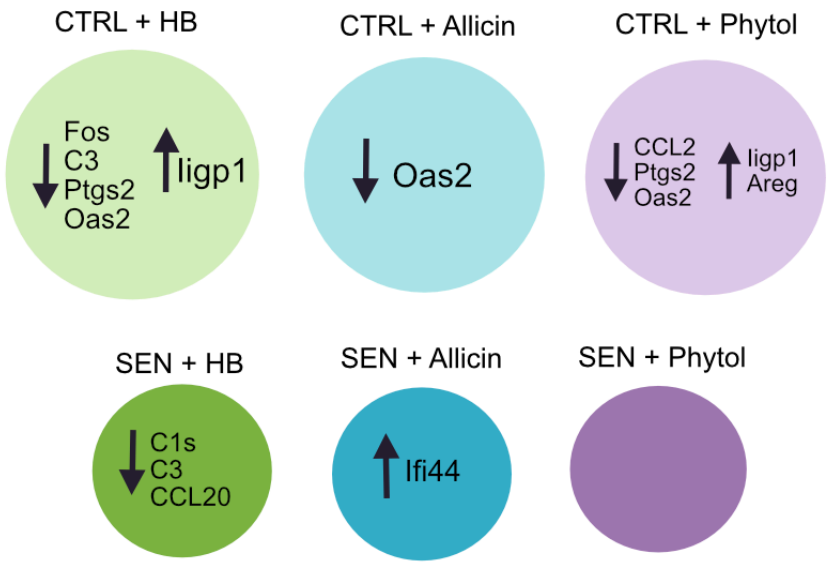

Figure 45: Genes identified that showed an increase or decrease in expression in CTRL and SEN + treatment cells compared to CTRL and SEN baseline when analysed using Nanostring. Application of Holy Basil to CTRL cells showed an increase in Iigp1 and decrease in Fos, C3, Ptgs2 and Oas2. SEN + HB showed dowregulation of C1s, C3 and CCL20. Allicin treatment in CTRL resulted in decreased Oas2 expression and in SEN it increased Ifi44 expression. CTRL + Phytol showed upregulation in Iigp1 and Areg and downregulation of CCL2, Ptgs2 and Oas2. However, in SEN + Phytol no genes showed differential expression.

5.7 Nutraceuticals: Marketed & Sold with limited evidence of efficacy

The consumer market is flooded with plant-based compounds claiming to provide health benefits to address an endless list of human ailments. Compounds like curcumin, garlic extract and holy basil supplements can be found available for purchasing through online portals. However, these supplements rarely come with clinical evidence to show beneficial effects of use not to mention the varying regulatory systems they go through across countries. In fact, use of these supplements could prove to be detrimental to health if taken with prescription drugs and an adverse reaction were to occur.

5.8 Conclusion

In this study an irradiation-mediated senescence cell line based model was developed and subsequently utilised in the general investigation of Holy Basil, Allicin and Phytol as potential senolytic and senostatic therapies. Overall, results indicate that all three nutraceuticals could be effective in combatting DNA-damage associated senescence when it becomes detrimental to health at an older age as a result of the exhaustion of DNA repair mechanisms. Further research of these plant-based compounds would need to be carried out in order to fully assess the benefits of these nutraceuticals. Additional work would be required to confirm low toxicity to healthy cells, define bioavailability, mechanisms of action and scrutinise long-term side effects. With the need to improve quality of life in a growing population of the elderly and combat age-related diseases it is important to continue researching into how and which plant-based compounds can be beneficial without harmful reactions and gather a greater biological understanding of the phenomenon of Cellular Senescence.

APPENDIX A

Thesis submitted for the degree of
Doctor of Philosophy

By
Amanpreet Kaur (BSc)
Department of Respiratory Sciences
University Of Leicester

May 2021

Appendix A Contents

Figure G1: Percentage of DEAD CTRL and SEN cell count following senostatic application.

Figure H1: Propidium Iodide Flow Cytometry analysis for L929 Fibroblast cells before serum starvation (BSS).

Figure H2: Propidium Iodide Flow Cytometry analysis for L929 Fibroblast cells before serum starvation (BSS).

Figure H3: Propidium Iodide Flow Cytometry analysis for L929 Fibroblast cells after serum starvation (ASS).

Figure H4: Propidium Iodide Flow Cytometry analysis for L929 Fibroblast cells after serum starvation (ASS).

Figure H5: Propidium Iodide Flow Cytometry analysis for CTRL cells with no treatment.

Figure H6: Propidium Iodide Flow Cytometry analysis for CTRL cells with no treatment.

Figure H7: Propidium Iodide Flow Cytometry analysis for SEN cells with no treatment.

Figure H8: Propidium Iodide Flow Cytometry analysis for SEN cells with no treatment.

Figure H9: Propidium Iodide Flow Cytometry analysis for CTRL + HB cells.

Figure H10: Propidium Iodide Flow Cytometry analysis for CTRL + HB cells.

Figure H11: Propidium Iodide Flow Cytometry analysis for SEN cells + HB.

Figure H12: Propidium Iodide Flow Cytometry analysis for SEN cells + HB.

Figure H13: Propidium Iodide Flow Cytometry analysis for CTRL cells + Allicin.

Figure H14: Propidium Iodide Flow Cytometry analysis for CTRL cells + Allicin.

Figure H15: Propidium Iodide Flow Cytometry analysis for SEN cells + Allicin.

Figure H16: Propidium Iodide Flow Cytometry analysis for SEN cells + Allicin.

Figure H17: Propidium Iodide Flow Cytometry analysis for CTRL cells + Phytol.

Figure H18: Propidium Iodide Flow Cytometry analysis for CTRL cells + Phytol.

Figure H19: Propidium Iodide Flow Cytometry analysis for SEN cells + Phytol.

Figure H20: Propidium Iodide Flow Cytometry analysis for SEN cells + Phytol.

	Mean ± SD	Mean ± SD
	CTRL	SEN
Seeding Density	150000 ± 0	150000 ± 0
BSS	340000 ± 28284	367500 ± 3536
ASS	740000 ± 28284	627500 ± 17678
Day 3	773333 ± 108424	292500 ± 48319
Day 6	1895000 ± 91924	310000 ± 84853
Day 10	2540000 ± 14142	242500 ± 31820

Table A1: Mean and standard deviation of CTRL and SEN cells counted over a 10-day period. In relation to Figure 8. BSS = Before serum starvation, ASS = After serum starvation. CTRL, (N=2) SEN, (N=4).

SA-B-Gal	*SEN*	*CTRL*
Mean	66.24802068	14.5089785
Variance	328.8910098	1.02859556
Observations	3	3
df	2	2
F	319.7476468	
P(F<=f) one-tail	0.003117716	
F Critical one-tail	19	

Table B1: F-Test to determine equal or unequal variance between SA-B-Gal positive CTRL and SEN cells. The F value (F) was found to be greater than F (Critical one-tail), indicating the rejection of the null hypothesis which is the variances of the two populations are not unequal. This means the variances of SEN and CTRL are unequal.

SA-B-Gal	*CTRL*	*SEN*
Mean	14.50897853	66.2480207
Variance	1.02859556	328.89101
Observations	3	3
Hypothesized Mean Difference	0	
df	2	
t Stat	-4.933725124	
P(T<=t) one-tail	0.019356007	
t Critical one-tail	2.91998558	
P(T<=t) two-tail	0.038712013	
t Critical two-tail	4.30265273	

Table B2: T-Test to determine significant difference between SA-B-Gal CTRL and SEN assuming unequal variance. The P-value (0.006) was found to be less than 0.05 (5% significance level) indicating a significant difference between SA-B-Gal CTRL and SEN.

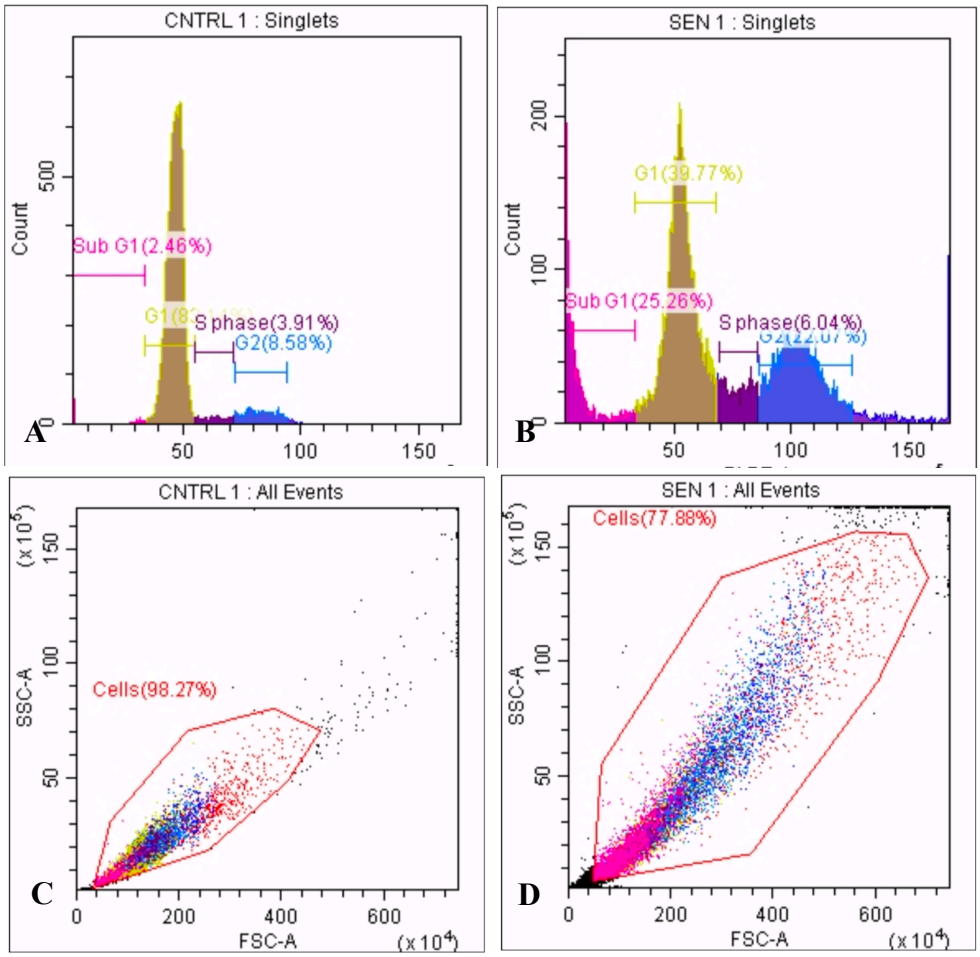

Figure C1: Cell cycle analysis of CTRL and SEN cells. Gating of cell cycle for CTRL and SEN (A-B) shows the individual phases of the cell cycle according to the peaks. Forward and Side scatter plots (C-D) show differences in cell size and granularity. Repeat 1.

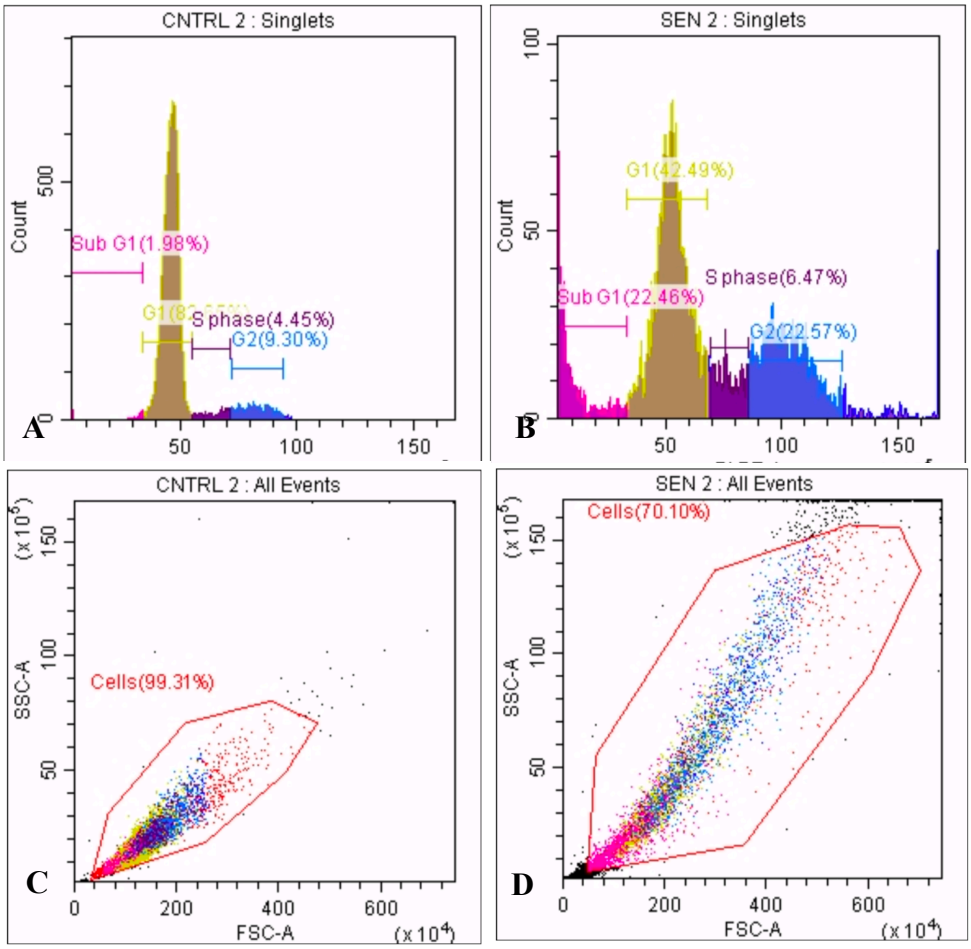

Figure C2: Cell cycle analysis of CTRL and SEN cells. Gating of cell cycle for CTRL and SEN (A-B) shows the individual phases of the cell cycle according to the peaks. Forward and Side scatter plots (C-D) show differences in cell size and granularity. Repeat 2.

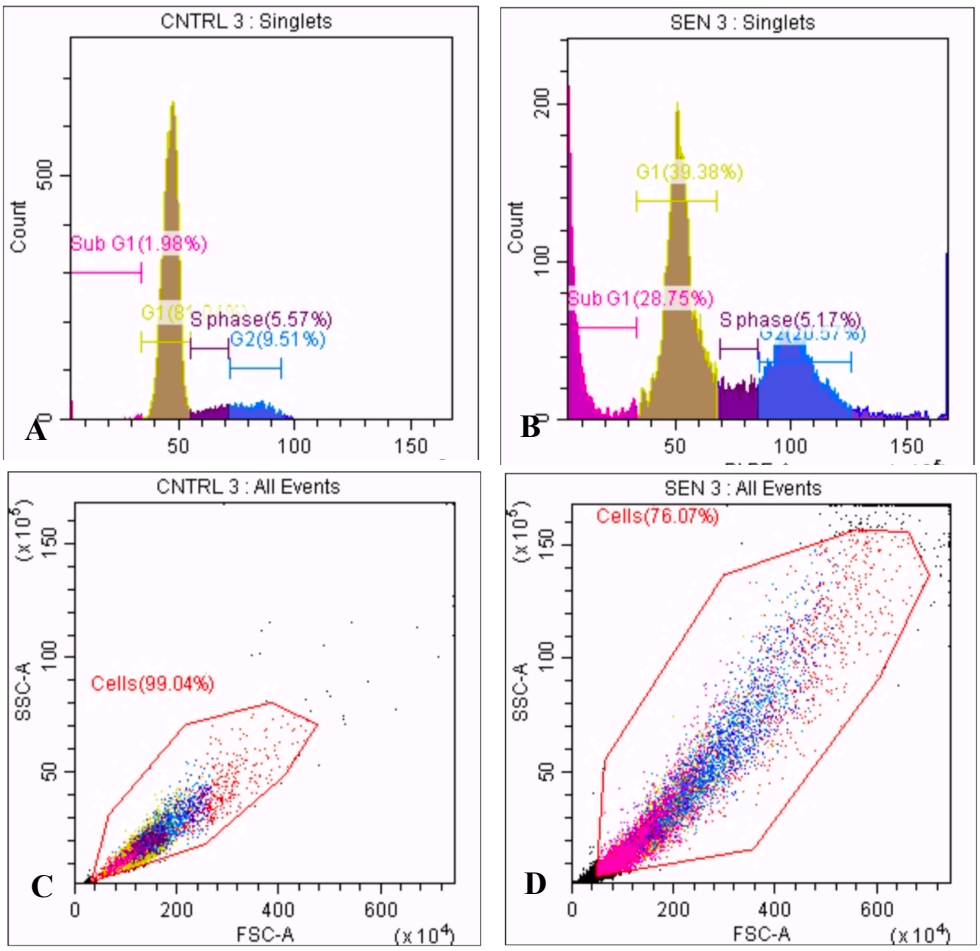

Figure C3: Cell cycle analysis of CTRL and SEN cells. Gating of cell cycle for CTRL and SEN (A-B) shows the individual phases of the cell cycle according to the peaks. Forward and Side scatter plots (C-D) show differences in cell size and granularity. Repeat 3.

	Mean ± SD	Mean ± SD	Mean ± SD	Mean ± SD
	Sub-G1	G1	S	G2
CTRL	2.14 ± 0.28	82.3 ± 1.10	4.64 ± 0.85	9.13 ± 0.49
SEN	25.49 ± 3.15	40.55 ± 1.69	5.89 ± 0.66	21.74 ± 1.04

Table C1: Mean and Standard deviation for Cell cycle analysis of CTRL and SEN cells.

F-Test Two-Sample for Variances		
SUB-G1	*SEN*	*CTRL*
Mean	25.49	2.14
Variance	9.9307	0.0768
Observations	3	3
df	2	2
F	129.30599	
P(F<=f) one-tail	0.00767424	
F Critical one-tail	19	
Unequal Variance		

Table C2: F-Test to determine equal or unequal variance between Sub-G1 CTRL and SEN. The F value (F) was found to be greater than F (Critical one-tail), indicating the rejection of the null hypothesis which is the variances of the two populations are not unequal. This means the variances of Sub-G1 SEN and Sub-G1 CTRL are unequal.

t-Test: Two-Sample Assuming Unequal Variances		
SUB-G1	*SEN*	*CTRL*
Mean	25.49	2.14
Variance	9.9307	0.0768
Observations	3	3
Hypothesized Mean Difference	0	
df	2	
t Stat	12.7845284	
P(T<=t) one-tail	0.00303136	
t Critical one-tail	2.91998558	
P(T<=t) two-tail	0.00606271	
t Critical two-tail	4.30265273	
Reject null hypothesis	Sig diff between groups	

Table C3: T-Test to determine significant difference between Sub-G1 CTRL and SEN assuming unequal variance. The P-value (0.006) was found to be less than 0.05 (5% significance level) indicating a significant difference between Sub-G1 CTRL and SEN.

F-Test Two-Sample for Variances		
G1	*SEN*	*CTRL*
Mean	40.5466667	82.2766667
Variance	2.87043333	1.20703333
Observations	3	3
df	2	2
F	2.37808953	
P(F<=f) one-tail	0.29602531	
F Critical one-tail	19	
Equal variance		

Table C4: F-Test to determine equal or unequal variance between G1 CTRL and SEN. The F value (F) was found to be less than F (Critical one-tail), indicating the acceptance of the null hypothesis which is the variances of the two populations are not unequal. This means the variances of G1 SEN and G1 CTRL are equal.

t-Test: Two-Sample Assuming Equal Variances		
	SEN	*CTRL*
Mean	40.5466667	82.2766667
Variance	2.87043333	1.20703333
Observations	3	3
Pooled Variance	2.03873333	
Hypothesized Mean Difference	0	
df	4	
t Stat	-35.794294	
P(T<=t) one-tail	1.8181E-06	
t Critical one-tail	2.13184679	
P(T<=t) two-tail	3.6361E-06	
t Critical two-tail	2.77644511	

Table C5: T-Test to determine significant difference between G1 CTRL and SEN assuming equal variance. The P-value (4.8E-05) was found to be less than 0.05 (5% significance level) indicating a significant difference between G1 CTRL and G1 SEN.

F-Test Two-Sample for Variances		
S	*SEN*	*CTRL*
Mean	5.89333333	4.64333333
Variance	0.43863333	0.71693333
Observations	3	3
df	2	2
F	0.61181886	
P(F<=f) one-tail	0.37958289	
F Critical one-tail	0.05263158	
equal variance		

Table C6: F-Test to determine equal or unequal variance between S Phase CTRL and SEN. The F value (F) was found to be greater than F (Critical one-tail), indicating the rejection of the null hypothesis which is the variances of the two populations are not unequal. This means the variances of S SEN and S CTRL are unequal.

t-Test: Two-Sample Assuming Unequal Variances		
	SEN	*CTRL*
Mean	5.89333333	4.64333333
Variance	0.43863333	0.71693333
Observations	3	3
Hypothesized Mean Difference	0	
df	4	
t Stat	2.0140634	
P(T<=t) one-tail	0.05713413	
t Critical one-tail	2.13184679	
P(T<=t) two-tail	0.11426826	
t Critical two-tail	2.77644511	

Table C7: T-Test to determine significant difference between S CTRL and SEN assuming equal variance. The P-value (0.11) was found to be greater than 0.05 (5% significance level) indicating no significant difference between S CTRL and S SEN.

F-Test Two-Sample for Variances		
G2	*SEN*	*CTRL*
Mean	21.7366667	9.13
Variance	1.08333333	0.2379
Observations	3	3
df	2	2
F	4.55373406	
P(F<=f) one-tail	0.18005904	
F Critical one-tail	19	
Equal variance		

Table C8: F-Test to determine equal or unequal variance between G2 Phase CTRL and SEN. The F value (F) was found to be greater than F (Critical one-tail), indicating the acceptance of the null hypothesis which is the variances of the two populations are not unequal. This means the variances of G2 SEN and G2 CTRL are equal.

t-Test: Two-Sample Assuming Equal Variances		
	SEN	*CTRL*
Mean	21.7366667	9.13
Variance	1.08333333	0.2379
Observations	3	3
Pooled Variance	0.66061667	
Hypothesized Mean Difference	0	
df	4	
t Stat	18.9963926	
P(T<=t) one-tail	2.2618E-05	
t Critical one-tail	2.13184679	
P(T<=t) two-tail	4.5236E-05	
t Critical two-tail	2.77644511	

Table C9: T-Test to determine significant difference between G2 CTRL and SEN assuming equal variance. The P-value (4.52E-05) was found to be less than 0.05 (5% significance level) indicating a significant difference between G2 CTRL and G2 SEN.

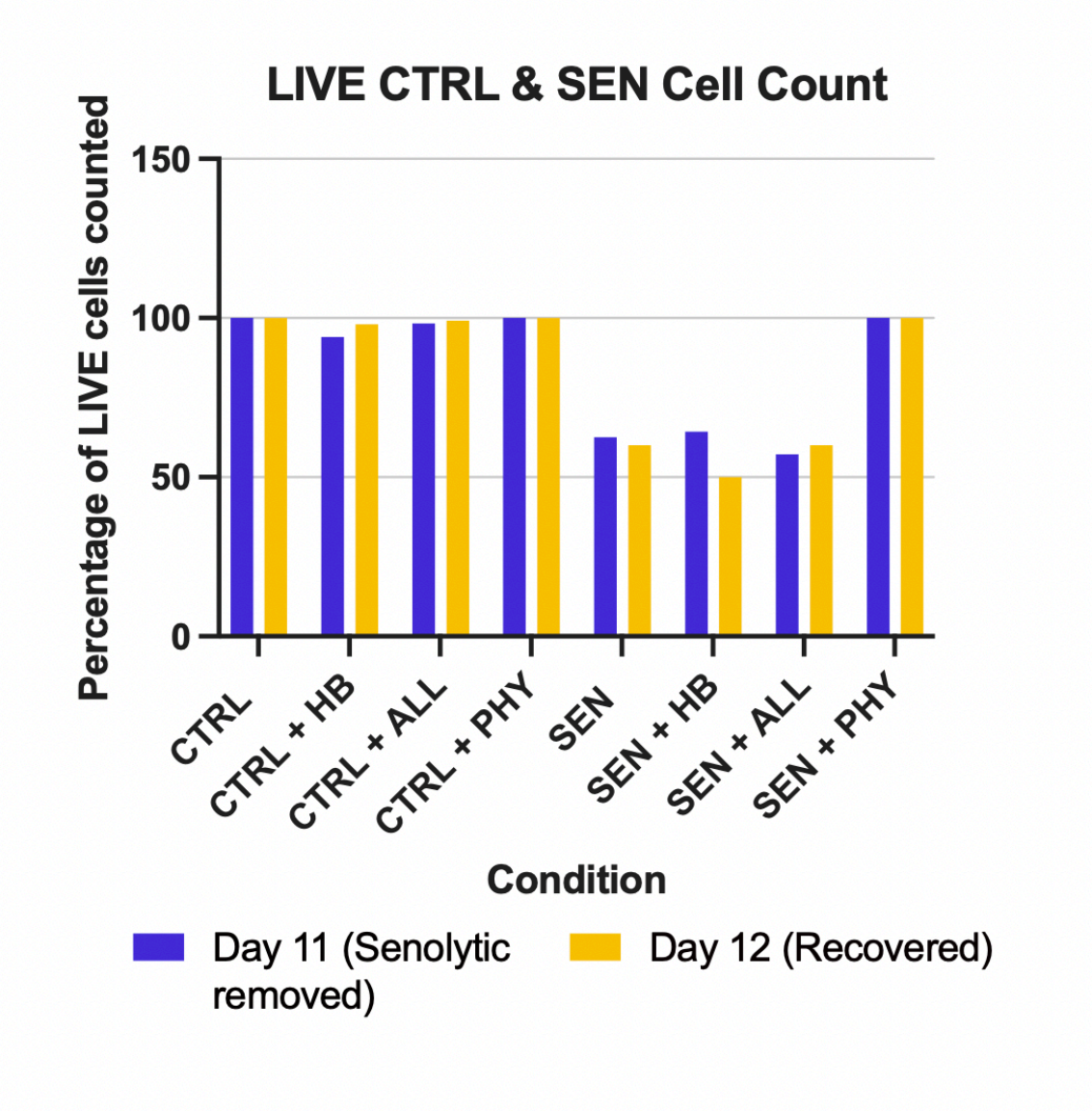

Figure D1: Percentage of LIVE CTRL and SEN cell count following senolytic application. Percentage of Live cells out of total cells counted was calculated. Counts were done in replicates and averaged. Graph shows that dosage of treatments are not detrimental to healthy cells as loss of live cells is minimal in CTRL + treatments.

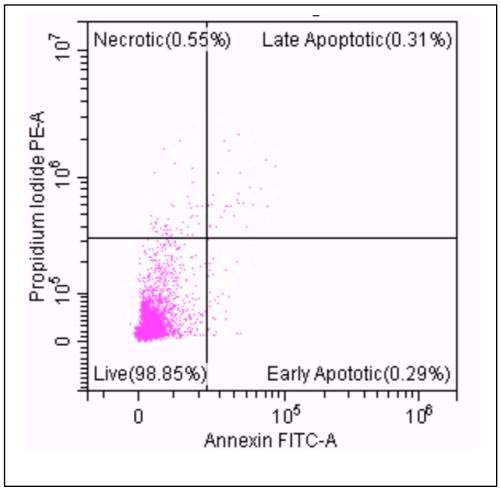

Figure E1: Annexin V-FITC analysis of CTRL cells using Flow Cytometry. (A) Forward and side scatter plot of CTRL cells. (B) Quadrant map of Annexin V-FITC vs PI. Q1 = Live, Q2 = Early Apoptotic, Q3 = Late Apoptotic, Q4 = Necrotic. Repeat 1.

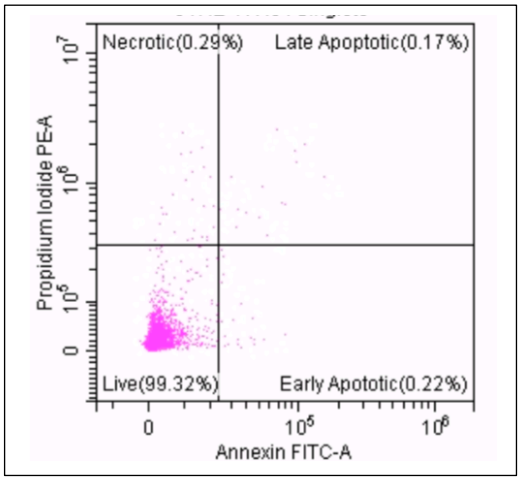

Figure E2: Annexin V-FITC analysis of CTRL cells using Flow Cytometry. (A) Forward and side scatter plot of CTRL cells. (B) Quadrant map of Annexin V-FITC vs PI. Q1 = Live, Q2 = Early Apoptotic, Q3 = Late Apoptotic, Q4 = Necrotic. Repeat 2.

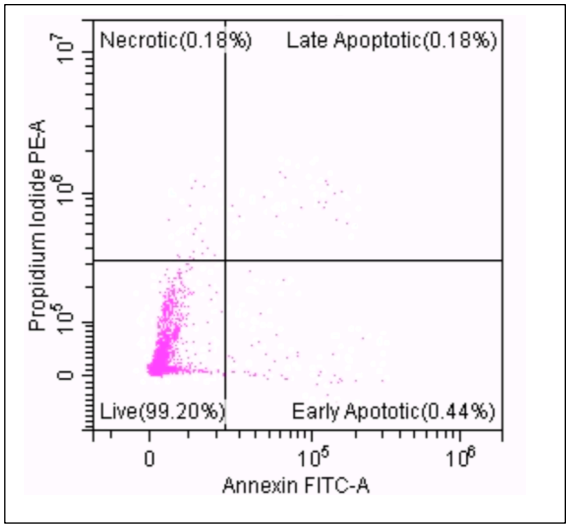

Figure E3: Annexin V-FITC analysis of CTRL + HB cells using Flow Cytometry. (A) Forward and side scatter plot of CTRL + HB cells. (B) Quadrant map of Annexin V-FITC vs PI. Q1 = Live, Q2 = Early Apoptotic, Q3 = Late Apoptotic, Q4 = Necrotic. Repeat 1.

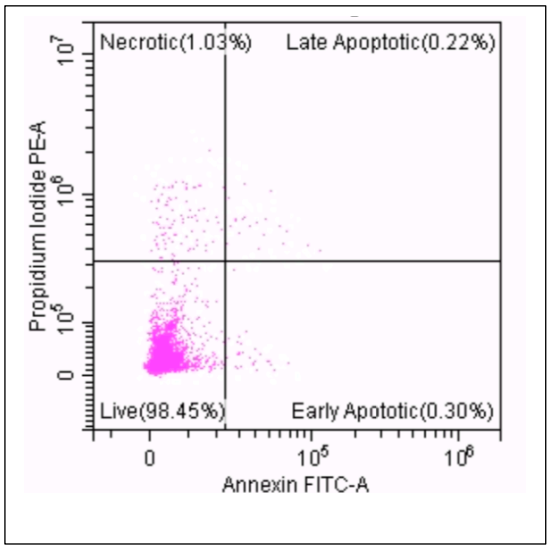

Figure E4: Annexin V-FITC analysis of CTRL + HB cells using Flow Cytometry. (A) Forward and side scatter plot of CTRL + HB cells. (B) Quadrant map of Annexin V-FITC vs PI. Q1 = Live, Q2 = Early Apoptotic, Q3 = Late Apoptotic, Q4 = Necrotic. Repeat 2.

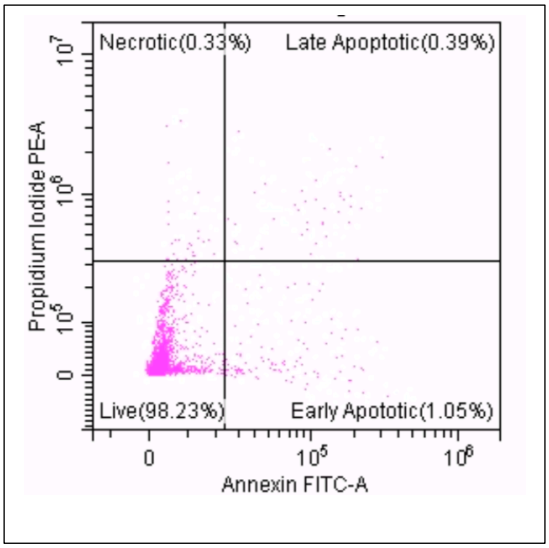

Figure E5: Annexin V-FITC analysis of CTRL + Allicin cells using Flow Cytometry. (A) Forward and side scatter plot of CTRL + Allicin cells. (B) Quadrant map of Annexin V-FITC vs PI. Q1 = Live, Q2 = Early Apoptotic, Q3 = Late Apoptotic, Q4 = Necrotic. Repeat 1.

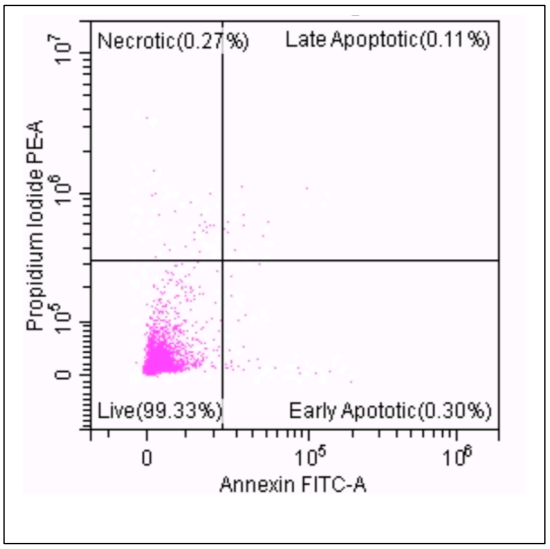

Figure E6: Annexin V-FITC analysis of CTRL + Allicin cells using Flow Cytometry. (A) Forward and side scatter plot of CTRL + Allicin cells. (B) Quadrant map of Annexin V-FITC vs PI. Q1 = Live, Q2 = Early Apoptotic, Q3 = Late Apoptotic, Q4 = Necrotic. Repeat 2.

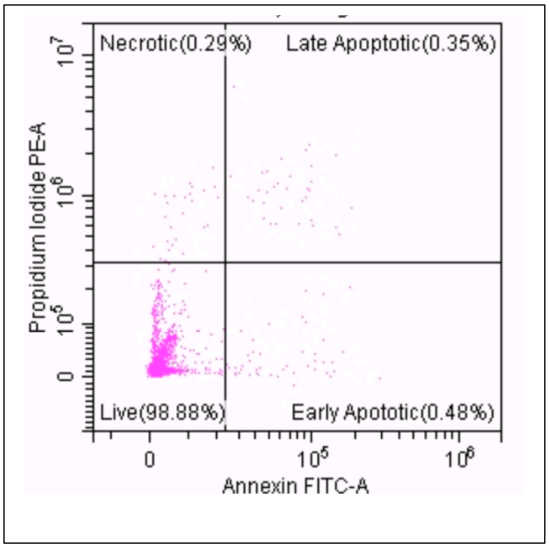

Figure E7: Annexin V-FITC analysis of CTRL + Phytol cells using Flow Cytometry. (A) Forward and side scatter plot of CTRL + Phytol cells. (B) Quadrant map of Annexin V-FITC vs PI. Q1 = Live, Q2 = Early Apoptotic, Q3 = Late Apoptotic, Q4 = Necrotic. Repeat 1.

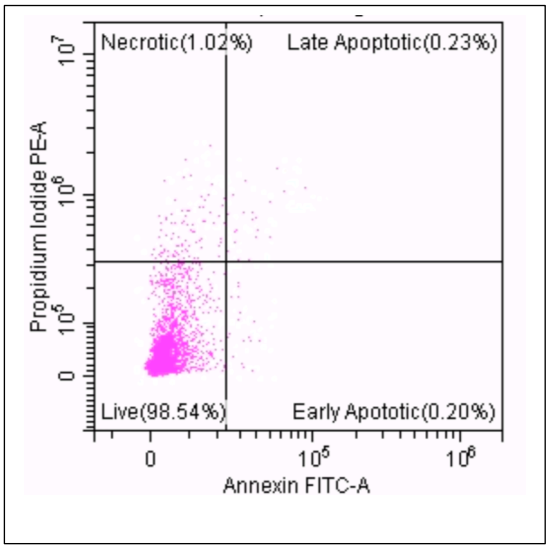

Figure E8: Annexin V-FITC analysis of CTRL + Phytol cells using Flow Cytometry. (A) Forward and side scatter plot of CTRL + Phytol cells. (B) Quadrant map of Annexin V-FITC vs PI. Q1 = Live, Q2 = Early Apoptotic, Q3 = Late Apoptotic, Q4 = Necrotic. Repeat 2.

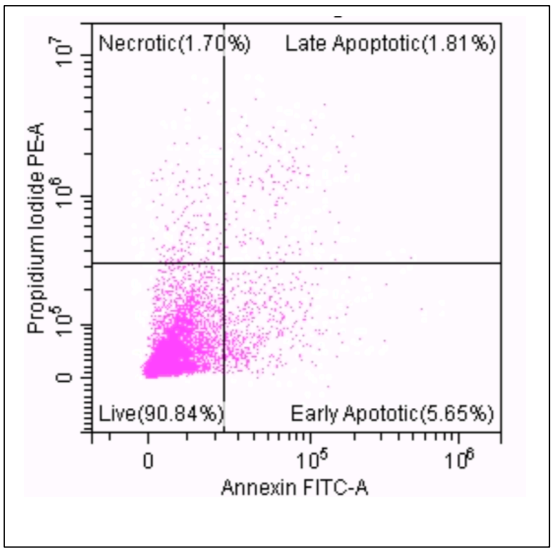

Figure E9: Annexin V-FITC analysis of SEN cells using Flow Cytometry. (A) Forward and side scatter plot of SEN cells. (B) Quadrant map of Annexin V-FITC vs PI. Q1 = Live, Q2 = Early Apoptotic, Q3 = Late Apoptotic, Q4 = Necrotic. Repeat 1.

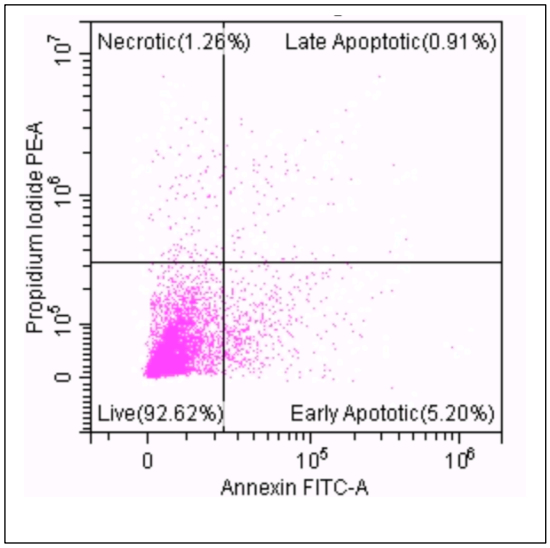

Figure E10: Annexin V-FITC analysis of SEN cells using Flow Cytometry. (A) Forward and side scatter plot of SEN cells. (B) Quadrant map of Annexin V-FITC vs PI. Q1 = Live, Q2 = Early Apoptotic, Q3 = Late Apoptotic, Q4 = Necrotic. Repeat 2.

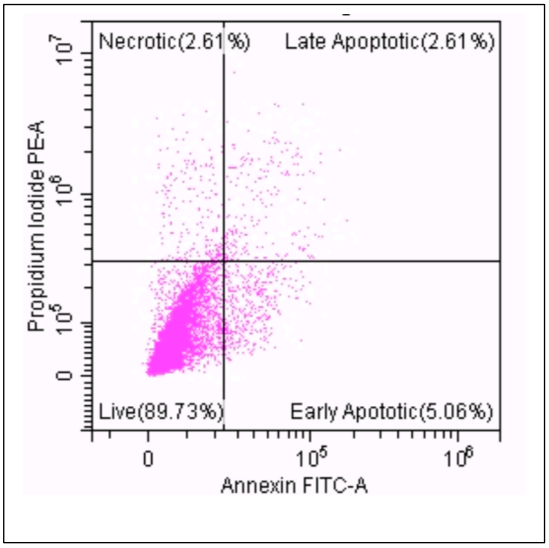

Figure E11: Annexin V-FITC analysis of SEN + HB cells using Flow Cytometry. (A) Forward and side scatter plot of SEN + HB cells. (B) Quadrant map of Annexin V-FITC vs PI. Q1 = Live, Q2 = Early Apoptotic, Q3 = Late Apoptotic, Q4 = Necrotic. Repeat 1.

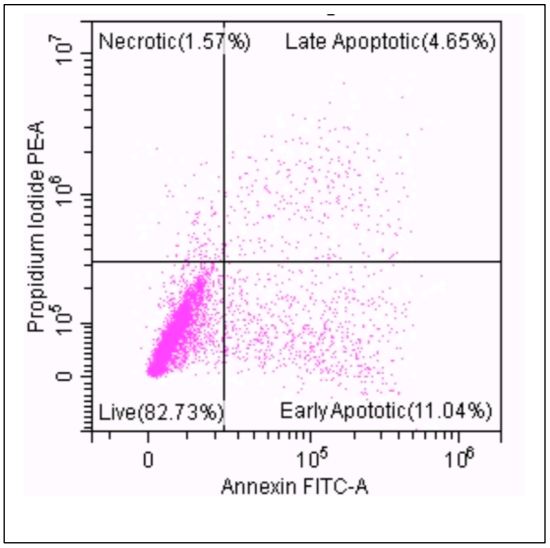

Figure E12: Annexin V-FITC analysis of SEN + HB cells using Flow Cytometry. (A) Forward and side scatter plot of SEN +HB cells. (B) Quadrant map of Annexin V-FITC vs PI. Q1 = Live, Q2 = Early Apoptotic, Q3 = Late Apoptotic, Q4 = Necrotic. Repeat 2.

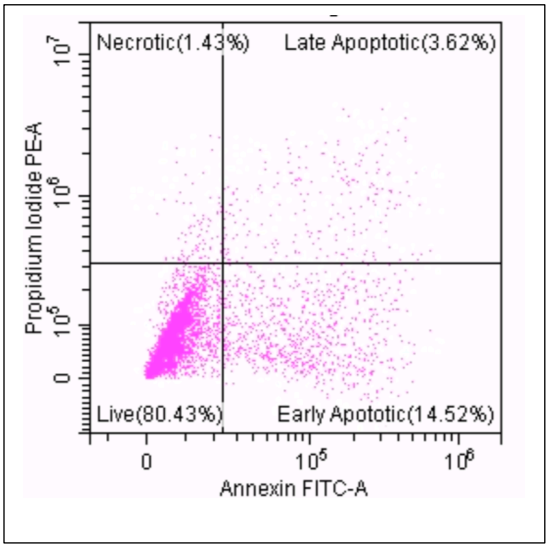

Figure E13: Annexin V-FITC analysis of SEN + Allicin cells using Flow Cytometry. (A) Forward and side scatter plot of SEN + Allicin cells. (B) Quadrant map of Annexin V-FITC vs PI. Q1 = Live, Q2 = Early Apoptotic, Q3 = Late Apoptotic, Q4 = Necrotic. Repeat 1.

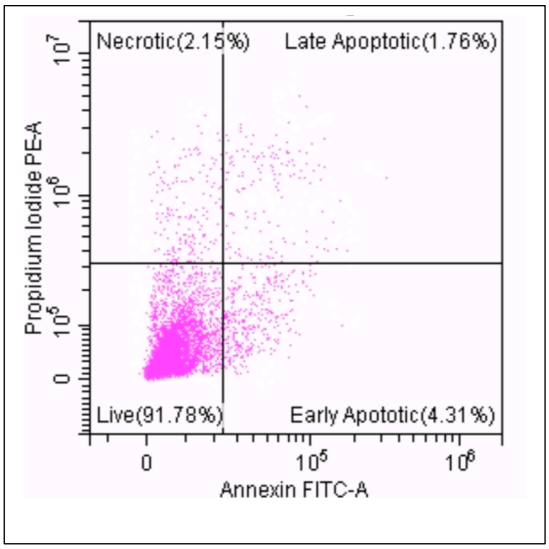

Figure E14: Annexin V-FITC analysis of SEN + Allicin cells using Flow Cytometry. (A) Forward and side scatter plot of SEN + Allicin cells. (B) Quadrant map of Annexin V-FITC vs PI. Q1 = Live, Q2 = Early Apoptotic, Q3 = Late Apoptotic, Q4 = Necrotic. Repeat 2.

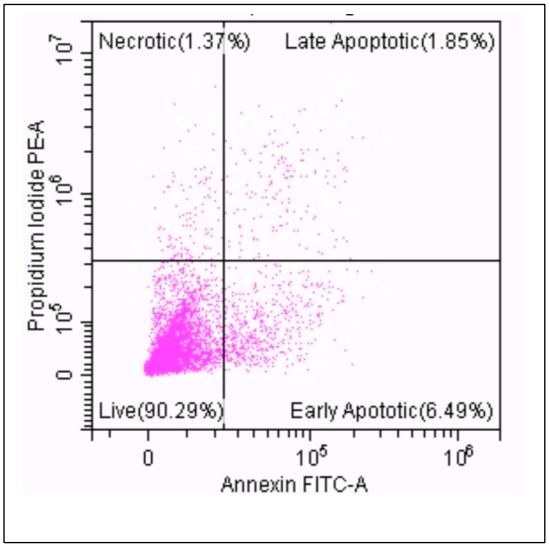

Figure E15: Annexin V-FITC analysis of SEN + Phytol cells using Flow Cytometry. (A) Forward and side scatter plot of SEN + Phytol cells. (B) Quadrant map of Annexin V-FITC vs PI. Q1 = Live, Q2 = Early Apoptotic, Q3 = Late Apoptotic, Q4 = Necrotic. Repeat 1.

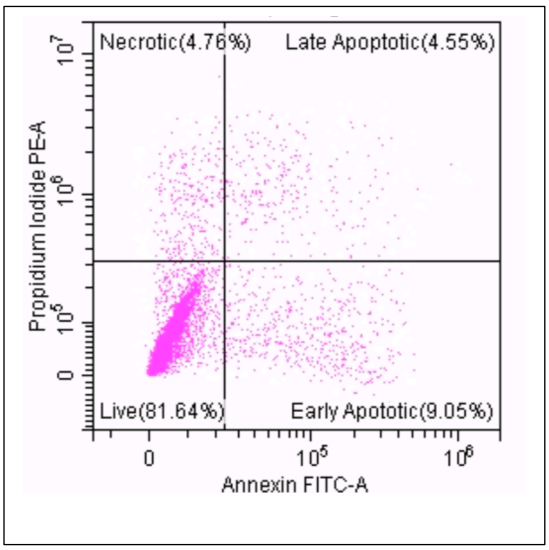

Figure E16: Annexin V-FITC analysis of SEN + Phytol cells using Flow Cytometry. (A) Forward and side scatter plot of SEN + Phytol cells. (B) Quadrant map of Annexin V-FITC vs PI. Q1 = Live, Q2 = Early Apoptotic, Q3 = Late Apoptotic, Q4 = Necrotic. Repeat 2.

Annexin V - FITC Results				
One way ANOVA				
P-value				
	Dead			Dead
SEN + HB	0.266112684		CTRL + HB	0.030152053
SEN +All	0.430441361		CTRL + All	0.4918776
SEN +Phy	0.32144033		CTRL + Phy	0.169552597
	Early Apoptotic			Early Apoptotic
SEN + HB	0.473651611		CTRL + HB	0.218341123
SEN + All	0.516650809		CTRL + All	0.400230636
SEN +Phy	0.212939889		CTRL + Phy	0.499591002
	Late Apoptotic			Late Apoptotic
SEN + HB	0.178672943		CTRL + HB	0.376149706
SEN + All	0.326847561		CTRL + All	0.632270971
SEN +Phy	0.325223711		CTRL + Phy	0.506374116
	Necrotic			Necrotic
SEN + HB	0.392937149		CTRL + HB	0.03212881
SEN + All	0.538953807		CTRL + All	0.579093087
SEN +Phy	0.451654744		CTRL + Phy	0.084160664

Table E1: One Way ANOVA performed on Annexin V FITC results. P-values shown for each sample in compared to its baseline control. DEAD = Early Apoptotic + Late Apoptotic + Necrotic. Analysis of two repeats for each sample was carried out. Green cells show p-value below 0.05 threshold indicating a significant difference.

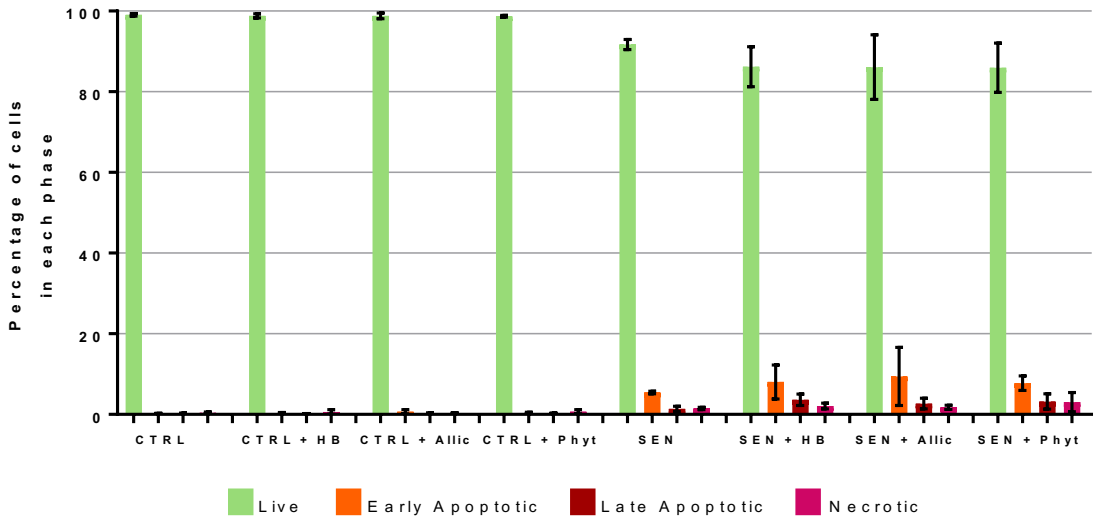

Figure E17: Annexin V-FITC detection of cells treated with HB, Allicin and Phytol as individual phases. The phases Live, Early Apoptotic, Late Apoptotic and Necrotic are shown. Results shown are averages over 2 repeats and small bars represent standard error of mean.

	Live	Early Apoptotic	Late Apoptotic	Necrotic
	Mean ± SD	**Mean ± SD**	**Mean ± SD**	**Mean ± SD**
CTRL	99.1 ± 0.33	0.3 ± 0.1	0.2 ± 0.1	0.4 ± 0.18
CTRL + HB	97.6 ± 0.18	0.6 ± 0.25	0.4 ± 0.11	1.5 ± 0.2
CTRL + Allic	97.8 ± 2.14	1.0 ± 1.0	0.4 ± 0.43	0.7 ± 0.66
CTRL + Phyt	98.2 ± 0.5	0.5 ± 0.44	0.4 ± 0.18	0.9 ± 0.13
SEN	91.7 ± 1.3	5.4 ± 0.32	1.4 ± 0.64	1.5 ± 0.31
SEN + HB	86.2 ± 4.9	8.1 ± 4.23	3.6 ± 1.44	2.1 ± 0.74
SEN + Allic	86.1 ± 8.0	9.4 ± 7.22	2.7 ± 1.3	1.8 ± 0.51
SEN + Phyt	86.0 ± 6.1	7.8 ± 1.8	3.2 ± 1.9	3.1 ± 2.4

Table E2: Mean and Standard deviation calculated for Annexin V-FITC detection of cells treated with HB, Allicin and Phytol as Senolytics as individual phases. Live, Early Apoptotic, Late Apoptotic and Necrotic calculated individually.

P Values		
TUNEL ASSAY		
	Normal	Apoptotic
CTRL + HB	0.1234318	0.12655771
CTRL + ALL	0.07671234	0.15050652
CTRL + PHY	0.12860653	0.21184792
SEN + HB	0.18485021	0.18485021
SEN + ALL	0.57326917	0.57326917
SEN + PHY	0.33043357	0.3292725

Table F1: One Way ANOVA performed on TUNEL Assay results. P-values shown for each sample in compared to its baseline control. Analysis of results carried out by two independent scorers.

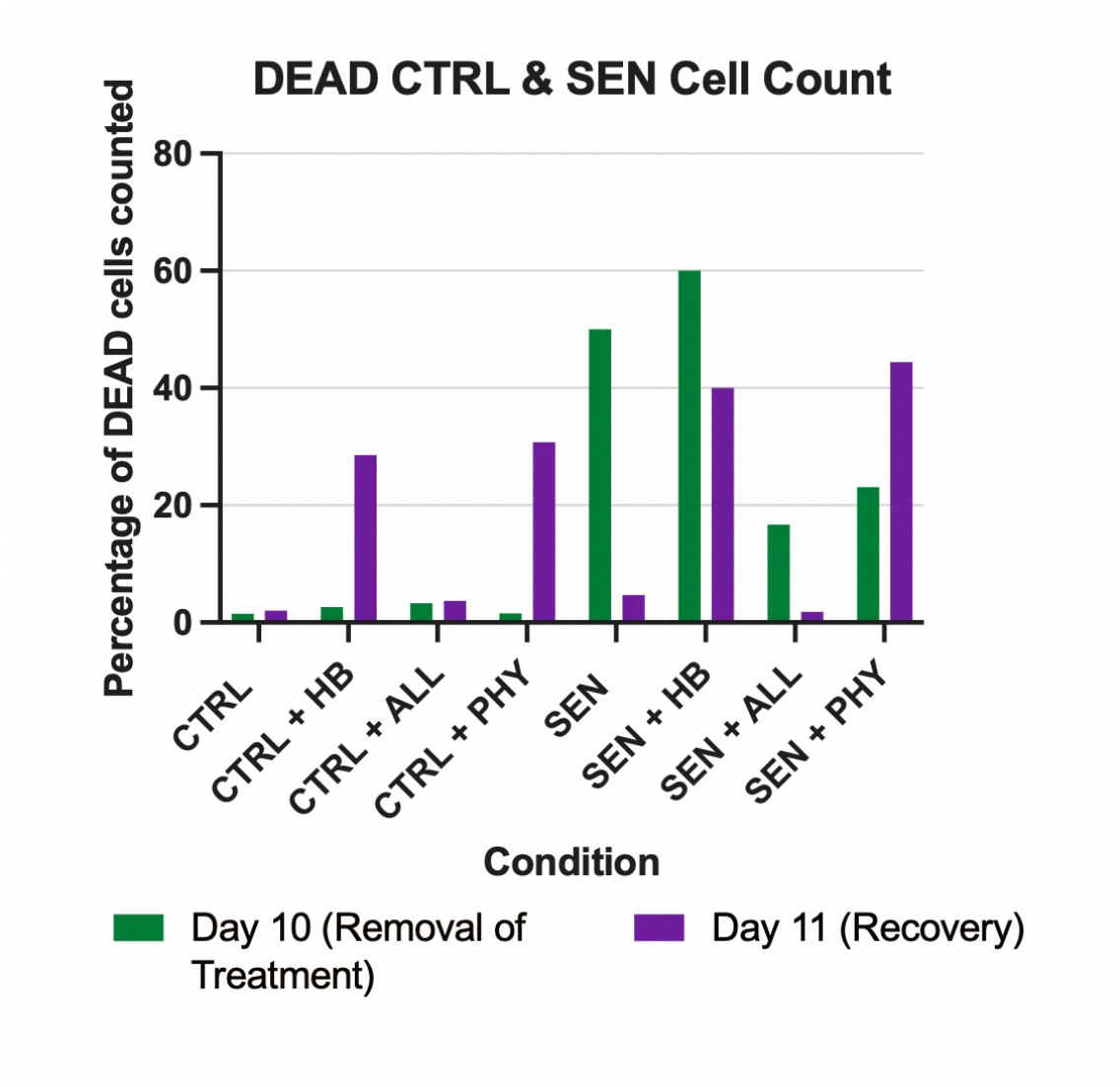

Figure G1: Percentage of Dead CTRL and SEN cells out of total cells counted following senostatic application of HB, Allicin and Phytol. The decrease in DEAD SEN cells with Allicin and Phytol treatment supports potential senostatic properties. Nutraceuticals have very small effect on percentage of dead CTRL cells.

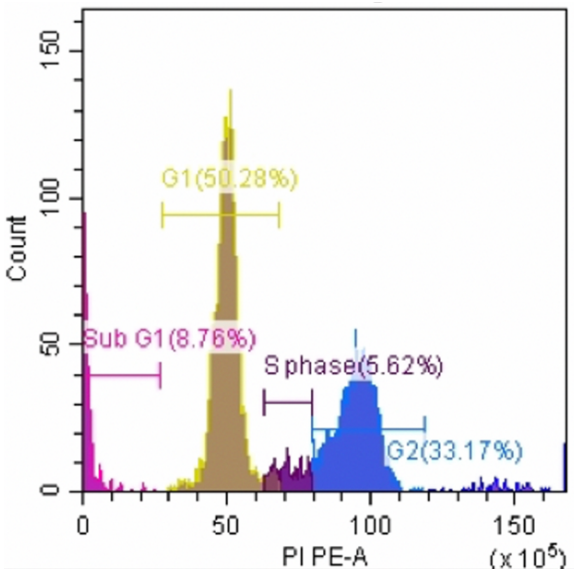

Figure H1: Propidium Iodide Flow Cytometry analysis for L929 Fibroblast cells before serum starvation (BSS). Repeat 1

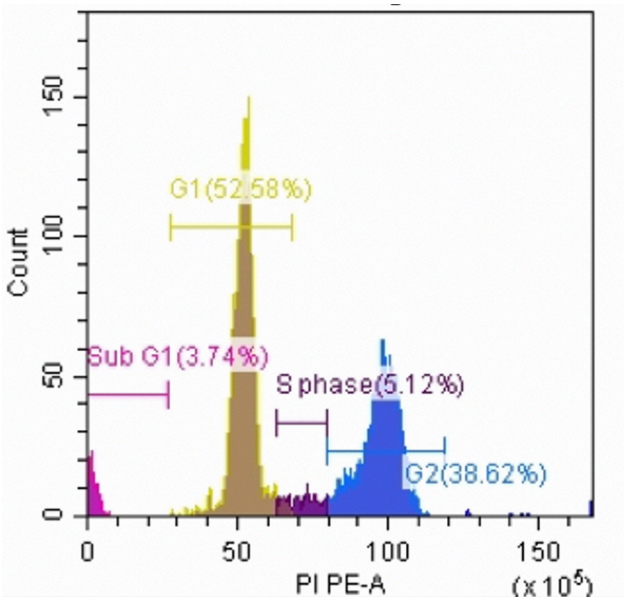

Figure H2: Propidium Iodide Flow Cytometry analysis for L929 Fibroblast cells before serum starvation (BSS). Repeat 2

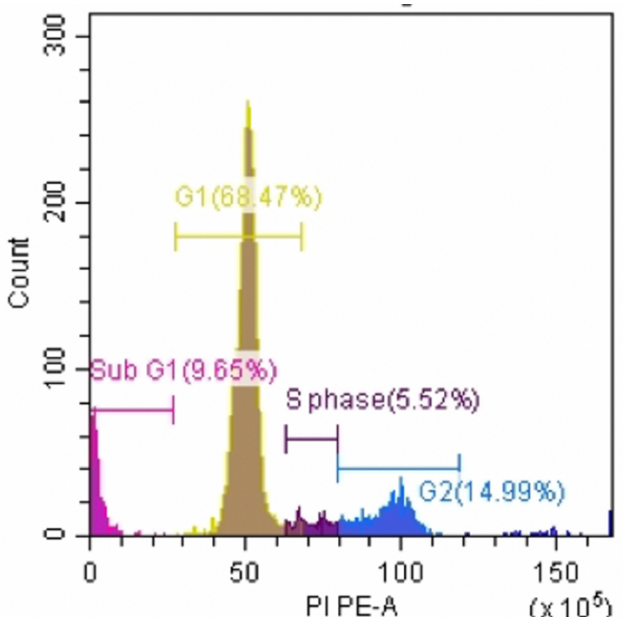

Figure H3: Propidium Iodide Flow Cytometry analysis for L929 Fibroblast cells after serum starvation (ASS). Repeat 1

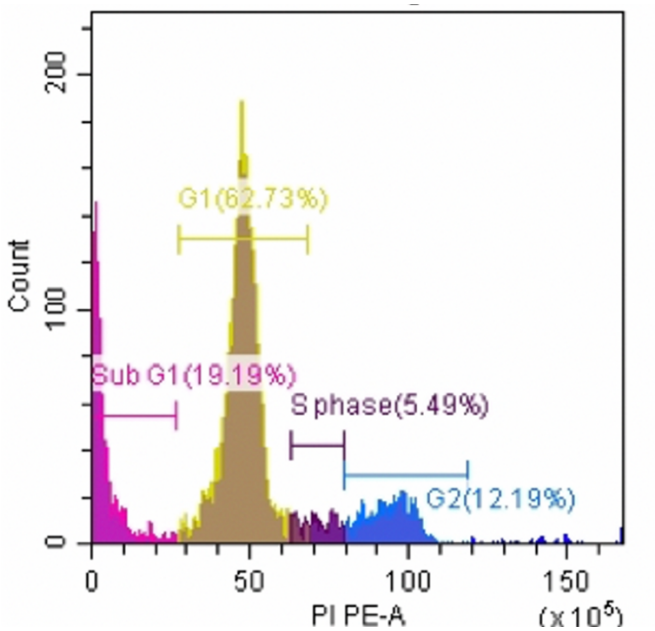

Figure H4: Propidium Iodide Flow Cytometry analysis for L929 Fibroblast cells after serum starvation (ASS). Repeat 2

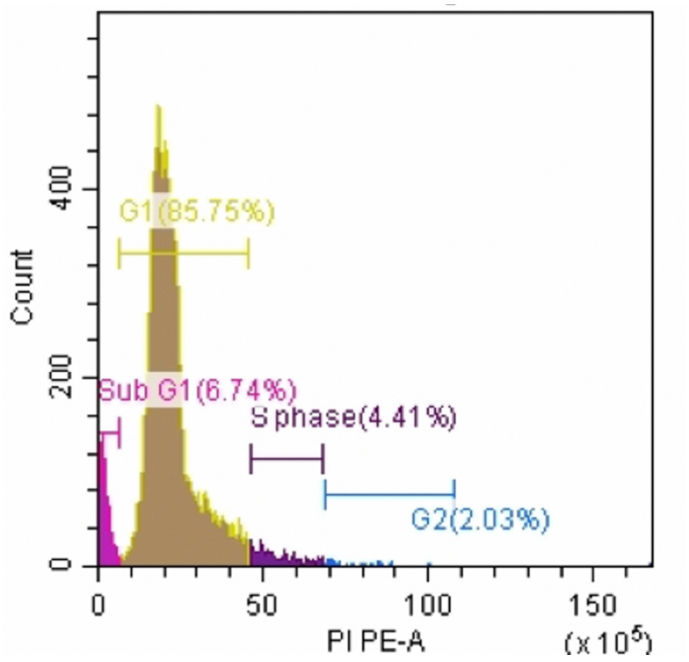

Figure H5: Propidium Iodide Flow Cytometry analysis for CTRL cells without treatment. Repeat 1.

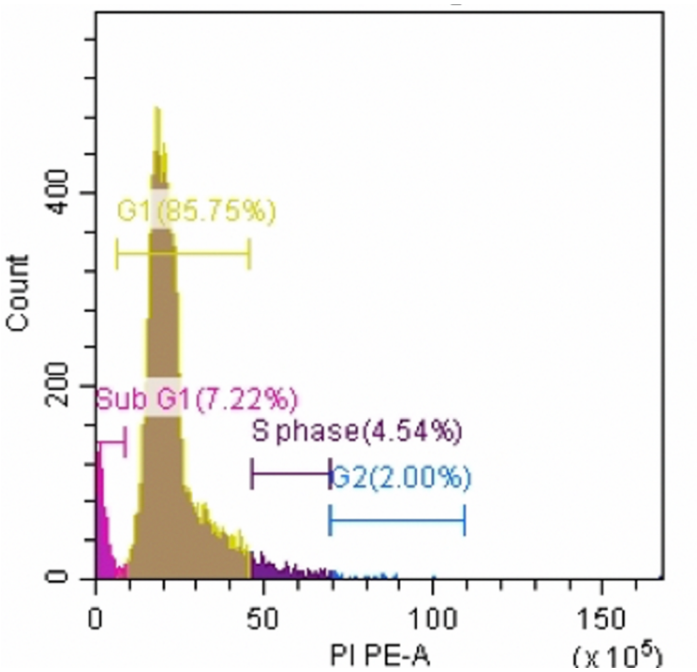

Figure H6: Propidium Iodide Flow Cytometry analysis for CTRL cells without treatment. Repeat 2.

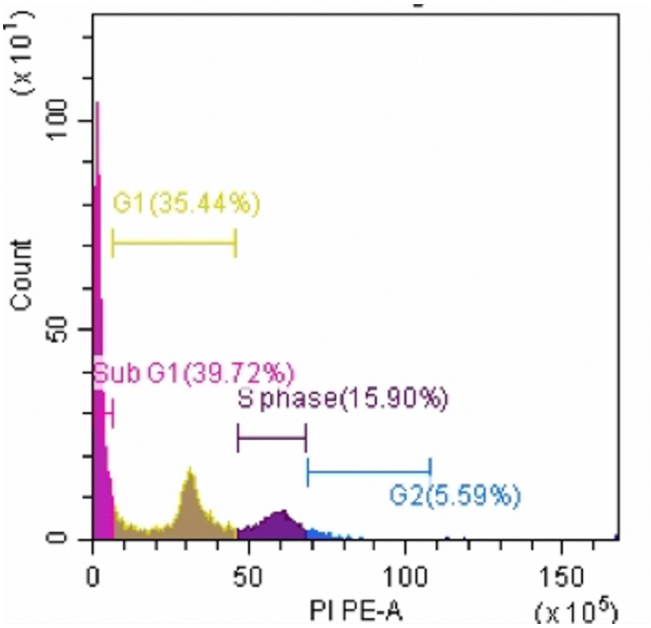

Figure H7: Propidium Iodide Flow Cytometry analysis for SEN cells without treatment. Repeat 1.

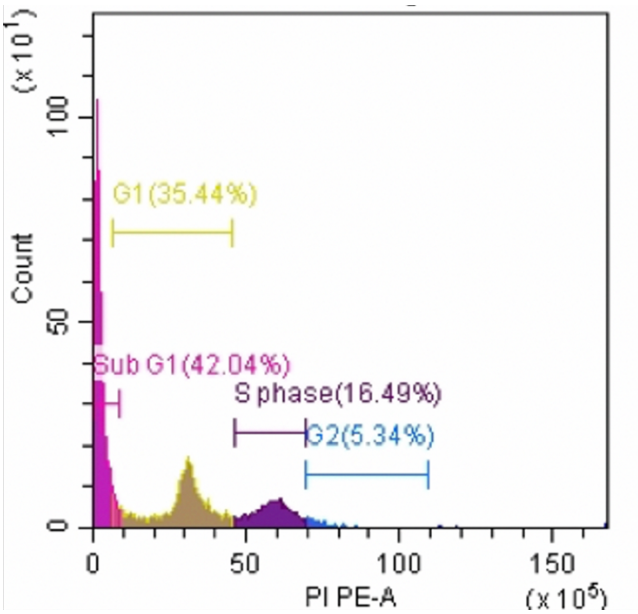

Figure H8: Propidium Iodide Flow Cytometry analysis for SEN cells without treatment. Repeat 2.

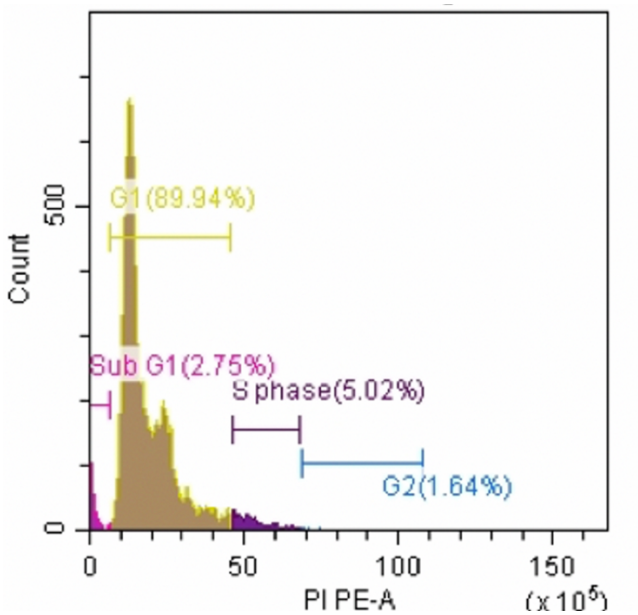

Figure H9: Propidium Iodide Flow Cytometry analysis for CTRL cells treated with Holy Basil. Repeat 1.

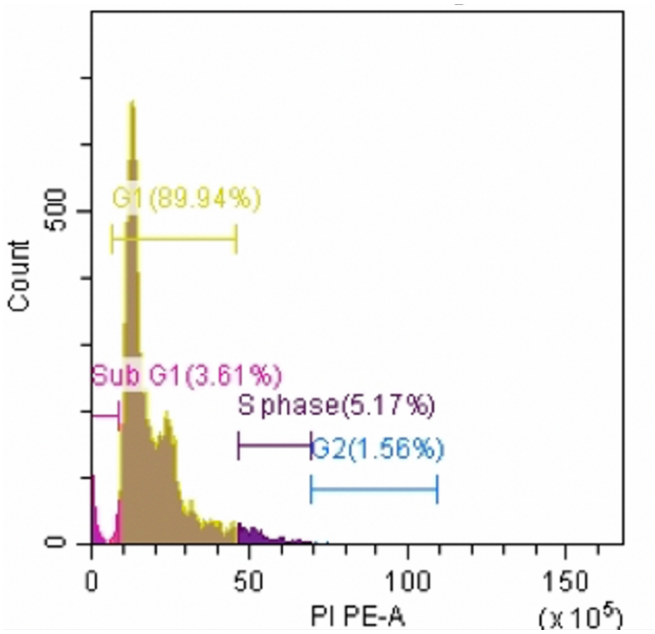

Figure H10: Propidium Iodide Flow Cytometry analysis for CTRL cells treated with Holy Basil. Repeat 1.

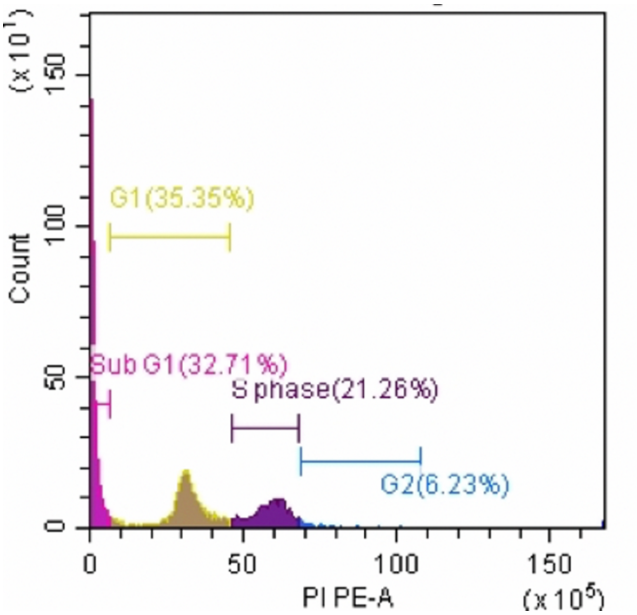

Figure H11: Propidium Iodide Flow Cytometry analysis for SEN cells treated with Holy Basil. Repeat 1.

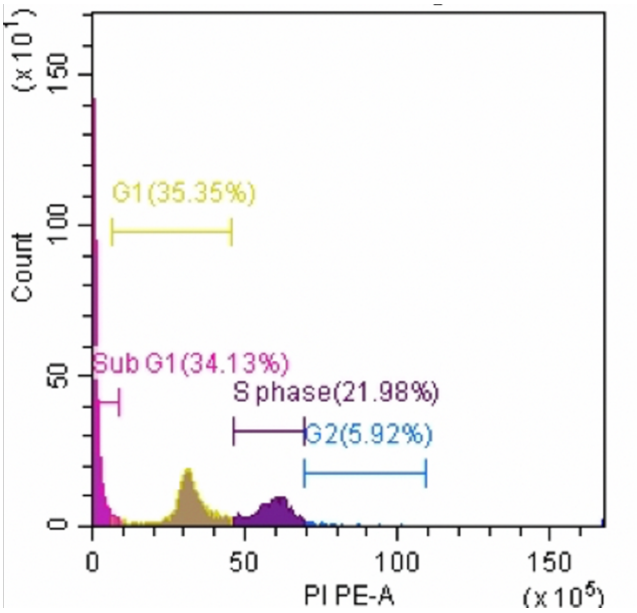

Figure H12: Propidium Iodide Flow Cytometry analysis for SEN cells treated with Holy Basil. Repeat 2.

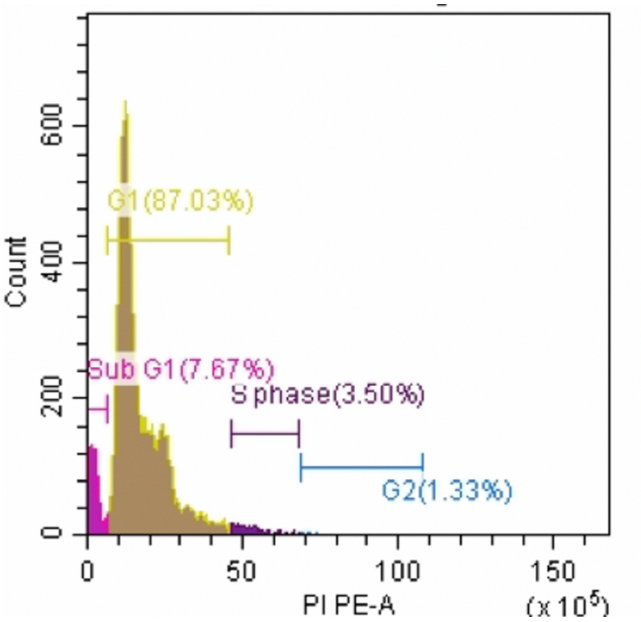

Figure H13: Propidium Iodide Flow Cytometry analysis for CTRL cells treated with Allicin. Repeat 1.

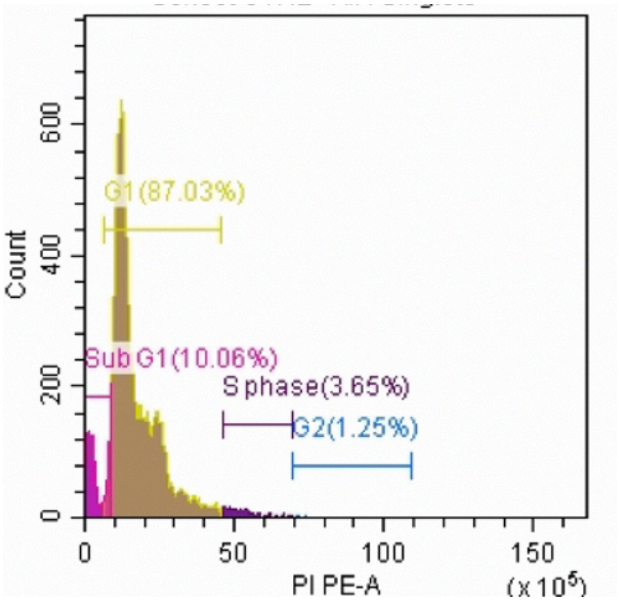

Figure H14: Propidium Iodide Flow Cytometry analysis for CTRL cells treated with Allicin. Repeat 2.

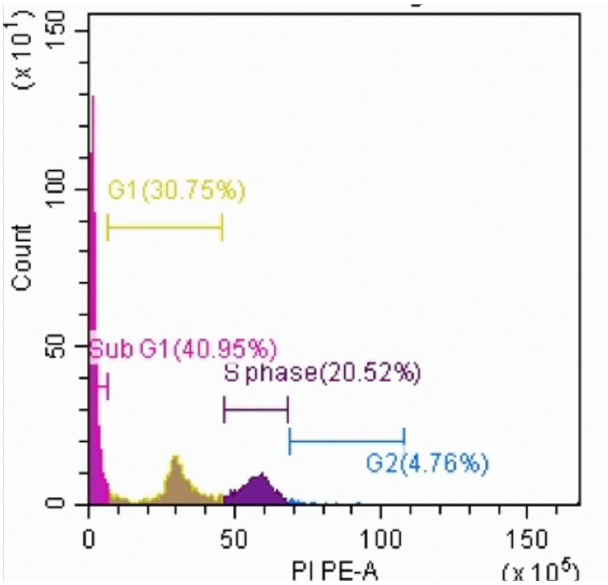

Figure H15: Propidium Iodide Flow Cytometry analysis for SEN cells treated with Allicin. Repeat 1.

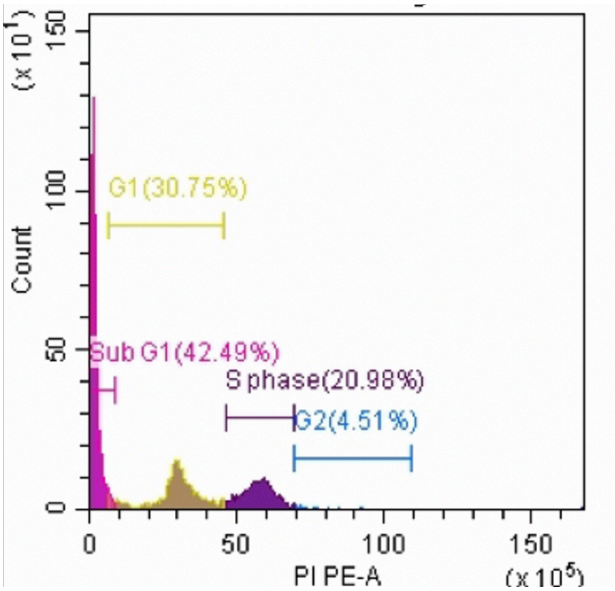

Figure H16: Propidium Iodide Flow Cytometry analysis for SEN cells treated with Allicin. Repeat 2.

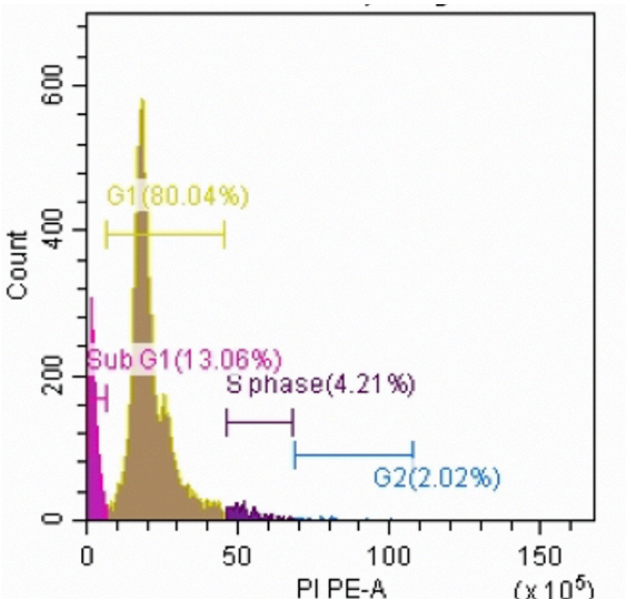

Figure H17: Propidium Iodide Flow Cytometry analysis for CTRL cells treated with Phytol. Repeat 1.

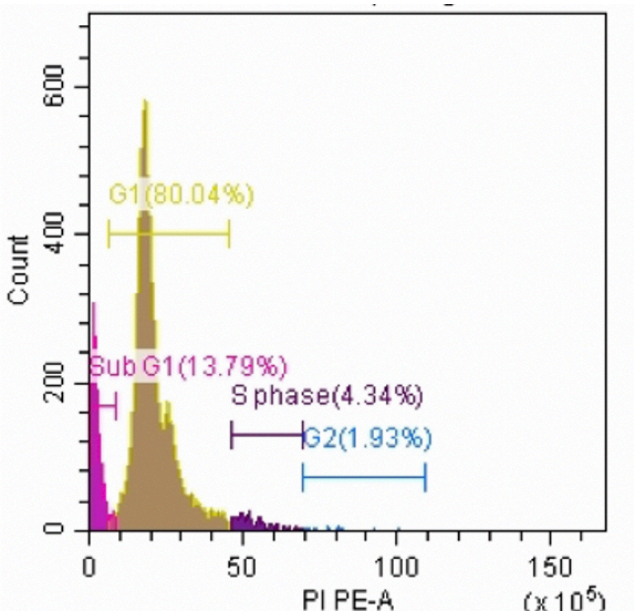

Figure H18: Propidium Iodide Flow Cytometry analysis for CTRL cells treated with Phytol. Repeat 2.

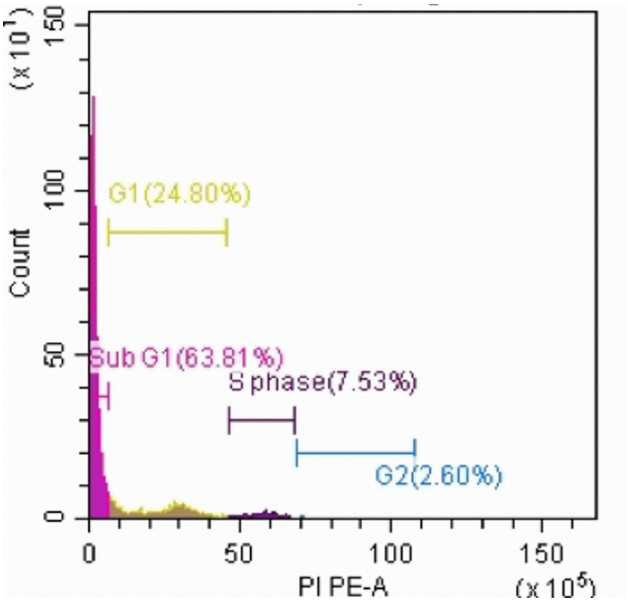

Figure H19: Propidium Iodide Flow Cytometry analysis for SEN cells treated with Phytol. Repeat 1.

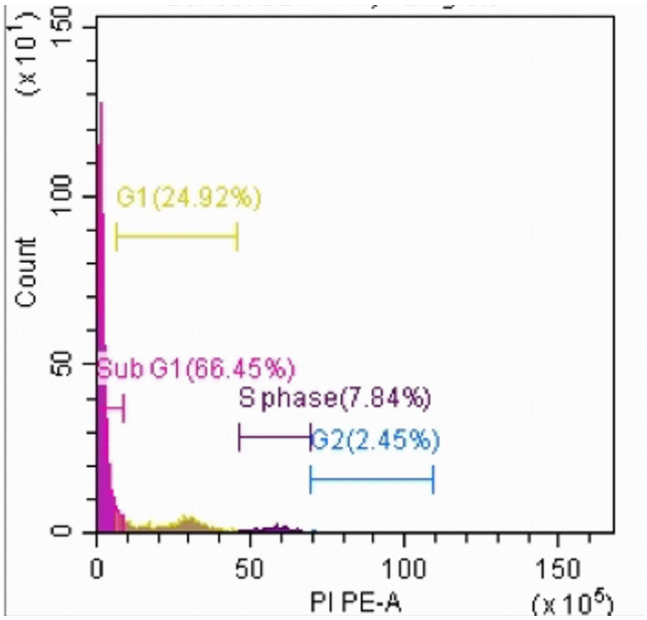

Figure H20: Propidium Iodide Flow Cytometry analysis for SEN cells treated with Phytol. Repeat 2.

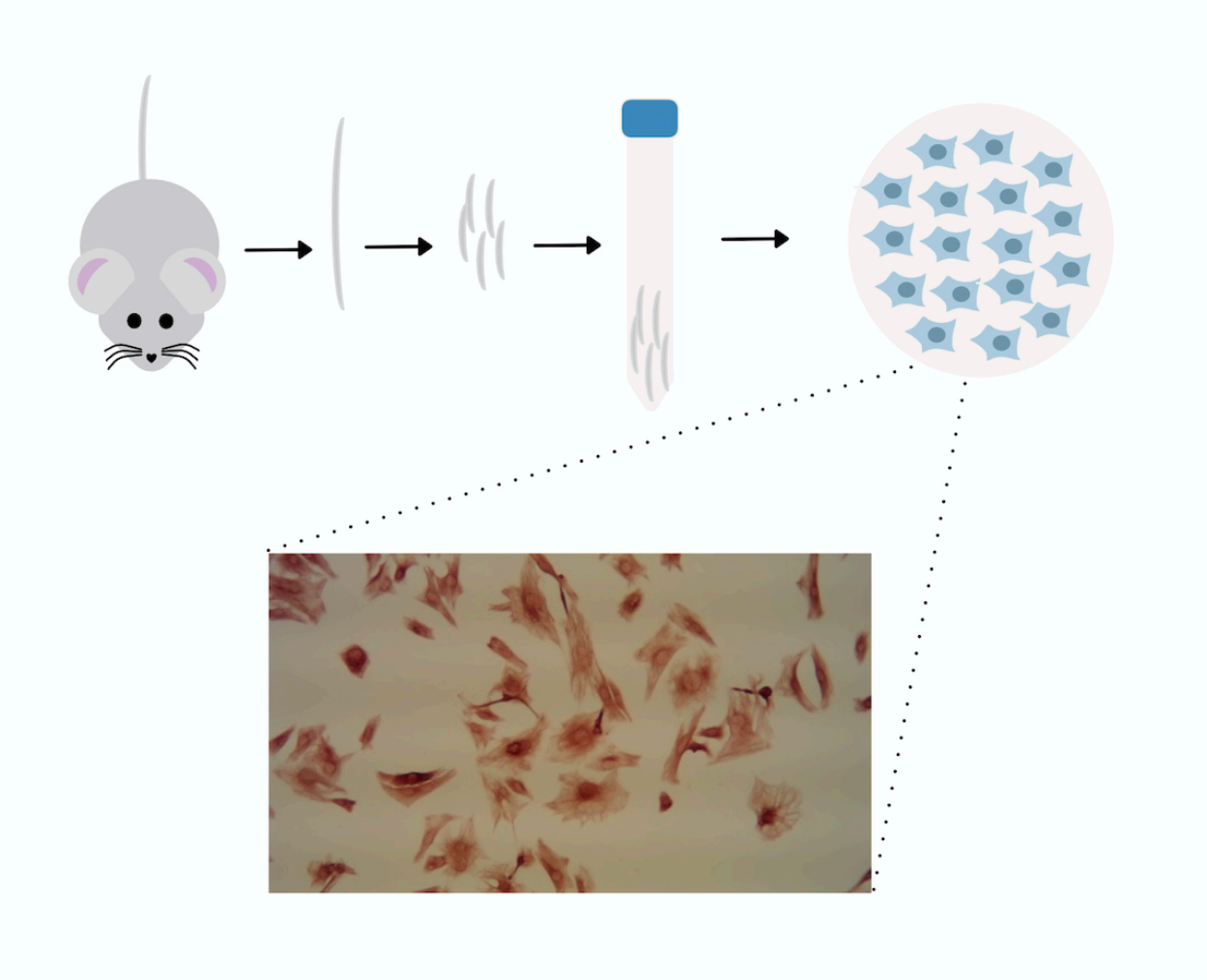

Figure I1: Illustration of Mouse Fibroblast Harvest Protocol. 5cm of mouse tail was excised, shaved and cut into small parts. Tail pieces were subjected to collagenase exposure for 90 minutes at 37^{o}c. Tissue was then sieved/pushed through 70um filter using cell culture media for washing. Cells were centrifuged, resuspended and seeded in to T25 flasks.

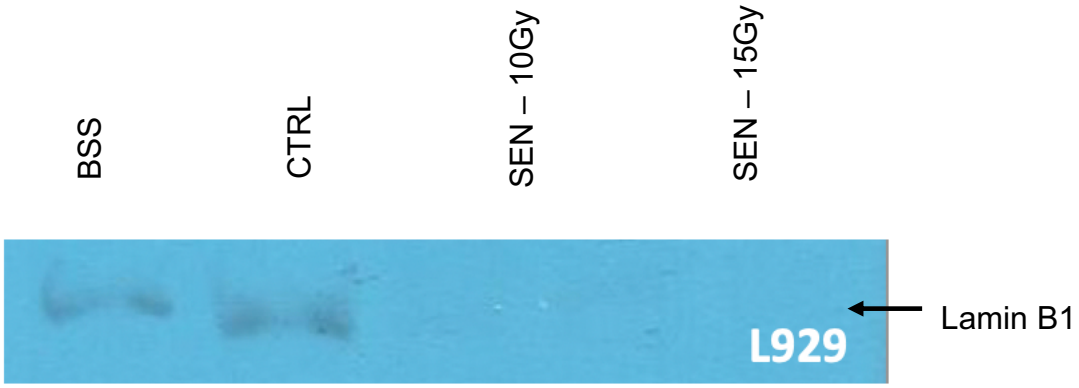

Figure J1: Western Blot for Lamin B1. L929 cells BSS = before serum starvation, CTRL = no irradiation, SEN – 10Gy, SEN – 15Gy were probed for Lamin B1. BSS and CTRL show positive signals for the protein whereas in SEN cells show no or minimal Lamin B1.

File Name			20201210_3010	20201210_30	20201210_3	20201210	20201210_3	20201210_3	20201210_3	20201210_3010253939 1221-01_SEN_04.RCC		
Description												
Sample ID			CTRL + All	CTRL + HB	CTRL + Phy	CTRL	SEN + All	SEN + HB	SEN + Phy	SEN		
Sample Date			10/12/20	10/12/20	10/12/20	########	10/12/20	10/12/20	10/12/20	10/12/20		
File Version			2	2	2	2	2	2	2	2		
Gene RLF			NS_INFL_MM_V2_	NS_INFL_MM_	NS_INFL_MM	NS_INFL_	NS_INFL_MM	NS_INFL_MM	NS_INFL_MM	NS_INFL_MM_V2_C2537		
Comments												
Lane ID			7	5	9	3	8	6	10	4		
FOV Count			194	194	194	194	194	194	194	194		
FOV Counted			194	194	194	194	194	194	194	194		
Scanner ID			1610P0142	1610P0142	1610P0142	1610P014	1610P0142	1610P0142	1610P0142	1610P0142		
Stage Position			1	1	1	1	1	1	1	1		
Binding Density			0.48	0.32	0.33	0.25	0.62	0.53	0.61	0.54		
Positive	POS_A	ERCC_00117.1	53448	50844	45401	55764	54545	40824	52144	46722		
Positive	POS_B	ERCC_00112.1	20424	18728	17269	20660	20284	14468	19416	16967		
Positive	POS_C	ERCC_00002.1	5469	5368	4745	5690	5366	4227	5225	4731		
Positive	POS_D	ERCC_00092.1	1281	1266	1179	1382	1353	1028	1315	1104		
Positive	POS_E	ERCC_00035.1	223	233	208	220	227	182	213	228		
Positive	POS_F	ERCC_00034.1	95	85	82	96	102	81	99	75		
Negative	NEG_A	ERCC_00096.1	23	21	16	22	13	23	23	24		
Negative	NEG_B	ERCC_00041.1	16	18	17	15	16	12	26	19		
Negative	NEG_C	ERCC_00019.1	26	15	25	27	26	27	19	19		
Negative	NEG_D	ERCC_00076.1	26	15	19	16	25	27	32	16		
Negative	NEG_E	ERCC_00098.1	24	22	21	24	16	16	19	23		
Negative	NEG_F	ERCC_00126.1	35	44	29	37	23	34	30	36		
Negative	NEG_G	ERCC_00144.1	6	5	4	4	5	3	5	6		
Negative	NEG_H	ERCC_00154.1	12	8	13	8	15	16	9	6		
		BACKGROUND	39.3614503	42.2366504	33.231546	40.4105	31.433551	39.570624	39.436929	38.27734	Background 70 counts	
Endogenous	Atf2	NM_001025093.1	1623.61	1430.99	1514.21	1726.36	2447.6	2002.22	2487.73	2405.66	8	
Endogenous	Bcl2l1	NM_009743.4	642.06	546.62	592.03	628.81	919.4	811.04	993.8	977.79	8	
Endogenous	Birc2	NM_007465.2	664.2	587.19	659.18	672.9	689.97	598.46	690.42	692.81	8	
Endogenous	C1ra	NM_023143.3	438.7	408.17	517.05	370.75	247.66	180.98	259.25	239.78	8	
Endogenous	C1s	NM_144938.2	2369.81	1353.41	3048.56	1710.02	1991.21	1003.5	2020.7	2026.34	8	
Endogenous	C2	NM_013484.2	798.68	620.61	823.69	779.07	743.81	477.81	709.73	675.12	8	
Endogenous	Ccl2	NM_011333.3	3867.13	3754.7	1351.93	4493.1	25070.75	21966.01	33009.73	24456.6	8	
Endogenous	Ccl7	NM_013654.2	627.3	683.87	384.99	710.47	2937.12	2585.36	3456.71	2921.58	8	
Endogenous	Cd40	NM_011611.2	268.96	311.5	336.86	315.22	863.08	675.07	953.35	736.05	8	
Endogenous	Cdc42	NM_009861.1	16328.71	17237.49	15287.56	16683.8	17235.11	15658.68	18484.2	17127.58	8	
Endogenous	Cebpb	NM_009883.3	7785.11	8896.23	8296.25	9141.36	5147.01	4139.45	4840.31	4952.84	8	
Endogenous	Cfl1	NM_007687.5	20427.91	19204.35	16699.93	18027.9	22350.64	22530	23162.71	21982.15	8	
Endogenous	Csf1	NM_001113530.1	39305.2	25773.29	29886.85	20786.5	82391.89	85702.88	91223.08	88310.87	8	
Endogenous	Cxcl1	NM_008176.1	321.44	330.6	229.43	277.65	3465.57	2633.24	4640.81	3617.34	8	
Endogenous	Daxx	NM_007829.3	247.64	200.51	213.76	236.82	281.62	269.07	254.66	240.76	8	
Endogenous	Ddit3	NM_007837.3	5822.84	5899.39	6280.66	5659.25	10256.74	7186.35	11321.64	10369.51	8	
Endogenous	Fos	NM_010234.2	1322.66	689.83	923.3	1442.17	249.32	151.29	189.38	156.25	8	
Endogenous	Gnaq	NM_008139.5	1662.15	1015.65	1291.5	841.13	2269.52	1925.62	2236.75	2391.91	8	
Endogenous	Gnas	NM_010309.3	25567.69	24806.57	23033.19	23798.3	25939.63	22880.46	27379.7	26954.64	8	
Endogenous	Gnb1	NM_008142.3	7079.08	5543.73	5689.75	5646.19	7557.34	7874.82	7931.12	8081.77	8	
Endogenous	Grb2	NM_008163.3	966.78	741.15	875.17	899.93	1251.55	1131.81	1302.7	1319.77	8	
Endogenous	Hc	NM_010406.1	417.38	214.83	302.17	253.16	212.87	215.45	212.37	248.62	8	
Endogenous	Hdac4	NM_207225.1	358.34	176.64	256.28	218.86	488.69	425.15	499.2	520.83	8	
Endogenous	Hif1a	NM_010431.2	8177.07	6616.68	6918.57	6302.76	7804.17	6240.3	7704.05	7714.24	8	
Endogenous	Hmgb1	NM_010439.3	5006.12	5843.3	5013.78	4744.62	4012.25	3323.63	3949.47	3872.84	8	
Endogenous	Hmgn1	NM_008251.3	8380.43	8754.21	7350.56	9288.36	7059.54	7726.41	7225.99	7454.81	8	
Endogenous	Ifit2	NM_008332.2	219.76	226.76	191.37	148.63	535.91	469.2	547.01	577.83	8	

Endogenous	Iigp1	NM_021792.3	630.58	1660.14	1447.06	643.51	1576.24	1128.94	1473.7	1174.33	8
Endogenous	Il10rb	NM_008349.5	458.38	479.78	494.66	470.38	653.52	659.75	721.68	733.1	8
Endogenous	Il1r1	NM_001123382.1	1379.24	1213.77	1194.13	1095.92	1530.68	1028.4	1360.62	1411.17	8
Endogenous	Il1rap	NM_008364.2	490.36	359.24	415.2	333.19	609.62	521.86	646.29	626.97	8
Endogenous	Il6	NM_031168.1	96.76	94.29	106.32	111.06	118.45	115.86	123.19	122.84	8
Endogenous	Irf1	NM_008390.1	82	201.7	149.97	124.13	662.63	447.17	729.03	578.81	8
Endogenous	Jun	NM_010591.2	1146.36	901.08	880.77	1518.93	1063.53	857	1074.71	1085.89	8
Endogenous	Keap1	NM_016679.4	1631.81	620.61	985.97	1156.35	697.42	690.39	767.65	751.77	8
Endogenous	Limk1	NM_010717.2	774.9	642.09	716.25	592.87	662.63	602.29	652.73	681.02	8
Endogenous	Ly96	NM_016923.1	682.24	387.88	414.08	529.18	613.76	726.77	672.95	706.57	8
Endogenous	Maff	NM_010755.3	260.76	404.59	310	272.75	387.64	336.1	442.2	408.81	8
Endogenous	Mafk	NM_010757.2	262.4	180.22	176.83	227.02	997.26	744.97	1026.9	875.59	8
Endogenous	Map2k1	NM_008927.3	314.06	205.28	207.04	241.72	414.15	378.23	448.64	394.07	8
Endogenous	Map2k4	NM_009157.4	2250.09	2093.37	2243.89	2002.38	3283.35	3043.07	3602.88	3280.27	8
Endogenous	Map2k6	NM_011943.2	1135.7	744.73	858.39	787.23	1375.79	1123.2	1456.23	1420.01	8
Endogenous	Map3k5	NM_008580.4	288.64	235.12	266.36	284.19	214.53	180.98	246.38	222.09	8
Endogenous	Map3k7	NM_172688.2	164.82	118.15	177.94	99.63	335.46	273.86	284.99	327.24	8
Endogenous	Mapk1	NM_001038663.1	1126.68	1002.53	1052	883.59	859.77	843.59	808.1	913.92	8
Endogenous	Mapk14	NM_011951.2	1790.89	1311.64	1459.37	1301.71	2088.95	1850.93	2112.64	2123.63	8
Endogenous	Mapk3	NM_011952.2	244.36	189.76	185.78	253.16	237.72	270.98	241.79	261.4	8
Endogenous	Mapk8	NM_016700.3	1266.9	804.41	952.4	816.63	1297.93	1182.56	1372.57	1459.32	8
Endogenous	Mapkapk2	NM_008551.1	1818.77	2006.25	1965.22	2090.57	1648.3	1455.46	1613.44	1663.72	8
Endogenous	Masp1	NM_008555.2	712.58	675.51	609.94	810.1	1017.97	1058.08	1049.88	1000.39	8
Endogenous	Max	NM_008558.1	1010.24	792.47	799.07	748.03	1316.16	1188.31	1375.33	1307.98	8
Endogenous	Mef2d	NM_133665.3	274.7	221.99	275.31	244.99	400.89	431.85	398.99	392.1	8
Endogenous	Mknk1	NM_021461.4	496.92	422.49	440.94	558.58	477.92	457.71	531.38	558.18	8
Endogenous	Myc	NM_010849.4	606.8	362.82	508.09	400.15	977.38	950.84	957.03	1003.34	8
Endogenous	Myd88	NM_010851.2	516.6	367.59	464.45	409.95	487.04	424.19	533.22	459.91	8
Endogenous	Myl2	NM_010861.3	10864.22	4111.55	6016.54	7722.06	3072.14	3343.74	2747.9	2962.86	8
Endogenous	Nfatc3	NM_010901.2	578.92	587.19	605.46	646.77	723.93	644.43	734.55	740.96	8
Endogenous	Nfe2l2	NM_010902.3	197.62	270.92	269.71	307.05	142.47	104.37	153.53	127.75	8
Endogenous	Nfkb1	NM_008689.2	494.46	307.92	373.8	292.35	726.41	636.77	764.89	800.91	8
Endogenous	Nod1	NM_172729.2	1782.69	1818.87	2013.35	1594.06	2151.9	1580.9	2280.88	2209.12	8
Endogenous	Nr3c1	NM_008173.3	1112.74	852.15	962.47	891.76	1106.6	1108.83	1146.41	1201.85	8
Endogenous	Oas1a	NM_145211.2	137.76	106.22	108.56	155.16	260.91	192.47	294.19	280.07	8
Endogenous	Pdgfa	NM_008808.3	2888.05	2073.08	2692.67	2623.02	3722.35	2988.49	3662.64	3709.71	8
Endogenous	Pla2g4a	NM_008869.2	644.52	770.99	750.95	895.03	2141.96	2124.79	2016.11	1505.51	8
Endogenous	Ppp1r12b	NM_001081307.1	6177.9	6981.88	5267.83	5285.23	5663.03	5678.22	6952.03	6289.32	8
Endogenous	Prkca	NM_011101.3	414.92	415.33	392.82	287.45	678.37	554.42	711.57	588.64	8
Endogenous	Prkcb	NM_008855.2	164.82	93.09	132.06	137.19	131.7	97.67	133.3	145.44	8
Endogenous	Ptger4	NM_008965.1	696.18	361.63	530.48	543.88	799.3	765.08	810.86	889.35	8
Endogenous	Ptgir	NM_008967.3	728.98	380.72	616.65	478.55	417.46	326.52	441.28	515.92	8
Endogenous	Ptk2	NM_007982.2	151.7	138.44	141.01	129.03	168.14	145.55	185.71	183.77	8
Endogenous	Rac1	NM_009007.2	546.12	453.52	550.62	472.01	549.16	581.23	558.04	587.66	8
Endogenous	Raf1	NM_029780.3	1496.51	1055.04	1216.51	1190.65	1316.98	1336.73	1286.15	1302.09	8
Endogenous	Rapgef2	NM_001099624.2	11913.82	9010.8	9211.71	9059.7	12762.33	11816.07	13688.93	13414.92	8
Endogenous	Rela	NM_009045.4	2040.99	1879.74	1808.54	1937.05	1600.26	1556.96	1569.31	1591	8
Endogenous	Relb	NM_009046.2	1440.74	1046.69	1226.59	1251.08	3019.95	2563.34	3180.91	3188.88	8
Endogenous	Rhoa	NM_016802.4	882.32	644.48	786.76	723.53	1755.15	1704.42	1827.64	1864.19	8
Endogenous	Ripk1	NM_009068.3	512.5	509.62	512.57	503.04	934.31	893.39	980.93	1033.81	8
Endogenous	Ripk2	NM_138952.3	6304.18	7296.96	5697.58	7676.33	6195.63	6058.37	6120.03	6173.36	8
Endogenous	Rock2	NM_009072.2	286.18	269.73	249.57	212.32	554.96	515.16	594.81	598.47	8
Endogenous	Rps6ka5	NM_153587.2	178.76	181.41	254.05	233.56	501.95	507.5	565.39	556.21	8
Endogenous	Shc1	NM_011368.4	606.8	417.72	458.85	454.05	1190.26	1077.23	1208.01	1175.32	8
Endogenous	Stat1	NM_009283.3	164.82	157.54	162.28	140.46	342.91	313.12	332.8	341.98	8
Endogenous	Stat2	NM_019963.1	1915.53	2176.91	1856.67	1773.72	2326.67	2016.58	2440.84	2469.54	8
Endogenous	Stat3	NM_213659.2	879.86	955.98	915.46	726.8	1356.74	1214.16	1201.57	1115.37	8
Endogenous	Tcf4	NM_013685.1	546.12	457.1	517.05	437.71	1709.6	1434.4	1679.63	1471.11	8

Endogenous	Tgfb1	NM_011577.1	2045.91	1436.95	1984.25	1659.39	2800.46	2053.93	2701.93	2725.04	8
Endogenous	Tgfb3	NM_009368.2	2900.35	1895.25	2582.99	2270.23	2576.82	1927.53	2479.45	2615.96	8
Endogenous	Tgfbr1	NM_009370.2	957.76	1119.49	951.28	756.2	1152.15	1170.12	1288.91	1277.52	8
Endogenous	Tlr2	NM_011905.2	382.94	262.57	343.58	256.42	445.62	398.34	518.51	514.94	8
Endogenous	Tlr4	NM_021297.2	242.72	173.06	224.95	194.36	641.1	516.12	649.05	653.5	8
Endogenous	Tlr6	NM_011604.3	177.94	187.38	168.99	166.59	263.4	248	298.78	276.14	8
Endogenous	Tnfaip3	NM_009397.2	728.98	711.32	694.99	607.57	757.06	655.92	837.52	774.37	8
Endogenous	Tollip	NM_023764.3	112.34	89.51	101.84	94.73	150.75	150.33	167.32	148.39	8
Endogenous	Tradd	NM_001033161.2	267.32	278.08	307.77	217.22	253.46	206.83	249.14	240.76	8
Endogenous	Traf2	NM_009422.2	127.1	100.25	107.44	122.49	361.96	297.8	387.96	356.72	8
Endogenous	Twist2	NM_007855.2	2232.87	1695.94	1797.35	1910.92	2517.18	2369.92	2657.8	2705.39	8
Endogenous	C3	NM_009778.2	193.52	184.99	203.68	238.46	215.36	168.53	208.69	193.59	8
Endogenous	Il23a	NM_031252.1	586.3	595.55	513.69	651.67	688.31	622.4	742.82	740.96	8
Endogenous	Map3k1	NM_011945.2	642.88	615.84	556.22	476.91	672.57	684.64	656.41	681.02	8
Endogenous	Tlr5	NM_016928.2	86.1	75.19	77.22	58.8	202.93	139.8	193.06	196.54	7
Endogenous	Il18	NM_008360.1	341.94	34.61	208.16	328.29	405.86	122.57	369.57	381.29	7
Endogenous	Irf7	NM_016850.2	76.26	60.87	90.65	80.03	482.89	377.27	392.56	247.64	7
Endogenous	Tlr1	NM_030682.1	161.54	51.32	76.1	88.2	415.8	452.92	459.67	412.74	7
Endogenous	Bcl6	NM_009744.3	105.78	66.84	154.44	86.56	93.6	71.82	102.05	83.53	7
Endogenous	Il18rap	NM_010553.2	67.24	60.87	104.08	107.8	102.71	76.6	107.56	101.22	6
Endogenous	Il6ra	NM_010559.2	179.58	23.87	38.05	104.53	712.33	539.1	536.89	384.24	6
Endogenous	Mafg	XM_001002362.1	32.8	74	66.03	35.93	580.63	566.86	534.13	438.29	5
Endogenous	Ptgs2	NM_011198.3	39.36	70.42	42.53	57.16	128.39	94.8	149.85	138.56	5
Endogenous	Smad7	NM_001042660.1	87.74	41.77	59.31	66.96	121.76	105.33	142.5	119.89	5
Endogenous	Ager	NM_007425.2	100.04	64.45	77.22	60.43	104.36	77.56	69.87	113.01	5
Endogenous	Areg	NM_009704.3	44.28	35.8	53.72	52.26	82	80.43	114	105.15	4
Endogenous	Ccl20	NM_016960.1	10.66	7.16	15.67	6.53	98.57	127.35	99.29	110.06	4
Endogenous	Ifi44	NM_133871.2	15.58	13.13	13.43	11.43	1702.14	376.31	1516.91	957.16	4
Endogenous	Ifit1	NM_008331.2	45.1	41.77	52.6	32.67	3385.23	2580.58	2969.46	1585.1	4
Endogenous	Ifit3	NM_010501.1	22.96	27.45	26.86	27.77	285.76	279.6	276.72	190.64	4
Endogenous	Il15	NM_008357.1	52.48	66.84	36.93	55.53	176.43	178.1	194.9	183.77	4
Endogenous	Il7	NM_008371.2	16.4	17.9	14.55	35.93	288.25	189.59	257.41	170.99	4
Endogenous	Oas2	NM_145227.2	36.08	45.35	33.57	44.1	92.77	96.71	88.26	97.29	4
Endogenous	Ptgs1	NM_008969.3	21.32	17.9	17.91	11.43	89.46	80.43	91.01	89.43	4
Endogenous	Tlr3	NM_126166.2	12.3	17.9	16.79	13.07	115.96	96.71	143.42	82.55	4
Endogenous	Tslp	NM_021367.1	10.66	13.13	14.55	13.07	83.66	48.83	83.66	70.75	3
Endogenous	Ccl5	NM_013653.1	47.56	40.58	39.17	35.93	120.93	91.92	114.92	66.82	3
Endogenous	Hmgb2	NM_008252.3	73.8	81.16	79.46	53.9	39.76	31.6	42.29	35.38	3
Endogenous	Oasl1	NM_145209.2	7.38	8.35	6.71	8.17	90.28	60.33	94.69	61.91	2
Endogenous	Ccl17	NM_011332.2	45.92	64.45	74.98	70.23	59.64	44.05	63.43	64.86	2
Endogenous	Ifi27l2a	NM_029803.1	59.04	46.55	36.93	45.73	75.37	50.75	72.63	57	2
Endogenous	Masp2	NM_010767.3	59.86	33.42	39.17	53.9	67.92	67.99	86.42	86.48	2
Endogenous	Mmp3	NM_010809.1	31.16	37	36.93	39.2	52.18	76.6	58.84	71.74	2
Endogenous	Mx2	NM_013606.1	27.06	26.26	32.46	37.57	72.06	57.45	72.63	47.17	2
Endogenous	Nod2	NM_145857.2	11.48	5.97	11.19	4.9	83.66	60.33	88.26	36.36	2
Endogenous	Ptger2	NM_008964.4	23.78	16.71	33.57	34.3	85.31	24.9	68.03	39.31	1
Endogenous	Cxcr4	NM_009911.3	26.24	47.74	32.46	73.5	47.21	41.17	29.42	32.43	1
Endogenous	H2-Eb1	NM_010382.2	5.74	5.97	3.36	9.8	2.48	1.92	3.68	1	0
Endogenous	Mx1	NM_010846.1	17.22	9.55	8.95	21.23	10.77	9.58	11.03	13.76	0
Endogenous	Trem2	NM_031254.2	18.04	8.35	10.07	11.43	8.28	6.7	13.79	10.81	0
Endogenous	Alox12	NM_007440.4	9.84	10.74	10.07	4.9	5.8	4.79	9.19	7.86	0
Endogenous	Alox15	NM_009660.3	10.66	10.74	6.71	11.43	10.77	4.79	7.35	5.9	0
Endogenous	Alox5	NM_009662.2	10.66	10.74	6.71	8.17	7.45	7.66	11.03	10.81	0
Endogenous	Arg1	NM_007482.3	12.3	5.97	8.95	17.97	19.05	11.49	25.74	20.64	0
Endogenous	C1qa	NM_007572.2	14.76	11.93	12.31	17.97	28.16	13.41	30.34	17.69	0
Endogenous	C1qb	NM_009777.2	7.38	5.97	10.07	16.33	10.77	7.66	7.35	7.86	0
Endogenous	C3ar1	NM_009779.2	6.56	7.16	7.83	6.53	6.63	1.92	7.35	6.88	0
Endogenous	C4a	NM_011413.2	4.92	4.77	4.48	8.17	6.63	2.87	9.19	4.91	0

Endogenous	C6	NM_016704.2	14.76	16.71	6.71	13.07	8.28	9.58	9.19	14.74	0
Endogenous	C7	XM_356827.6	8.2	16.71	14.55	19.6	10.77	10.53	11.03	13.76	0
Endogenous	C8a	NM_146148.1	12.3	15.52	13.43	16.33	13.25	23.94	27.58	19.65	0
Endogenous	C8b	NM_133882.2	5.74	10.74	7.83	8.17	6.63	5.75	7.35	7.86	0
Endogenous	C9	NM_013485.1	23.78	21.48	19.03	26.13	13.25	12.45	18.39	18.67	0
Endogenous	Ccl11	NM_011330.3	7.38	13.13	15.67	16.33	13.25	15.32	22.06	15.72	0
Endogenous	Ccl19	NM_011888.2	19.68	20.29	13.43	19.6	8.28	17.24	20.23	22.6	0
Endogenous	Ccl21a	NM_011124.4	6.56	15.52	12.31	14.7	9.94	5.75	14.71	6.88	0
Endogenous	Ccl22	NM_009137.2	6.56	5.97	2.24	4.9	6.63	13.41	6.44	12.78	0
Endogenous	Ccl24	NM_019577.4	15.58	10.74	13.43	19.6	19.05	13.41	34.02	26.53	0
Endogenous	Ccl3	NM_011337.1	11.48	15.52	8.95	9.8	8.28	4.79	12.87	6.88	0
Endogenous	Ccl4	NM_013652.1	30.34	28.64	48.12	47.36	43.07	40.22	45.05	56.01	0
Endogenous	Ccl8	NM_021443.2	20.5	8.35	11.19	24.5	8.28	8.62	11.95	8.84	0
Endogenous	Ccr1	NM_009912.4	16.4	19.1	16.79	32.67	10.77	9.58	10.11	9.83	0
Endogenous	Ccr2	NM_009915.2	6.56	8.35	5.6	8.17	5.8	6.7	10.11	4.91	0
Endogenous	Ccr3	NM_009914.4	18.86	17.9	17.91	17.97	17.39	15.32	18.39	12.78	0
Endogenous	Ccr4	NM_009916.2	13.94	8.35	7.83	17.97	13.25	7.66	11.95	8.84	0
Endogenous	Ccr7	NM_007719.2	12.3	13.13	12.31	11.43	13.25	13.41	17.47	5.9	0
Endogenous	Cd163	NM_053094.2	9.84	13.13	15.67	14.7	8.28	8.62	11.03	20.64	0
Endogenous	Cd4	NM_013488.2	9.02	9.55	10.07	8.17	5.8	5.75	4.6	3.93	0
Endogenous	Cd40lg	NM_011616.2	20.5	22.68	33.57	21.23	26.51	16.28	25.74	24.57	0
Endogenous	Cd55	NM_010016.2	9.02	4.77	4.48	19.6	4.14	6.7	8.27	5.9	0
Endogenous	Cd86	NM_019388.3	3.28	8.35	8.95	16.33	9.94	11.49	6.44	7.86	0
Endogenous	Cfb	NM_008198.2	22.96	26.26	14.55	22.87	20.71	22.98	13.79	25.55	0
Endogenous	Cfd	NM_013459.1	4.92	8.35	10.07	9.8	6.63	4.79	6.44	9.83	0
Endogenous	Chi3l3	NM_009892.1	4.1	3.58	2.24	8.17	28.16	34.47	38.61	26.53	0
Endogenous	Creb1	NM_133828.2	6.56	5.97	8.95	17.97	6.63	9.58	8.27	1.97	0
Endogenous	Crp	NM_007768.4	18.04	11.93	15.67	16.33	36.44	23.94	39.53	30.46	0
Endogenous	Csf2	NM_009969.4	9.84	14.32	13.43	13.07	14.91	10.53	16.55	16.71	0
Endogenous	Csf3	NM_009971.1	8.2	11.93	8.95	6.53	10.77	3.83	15.63	7.86	0
Endogenous	Cxcl10	NM_021274.1	4.1	7.16	11.19	4.9	12.42	8.62	6.44	4.91	0
Endogenous	Cxcl2	NM_009140.2	14.76	15.52	15.67	13.07	55.5	44.05	56.08	36.36	0
Endogenous	Cxcl3	NM_203320.2	5.74	3.58	4.48	6.53	4.97	5.75	7.35	5.9	0
Endogenous	Cxcl5	NM_009141.2	15.58	11.93	20.14	11.43	13.25	10.53	15.63	9.83	0
Endogenous	Cxcl9	NM_008599.2	4.1	9.55	12.31	9.8	13.25	8.62	10.11	7.86	0
Endogenous	Cxcr1	NM_178241.4	17.22	21.48	15.67	17.97	20.71	18.19	28.5	16.71	0
Endogenous	Cxcr2	NM_009909.3	9.02	10.74	11.19	13.07	6.63	2.87	11.95	9.83	0
Endogenous	Cysltr1	NM_021476.4	34.44	31.03	23.5	32.67	30.65	43.09	37.69	40.29	0
Endogenous	Cysltr2	NM_001162412.1	4.92	13.13	7.83	9.8	11.6	4.79	11.03	6.88	0
Endogenous	Defa-rs1	NM_007844.2	7.38	11.93	10.07	8.17	8.28	6.7	9.19	10.81	0
Endogenous	Elk1	NM_007922.4	7.38	11.93	6.71	8.17	8.28	3.83	10.11	19.65	0
Endogenous	Fasl	NM_010177.3	24.6	25.06	23.5	42.46	21.54	24.9	12.87	21.62	0
Endogenous	Flt1	NM_010228.3	13.94	23.87	10.07	6.53	6.63	6.7	12.87	10.81	0
Endogenous	Fxyd2	NM_052823.2	9.02	14.32	10.07	14.7	4.14	9.58	8.27	9.83	0
Endogenous	Gngt1	NM_010314.2	19.68	20.29	26.86	27.77	60.47	44.05	58.84	55.03	0
Endogenous	Gpr44	NM_009962.2	27.06	26.26	24.62	16.33	34.79	47.88	33.1	39.31	0
Endogenous	H2-Ea-ps	NM_010381.2	19.68	17.9	13.43	24.5	19.05	16.28	17.47	20.64	0
Endogenous	Hras1	NM_008284.2	7.38	7.16	5.6	3.27	7.45	3.83	8.27	4.91	0
Endogenous	Hsh2d	NM_197944.1	21.32	19.1	19.03	13.07	28.16	28.73	41.37	24.57	0
Endogenous	Hspb1	NM_013560.2	13.12	11.93	24.62	9.8	9.94	15.32	4.6	7.86	0
Endogenous	Hspb2	NM_024441.3	22.96	9.55	16.79	14.7	18.22	21.07	20.23	19.65	0
Endogenous	Ifna1	NM_010502.2	9.84	3.58	12.31	11.43	7.45	6.7	8.27	9.83	0
Endogenous	Ifnb1	NM_010510.1	15.58	21.48	15.67	16.33	14.08	19.15	27.58	20.64	0
Endogenous	Ifng	NM_008337.1	12.3	9.55	13.43	14.7	7.45	6.7	9.19	3.93	0
Endogenous	Il10	NM_010548.1	29.52	32.22	43.65	26.13	34.79	33.51	33.1	25.55	0
Endogenous	Il11	NM_008350.2	6.56	13.13	16.79	16.33	7.45	3.83	11.03	10.81	0
Endogenous	Il12a	NM_008351.1	4.92	14.32	8.95	13.07	6.63	6.7	9.19	6.88	0
Endogenous	Il12b	NM_008352.1	6.56	4.77	10.07	8.17	9.11	5.75	14.71	13.76	0

Endogenous	Il12b	NM_008352.1	6.56	4.77	10.07	8.17	9.11	5.75	14.71	13.76	0
Endogenous	Il13	NM_008355.2	12.3	13.13	14.55	14.7	19.05	17.24	23.9	28.5	0
Endogenous	Il17a	NM_010552.3	14.76	27.45	24.62	14.7	9.94	11.49	19.31	15.72	0
Endogenous	Il1a	NM_010554.4	8.2	4.77	8.95	11.43	9.94	9.58	7.35	7.86	0
Endogenous	Il1b	NM_008361.3	13.12	15.52	7.83	4.9	11.6	8.62	26.66	15.72	0
Endogenous	Il1rn	NM_031167.4	12.3	26.26	15.67	19.6	12.42	23.94	16.55	7.86	0
Endogenous	Il2	NM_008366.3	1	5.97	5.6	9.8	9.11	4.79	4.6	2.95	0
Endogenous	Il21	NM_021782.2	9.02	8.35	5.6	11.43	11.6	15.32	20.23	15.72	0
Endogenous	Il22	NM_016971.1	13.94	16.71	8.95	11.43	11.6	11.49	13.79	12.78	0
Endogenous	Il22ra2	NM_178258.5	9.84	9.55	13.43	8.17	12.42	6.7	10.11	7.86	0
Endogenous	Il23r	NM_144548.1	9.02	4.77	10.07	16.33	4.14	5.75	6.44	6.88	0
Endogenous	Il3	NM_010556.4	12.3	5.97	6.71	9.8	17.39	11.49	8.27	9.83	0
Endogenous	Il4	NM_021283.1	5.74	8.35	4.48	11.43	8.28	3.83	11.03	11.79	0
Endogenous	Il5	NM_010558.1	31.16	34.61	32.46	49	28.16	26.81	29.42	26.53	0
Endogenous	Il9	NM_008373.1	18.04	16.71	13.43	29.4	38.1	34.47	39.53	39.31	0
Endogenous	Irf3	NM_016849.3	22.14	48.93	39.17	37.57	26.51	22.02	34.02	43.24	0
Endogenous	Irf5	NM_012057.3	10.66	13.13	14.55	11.43	28.16	23.94	27.58	21.62	0
Endogenous	Itgb2	NM_008404.4	8.2	8.35	10.07	6.53	15.74	11.49	22.98	13.76	0
Endogenous	Kng1	NM_023125.3	21.32	21.48	11.19	16.33	19.05	30.64	31.26	18.67	0
Endogenous	Lta	NM_010735.1	21.32	28.64	15.67	19.6	16.57	19.15	24.82	20.64	0
Endogenous	Ltb	NM_008518.2	13.94	7.16	7.83	8.17	15.74	12.45	11.03	12.78	0
Endogenous	Ltb4r1	NM_008519.2	8.2	9.55	7.83	3.27	9.11	7.66	9.19	5.9	0
Endogenous	Ltb4r2	NM_020490.2	32.8	31.03	25.74	31.03	38.1	36.39	34.93	30.46	0
Endogenous	Map3k9	NM_177395.4	4.1	2.39	3.36	13.07	6.63	4.79	5.52	2.95	0
Endogenous	Mapkapk5	XM_990515.1	7.38	11.93	10.07	13.07	5.8	3.83	4.6	9.83	0
Endogenous	Mbl2	NM_010776.1	11.48	13.13	12.31	16.33	14.08	12.45	27.58	14.74	0
Endogenous	Mef2a	XM_976032.1	9.84	9.55	8.95	13.07	13.25	13.41	14.71	12.78	0
Endogenous	Mef2b	NM_001045484.1	8.2	10.74	13.43	13.07	9.11	12.45	6.44	7.86	0
Endogenous	Mef2c_Mm	NM_025282.2	59.04	52.51	51.48	45.73	33.13	33.51	41.37	32.43	0
Endogenous	Mmp9	NM_013599.2	10.66	14.32	13.43	14.7	14.91	13.41	11.95	16.71	0
Endogenous	Mrc1	NM_008625.1	41	38.19	44.77	26.13	65.44	43.09	68.95	57.98	0
Endogenous	Nlrp3	NM_145827.3	39.36	22.68	33.57	55.53	21.54	17.24	22.06	24.57	0
Endogenous	Nos2	NM_010927.3	9.02	3.58	5.6	8.17	9.11	8.62	13.79	13.76	0
Endogenous	Nox1	NM_172203.1	6.56	8.35	5.6	3.27	4.97	4.79	7.35	3.93	0
Endogenous	Pik3c2g	NM_011084.2	14.76	20.29	17.91	19.6	17.39	14.36	12.87	15.72	0
Endogenous	Plcb1	NM_019677.1	13.94	13.13	8.95	8.17	9.11	11.49	18.39	12.78	0
Endogenous	Ptger1	NM_013641.2	8.2	10.74	8.95	8.17	4.97	5.75	11.03	5.9	0
Endogenous	Ptger3	NM_011196.2	15.58	17.9	22.38	19.6	24.02	22.98	28.5	18.67	0
Endogenous	Ptgfr	NM_008966.3	13.12	8.35	8.95	13.07	7.45	8.62	9.19	8.84	0
Endogenous	Retnla	NM_020509.3	36.9	37	34.69	31.03	39.76	40.22	29.42	24.57	0
Endogenous	Tbxa2r	NM_001277265.1	8.2	9.55	10.07	13.07	11.6	17.24	15.63	12.78	0
Endogenous	Tgfb2	NM_009367.1	5.74	15.52	4.48	13.07	5.8	13.41	8.27	10.81	0
Endogenous	Tlr7	NM_133211.3	23.78	23.87	25.74	14.7	40.59	49.79	30.34	35.38	0
Endogenous	Tlr8	NM_133212.2	14.76	26.26	11.19	13.07	17.39	17.24	29.42	14.74	0
Endogenous	Tlr9	NM_031178.2	16.4	8.35	10.07	14.7	21.54	16.28	18.39	17.69	0
Endogenous	Tnf	NM_013693.1	4.92	5.97	2.24	6.53	5.8	2.87	7.35	6.88	0
Endogenous	Tnfsf14	NM_019418.2	41.82	21.48	68.27	58.8	66.26	54.58	56.08	52.08	0
Endogenous	Tyrobp	NM_011662.2	13.94	13.13	10.07	8.17	13.25	13.41	13.79	18.67	0
TOTAL NO OF TARGETS ABOVE BACKGROUND			108	103	108	107	127	122	126	123	
Housekeeping	Cltc	NM_001003908.1	14046	8027	8560	4979	12925	10304	11405	10842	
Housekeeping	Gapdh	NM_008084.1	14114	10009	12117	7742	12208	10397	11173	10322	
Housekeeping	Gusb	NM_010368.1	3245	2227	2203	1546	2281	1934	2275	2219	
Housekeeping	Hprt	NM_013556.2	1169	803	845	724	1812	1587	1701	1556	
Housekeeping	Pgk1	NM_008828.2	2884	2388	2507	1836	3701	3297	3245	2844	
Housekeeping	Tubb5	NM_011655.4	6504	4325	4509	2852	5502	5132	4439	4333	

Table K1: Table of Normalised Counts for Nanostring analysis of Inflammation Panel for CTRL and SEN cells with nutraceutical treatments. 254 genes were analysed for all following samples: CTRL, CTRL + HB, CTRL + Allicin, CTRL + Phytol, SEN , SEN + HB, SEN + Allicin, SEN + Phytol.

	CTRL + All	CTRL + HB	CTRL + Phy	CTRL	SEN + All	SEN + HB	SEN + Phy	SEN
Atf2	41.25	33.88	45.57	42.72	77.87	50.60	63.08	62.85
Bcl2l1	16.31	12.94	17.82	15.56	29.25	20.50	25.20	25.54
Birc2	16.87	13.90	19.84	16.65	21.95	15.12	17.51	18.10
C1ra	11.15	9.66	15.56	9.17	7.88	4.57	6.57	6.26
C1s	60.21	32.04	91.74	42.32	63.35	25.36	51.24	52.94
C2	20.29	14.69	24.79	19.28	23.66	12.07	18.00	17.64
Ccl2	98.25	88.90	40.68	111.19	797.58	555.11	837.03	638.93
Ccl7	15.94	16.19	11.59	17.58	93.44	65.34	87.65	76.33
Cd40	6.83	7.38	10.14	7.80	27.46	17.06	24.17	19.23
Cdc42	414.84	408.12	460.03	412.86	548.30	395.71	468.70	447.46
Cebpb	197.79	210.63	249.65	226.21	163.74	104.61	122.74	129.39
Cfl1	518.98	454.68	502.53	446.12	711.04	569.36	587.34	574.29
Csf1	998.57	610.21	899.35	514.38	2621.14	2165.82	2313.14	2307.13
Cxcl1	8.17	7.83	6.90	6.87	110.25	66.55	117.68	94.50
Daxx	6.29	4.75	6.43	5.86	8.96	6.80	6.46	6.29
Ddit3	147.93	139.67	189.00	140.04	326.30	181.61	287.08	270.90
Fos	33.60	16.33	27.78	35.69	7.93	3.82	4.80	4.08
Gnaq	42.23	24.05	38.86	20.81	72.20	48.66	56.72	62.49
Gnas	649.56	587.32	693.11	588.91	825.22	578.22	694.27	704.19
Gnb1	179.85	131.25	171.22	139.72	240.42	199.01	201.11	211.14
Grb2	24.56	17.55	26.34	22.27	39.82	28.60	33.03	34.48
Hc	10.60	5.09	9.09	6.26	6.77	5.44	5.39	6.50
Hdac4	9.10	4.18	7.71	5.42	15.55	10.74	12.66	13.61
Hif1a	207.74	156.66	208.19	155.97	248.28	157.70	195.35	201.54
Hmgb1	127.18	138.35	150.87	117.41	127.64	83.99	100.15	101.18
Hmgn1	212.91	207.27	221.19	229.85	224.59	195.26	183.23	194.76
Ifit2	5.58	5.37	5.76	3.68	17.05	11.86	13.87	15.10
Iigp1	16.02	39.31	43.54	15.92	50.15	28.53	37.37	30.68
Il10rb	11.65	11.36	14.89	11.64	20.79	16.67	18.30	19.15
Il1r1	35.04	28.74	35.93	27.12	48.70	25.99	34.50	36.87
Il1rap	12.46	8.51	12.49	8.25	19.39	13.19	16.39	16.38
Il23a	2.46	2.23	3.20	2.75	3.77	2.93	3.12	3.21
Il6	2.08	4.78	4.51	3.07	21.08	11.30	18.49	15.12
Irf1	29.12	21.33	26.50	37.59	33.83	21.66	27.25	28.37
Jun	41.46	14.69	29.67	28.62	22.19	17.45	19.47	19.64
Keap1	19.69	15.20	21.55	14.67	21.08	15.22	16.55	17.79
Limk1	17.33	9.18	12.46	13.10	19.53	18.37	17.06	18.46
Ly96	6.62	9.58	9.33	6.75	12.33	8.49	11.21	10.68
Maff	6.67	4.27	5.32	5.62	31.73	18.83	26.04	22.87
Mafk	7.98	4.86	6.23	5.98	13.18	9.56	11.38	10.30
Map2k1	57.16	49.56	67.52	49.55	104.45	76.90	91.36	85.70
Map2k4	28.85	17.63	25.83	19.48	43.77	28.38	36.93	37.10
Map2k6	7.33	5.57	8.02	7.03	6.82	4.57	6.25	5.80
Map3k1	4.19	2.80	5.35	2.47	10.67	6.92	7.23	8.55
Map3k5	28.62	23.74	31.66	21.87	27.35	21.32	20.49	23.88
Map3k7	45.50	31.05	43.92	32.21	66.46	46.78	53.57	55.48
Mapk1	6.21	4.49	5.59	6.26	7.56	6.85	6.13	6.83
Mapk14	32.19	19.05	28.66	20.21	41.29	29.88	34.80	38.12
Mapk3	46.21	47.50	59.14	51.73	52.44	36.78	40.91	43.46
Mapk8	18.10	15.99	18.35	20.05	32.38	26.74	26.62	26.14
Mapkapk2	25.67	18.76	24.05	18.51	41.87	30.03	34.87	34.17
Masp1	6.98	5.26	8.28	6.06	12.75	10.91	10.12	10.24
Max	12.62	10.00	13.27	13.82	15.20	11.57	13.47	14.58
Mef2d	15.42	8.59	15.29	9.90	31.09	24.03	24.27	26.21
Mknk1	13.12	8.70	13.98	10.14	15.49	10.72	13.52	12.02
Myc	276.01	97.35	181.05	191.09	97.73	84.50	69.68	77.41
Myd88	14.71	13.90	18.22	16.01	23.03	16.29	18.63	19.36
Myl2	5.02	6.41	8.12	7.60	4.53	2.64	3.89	3.34

Nfatc3	12.56	7.29	11.25	7.23	23.11	16.09	19.40	20.92
Nfe2l2	45.29	43.06	60.59	39.45	68.46	39.95	57.84	57.71
Nfkb1	28.27	20.18	28.96	22.07	35.20	28.02	29.07	31.40
Nod1	3.50	2.51	3.27	3.84	8.30	4.86	7.46	7.32
Nr3c1	73.37	49.08	81.03	64.91	118.42	75.52	92.87	96.92
Oas1a	16.37	18.25	22.60	22.15	68.14	53.70	51.12	39.33
Pdgfa	156.95	165.30	158.52	130.79	180.16	143.50	176.28	164.31
Pla2g4a	10.54	9.83	11.82	7.11	21.58	14.01	18.04	15.38
Ppp1r12b	4.19	2.20	3.97	3.39	4.19	2.47	3.38	3.80
Prkca	17.69	8.56	15.96	13.46	25.43	19.33	20.56	23.23
Prkcb	18.52	9.01	18.56	11.84	13.28	8.25	11.19	13.48
Ptger4	3.85	3.28	4.24	3.19	5.35	3.68	4.71	4.80
Ptgir	13.87	10.74	16.57	11.68	17.47	14.69	14.15	15.35
Ptk2	38.02	24.98	36.61	29.46	41.90	33.78	32.61	34.02
Rac1	302.68	213.34	277.20	224.19	406.01	298.61	347.11	350.47
Raf1	51.85	44.50	54.42	47.93	50.91	39.35	39.79	41.57
Rapgef2	36.60	24.78	36.91	30.96	96.07	64.78	80.66	83.31
Rela	22.42	15.26	23.68	17.90	55.84	43.07	46.34	48.70
Relb	13.02	12.07	15.42	12.45	29.72	22.58	24.87	27.01
Rhoa	160.16	172.76	171.45	189.96	197.10	153.10	155.19	161.28
Ripk1	7.27	6.39	7.51	5.25	17.66	13.02	15.08	15.64
Ripk2	4.54	4.30	7.64	5.78	15.97	12.83	14.34	14.53
Rock2	15.42	9.89	13.81	11.24	37.87	27.22	30.63	30.71
Rps6ka5	4.19	3.73	4.88	3.48	10.91	7.91	8.44	8.93
Shc1	48.67	51.54	55.87	43.89	74.02	50.96	61.89	64.52
Stat1	22.35	22.63	27.55	17.99	43.16	30.68	30.47	29.14
Stat2	13.87	10.82	15.56	10.83	54.39	36.25	42.59	38.43
Stat3	51.98	34.02	59.71	41.06	89.09	51.91	68.51	71.19
Tcf4	73.69	44.87	77.73	56.18	81.98	48.71	62.87	68.34
Tgfb1	24.33	26.51	28.63	18.71	36.65	29.57	32.68	33.38
Tgfb3	9.73	6.22	10.34	6.35	14.18	10.07	13.15	13.45
Tgfbr1	6.17	4.10	6.77	4.81	20.40	13.04	16.46	17.07
Tlr2	4.52	4.44	5.09	4.12	8.38	6.27	7.58	7.21
Tlr4	18.52	16.84	20.91	15.03	24.08	16.58	21.24	20.23
Tlr5	2.85	2.12	3.06	2.34	4.80	3.80	4.24	3.88
Tlr6	6.79	6.58	9.26	5.38	8.06	5.23	6.32	6.29
Tnfaip3	3.23	2.37	3.23	3.03	11.52	7.53	9.84	9.32
Tollip	56.73	40.15	54.09	47.29	80.08	59.89	67.39	70.68
Tradd	4.92	4.38	6.13	5.90	6.85	4.26	5.29	5.06
Traf2	14.90	14.10	15.46	16.13	21.90	15.73	18.84	19.36
Twist2	16.33	14.58	16.74	11.80	21.40	17.30	16.64	17.79
Bcl6	2.19	1.78	2.32	1.46	6.46	3.53	4.90	5.13
C3	8.69	0.82	6.26	8.12	12.91	3.10	9.37	9.96
Irf7	1.94	1.44	2.73	1.98	15.36	9.53	9.95	6.47
Smad7	4.10	1.22	2.29	2.18	13.23	11.45	11.66	10.78
Tlr1	2.69	1.58	4.65	2.14	2.98	1.81	2.59	2.18
Il18	1.71	1.44	3.13	2.67	3.27	1.94	2.73	2.64
Ptgs2	4.56	0.57	1.14	2.59	22.66	13.62	13.61	10.04
Ifit3	0.83	1.75	1.99	0.89	18.47	14.33	13.54	11.45
Il15	1.00	1.67	1.28	1.41	4.08	2.40	3.80	3.62
Il18rap	2.23	0.99	1.78	1.66	3.87	2.66	3.61	3.13
Il6ra	2.54	1.53	2.32	1.50	3.32	1.96	1.77	2.95
Areg	0.27	0.17	0.47	0.16	3.14	3.22	2.52	2.88
Ccl20	0.40	0.31	0.40	0.28	54.15	9.51	38.46	25.01
Ifi44	1.15	0.99	1.58	0.81	107.69	65.21	75.30	41.41
Ifit1	0.58	0.65	0.81	0.69	9.09	7.07	7.02	4.98
Il7	1.33	1.58	1.11	1.37	5.61	4.50	4.94	4.80
Oas2	0.42	0.42	0.44	0.89	9.17	4.79	6.53	4.47

Table K2: Signal: Noise Ratio of target genes with a signal:noise ratio above 3 (yellow cells) and above 5 (green cells).

	CTRL/CTRL + HB	CTRL/CTRL + ALL	CTRL/CTRL + PHY	CTRL/SEN	SEN/SEN + HB	SEN/SEN + ALL	SEN/SEN + PHY
Atf2	0.83	0.94	0.88	1.39	0.83	1.02	1.03
Bcl2l1	0.87	1.02	0.94	1.55	0.83	0.94	1.02
Birc2	0.87	0.99	0.98	1.03	0.86	1.00	1.00
C1ra	1.10	1.18	1.39	0.65	0.75	1.03	1.08
C1s	0.79	1.39	1.78	1.18	0.50	0.98	1.00
C2	0.80	1.03	1.06	0.87	0.71	1.10	1.05
Ccl2	0.84	0.86	0.30	5.44	0.90	1.03	1.35
Ccl7	0.96	0.88	0.54	4.11	0.88	1.01	1.18
Cd40	0.99	0.85	1.07	2.34	0.92	1.17	1.30
Cdc42	1.03	0.98	0.92	1.03	0.91	1.01	1.08
Cebpb	0.97	0.85	0.91	0.54	0.84	1.04	0.98
Cfl1	1.07	1.13	0.93	1.22	1.02	1.02	1.05
Csf1	1.24	1.89	1.44	4.25	0.97	0.93	1.03
Cxcl1	1.19	1.16	0.83	13.03	0.73	0.96	1.28
Daxx	0.85	1.05	0.90	1.02	1.12	1.17	1.06
Ddit3	1.04	1.03	1.11	1.83	0.69	0.99	1.09
Fos	0.48	0.92	0.64	0.11	0.97	1.60	1.21
Gnaq	1.21	1.98	1.54	2.84	0.81	0.95	0.94
Gnas	1.04	1.07	0.97	1.13	0.85	0.96	1.02
Gnb1	0.98	1.25	1.01	1.43	0.97	0.94	0.98
Grb2	0.82	1.07	0.97	1.47	0.86	0.95	0.99
Hc	0.85	1.65	1.19	0.98	0.87	0.86	0.85
Hdac4	0.81	1.64	1.17	2.38	0.82	0.94	0.96
Hif1a	1.05	1.30	1.10	1.22	0.81	1.01	1.00
Hmgb1	1.23	1.06	1.06	0.82	0.86	1.04	1.02
Hmgn1	0.94	0.90	0.79	0.80	1.04	0.95	0.97
Ifit2	1.53	1.48	1.29	3.89	0.81	0.93	0.95
Iigp1	2.58	0.98	2.25	1.82	0.96	1.34	1.25
Il10rb	1.02	0.97	1.05	1.56	0.90	0.89	0.98
Il1r1	1.11	1.26	1.09	1.29	0.73	1.08	0.96
Il1rap	1.08	1.47	1.25	1.88	0.83	0.97	1.03
Il23a	0.85	0.87	0.96	1.11	0.94	0.96	1.00
Il6	1.62	0.66	1.21	4.66	0.77	1.14	1.26
Irf1	0.59	0.75	0.58	0.71	0.79	0.98	0.99
Jun	0.54	1.41	0.85	0.65	0.92	0.93	1.02
Keap1	1.08	1.31	1.21	1.15	0.88	0.97	0.96
Limk1	0.73	1.29	0.78	1.34	1.03	0.87	0.95
Ly96	1.48	0.96	1.14	1.50	0.82	0.95	1.08
Maff	0.79	1.16	0.78	3.86	0.85	1.14	1.17

Mafk	0.85	1.30	0.86	1.63	0.96	1.05	1.14
Map2k1	1.05	1.12	1.12	1.64	0.93	1.00	1.10
Map2k4	0.95	1.44	1.09	1.80	0.79	0.97	1.03
Map2k6	0.83	1.02	0.94	0.78	0.81	0.97	1.11
Map3k1	1.19	1.65	1.79	3.28	0.84	1.03	0.87
Map3k5	1.13	1.28	1.19	1.03	0.92	0.94	0.88
Map3k7	1.01	1.38	1.12	1.63	0.87	0.98	0.99
Mapk1	0.75	0.97	0.73	1.03	1.04	0.91	0.92
Mapk14	0.99	1.55	1.17	1.79	0.81	0.89	0.94
Mapk3	0.96	0.87	0.94	0.80	0.87	0.99	0.97
Mapk8	0.83	0.88	0.75	1.23	1.06	1.02	1.05
Mapkapk2	1.06	1.35	1.07	1.75	0.91	1.01	1.05
Masp1	0.91	1.12	1.12	1.60	1.10	1.02	1.02
Max	0.76	0.89	0.79	1.00	0.82	0.86	0.95
Mef2d	0.91	1.52	1.27	2.51	0.95	0.97	0.95
Mknk1	0.90	1.26	1.13	1.12	0.92	1.06	1.16
Myc	0.53	1.41	0.78	0.38	1.13	1.04	0.93
Myd88	0.91	0.90	0.94	1.15	0.87	0.98	0.99
Myl2	0.88	0.64	0.88	0.42	0.82	1.12	1.20
Nfatc3	1.05	1.69	1.28	2.74	0.80	0.91	0.96
Nfe2l2	1.14	1.12	1.26	1.39	0.72	0.97	1.03
Nfkb1	0.96	1.25	1.08	1.35	0.92	0.92	0.95
Nod1	0.68	0.89	0.70	1.81	0.69	0.93	1.05
Nr3c1	0.79	1.10	1.03	1.41	0.81	1.00	0.99
Oas1a	0.86	0.72	0.84	1.68	1.41	1.42	1.34
Pdgfa	1.32	1.17	1.00	1.19	0.90	0.90	1.11
Pla2g4a	1.44	1.44	1.37	2.05	0.94	1.15	1.21
Ppp1r12b	0.68	1.20	0.96	1.06	0.67	0.91	0.92
Prkca	0.66	1.28	0.98	1.64	0.86	0.90	0.91
Prkcb	0.80	1.52	1.29	1.08	0.63	0.81	0.86
Ptger4	1.07	1.18	1.09	1.42	0.79	0.91	1.01
Ptgir	0.96	1.16	1.17	1.25	0.99	0.93	0.95
Ptk2	0.89	1.26	1.02	1.09	1.03	1.01	0.99
Rac1	0.99	1.32	1.02	1.48	0.88	0.95	1.02
Raf1	0.97	1.05	0.93	0.82	0.98	1.01	0.99
Rapgef2	0.84	1.15	0.98	2.55	0.80	0.95	1.00
Rela	0.89	1.22	1.09	2.58	0.91	0.94	0.98
Relb	1.01	1.02	1.02	2.06	0.86	0.90	0.95
Rhoa	0.95	0.82	0.74	0.80	0.98	1.00	0.99
Ripk1	1.27	1.35	1.18	2.82	0.86	0.93	0.99
Ripk2	0.78	0.77	1.09	2.38	0.91	0.90	1.02
Rock2	0.92	1.34	1.01	2.59	0.92	1.01	1.03

Rps6ka5	1.12	1.17	1.16	2.43	0.92	1.00	0.97
Shc1	1.23	1.08	1.05	1.39	0.82	0.94	0.99
Stat1	1.32	1.21	1.26	1.53	1.09	1.22	1.08
Stat2	1.04	1.25	1.18	3.36	0.98	1.16	1.14
Stat3	0.87	1.23	1.20	1.64	0.75	1.03	0.99
Tcf4	0.83	1.28	1.14	1.15	0.74	0.99	0.95
Tgfb1	1.48	1.27	1.26	1.69	0.92	0.90	1.01
Tgfb3	1.02	1.49	1.34	2.01	0.77	0.87	1.01
Tgfbr1	0.89	1.25	1.16	3.36	0.79	0.98	0.99
Tlr2	1.12	1.07	1.01	1.66	0.90	0.95	1.08
Tlr4	1.17	1.20	1.14	1.27	0.85	0.98	1.08
Tlr5	0.94	1.19	1.08	1.57	1.01	1.02	1.13
Tlr6	1.28	1.23	1.42	1.11	0.86	1.05	1.03
Tnfaip3	0.82	1.04	0.88	2.91	0.83	1.01	1.09
Tollip	0.89	1.17	0.94	1.42	0.88	0.93	0.98
Tradd	0.78	0.81	0.85	0.81	0.87	1.11	1.08
Traf2	0.91	0.90	0.79	1.14	0.84	0.93	1.00
Twist2	1.29	1.35	1.17	1.43	1.01	0.99	0.96
Bcl6	1.28	1.46	1.31	3.34	0.71	1.03	0.98
C3	0.11	1.04	0.63	1.16	0.32	1.06	0.97
Irf7	0.76	0.95	1.13	3.09	1.52	1.95	1.59
Smad7	0.58	1.83	0.86	4.68	1.10	1.01	1.11
Tlr1	0.77	1.22	1.78	0.96	0.86	1.12	1.22
Il18	0.56	0.62	0.97	0.94	0.76	1.01	1.06
Ptgs2	0.23	1.72	0.36	3.68	1.40	1.85	1.40
Ifit3	2.06	0.91	1.84	12.20	1.29	1.32	1.22
Il15	1.23	0.69	0.74	2.42	0.68	0.93	1.08
Il18rap	0.62	1.31	0.89	1.79	0.88	1.02	1.19
Il6ra	1.07	1.66	1.28	1.87	0.69	0.92	0.62
Areg	1.10	1.63	2.40	16.85	1.16	0.90	0.90
Ccl20	1.15	1.36	1.17	83.74	0.39	1.78	1.58
Ifi44	1.28	1.38	1.61	48.52	1.63	2.14	1.87
Ifit1	0.99	0.83	0.97	6.86	1.47	1.50	1.45
Il7	1.20	0.95	0.67	3.31	0.97	0.96	1.06
Oas2	0.50	0.46	0.40	4.76	1.11	1.69	1.51

Table K3: Fold change for target genes selected from Nanostring Analysis

	CTRL/CTRL + HB	CTRL/CTRL + ALL	CTRL/CTRL + PHY	CTRL/SEN	SEN/SEN + HB	SEN/SEN + ALL	SEN/SEN + PHY
Atf2	-0.27	-0.09	-0.19	0.48	-0.26	0.02	0.05
Bcl2l1	-0.20	0.03	-0.09	0.64	-0.27	-0.09	0.02
Birc2	-0.20	-0.02	-0.03	0.04	-0.21	-0.01	0.00
C1ra	0.14	0.24	0.48	-0.63	-0.41	0.05	0.11
C1s	-0.34	0.47	0.83	0.24	-1.01	-0.03	0.00
C2	-0.33	0.04	0.08	-0.21	-0.50	0.14	0.07
Ccl2	-0.26	-0.22	-1.73	2.44	-0.15	0.04	0.43
Ccl7	-0.06	-0.18	-0.88	2.04	-0.18	0.01	0.24
Cd40	-0.02	-0.23	0.10	1.22	-0.12	0.23	0.37
Cdc42	0.05	-0.03	-0.13	0.04	-0.13	0.01	0.11
Cebpb	-0.04	-0.23	-0.14	-0.88	-0.26	0.06	-0.03
Cfl1	0.09	0.18	-0.11	0.29	0.04	0.02	0.08
Csf1	0.31	0.92	0.52	2.09	-0.04	-0.10	0.05
Cxcl1	0.25	0.21	-0.28	3.70	-0.46	-0.06	0.36
Daxx	-0.24	0.06	-0.15	0.02	0.16	0.23	0.08
Ddit3	0.06	0.04	0.15	0.87	-0.53	-0.02	0.13
Fos	-1.06	-0.12	-0.64	-3.21	-0.05	0.67	0.28
Gnaq	0.27	0.98	0.62	1.51	-0.31	-0.08	-0.10
Gnas	0.06	0.10	-0.05	0.18	-0.24	-0.06	0.02
Gnb1	-0.03	0.33	0.01	0.52	-0.04	-0.10	-0.03
Grb2	-0.28	0.10	-0.04	0.55	-0.22	-0.08	-0.02
Hc	-0.24	0.72	0.26	-0.03	-0.21	-0.22	-0.23
Hdac4	-0.31	0.71	0.23	1.25	-0.29	-0.09	-0.06
Hif1a	0.07	0.38	0.13	0.29	-0.31	0.02	0.00
Hmgb1	0.30	0.08	0.08	-0.29	-0.22	0.05	0.03
Hmgn1	-0.09	-0.15	-0.34	-0.32	0.05	-0.08	-0.04
Ifit2	0.61	0.56	0.36	1.96	-0.30	-0.11	-0.08
Iigp1	1.37	-0.03	1.17	0.87	-0.06	0.42	0.33
Il10rb	0.03	-0.04	0.07	0.64	-0.15	-0.17	-0.02
Il1r1	0.15	0.33	0.12	0.36	-0.46	0.12	-0.05
Il1rap	0.11	0.56	0.32	0.91	-0.26	-0.04	0.04
Il23a	-0.24	-0.20	-0.06	0.15	-0.08	-0.05	0.00
Il6	0.70	-0.60	0.27	2.22	-0.37	0.20	0.33
Irf1	-0.75	-0.41	-0.79	-0.48	-0.34	-0.03	-0.01
Jun	-0.90	0.50	-0.23	-0.62	-0.12	-0.11	0.03
Keap1	0.12	0.39	0.27	0.20	-0.18	-0.04	-0.06
Limk1	-0.45	0.37	-0.35	0.42	0.04	-0.20	-0.07
Ly96	0.57	-0.06	0.18	0.58	-0.28	-0.08	0.11
Maff	-0.33	0.21	-0.36	1.95	-0.23	0.19	0.23

Mafk	-0.24	0.38	-0.22	0.71	-0.06	0.07	0.19
Map2k1	0.06	0.17	0.16	0.71	-0.11	0.00	0.14
Map2k4	-0.08	0.53	0.12	0.85	-0.34	-0.05	0.04
Map2k6	-0.27	0.02	-0.09	-0.36	-0.30	-0.05	0.15
Map3k1	0.25	0.73	0.84	1.72	-0.26	0.04	-0.20
Map3k5	0.18	0.35	0.25	0.05	-0.12	-0.09	-0.18
Map3k7	0.01	0.46	0.16	0.71	-0.20	-0.02	-0.01
Mapk1	-0.42	-0.05	-0.45	0.05	0.05	-0.14	-0.11
Mapk14	-0.02	0.63	0.22	0.84	-0.30	-0.17	-0.09
Mapk3	-0.06	-0.20	-0.09	-0.33	-0.19	-0.01	-0.04
Mapk8	-0.26	-0.19	-0.41	0.30	0.08	0.03	0.07
Mapkapk2	0.08	0.43	0.10	0.81	-0.14	0.01	0.07
Masp1	-0.14	0.17	0.17	0.68	0.14	0.03	0.03
Max	-0.40	-0.17	-0.34	0.00	-0.29	-0.22	-0.07
Mef2d	-0.14	0.60	0.34	1.33	-0.08	-0.04	-0.07
Mknk1	-0.16	0.33	0.18	0.17	-0.12	0.08	0.21
Myc	-0.91	0.49	-0.36	-1.38	0.17	0.05	-0.11
Myd88	-0.14	-0.16	-0.10	0.20	-0.20	-0.03	-0.01
Myl2	-0.18	-0.64	-0.19	-1.27	-0.29	0.16	0.27
Nfatc3	0.07	0.76	0.35	1.45	-0.33	-0.14	-0.07
Nfe2l2	0.19	0.16	0.34	0.47	-0.48	-0.04	0.05
Nfkb1	-0.07	0.32	0.11	0.43	-0.12	-0.12	-0.07
Nod1	-0.55	-0.17	-0.52	0.85	-0.54	-0.10	0.07
Nr3c1	-0.34	0.14	0.04	0.50	-0.31	0.00	-0.02
Oas1a	-0.22	-0.47	-0.25	0.75	0.50	0.51	0.42
Pdgfa	0.40	0.23	0.00	0.25	-0.15	-0.15	0.14
Pla2g4a	0.53	0.53	0.45	1.03	-0.09	0.20	0.27
Ppp1r12b	-0.56	0.26	-0.05	0.08	-0.57	-0.14	-0.13
Prkca	-0.59	0.36	-0.04	0.71	-0.22	-0.15	-0.13
Prkcb	-0.33	0.61	0.37	0.11	-0.66	-0.31	-0.23
Ptger4	0.10	0.23	0.13	0.51	-0.34	-0.13	0.02
Ptgir	-0.06	0.21	0.22	0.32	-0.02	-0.10	-0.07
Ptk2	-0.17	0.33	0.03	0.13	0.04	0.02	-0.02
Rac1	-0.01	0.40	0.02	0.57	-0.18	-0.07	0.03
Raf1	-0.04	0.08	-0.10	-0.28	-0.03	0.01	-0.02
Rapgef2	-0.26	0.20	-0.03	1.35	-0.32	-0.08	0.00
Rela	-0.17	0.29	0.12	1.37	-0.13	-0.09	-0.03
Relb	0.02	0.03	0.03	1.04	-0.21	-0.15	-0.08
Rhoa	-0.07	-0.28	-0.43	-0.31	-0.03	0.01	-0.01
Ripk1	0.35	0.43	0.23	1.50	-0.22	-0.11	-0.01
Ripk2	-0.36	-0.39	0.12	1.25	-0.13	-0.15	0.02
Rock2	-0.12	0.42	0.02	1.37	-0.13	0.02	0.04

Rps6ka5	0.17	0.23	0.21	1.28	-0.13	0.00	-0.04
Shc1	0.30	0.11	0.07	0.48	-0.29	-0.09	-0.02
Stat1	0.40	0.28	0.33	0.62	0.12	0.28	0.11
Stat2	0.06	0.32	0.24	1.75	-0.04	0.22	0.19
Stat3	-0.21	0.30	0.26	0.72	-0.41	0.04	-0.01
Tcf4	-0.26	0.35	0.19	0.20	-0.44	-0.02	-0.08
Tgfb1	0.57	0.34	0.33	0.76	-0.13	-0.15	0.01
Tgfb3	0.03	0.58	0.42	1.01	-0.37	-0.21	0.01
Tgfbr1	-0.17	0.32	0.21	1.75	-0.34	-0.03	-0.01
Tlr2	0.17	0.10	0.02	0.73	-0.16	-0.07	0.11
Tlr4	0.23	0.26	0.19	0.35	-0.24	-0.03	0.11
Tlr5	-0.08	0.25	0.10	0.65	0.02	0.02	0.17
Tlr6	0.36	0.30	0.50	0.15	-0.22	0.07	0.05
Tnfaip3	-0.29	0.05	-0.19	1.54	-0.26	0.02	0.12
Tollip	-0.17	0.22	-0.09	0.50	-0.19	-0.10	-0.03
Tradd	-0.37	-0.30	-0.23	-0.30	-0.20	0.15	0.11
Traf2	-0.13	-0.15	-0.34	0.19	-0.25	-0.11	0.00
Twist2	0.37	0.43	0.22	0.51	0.01	-0.02	-0.05
Bcl6	0.35	0.55	0.39	1.74	-0.49	0.05	-0.03
C3	-3.25	0.06	-0.66	0.22	-1.64	0.09	-0.05
Irf7	-0.39	-0.07	0.18	1.63	0.61	0.96	0.66
Smad7	-0.78	0.87	-0.21	2.23	0.13	0.01	0.16
Tlr1	-0.37	0.29	0.84	-0.05	-0.22	0.16	0.29
Il18	-0.82	-0.68	-0.05	-0.09	-0.40	0.02	0.09
Ptgs2	-2.13	0.78	-1.46	1.88	0.49	0.89	0.48
Ifit3	1.04	-0.13	0.88	3.61	0.37	0.41	0.29
Il15	0.30	-0.54	-0.43	1.28	-0.55	-0.11	0.11
Il18rap	-0.68	0.39	-0.18	0.84	-0.19	0.02	0.25
Il6ra	0.09	0.73	0.35	0.90	-0.54	-0.11	-0.69
Areg	0.13	0.71	1.26	4.08	0.21	-0.16	-0.15
Ccl20	0.20	0.45	0.23	6.39	-1.35	0.83	0.66
Ifi44	0.35	0.47	0.69	5.60	0.70	1.09	0.91
Ifit1	-0.02	-0.27	-0.05	2.78	0.55	0.58	0.54
Il7	0.27	-0.08	-0.59	1.73	-0.05	-0.06	0.08
Oas2	-1.01	-1.13	-1.30	2.25	0.15	0.75	0.59

Table K4: Log2(Fold Change) Values for all target genes selected from Nanostring analysis.

APPENDIX B

Thesis submitted for the degree of
Doctor of Philosophy

By
Amanpreet Kaur (BSc)
Department of Respiratory Sciences
University Of Leicester

May 2021

frontiers in Cell and Developmental Biology

REVIEW
published: 03 April 2020
doi: 10.3389/fcell.2020.00218

An Appraisal on the Value of Using Nutraceutical Based Senolytics and Senostatics in Aging

Amanpreet Kaur[1], Salvador Macip[2,3] and Cordula M. Stover[1]*

[1] Department of Respiratory Sciences, University of Leicester, Leicester, United Kingdom, [2] Mechanisms of Cancer and Ageing Laboratory, Department of Molecular and Cell Biology, University of Leicester, Leicester, United Kingdom, [3] Faculty of Health Sciences, Universitat Oberta de Catalunya, Barcelona, Spain

The average human life expectancy has increased globally, and continues to rise, owing to the substantive progress made in healthcare, medicine, sanitation, housing and education. This ultimately enriches society with a greater proportion of elderly people. Sustaining a healthy aged population is key to diminish the societal and economic impact of age-related infirmities. This is especially challenging because tissue function, and thus wellbeing, naturally progressively decline as humans age. With age increasing the risk of developing diseases, one of the therapeutic options is to interfere with the molecular and cellular pathways involved in age-related tissue dysfunction, which is in part caused by the accumulation of senescent cells. One strategy to prevent this could be using drugs that selectively kill these cells (senolytics). In parallel, some compounds have been identified that prevent or slow down the progression of senescence or some of its features (senostatics). Senolytic and senostatic therapies have been shown to be efficient *in vivo*, but they also have unwanted dose-dependent side effects, including toxicity. Important advances might be made using bioactive compounds from plants and foods (nutraceuticals) if, as is proposed, they offer similar effectiveness with fewer side effects. The focus of this review is on the use of nutraceuticals in interfering with cellular senescence.

Keywords: senescence, senolytics, senostatics, nutraceuticals, aging

OPEN ACCESS

Edited by:
Isabel Varela-Nieto, Spanish National Research Council, Spain

Reviewed by:
Shang Li, Duke-NUS Medical School, Singapore
José Marco-Contelles, Spanish National Research Council, Spain

****Correspondence:***
Amanpreet Kaur
ak699@leicester.ac.uk

Specialty section:
This article was submitted to Cell Growth and Division, a section of the journal Frontiers in Cell and Developmental Biology

Received: *16 January 2020*
Accepted: *13 March 2020*
Published: *03 April 2020*

Citation:
Kaur A, Macip S and Stover CM (2020) An Appraisal on the Value of Using Nutraceutical Based Senolytics and Senostatics in Aging. Front. Cell Dev. Biol. 8:218. doi: 10.3389/fcell.2020.00218

INTRODUCTION

Aging is the time-related deterioration of physiological functions necessary for survival and fertility (Gilbert, 2000). On a cellular level, aging is accompanied by the accumulation of cells that adopt a specific phenotype, known as senescence, a process which is conserved across species. Senescence is mainly characterized by an irreversible cell cycle arrest and the secretion of a group of factors, known as the senescence-associated secretory phenotype (SASP), whilst maintaining metabolic activity (Wiley and Campisi, 2016). Over time, senescent cells accumulate in all tissues and organs, contributing to their functional deterioration (van Deursen, 2014). The permanent cessation of cell proliferation is seen as a way to avoid neoplastic outgrowth, which means that in this context, senescence can be considered a tumor supressor mechanism (Dimri, 2005). For growth arrest to take place, senescent cells increase the expression of cyclin dependent kinase inhibitors (CDKIs) expression such as p21, p16 or p27 (Alcorta et al., 1996; Hernández-Segura et al., 2018).

The SASP, which is capable of promoting tissue repair and regeneration, creates a microenvironment that can drive neighboring cells into proliferation or even senescence, thus contributing to the disruption of tissue homeostasis (Rodier and Campisi, 2011). Therefore, with beneficial attributes early in life and detrimental consequences late in life, the senescence phenomenon is as an example of so-called antagonistic pleiotropy (Rodier and Campisi, 2011; Giaimo and d'Adda di Fagagna, 2012).

Due to general lack of specificity, multiple markers have to be considered and validated in conjunction for the identification of senescent cells. These markers include, but are not limited to, senescence associated beta-galactosidase staining (SA-β-Gal), cell cycle arrest, morphological and nuclear changes, and expression of certain proteins (Hooten and Evans, 2017). It is important to differentiate senescent cells from quiescent and terminally differentiated cells such as neurons, macrophages and muscle cells (Rodier and Campisi, 2011). Quiescent cells retain the ability to re-enter the growth cycle when stimulated with growth signals and are key to tissue regeneration by maintaining a constant state of balanced proliferation (Yao, 2014).

CAUSES OF CELLULAR SENESCENCE

Replicative Senescence

Hayflick and Moorhead first observed senescence in somatic cells serially passaged in culture (Hayflick and Moorhead, 1961). Normal cells undergo multiple mitotic cell divisions, eventually reaching a limit at which their proliferative capabilities are lost. This is now referred to as replicative senescence. Human fibroblasts, the cell type originally described, had a limit of around 50 passages. Since then, other forms of senescence have been discovered and applied in models of *in vitro* and *in vivo* research.

Most types of senescence are largely triggered through the DNA damage response pathways (DDR) (Fumagalli et al., 2014). The DDR consists of upstream components such as ATM (Ataxia telangiectasia mutated) and ATR (Ataxia telangiectasia and Rad3 related) kinases, which activate cell cycle checkpoint proteins CHK1 and CHK2. Eventually, cyclin dependent kinases (CDKs) are inhibited to arrest the cell cycle (Jackson and Bartek, 2009). In senescent cells, the main proteins involved in proliferative arrest are CDKIs p21 and p16. These are found to be overexpressed and are often used as markers for cell cycle arrest and senescence.

In replicative senescence, activation of the DDR is triggered through the shortening of telomeres. The change in DNA content following loss of telomeric length is recognized as damage, resulting in the initiation of the DDR response (Serrano and Muñoz-Espín, 2014). Telomeres are complexes composed of proteins and nucleotides of TTAGGG repeats at the ends of eukaryotic chromosomes that are considered protective structures (Bernadotte et al., 2016). When a cell divides, chromosomes are replicated and telomeres shorten in length with each cell division. An increase in the presence of telomere associated foci is seen in connection to aging (Hewitt et al., 2012). Loss of telomeric length has been suggested to be the biomarker of choice in replicative senescence (Bernadotte et al., 2016). Of note, lifestyle choices such as smoking, diet, stress and exercise can have an effect on telomere attrition (Shammas, 2011). Telomere attrition occurs in cells in which the expression of telomerase is repressed, as is the case in adult human somatic cells (Calado and Dumitriu, 2013). By contrast, mice regulate telomere length and telomerase activity differently from humans and are therefore inherently limited in studies of replicative aging (Zhang et al., 2016).

Stress-Induced Premature Senescence (SIPS)

DNA single and double strand breaks (induced by exposure to radiation, overexpression of oncogenes, oxidative stress, etc.) result in the activation of the DDR and can eventually lead to a stress-induced premature senescence (SIPS), which is independent of telomere length (Boothman and Suzuki, 2008). *In vitro* SIPS models have been established using oxidative stress, ionizing radiation or DNA damage causing agents such as bleomycin (González-Hunt et al., 2018).

Overexpression of the *ras* oncogene in human and rodent cells was found to elicit a phenotype similar to cellular senescence, supporting the fact that senescence is a tumor-suppressor mechanism. Since then, other oncogenes have also been found to induce senescence including; Raf, c-Myc, Akt and E2F3 (Serrano et al., 1997; Astle et al., 2011; Qian and Chen, 2012; Ko et al., 2018).

In vivo models of SIPS include accelerated aging of mice as a result of gene defects. For example, mutations in the *LMNA* gene of mice can result in the onset of Hutchinson-Gilford progeria syndrome, deficiencies in *nfkb1* can lead to early aging phenotype in middle-aged mice and WRN protein deficient mice develop Werners syndrome, a disease of premature aging (Kõks et al., 2016). Recent models include the syngeneic transplantation of senescent cells in mice, leading to signs of physical dysfunction (Xu et al., 2018). These models have become the basis for senescence research, specifically for the testing of potential anti-aging drugs.

CHARACTERISTICS OF CELLULAR SENESCENCE

As outlined below and illustrated in **Figure 1**, senescent cells display changes in morphology, increases in certain cell cycle related proteins, nuclear changes and the presence of SASP.

Morphology

Senescent cells in culture have a characteristic morphology that makes them distinguishable from proliferating cells (Dimri, 1995). Once in senescence, cells become flatter and the nucleus becomes enlarged. The cause for these morphological changes is not fully understood but the increase in cell size may be associated with the process of cell cycle arrest, where the imbalance of DNA: cytoplasm ratio in itself may contribute to aging (Neurohr et al., 2019).

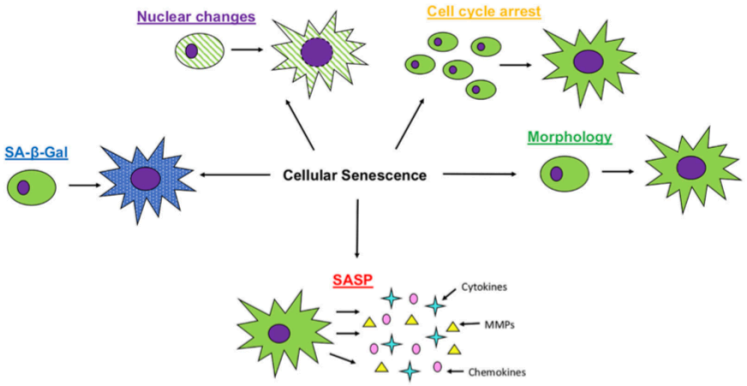

FIGURE 1 | Characteristics of Cellular Senescence. Senescent cells will undergo multiple changes, with morphology becoming larger and flatter, an increased expression of SA- β -Gal activity, loss of nuclear membrane integrity, cease in cell proliferation and the production of SASP, including an increased expression of matrix metalloproteases (MMPs), cytokines and chemokines.

SA-β-Gal Activity

The cytoplasmic content of senescent cells also changes, with an increase in lysosomal SA- β-Gal activity. This enzyme is thought to exist in cell lysosomes, which are known to increase in size as cells age. Therefore, a high SA- β-Gal activity would be expected in senescent cells. However, this is not considered to be exclusive, as it can also be found in other cell types of non-senescent nature and in some cases may not be established in senescence (Dimri, 1995; Lee et al., 2006; Huang and Rivera-Pérez, 2014).

Cell Cycle Arrest

The CDK/Cyclin complexes are necessary to progress through the cell cycle. In senescent cells, this interaction between cyclins and CDKs is blocked by CDKIs (Blagosklonny, 2011). The *INK4A* gene encodes the p16 protein, which inhibits the Cyclin D/CDK4/6 complex to stop the progression of G1 phase to S phase (Jingwen et al., 2017). It is often used as a marker for senescent cells due to its increased levels of expression. The *CDKN1A* gene encodes p21, which inhibits the Cyclin E/CDK2 and Cyclin B/CDK1 complexes (Jingwen et al., 2017). The inhibitor is commonly used a marker as well, but is less specific, since it can be upregulated in other situations (Hernández-Segura et al., 2018).

Nuclear Changes

In addition to the increase in nuclear size, senescent cells have changes to the nuclear lamina, which impact on nuclear stability (Hernández-Segura et al., 2018). The nuclear lamina is made up of lamin proteins, which are type V intermediate filaments, and is disassembled and reassembled with every mitotic division (Freund et al., 2012). Lamin B1 is expressed differentially between pre-senescent and senescent cells: in various primary human fibroblast cell lines, a decrease of protein and mRNA expression of Lamin B1 can be observed, suggesting its use as a senescent cell biomarker (Freund et al., 2012).

Changes in chromatin structure are also exhibited in senescent cells. Heterochromatin becomes more prominent, with areas of nucleus having denser DAPI (diamidinophenylindole) stained foci that have been called senescence associated heterochromatin foci (SAHFs) and may be involved in gene silencing of proliferation genes (Aird and Zhang, 2012). These SAHFs can also be distinguished with specific epigenetic markers, such as H3K9me3, H3K27me3, and macroH2A, a facultative heterochromatin histone variant (Parry and Narita, 2016). DNA methylation patterns change during the process of aging as well, with hypomethylation in heterochromatic regions and focal hypermethylation in gene-associated cytosine-guanine islands (CGIs) (Ciccarone et al., 2018). Histone modifications can cause repression of certain genes, silencing those involved in cell cycle progression.

SASP

The SASP consists of a collection of molecules secreted by senescent cells that shape the microenvironment. These molecules include proteases and growth factors, chemokines and cytokines such as IL-6, IL-8 and IL-1β (Borodkina et al., 2018). Interleukins take part in activating signaling pathways such as Jak/STAT, PI3K, and MAPK (Garbers et al., 2013). Proteases, such as matrix metalloproteases (MMPs) and serine proteases, are involved in the development and regeneration of the extracellular matrix. The inhibitors of these proteins and signaling molecules are also secreted by senescent cells to regulate their functions (Borodkina et al., 2018), so the net effect is dependent on this balance. Although the SASP works to promote tissue repair and regeneration and encourages immune surveillance, it

can also be detrimental to health. For example, through paracrine induction of epithelial to mesenchymal transition and attraction of immunosuppressive immune cells, it can contribute to tumorigenesis and metastasis in cancer (González-Meljem et al., 2018).

CHEMICAL APPROACHES TO REGULATE SENESCENT CELL ACCUMULATION AND ACTIVITY

The characterization of compounds that could counteract the process of senescence has recently become a priority, given its immense therapeutic potential. These anti-senescence compounds are divided into two categories: senolytics and senostatics. Senolytic drugs are agents that selectively induce apoptosis of senescent cells. They were first discovered by Zhu et al. (2015), in whose work the combination of quercetin and dasatinib showed potential apoptotic activity in eliminating senescent cells (Zhu et al., 2015). On the other hand, senostatics are drugs capable of interfering with the progression of cells entering senescence or modulate their activity by reducing SASP generation (Short et al., 2019).

Senolytics can work by overriding anti-apoptotic pathways in senescent cells (Short et al., 2019). One of the most well studied senolytics is the combination of dasatinib and quercetin. Dasatinib is an established anti-cancer drug that, when administered in mice alongside quercetin, selectively eliminates senescent cells, leading to improved physical function and increased survival *in vivo* (Xu et al., 2018). This combination is now being tested as part of clinical trials to investigate its potential in patients with idiopathic pulmonary fibrosis, with preliminary results already showing improvements in cardiopulmonary function (Justice et al., 2019). Many compounds are under investigation for their potential senolytic properties. Other synthetic senolytic drugs include BCL inhibitor ABT-737, Panobinostat, HSP90 inhibitors or cardiac glycosides (Yosef et al., 2016; Fuhrmann-Stroissnigg et al., 2017; Samaraweera et al., 2017; Xu et al., 2018; Guerrero et al., 2019; Triana-Martínez et al., 2019).

Senostatics can work by inhibiting paracrine signaling or by counteracting the effects of the SASP in senescence (Short et al., 2019). They can also prevent the emergence of senescent cells by blocking fundamental steps of the effector mechanisms of the phenotype, such as activation of the p53 pathway (Althubiti et al., 2016). Examples of senostatic that have proven to be effective therapies in mouse models include rapamycin and metformin (Short et al., 2019). Rapamycin is a naturally derived antibiotic with additional anti-fungal and immunosuppressant properties. The macrolide compound is an mTOR inhibitor and it delays the progression of senescence and improves health in animal models (Blenis et al., 2014; Wang et al., 2017). Metformin, originally derived from *Galega officinalis* also known as Goat's Rue (Bailey, 2017), is a well-established anti-diabetic drug that, has previously been shown to inhibit the SASP by interfering with the NFκB pathway (Moiseeva et al., 2013).

NUTRACEUTICAL-BASED SENOLYTICS AND SENOSTATICS

Synthetic compounds with senolytic or senostatic properties can be effective, however, they are not specific, and systemic side effects can be severe and deleterious to healthy cells (Malavolta et al., 2018). Hence, a movement toward the research of natural based compounds (nutraceuticals) with potential anti-senescence properties has begun. Nutraceuticals are bioactive compounds derived from food, including plant material, with physiological benefits in the prevention or treatment of disease (Rafieian-Kopaei et al., 2014). For instance, polyphenols, found in high abundance in plants, are bio-active compounds with anti-oxidant and anti-inflammatory properties making them potential senostatics by negating the pro-oxidant and pro-inflammatory signaling of senescent cells (Gurău et al., 2018). The aim remains to find potential anti-aging therapies that are effective but exhibit minimal side effects, and some natural plant-based compounds could fit this criterion. Below, we will discuss studied examples of nutraceuticals that could act as senolytics or senostatics as illustrated in **Figure 2**.

Olive Phenols

The olive oil plant contains high amounts of phenolic compounds, which exhibit potential beneficial properties regarding cardiac health, cancer protection and antimicrobial effects (Tuck and Hayball, 2002; Marković et al., 2019). *In vitro,* two olive phenols called hydroxytyrosol (HT) and oleuropein aglycone (OLE) have shown to counteract senescence via significant reductions in SA-β-Gal staining, p16 levels and SASP levels in pre-senescent human lung fibroblasts (MRC5) and neonatal human dermal fibroblasts (Menicacci et al., 2017). HT has also been investigated in a UVA-induced senescence model in human dermal fibroblasts (HDFs) and significant reductions in SA-β-Gal positivity and mRNA expression levels for SASP related genes were observed after treatment (Jeon and Choi, 2018).

OLE reduces oxidative stress and inhibits mTOR, which is a key modulator in aging (Johnson et al., 2013; Sun et al., 2017). However, there are no data yet on the potential effects of OLE on organismal ageing. During the process of aging, the accumulation of misfolded and damaged proteins takes place, and these are degraded and removed through proteasome activity (Sáez and Vílchez, 2014). OLE has shown to improve proteasome activity, thereby delaying senescence in human fibroblasts. Furthermore, continuous OLE treatment of early passage human embryonic fibroblasts was shown to reduce ROS levels, curb the progression of the senescence phenotype by abating the changes in morphology seen in senescence, and lower cell mortality (Katsiki et al., 2007; Giovannelli, 2012; Menicacci et al., 2017).

Green Tea Catechins

Catechin is a tannin found in green tea that has high antioxidant properties. As a polyphenol, it exists in multiple forms, including Epigallocatechin gallate (EGCG), which is found abundantly in tea leaves (Unno, 2016). Research investigating the effects of EGCG against replicative senescence in primary cells (rat vascular smooth muscle cells, HDF (human dermal fibroblasts)

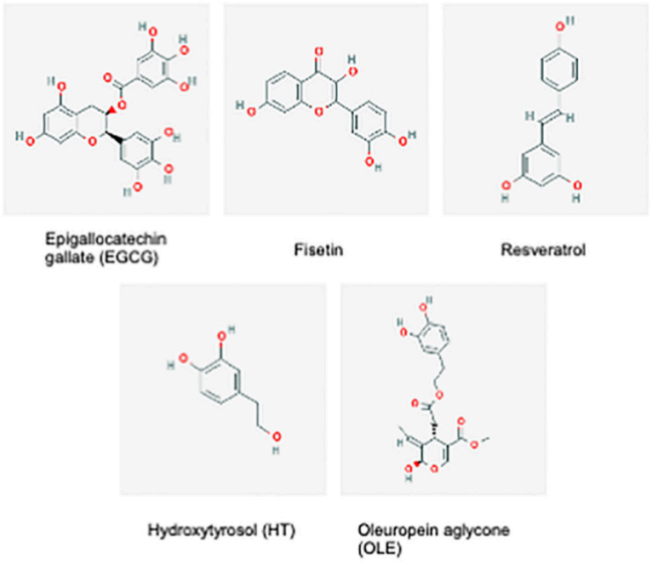

FIGURE 2 | Chemical structures of Epigallocatchin gallate (EGCG), Fisetin, Resveratrol, Hydroxytyrosol (HT) and Oleuropein aglycone (OLE). These compounds consist of either phenolic of polyphenolic alcohol groups (National Center for Biotechnology Information, 2019a,b,c,d,e).

and human articular chondrocytes), has shown the potential senostatics effects of the nutraceutical (Han et al., 2012). SA-β-Gal staining of HDF cells treated with EGCG at early and late passages showed fewer positive cells in treated than controls (Han et al., 2012). Moreover, p53 was shown to be significant reduced in EGCG treated cells (Han et al., 2012). However, cell cycle analysis of HDFs with and without EGCG treatment showed that treated cells had a similar percentage of cell in S phase as control cells.

EGCG was found to suppress premature senescence in preadipocytes, with treated cells showing significant downregulation of ROS, SASP and p53 mediated cell cycle arrest, in addition to the suppression of the anti-apoptotic protein BCL-2 and an increase in cell death (Kumar et al., 2018). This suggests that EGCG could have senolytic properties.

The effect of green tea catechins in aging was studied using a senescence accelerated mouse model ($SAMP_{10}$), which exhibits a short life span, cerebral atrophy and cognitive dysfunction (Unno et al., 2006). Between the ages of 1 and 15 months, mice were fed 35 mg/kg/day of green tea catechins. Analysis of blood and brain tissue found a decrease in oxidative DNA damage in the catechin-fed mice along with higher memory retention (Unno et al., 2006). A study investigating the effects of EGCG in healthy rats showed a median increase of lifespan by 8–12 weeks compared to controls. There was a significant decrease in liver and kidney IL-6 and ROS levels of the EGCG treated group, both of which are known to be upregulated with increasing age (Niu et al., 2013). This shows the potential beneficial systemic effects of EGCG in various organs.

However, an Intervention Testing Program was carried out, in which green tea extract was administered to a genetically heterogenous mouse model from a young age. Results showed no significant changes to lifespan (Strong et al., 2012). Although, the limited research of EGCG in connection to aging does not allow for definite conclusions, it has been widely used as a cosmetic for its potential skin protective effects its widely researched as a cosmetic additive having shown skin protective effects (Kim et al., 2018) and is available commercially in the form of green tea extract tablets.

Fisetin

Fisetin is bioactive flavonol molecule found in fruits and vegetables such as cucumber, apple, grape and onions, with the highest concentration being found in strawberries (Khan et al., 2013). It has established antioxidant, apoptotic and anti-proliferative qualities (Khan et al., 2013). Application of 5 μM Fisetin for 48 h led to a significant reduction in SA-β-Gal positivity in oxidative-stress induced senescent murine embryonic fibroblasts (Yousefzadeh et al., 2018b). Progeroid $Ercc1^{-/\Delta}$ and aged wild type mice receiving a diet supplemented with fisetin for two 14-day periods over 14 weeks at a concentration of 60 mg/kg/day had significantly lowered p16 expression in adipose tissue, in addition to decreased SASP.

Naturally aged C57BL/6 mice treated orally at 22–24 months with 100 mg/kg fisetin for 5 days showed a reduction in senescent cells in white adipose tissue (Yousefzadeh et al., 2018b). This result was mimicked in human adipose tissue explants that had been treated with fisetin and cultured *ex vivo*, showing reduction in SASP markers, IL-6, IL-8, MCP-1, and SA-β-Gal activity (Yousefzadeh et al., 2018b). Additionally, fisetin treatment at 85 weeks of age significantly prolonged life-span of these mice by an additional 3 months.

This research has given rise to the Alleviation by Fisetin of frailty, Inflammation and related measures in Older Adults (AFFIRM-LITE) clinical trial. Currently in the recruiting phase, the trial hopes to recruit 40 participants between the ages of 70–90 to take an oral 2-day dose of a placebo or fisetin at 20 mg/kg/day with analysis focusing on markers of frailty, inflammation, insulin resistance and bone metabolism (Clinicaltrials.gov, 2019a).

Resveratrol

Resveratrol is a stilbene polyphenol commonly found in pigmented fruits and vegetables, such as grapes and berries (Risuleo, 2016; Salehi et al., 2018). Biological activities of resveratrol include being antitumor, phytoestrogenic, antioxidant and antiviral (Risuleo, 2016). In senescence, resveratrol has been investigated for its effects on WI-38 human fibroblasts and HT-1080 cells with inducible ectopic p21. With the application of resveratrol at 50 μM, the senescent morphology of both SIPS model-based cell types was prevented, suggesting a senostatic effect. Moreover, at these concentrations, there was a 2-fold increase in cell number, showing that resveratrol helps overcome the cell cycle arrest. Of note, the polyphenol proved to be cytotoxic only at concentrations over 200 μM (Demidenko and Blagosklonny, 2009).

Resveratrol treatment in endothelial progenitor cells (EPCs) also showed prevention of replicative senescence, with reduced SA-β-Gal positive staining in comparison to controls (Xia et al., 2009). Treatment also demonstrated an increase in proliferative and migrating capabilities of EPCs, alongside a dose-dependent increase in telomerase activity, further highlighting the potential anti-senescence effects of resveratrol. This increase in telomerase activity was attributed to the activation of the PI3K-AKT pathway, which was shown to be phosphorylated in a resveratrol dose-dependent manner (Xia et al., 2009).

Moreover, when a large-scale *in vivo* study of resveratrol in genetically heterogenous (outbred) mice was conducted in parallel with rapamycin treatment, analysis of activity showed that there was no significant difference between control and resveratrol-treated mice. However, rapamycin-treated mice showed a 10% and 18% increase in median survival in males and females, respectively (Miller et al., 2010). The study highlighted the minimal effect resveratrol has on overall survival *in vivo*, even if *in vitro* studies suggested potential anti-senescence properties. In line with this, *in vivo* research from an Interventions Testing Program, which investigated the effect of administering resveratrol to a genetically heterogenous mouse model from a young age, showed no significant positive or negative effects in lifespan (Strong et al., 2012).

Nevertheless, a clinical trial involving the administration of resveratrol in older patients is underway, with participants taking a placebo, 1000 mg or 1500 mg per day in capsule form. The study will look at mitochondrial and physical function, focusing on the effects in muscle. Measures of output include levels of mitochondrial enzymes, walking speed, blood glucose, blood pressure, AMPK protein levels and resistance to muscle fatigue (REVIVE – Clinicaltrials.gov, 2019b). Despite studies and research still being conducted on resveratrol, it is also widely available to the public in tablet form, and is found in many anti-aging based cosmetics.

CONCLUSION: A LONG ROAD AHEAD

With life expectancy on the increase and a greater geriatric population with chronic illnesses, management of the elderly should be focused on prevention of tissue dysfunction and maintaining a better quality of life for longer times, what is known as increasing health span. In the last decade, the field of senescence has seen the emergence of senolytic therapies, which are being investigated intensively through *in vivo* research and, recently, a move toward clinical trials. Currently, a universal standard for senescence research isn't recognized. Different groups were able to create models *in vitro* using multiple inducers to cause DNA damage. All research should aim to test nutraceuticals first on an *in vitro* model preferably in human derived cells which have entered replicative senescence through multiple passaging. However, this kind of cell preparation would take a long time to reach senescence and only produce a finite number of cells for testing. Alternatively, using an *in vitro* mouse replicative senescence model is more feasible, as cells they stop proliferating after 5–6 passages (Khan and Gasser, 2016). Senolytics or senostatics could next be applied *in vivo* using aged wild-type mice. Despite this, multiple mouse models exist to test senolytic and senostatic application such as progeroid mice, which mimic the human syndrome known as progeria. Mice naturally reach full term within 6 months and can arise from BubR1$^{H/H}$, Zmpste24$^{-/-}$, Sod1$^{-/-}$ or Ercc$^{-/\Delta}$ strains (Yousefzadeh et al., 2018a).

Senolytics could be used as a preventative in the elderly, as a supplement to clear senescent cells to thus improve or maintain tissue and organ health. They are also being looked at as an adjuvant cancer therapy, with the aim of clearing treatment-induced senescent cells and thus reducing the probability of relapse (Tabasso et al., 2019). They are also being investigated in telomere biology. Telomerase is capable of reversing telomere erosion and has been targeted in peripheral blood mononuclear cells by plant derived telomerase activators (Tsoukalas et al., 2019). TA-65, a derivative of *Astragalus membranaceus*, has been shown to elongate telomerase in a telomere deficient mouse model (de Jesus et al., 2011).

Recent studies argue for a pathogenic role of senescent cells, which would contribute to a range of aging related diseases, such as osteoarthritis (Jeon et al., 2018), cardiovascular disease (Childs et al., 2018) and cataract (Fu et al., 2016). Senescent cells are found in aging related cognitive decline but

also in neurodegenerative diseases such as Alzheimer's disease and Parkinson's disease (Baker and Petersen, 2018) which are typically identified clinically and further characterized through imaging or at autopsy. Therefore, the possible application of senolytics in a wide range of clinical scenarios is becoming an attractive concept (Paez-Ribes et al., 2019).

However, for senolytics to be widely used in aged but otherwise healthy populations to prevent tissue dysfunction, unwanted side effects have to be kept to the minimum. The use of nutraceutical based senolytics could result in fewer complications, while retaining anti-senescent effects. Despite promising *in vitro* reports, the data on the *in vivo* efficacy of nutraceutical senolytics is still sparse and, in some cases, contradictory. Thus, more research is still needed to determine whether they could be an attractive alternative to the most used chemical senolytics, such as dasatinib + quercetin, which have shown promising results in preliminary short-term clinical trials (Hickson et al., 2019).

It also has to be taken in consideration that this therapeutic field is new, and the use of nutraceuticals as senolytics may also come with its drawbacks. The potential toxicity of the compounds and their adverse interactions with existing therapies for other health issues, needs to be carefully investigated. Because of this, it is worrying that some of these compounds have reached the wider public without proper validation or complete safety studies. Caution should be exerted when dealing with them. The adoption of nutraceutical senolytics as harmless complements may need to be discouraged until more information is available.

AUTHOR CONTRIBUTIONS

AK researched and composed the manuscript. CS discussed the data. CS and SM edited the manuscript.

FUNDING

AK is in receipt of a funded scholarship on the MIBTP (Midlands Integrative Biosciences Training Partnership) program funded by the BBSRC (Biotechnology and Biological Sciences Research Council).

REFERENCES

Aird, K., and Zhang, R. (2012). Detection of senescence-associated heterochromatin foci (SAHF). *Methods Mol. Biol.* 965, 185–196. doi: 10.1007/978-1-62703-239-1_12

Alcorta, D., Xiong, Y., Phelps, D., Hannon, G., Beach, D., and Barrett, J. (1996). Involvement of the cyclin-dependent kinase inhibitor p16 (INK4a) in replicative senescence of normal human fibroblasts. *Proc. Natl. Acad. Sci. U.S.A.* 93, 13742–13747. doi: 10.1073/pnas.93.24.13742

Althubiti, M., Rada, M., Samuel, J., Escorsa, J., Najeeb, H., Lee, K., et al. (2016). BTK modulates p53 activity to enhance apoptotic and senescent responses. *Cancer Res.* 76, 5405–5414. doi: 10.1158/0008-5472.CAN-16-0690

Astle, M., Hannan, K., Ng, P., Lee, R., George, A., Hsu, A., et al. (2011). AKT induces senescence in human cells via mTORC1 and p53 in the absence of DNA damage: implications for targeting mTOR during malignancy. *Oncogene* 31, 1949–1962. doi: 10.1038/onc.2011.394

Bailey, C. (2017). Metformin: historical overview. *Diabetologia* 60, 1566–1576. doi: 10.1007/s00125-017-4318-z

Baker, D. J., and Petersen, R. C. (2018). Cellular senescence in brain aging and neurodegenerative diseases: evidence and perspectives. *J. Clin. Investig.* 128, 1208–1216. doi: 10.1172/JCI95145

Bernadotte, A., Mikhelson, V., and Spivak, I. (2016). Markers of cellular senescence. Telomere shortening as a marker of cellular senescence. *Aging* 8, 3–11. doi: 10.18632/aging.100871

Blagosklonny, M. (2011). Cell cycle arrest is not senescence. *Aging* 3, 94–101. doi: 10.18632/aging.100281

Blenis, J., Kim, S. G., and Li, J. (2014). Rapamycin: one drug, many effects. *Cell Metab.* 19, 373–379. doi: 10.1016/j.cmet.2014.01.001

Boothman, D. A., and Suzuki, M. (2008). Stress-induced premature senescence (SIPS) – influence of SIPS on radiotherapy. *J. Radiat. Res.* 49, 105–112. doi: 10.1269/jrr.07081

Borodkina, A. V., Deryabin, P. I., Glukova, A. A., and Nikolsky, N. N. (2018). "Social Life" of senescent cells: what is SASP and why study it? *Acta Nat.* 10, 4–14. doi: 10.32607/20758251-2018-10-1-4-14

Calado, R. T., and Dumitriu, B. (2013). Telomere dynamics in mice and humans. *Semin. Hematol.* 50, 165–174. doi: 10.1053/j.seminhematol.2013.03.030

Childs, B., Li, H., and van Deursen, J. (2018). Senescent cells: a therapeutic target for cardiovascular disease. *J. Clin. Investig.* 128, 1217–1228. doi: 10.1172/jci95146

Ciccarone, F., Tagliatesta, S., Caiafa, P., and Zampieri, M. (2018). DNA methylation dynamics in aging: how far are we from understanding the mechanisms? *Mech. Age. Dev.* 174, 3–17. doi: 10.1016/j.mad.2017.12.002

Clinicaltrials.gov (2019a). *Alleviation by Fisetin of Frailty, Inflammation, and Related Measures in Older Adults - ClinicalTrials.gov*. Available online at: https://clinicaltrials.gov/ct2/show/NCT03675724 (accessed August 14, 2019).

Clinicaltrials.gov (2019b). *Resveratrol to Enhance Vitality and Vigor in Elders - ClinicalTrials.gov*. Available online at: https://www.clinicaltrials.gov/ct2/show/record/NCT02123121?term=resveratrol+aging&rank=10&view=record (accessed October 3, 2019).

de Jesus, B., Schneeberger, K., Vera, E., Tejera, A., Harley, C., and Blasco, M. (2011). The telomerase activator TA-65 elongates short telomeres and increases health span of adult/old mice without increasing cancer incidence. *Aging Cell* 10, 604–621. doi: 10.1111/j.1474-9726.2011.00700.x

Demidenko, Z. N., and Blagosklonny, M. V. (2009). At concentrations that inhibit mTOR, resveratrol suresses cellular senescence. *Cell Cycle* 8, 1901–1904. doi: 10.4161/cc.8.12.8810

Dimri, G. (1995). A biomarker that identifies senescent human cells in culture and in aging skin in vivo. *Cell Biol.* 92, 9363–9367. doi: 10.1073/pnas.92.20.9363

Dimri, G. (2005). What has senescence got to do with cancer? *Cancer Cell* 7, 505–512. doi: 10.1016/j.ccr.2005.05.025

Freund, A., Laberge, R., Demaria, M., and Campisi, J. (2012). Lamin B1 loss is a senescence-associated biomarker. *Mol. Biol. Cell* 23, 2066–2075. doi: 10.1091/mbc.E11-10-0884

Fu, Q., Qin, Z., Yu, J., Yu, Y., Tang, Q., Lyu, D., et al. (2016). Effects of senescent lens epithelial cells on the severity of age-related cortical cataract in humans. *Medicine* 95:3869. doi: 10.1097/MD.0000000000003869

Fuhrmann-Stroissnigg, H., Ling, Y., Zhao, J., McGowan, S., Zhu, Y., Brooks, R., et al. (2017). Identification of HSP90 inhibitors as a novel class of senolytics. *Nat. Commun.* 8:422. doi: 10.1038/s41467-017-00314-z

Fumagalli, M., Rossiello, F., Mondello, C., and d'Adda di Fagagna, F. (2014). Stable cellular senescence is associated with persistent DDR activation. *PLoS One* 9:110969. doi: 10.1371/journal.pone.0110969

Garbers, C., Kuck, F., Aparicio-Siegmund, S., Konzak, K., Kessenbrock, M., Sommerfeld, A., et al. (2013). Cellular senescence or EGFR signaling induces Interleukin 6 (IL-6) receptor expression controlled by mammalian target of rapamycin (mTOR). *Cell Cycle* 12, 3421–3432. doi: 10.4161/cc.26431

Giaimo, S., and d'Adda di Fagagna, F. (2012). Is cellular senescence an example of antagonistic pleiotropy? *Aging Cell* 11, 378–383. doi: 10.1111/j.1474-9726.2012.00807.x

Gilbert, S. F. (2000). "Developmental biology," in *Aging: The Biology of Senescence*, 6th Edn, eds T. J. Mauch and G. C. Schoenwolf (Sunderland, MA: Sinauer Associates).

Giovannelli, L. (2012). Beneficial effects of olive oil phenols on the aging process: experimental evidence and possible mechanisms of action. *Nutr. Aging* 1, 207–223. doi: 10.3233/nua-130016

González-Hunt, C., Wadhwa, M., and Sanders, L. (2018). DNA damage by oxidative stress: measurement strategies for two genomes. *Curr. Opin. Toxicol.* 7, 87–94. doi: 10.1016/j.cotox.2017.11.001

González-Meljem, J., As, J., Fraser, H., and Martínez-Barberá, J. (2018). Paracrine roles of cellular senescence in promoting tumourigenesis. *Br. J. Cancer* 118, 1283–1288. doi: 10.1038/s41416-018-0066-1

Guerrero, A., Herranz, N., Sun, B., Wagner, V., Gallage, S., Guiho, R., et al. (2019). Cardiac glycosides are broad-spectrum senolytics. *Nat. Metab.* 1, 1074–1088. doi: 10.1038/s42255-019-0122-z

Gurău, F., Baldoni, S., Prattichizzo, F., Espinosa, E., Amenta, F., Procopio, A., et al. (2018). Anti-senescence compounds: a potential nutraceutical aroach to healthy aging. *Ageing Res. Rev.* 46, 14–31. doi: 10.1016/j.arr.2018.05.001

Han, D. W., Lee, M. H., Kim, B., Lee, J. J., Hyon, S. H., and Parl, J. C. (2012). Preventative effects of Epigallocatechin-3-O-Gallate against replicative senescence associated with p53 acetylation in human dermal fibroblasts. *Oxid. Med. Cell. Longev.* 2012:850684.

Hayflick, L., and Moorhead, P. (1961). The serial cultivation of human diploid cell strains. *Exp. Cell Res.* 25, 585–621. doi: 10.1016/0014-4827(61)90192-6

Hernández-Segura, A., Nehme, J., and Demaría, M. (2018). Hallmarks of cellular senescence. *Trends Cell Biol.* 28, 436–453. doi: 10.1016/j.tcb.2018.02.001

Hewitt, G., Jurk, D., Marques, F., Correia-Melo, C., Hardy, T., Gackowska, A., et al. (2012). Telomeres are favoured targets of a persistent DNA damage response in ageing and stress-induced senescence. *Nat. Commun.* 3:708. doi: 10.1038/ncomms1708

Hickson, L., Langhi Prata, L., Bobart, S., Evans, T., Giorgadze, N., Hashmi, S., et al. (2019). Senolytics decrease senescent cells in humans: preliminary report from a clinical trial of Dasatinib plus Quercetin in individuals with diabetic kidney disease. *EBioMedicine* 47, 446–456. doi: 10.1016/j.ebiom.2019.08.069

Hooten, N., and Evans, M. (2017). Techniques to induce and quantify cellular senescence. *J. Vis. Exp.* 123:55533.

Huang, T., and Rivera-Pérez, J. (2014). Senescence-associated β-galactosidase activity marks the visceral endoderm of mouse embryos but is not indicative of senescence. *Genesis* 52, 300–308. doi: 10.1002/dvg.22761

Jackson, S., and Bartek, J. (2009). The DNA-damage response in human biology and disease. *Nature* 461, 1071–1078. doi: 10.1038/nature08467

Jeon, O., David, N., Campisi, J., and Elisseeff, J. (2018). Senescent cells and osteoarthritis: a painful connection. *J. Clin. Investig.* 128, 1229–1237. doi: 10.1172/JCI95147

Jeon, S., and Choi, M. (2018). Anti-inflammatory and anti-aging effects of hydroxytyrosol on human dermal fibroblasts (HDFs). *Biomed. Dermatol.* 2:21.

Jingwen, B., Yaochen, L., and Guojun, Z. (2017). Cell cycle regulation and anticancer drug discovery. *Cancer Biol. Med.* 14, 348–362.

Johnson, S., Rabinovitch, P., and Kaeberlein, M. (2013). mTOR is a key modulator of ageing and age-related disease. *Nature* 493, 338–345. doi: 10.1038/nature11861

Justice, J., Nambiar, A., Tchkonia, T., LeBrasseur, N., Pascual, R., Hashmi, S., et al. (2019). Senolytics in idiopathic pulmonary fibrosis: results from a first-in-human, open-label, pilot study. *EBioMedicine* 40, 554–563. doi: 10.1016/j.ebiom.2018.12.052

Katsiki, M., Chondrogianni, N., Chinou, I., Rivett, A., and Gonos, E. (2007). The olive constituent oleuropein exhibits proteasome stimulatory properties in vitro and confers life span extension of human embryonic fibroblasts. *Rejuvenat. Res.* 10, 157–172. doi: 10.1089/rej.2006.0513

Khan, M., and Gasser, S. (2016). Generating primary fibroblast cultures from mouse ear and tail tissues. *J. Vis. Exp.* 107:53565. doi: 10.3791/53565

Khan, N., Syed, D., Ahmad, N., and Mukhtar, H. (2013). Fisetin: a dietary antioxidant for health promotion. *Antioxid. Redox Signal.* 19, 151–162. doi: 10.1089/ars.2012.4901

Kim, E., Hwang, K., Lee, J., Han, S., Kim, E., Park, J., et al. (2018). Skin protective effect of epigallocatechin gallate. *Int. J. Mol. Sci.* 19:173. doi: 10.3390/ijms19010173

Ko, A., Han, S., Choi, C., Cho, H., Lee, M., Kim, S., et al. (2018). Oncogene-induced senescence mediated by c-Myc requires USP10 dependent deubiquitination and stabilization of p14ARF. *Cell Death Diff.* 25, 1050–1062. doi: 10.1038/s41418-018-0072-0

Kõks, S., Dogan, S., Tuna, B., González-Navarro, H., Potter, P., and Vandenbroucke, R. (2016). Mouse models of ageing and their relevance to disease. *Mech. Ageing Dev.* 160, 41–53. doi: 10.1016/j.mad.2016.10.001

Kumar, R., Sharma, A., Kumari, A., Gulati, A., Paćwad, Y., and Sharma, R. (2018). Epigallocatechin gallate suresses premature senescence of preadipocytes by inhibition of PI3K/Akt/mTOR pathway and induces senescent cell death by regulation of Bax/Bcl-2 pathway. *Biogerontology* 20, 171–189. doi: 10.1007/s10522-018-9785-1

Lee, B., Han, J., Im, J., Morrone, A., Johung, K., Goodwin, E., et al. (2006). Senescence-associated β-galactosidase is lysosomal β-galactosidase. *Aging Cell* 5, 187–195. doi: 10.1111/j.1474-9726.2006.00199.x

Malavolta, M., Bracci, M., Santarelli, L., Sayeed, M., Pierpaoli, E., Giacconi, R., et al. (2018). Inducers of senescence, toxic compounds, and senolytics: the multiple faces of Nrf2-activating phytochemicals in cancer adjuvant therapy. *Mediators Inflamm.* 2018, 1–32. doi: 10.1155/2018/4159013

Marković, A. K., Torić, J., Barbarić, M., and Brala, C. J. (2019). Hydroxytyrosol, tyrosol and derivatives and their potential effects on human health. *Molecules* 24:2001. doi: 10.3390/molecules24102001

Menicacci, B., Cipriani, C., Margheri, F., Mocali, A., and Giovannelli, L. (2017). Modulation of the senescence-associated inflammatory phenotype in human fibroblasts by olive phenols. *Int. J. Mol. Sci.* 18:2275. doi: 10.3390/ijms18112275

Miller, R., Harrison, D., Astle, C., Baur, J., Boyd, A., de Cabo, R., et al. (2010). Rapamycin, but not resveratrol or simvastatin, extends life span of genetically heterogeneous mice. *J. Gerontol. Ser. A* 66A, 191–201. doi: 10.1093/gerona/glq178

Moiseeva, O., Deschênes-Simard, X., St-Germain, E., Igelmann, S., Huot, G., Cadar, A., et al. (2013). Metformin inhibits the senescence-associated secretory phenotype by interfering with IKK/NF-κB activation. *Aging Cell* 12, 489–498. doi: 10.1111/acel.12075

National Center for Biotechnology Information (2019a). *PubChem Database(-)-Epigallocatechin gallate, CID=65064*. Available online at: https://pubchem.ncbi.nlm.nih.gov/compound/Epigallocatechin-gallate (accessed Feburary 18, 2020).

National Center for Biotechnology Information (2019b). *PubChem Database Fisetin, CID=5281614*. Available online at: https://pubchem.ncbi.nlm.nih.gov/compound/Fisetin (accessed Feburary 18, 2020).

National Center for Biotechnology Information (2019c). *PubChem Database Hydroxytyrosol, CID=82755*. Available online at: https://pubchem.ncbi.nlm.nih.gov/compound/Hydroxytyrosol (accessed Feburary 18, 2020).

National Center for Biotechnology Information (2019d). *PubChem Database Oleuropein aglycone, CID=56842347*. Available online at: https://pubchem.ncbi.nlm.nih.gov/compound/Oleuropein-aglycone (accessed Feburary 18, 2020).

National Center for Biotechnology Information (2019e). *PubChem Database Resveratrol, CID=445154*. Available online at: https://pubchem.ncbi.nlm.nih.gov/compound/Resveratrol (accessed Feburary 18, 2020).

Neurohr, G., Terry, R., Lengefeld, J., Bonney, M., Brittingham, G., Moretto, F., et al. (2019). Excessive cell growth causes cytoplasm dilution and contributes to senescence. *Cell* 176, 1083–1097. doi: 10.1015/j.cell.2019.01.018

Niu, Y., Na, L., Feng, R., Gong, L., Zhao, Y., Li, Q., et al. (2013). The phytochemical, EGCG, extends lifespan by reducing liver and kidney function damage and improving age-associated inflammation and oxidative stress in healthy rats. *Aging Cell* 12, 1041–1049. doi: 10.1111/acel.12133

Paez-Ribes, M., González-Gualda, E., Doherty, G., and Muñoz-Espín, D. (2019). Targeting senescent cells in translational medicine. *EMBO Mol. Med.* 11:e10234.

Parry, A., and Narita, M. (2016). Old cells, new tricks: chromatin structure in senescence. *Mamm. Genome* 27, 320–331. doi: 10.1007/s00335-016-9628-9

Qian, Y., and Chen, X. (2012). Senescence regulation by the p53 protein family. *Methods Mol. Biol.* 965, 37–61. doi: 10.1007/978-1-62703-239-1_3

Rafieian-Kopaei, M., Shirzad, H., Baradaran, A., and Nasri, H. (2014). New concepts in nutraceuticals as an alternative for pharmaceuticals. *Int. J. Prevent. Med.* 5, 1487–1499.

Risuleo, G. (2016). Resveratrol. *Nutraceuticals* 5, 453–464.

Rodier, F., and Campisi, J. (2011). Four faces of cellular senescence. *J. Cell Biol.* 192, 547–556. doi: 10.1083/jcb.201009094

Sáez, I., and Vílchez, D. (2014). The mechanistic links between proteasome activity, aging and age-related diseases. *Curr. Genomics* 15, 38–51. doi: 10.2174/1389202915011403061133 44

Salehi, B., Mishra, A., Nigam, M., Sener, B., Kilic, M., Sharifi-Rad, M., et al. (2018). Resveratrol: a double-edged sword in health benefits. *Biomedicines* 6:91. doi: 10.3390/biomedicines6030091

Samaraweera, L., Adomako, A., Rodriguez-Gabin, A., and McDaid, H. (2017). A novel indication for panobinostat as a senolytic drug in NSCLC and HNSCC. *Sci. Rep.* 7:1900. doi: 10.1038/s41598-017-01964-1

Serrano, M., Lin, A., McCurrach, M., Beach, D., and Lowe, S. (1997). Oncogenic ras provokes premature cell senescence associated with accumulation of p53 and p16INK4a. *Cell* 88, 593–602. doi: 10.1016/s0092-8674(00)81902-9

Serrano, M., and Muñoz-Espín, D. (2014). Cellular senescence: from physiology to pathology. *Nat. Rev. Mol. Cell Biol.* 15, 482–496. doi: 10.1038/nrm3823

Shammas, M. (2011). Telomeres, lifestyle, cancer, and aging. *Curr. Opin. Clin. Nutr. Metab. Care* 14, 28–34. doi: 10.1097/mco.0b013e32834121b1

Short, S., Fielder, E., Miwa, S., and von Zglinicki, T. (2019). Senolytics and senostatics as adjuvant tumour therapy. *EBioMedicine* 41, 683–692. doi: 10.1016/j.ebiom.2019.01.056

Strong, R., Miller, R., Astle, C., Baur, J., de Cabo, R., Fernández, E., et al. (2012). Evaluation of resveratrol, green tea extract, curcumin, oxaloacetic acid, and medium-chain triglyceride oil on life span of genetically heterogeneous mice. *J. Gerontol. Ser. A Biol. Sci. Med. Sci.* 68, 6–16. doi: 10.1093/gerona/gls070

Sun, W., Frost, B., and Liu, J. (2017). Oleuropein, unexpected benefits! *Oncotarget* 8:17409.

Tabasso, A., Jones, D., Jones, G., and Macip, S. (2019). Radiotherapy-induced senescence and its effects on responses to treatment. *Clin. Oncol.* 31, 283–289. doi: 10.1016/j.clon.2019.02.003

Triana-Martínez, F., Picallos-Rabina, P., Da Silva-Álvarez, S., Pietrocola, F., Llanos, S., Rodilla, V., et al. (2019). Identification and characterization of Cardiac Glycosides as senolytic compounds. *Nat. Commun.* 10:4731. doi: 10.1038/s41467-019-12888-x

Tsoukalas, D., Fragkiadaki, P., Docea, A. O., Alegakis, A. K., Sarandi, E., Thanasoula, M., et al. (2019). Discovery of potent telomerase activators: unfolding new therapeutic, and anti-aging perspectives. *Mol. Med. Rep.* 20, 3701–3708. doi: 10.3892/mmr.2019.10614

Tuck, K., and Hayball, P. (2002). Major phenolic compounds in olive oil: metabolism and health effects. *J. Nutr. Biochem.* 13, 636–644. doi: 10.1016/s0955-2863(02)00229-2

Unno, K. (2016). Prevention of brain aging by green tea components: role of catechins and theanine. *J. Phys. Fitness Sports Med.* 5, 117–122. doi: 10.7600/jpfsm.5.117

Unno, K., Takabayashi, F., Yoshida, H., Choba, D., Fukutomi, R., Kikunaga, N., et al. (2006). Daily consumption of green tea catechin delays memory regression in aged mice. *Biogerontology* 8, 89–95. doi: 10.1007/s10522-006-9036-8

van Deursen, J. (2014). The role of senescent cells in ageing. *Nature* 509, 439–446. doi: 10.1038/nature13193

Wang, R., Yu, Z., Sunchu, B., Shoaf, J., Dang, I., Zhao, S., et al. (2017). Rapamycin inhibits the secretory phenotype of senescent cells by a Nrf2-independent mechanism. *Aging Cell* 16, 564–574. doi: 10.1111/acel.12587

Wiley, C., and Campisi, J. (2016). From ancient pathways to aging cells—connecting metabolism and cellular senescence. *Cell Metab.* 23, 1013–1021. doi: 10.1016/j.cmet.2016.05.010

Xia, L., Wang, X., Hu, X., Guo, X., Shang, Y., Chen, H., et al. (2009). Resveratrol reduces endothelial progenitor cells senescence through augmentation of telomerase activity by Akt-dependent mechanisms. *Br. J. Pharmacol.* 155, 387–394. doi: 10.1038/bjp.2008.272

Xu, M., Pirtskhalava, T., Farr, J., Weigand, B., Palmer, A., Weivoda, M., et al. (2018). Senolytics improve physical function and increase lifespan in old age. *Nat. Med.* 24, 1246–1256. doi: 10.1038/s41591-018-0092-9

Yao, G. (2014). Modelling mammalian cellular quiescence. *Interface Focus* 4:20130074. doi: 10.1098/rsfs.2013.0074

Yosef, R., Pilpel, N., Tokarsky-Amiel, R., Biran, A., Ovadya, Y., Cohen, S., et al. (2016). Directed elimination of senescent cells by inhibition of BCL-W and BCL-XL. *Nat. Commun.* 7:11190. doi: 10.1038/ncomms11190

Yousefzadeh, M., Melos, K., Angelini, L., Burd, C., Robbins, P., and Niedernhofer, L. (2018a). Mouse models of accelerated cellular senescence. *Methods Mol. Biol.* 1896, 203–230. doi: 10.1007/978-1-4939-8931-7_17

Yousefzadeh, M., Zhu, Y., McGowan, S., Angelini, L., Fuhrmann-Stroissnigg, H., Xu, M., et al. (2018b). Fisetin is a senotherapeutic that extends health and lifespan. *EBioMedicine* 36, 18–28. doi: 10.1016/j.ebiom.2018.09.015

Zhang, F., Cheng, D., Wang, S., and Zhu, J. (2016). Human specific regulation of the telomerase reverse transcriptase gene. *Genes* 7:30. doi: 10.3390/genes7070030

Zhu, Y., Tchkonia, T., Pirtskhalava, T., Gower, A., Ding, H., Giorgadze, N., et al. (2015). The Achilles' heel of senescent cells: from transcriptome to senolytic drugs. *Aging Cell* 14, 644–658. doi: 10.1111/acel.12344

Conflict of Interest: The authors declare that the research was conducted in the absence of any commercial or financial relationships that could be construed as a potential conflict of interest.

REFERENCES

Thesis submitted for the degree of
Doctor of Philosophy

By
Amanpreet Kaur (BSc)
Department of Respiratory Sciences
University Of Leicester

May 2021

Absalan A, Mesbah-Namin SA, Tiraihi T, Taheri T. (2017). Cinnamaldehyde and eugenol change the expression folds of AKT1 and DKC1 genes and decrease the telomere length of human adipose-derived stem cells (hASCs): An experimental and in silico study. *Iran J Basic Med Sci.* Mar;20(3):316-326.

Abubakar, A. and Haque, M., (2020). Preparation of medicinal plants: Basic extraction and fractionation procedures for experimental purposes. *Journal of Pharmacy And Bioallied Sciences*, 12(1).

Acosta, J., Banito, A., Wuestefeld, T., Georgilis, A., Janich, P., Morton, J., Athineos, D., Kang, T., Lasitschka, F., Andrulis, M., Pascual, G., Morris, K., Khan, S., Jin, H., Dharmalingam, G., Snijders, A., Carroll, T., Capper, D., Pritchard, C., Inman, G., Longerich, T., Sansom, O., Benitah, S., Zender, L. and Gil, J., (2013). A complex secretory program orchestrated by the inflammasome controls paracrine senescence. *Nature Cell Biology*, 15(8), pp.978-990.

Acun, A., Nguyen, T. and Zorlutuna, P., (2019). In vitro aged, hiPSC-origin engineered heart tissue models with age-dependent functional deterioration to study myocardial infarction. *Acta Biomaterialia*, 94, pp.372-391.

Agostinis, P., (2003). Bcl2 phosphorylation: a tie between cell survival, growth, and ROS. *Blood*, 102(9), pp.3079-3079.

Aird, K. and Zhang, R., (2012). Detection of Senescence-Associated Heterochromatin Foci (SAHF). *Methods in Molecular Biology*, pp.185-196.

Alexander, E., Hildebrand, D., Kriebs, A., Obermayer, K., Manz, M., Rothfuss, O., Schulze-Osthoff, K. and Essmann, F., (2013). IFKB is a regulator of the senescence-associated secretory phenotype in DNA damage- and oncogene-induced senescence. *Journal of Cell Science*, 126(16), pp.3738-3745.

Ahmad, S. and Tahir, I., 2016. Regulatory role of phenols in flower development and senescence in the genus Iris. *Indian Journal of Plant Physiology*, 22(1), pp.135-140.

Nobel Prize.org (2019) Alexis Carrel – Nobel Media AB 2019. Available at: https://www.nobelprize.org/prizes/medicine/1912/carrel/biographical/

Althubiti, M., Rada, M., Samuel, J., Escorsa, J., Najeeb, H., Lee, K., et al. (2016). BTK modulates p53 activity to enhance apoptotic and senescent responses. *Cancer Res.* 76, pp.5405–5414

TAME - American Federation for Aging Research. (2021). *TAME - Targeting Aging with Metformin - American Federation for Aging Research*. [online] Available at: <https://www.afar.org/tame-trial>

Ankri, S. and Mirelman, D., (1999). Antimicrobial properties of allicin from garlic. *Microbes and Infection*, 1(2), pp.125-129.

Arreola, R., Quintero-Fabián, S., López-Roa, R., Flores-Gutiérrez, E., Reyes-Grajeda, J., Carrera-Quintanar, L. and Ortuño-Sahagún, D., (2015). Immunomodulation and Anti-Inflammatory Effects of Garlic Compounds. *Journal of Immunology Research*, Vol 2015: 401630

Astle, M., Hannan, K., Ng, P., Lee, R., George, A., Hsu, A., Haupt, Y., Hannan, R. and Pearson, R. (2011). AKT induces senescence in human cells via mTORC1 and p53 in the absence of DNA damage: implications for targeting mTOR during malignancy. *Oncogene*, 31(15), pp.1949-1962.

Aw, D., Silva, A. and Palmer, D. (2007). Immunosenescence: emerging challenges for an ageing population. *Immunology*, 120(4), pp.435-446.

Bailey, C. (2017). Metformin: historical overview. *Diabetologia,* 60, pp.1566–1576.

Baliga, M., Rao, S., Rai, M. and D'souza, P., 2016. Radio protective effects of the Ayurvedic medicinal plant Ocimum sanctum Linn. (Holy Basil): A memoir. *Journal of Cancer Research and Therapeutics*, 12(1), pp.20.

Bayan, L., Koulivand, P. H., & Gorji, A. (2014). Garlic: a review of potential therapeutic effects. *Avicenna journal of phytomedicine*, *4*(1), pp.1–14.

Bernadotte, A., Mikhelson, V. and Spivak, I. (2016). Markers of cellular senescence. Telomere shortening as a marker of cellular senescence. *Aging*, 8(1), pp.3-11.

Betteridge, D., (2000). What is oxidative stress?. *Metabolism*, 49(2), pp.3-8.

Beyne-Rauzy, O., Recher, C., Dastugue, N., Demur, C., Pottier, G., Laurent, G., Sabatier, L. and Mansat-De Mas, V., (2004). Tumor necrosis factor alpha induces senescence and chromosomal instability in human leukemic cells. *Oncogene*, 23(45), pp.7507-7516.

Birch, J. and Gil, J., (2020). Blunting senescence boosts liver regeneration. *Genes & Development*, 34(7-8), pp.463-464.

Blackburn, E. (2004). Telomeres and telomerase: their mechanisms of action and the effects of altering their functions. *FEBS Letters*, 579(4), pp.859-862.

Blenis, J., Kim, S. G., and Li, J. (2014). Rapamycin: one drug, many effects. *Cell Metab.* 19, pp.373–379.

Boncler, M., Golanski, J., Lukasiak, M., Redzynia, M., Dastych, J. and Watala, C., (2017). A new approach for the assessment of the toxicity of polyphenol-rich compounds with the use of high content screening analysis. *PLOS ONE*, 12(6).

Bonda, T., Dziemidowicz, M., Cieślińska, M., Tarasiuk, E., Wawrusiewicz-Kurylonek, N., Bialuk, I., Winnicka, M. and Kamiński, K., (2018). Interleukin 6 Knockout Inhibits Aging-Related Accumulation of p53 in the Mouse Myocardium. *The Journals of Gerontology: Series A*, 74(2), pp.176-182.

Bondar, G., Xu, W., Elashoff, D., Li, X., Faure-Kumar, E., Bao, T., Grogan, T., Moose, J. and Deng, M., (2020). Comparing NGS and NanoString platforms in peripheral blood mononuclear cell transcriptome profiling for advanced heart failure biomarker development. *Journal of Biological Methods*, 7(1), pp.123.

Boothman, D.A. & Suzuki, M. (2008). Stress-induced premature senescence (SIPS) – Influence of SIPS on Radiotherapy. *Journal of Radiation Research.* 49 (2). pp105-112

Borodkina, A. V., Deryabin, P. I., Giukova, A. A., & Nikolsky, N. N. (2018). "Social Life" of Senescent Cells: What Is SASP and Why Study It?. *Acta naturae*, *10*(1), pp.4–14.

Bracken, A.P., Geraghty, J.G. & Lanigan, F. (2011). Transcriptional regulation of cellular senescence. *Oncogene*, 30 pp. 2901-2911.

Bratic, A. and Larsson, N. (2013). The role of mitochondria in aging. *Journal of Clinical Investigation*, 123(3), pp.951-957.

Bussian, T., Aziz, A., Meyer, C., Swenson, B., van Deursen, J. and Baker, D. (2018). Clearance of senescent glial cells prevents tau-dependent pathology and cognitive decline. *Nature*, 562(7728), pp.578-582.

Cai, Y., Zhou, H., Zhu, Y., Sun, Q., Ji, Y., Xue, A., Wang, Y., Chen, W., Yu, X., Wang, L., Chen, H., Li, C., Luo, T. and Deng, H., (2020). Elimination of senescent cells by β-galactosidase-targeted prodrug attenuates inflammation and restores physical function in aged mice. *Cell Research*, 30(7), pp.574-589.

Calado, R. and Dumitriu, B., (2013). Telomere Dynamics in Mice and Humans. *Seminars in Hematology*, 50(2), pp.165-174.

Callaway, E. (2013). Deal done over HeLa cell line. *Nature*, 500(7461), pp.132-133.

Campisi, J. (1997). The biology of replicative senescence. *European Journal of Cancer*, 33(5), pp.703-709.

Capurso, C., Bellanti, F., Lo Buglio, A. and Vendemiale, G., (2019). The Mediterranean Diet Slows Down the Progression of Aging and Helps to Prevent the Onset of Frailty: A Narrative Review. *Nutrients*, 12(1), p.35.

Carrel, A. (1912). *On the permanent life of tissue outside of the organism*. [online] Ncbi.nlm.nih.gov. Available at: https://www.ncbi.nlm.nih.gov/pmc/articles/PMC2124948/pdf/516.pdf.

Cedzyński, M., Thielens, N., Mollnes, T. and Vorup-Jensen, T., (2019). Editorial: The Role of Complement in Health and Disease. *Frontiers in Immunology*, 10.
Chaiyana, W., Anuchapreeda, S., Punyoyai, C., Neimkhum, W., Lee, K., Lin, W., Lue, S., Viernstein, H. and Mueller, M., 2019. Ocimum sanctum Linn. as a natural source of skin anti-ageing compounds. *Industrial Crops and Products*, 127, pp.217-224.

Chaudhary, A., Sharma, S., Mittal, A., Gupta, S. and Dua, A., (2020). Phytochemical and antioxidant profiling of Ocimum sanctum. *Journal of Food Science and Technology*, 57(10), pp.3852-3863.

Chen, C., Wu, W., Panyod, S., Wu, M. and Lee-Yan, S., (2019). Cardiovascular Disease Protective Effect of Allicin Through Gut Microbiota Modulation (FS07-08-19). *Current Developments in Nutrition*, 3.

Chen, H., Zhu, B., Zhao, L., Liu, Y., Zhao, F., Feng, J., Jin, Y., Sun, J., Geng, R. and Wei, Y., (2018). Allicin Inhibits Proliferation and Invasion in Vitro and in Vivo via SHP-1-Mediated STAT3 Signaling in Cholangiocarcinoma. *Cellular Physiology and Biochemistry*, 47(2), pp.641-653.

Chen, J., Ou, Y., Li, Y., Hu, S., Shao, L. and Liu, Y., (2017). Metformin extends *C. elegans* lifespan through lysosomal pathway. *eLife*, 6.

Chen, J., Ozanne, S. and Hales, C., (2007). Methods of Cellular Senescence Induction Using Oxidative Stress. *Methods in Molecular Biology*, pp.179-189
.

Chen, M., Huang, J., Yang, X., Liu, B., Zhang, W., Huang, L., Deng, F., Ma, J., Bai, Y., Lu, R., Huang, B., Gao, Q., Zhuo, Y. and Ge, J., (2012). Serum Starvation Induced Cell Cycle Synchronization Facilitates Human Somatic Cells Reprogramming. *PLoS ONE*, 7(4).

Chen, Q. and Ames, B., (1994). Senescence-like growth arrest induced by hydrogen peroxide in human diploid fibroblast F65 cells. *Proceedings of the National Academy of Sciences*, 91(10), pp.4130-4134.

Cheng, Y., Patterson, C. and Staeheli, P., (1991). Interferon-induced guanylate-binding proteins lack an N(T)KXD consensus motif and bind GMP in addition to GDP and GTP. *Molecular and Cellular Biology*, 11(9), pp.4717-4725.

Chien, Y., Scuoppo, C., Wang, X., Fang, X., Balgley, B., Bolden, J., Premsrirut, P., Luo, W., Chicas, A., Lee, C., Kogan, S. and Lowe, S., (2011). Control of the senescence-associated secretory phenotype by NF- B promotes senescence and enhances chemosensitivity. *Genes & Development*, 25(20), pp.2125-2136.

Choi, U., Kang, J., Hwang, Y. and Kim, Y., (2015). Oligoadenylate synthase-like (OASL) proteins: dual functions and associations with diseases. *Experimental & Molecular Medicine*, 47(3), pp.144.

Christofferson, D., Li, Y. and Yuan, J., (2014). Control of Life-or-Death Decisions by RIP1 Kinase. *Annual Review of Physiology*, 76(1), pp.129-150.

Chung, H., (2019). Therapeutic Role of Garlic Extracts in Aging and Age-Related Diseases. *Biomedical Journal of Scientific & Technical Research*, 18(5).

Chung, L., (2006). The Antioxidant Properties of Garlic Compounds: Allyl Cysteine, Alliin, Allicin, and Allyl Disulfide. *Journal of Medicinal Food*, 9(2), pp.205-213.

Clinicaltrials.gov. (2021). *Participatory Evaluation (of) Aging (With) Rapamycin (for) Longevity Study - Full Text View - ClinicalTrials.gov*. [online] Available at: <https://clinicaltrials.gov/ct2/show/NCT04488601> [Accessed 12 May 2021].

Cohen, M., (2014). Tulsi - Ocimum sanctum: A herb for all reasons. *Journal of Ayurveda and Integrative Medicine*, 5(4), p.251.

Colombo, A., Elias, H. and Ramsingh, G., (2018). Senescence induction universally activates transposable element expression. *Cell Cycle*, 17(14), pp.1846-1857.

Coppé, J., Desprez, P., Krtolica, A. and Campisi, J. (2010). The Senescence-Associated Secretory Phenotype: The Dark Side of Tumor Suppression. *Annual Review of Pathology: Mechanisms of Disease*, 5(1), pp.99-118.

Cox, A. and Hampton, M., (2007). Bcl-2 over-expression promotes genomic instability by inhibiting apoptosis of cells exposed to hydrogen peroxide. *Carcinogenesis*, 28(10), pp.2166-2171.

Genecards Database., (2021). *PTGS2 Gene – GeneCards | PGH2 Protein | PGH2 Antibody*. [online] Genecards.org. Available at: <https://www.genecards.org/cgi-bin/carddisp.pl?gene=PTGS2>

Davalos, A., Coppe, J., Campisi, J. and Desprez, P., (2010). Senescent cells as a source of inflammatory factors for tumor progression. *Cancer and Metastasis Reviews*, 29(2), pp.273-283.

de Alencar, M., Islam, M., de Lima, R., Paz, M., dos Reis, A., da Mata, A., Filho, J., Cerqueira, G., Ferreira, P., e Sousa, J., Mubarak, M. and Melo-Cavalcante, A., (2018). Phytol as an anticarcinogenic and antitumoral agent: An in vivo study in swiss mice with DMBA-Induced breast cancer. *IUBMB Life*, 71(2), pp.200-212.

de Jesus, B. and Blasco, M., (2012). Assessing Cell and Organ Senescence Biomarkers. *Circulation Research*, 111(1), pp.97-109.

de Moraes, J., de Oliveira, R., Costa, J., Junior, A., de Sousa, D., Freitas, R., Allegretti, S. and Pinto, P., (2014). Phytol, a Diterpene Alcohol from Chlorophyll, as a Drug against Neglected Tropical Disease Schistosomiasis Mansoni. *PLoS Neglected Tropical Diseases*, 8(1), p.e2617.

Debacq-Chainiaux, F., Borlon, C., Pascal, T., Royer, V., Eliaers, F., Ninane, N., Carrard, G., Friguet, B., de Longueville, F., Boffe, S., Remacle, J. and Toussaint, O., (2005). Repeated exposure of human skin fibroblasts to UVB at subcytotoxic level triggers premature senescence through the TGF- 1 signaling pathway. *Journal of Cell Science*, 118(4), pp.743-758.

Debacq-Chainiaux, F., Erusalimsky, J., Campisi, J. and Toussaint, O. (2009). Protocols to detect senescence-associated beta-galactosidase (SA-βgal) activity, a biomarker of senescent cells in culture and in vivo. *Nature Protocols*, 4(12), pp.1798-1806.

Demidenko, Z., Zubova, S., Bukreeva, E., Pospelov, V., Pospelova, T. and Blagosklonny, M., (2009). Rapamycin decelerates cellular senescence. *Cell Cycle*, 8(12), pp.1888-1895.

Deshmane, S., Kremlev, S., Amini, S. and Sawaya, B., (2009). Monocyte Chemoattractant Protein-1 (MCP-1): An Overview. *Journal of Interferon & Cytokine Research*, 29(6), pp.313-326.

Di, G., Liu, Y., Lu, Y., Liu, J., Wu, C. and Duan, H., (2014). IL-6 Secreted from Senescent Mesenchymal Stem Cells Promotes Proliferation and Migration of Breast Cancer Cells. *PLoS ONE*, 9(11), p.e113572.

Dimri, G. (2005). What has senescence got to do with cancer?. *Cancer Cell*, 7(6), pp.505-512.

Dunn, G.P., Old, L.J. & Schreiber, R.D. (2004) The three Es of cancer immunoediting. *Annu Rev Immunol*. 22, pp.329-360

Eggert, T., Wolter, K., Ji, J., Ma, C., Yevsa, T., Klotz, S., Medina-Echeverz, J., Longerich, T., Forgues, M., Reisinger, F., Heikenwalder, M., Wang, X., Zender, L. and Greten, T., (2016). *Distinct Functions of Senescence-Associated Immune Responses in Liver Tumor Surveillance and Tumor Progression*. Cancer cell 30, 533-547.

Ellison-Hughes, G., (2020). First evidence that senolytics are effective at decreasing senescent cells in humans. *EBioMedicine*, 56, p.102473.

Ershler, W., (1993). Interleukin-6: A Cytokine for Gerontolgists. *Journal of the American Geriatrics Society*, 41(2), pp.176-181.

Espia, M., Sebastian, C., Mulero, M., Giralt, M., Mallol, J., Celada, A. and Lloberas, J., (2008). Granulocyte Macrophage-Colony-Stimulating Factor-Dependent Proliferation Is Impaired in Macrophages From Senescence-Accelerated Mice. *The Journals of Gerontology Series A: Biological Sciences and Medical Sciences*, 63(11), pp.1161-1167.

Feng, Y., Zhu, X., Wang, Q., Jiang, Y., Shang, H., Cui, L. and Cao, Y., (2012). Allicin enhances host pro-inflammatory immune responses and protects against acute murine malaria infection. *Malaria Journal*, 11(1), p.268.

Feringa, F., Raaijmakers, J., Hadders, M., Vaarting, C., Macurek, L., Heitink, L., Krenning, L. and Medema, R., (2018). Persistent repair intermediates induce senescence. *Nature Communications*, 9(1).

Ferrucci, L. and Fabbri, E., (2018). Inflammageing: chronic inflammation in ageing, cardiovascular disease, and frailty. *Nature Reviews Cardiology*, 15(9), pp.505-522.

Ford, J., Hughson, A., Lim, K., Bardina, S., Lu, W., Charo, I., Lim, J. and Fowell, D., (2019). CCL7 Is a Negative Regulator of Cutaneous Inflammation Following Leishmania major Infection. *Frontiers in Immunology*, 9.

Fraga, M. and Esteller, M. (2007). Epigenetics and aging: the targets and the marks. *Trends in Genetics*, 23(8), pp.413-418.

Franceschi, C. and Campisi, J. (2014). Chronic Inflammation (Inflammaging) and Its Potential Contribution to Age-Associated Diseases. *The Journals of Gerontology Series A: Biological Sciences and Medical Sciences*, 69(Suppl 1), pp.4-9.

Franzen, J., Wagner, W. and Fernandez-Rebollo, E. (2016). Epigenetic Modifications upon Senescence of Mesenchymal Stem Cells. *Current Stem Cell Reports*, 2(3), pp.248-254.

Freund, A., Laberge, R., Demaria, M. and Campisi, J. (2012). Lamin B1 loss is a senescence-associated biomarker. *Molecular Biology of the Cell*, 23(11), pp.2066-2075.

Frick, V., Rubie, C., Keilholz, U. and Ghadjar, P., (2016). Chemokine/chemokine receptor pair CCL20/CCR6 in human colorectal malignancy: An overview. *World Journal of Gastroenterology*, 22(2), p.833.

Frisch, S. and MacFawn, I., (2020). Type I interferons and related pathways in cell senescence. *Aging Cell*, 19(10).

Fuhrmann-Stroissnigg, H., Ling, Y., Zhao, J., McGowan, S., Zhu, Y., Brooks, R., et al. (2017). Identification of HSP90 inhibitors as a novel class of senolytics. *Nat. Commun.* 8:422.

Fulop, T., Larbi, A., Dupuis, G., Le Page, A., Frost, E., Cohen, A., Witkowski, J. and Franceschi, C. (2018). Immunosenescence and Inflamm-Aging As Two Sides of the Same Coin: Friends or Foes?. *Frontiers in Immunology*, 8.

Gajula., D, M. Verghese, J. Boateng, L.T. Walker, L. Shackelford, S.R. Mentreddy and S. Cedric, (2009). Determination of Total Phenolics, Flavonoids and Antioxidant and Chemopreventive Potential of Basil (*Ocimum basilicum* L. and *Ocimum tenuiflorum* L.). *International Journal of Cancer Research, 5: 130-143*

Garbers, C., Kuck, F., Aparicio-Siegmund, S., Konzak, K., Kessenbrock, M., Sommerfeld, A., Häussinger, D., Lang, P., Brenner, D., Mak, T., Rose-John, S., Essmann, F., Schulze-Osthoff, K., Piekorz, R. and Scheller, J. (2013). Cellular

senescence or EGFR signaling induces Interleukin 6 (IL-6) receptor expression controlled by mammalian target of rapamycin (mTOR). *Cell Cycle*, 12(21), pp.3421-3432.

Garces de los Fayos Alonso, I., Liang, H., Turner, S., Lagger, S., Merkel, O. and Kenner, L., (2018). The Role of Activator Protein-1 (AP-1) Family Members in CD30-Positive Lymphomas. *Cancers*, 10(4), p.93.

Garnier, G., Cirocolo, A., Xu, Y. and Volanakis, J., (2003). Complement C1r and C1s genes are duplicated in the mouse: differential expression generates alternative isomorphs in the liver and in the male reproductive system. *Biochemical Journal*, 371(2), pp.631-640.

Gaya da Costa, M., Poppelaars, F., van Kooten, C., Mollnes, T., Tedesco, F., Würzner, R., Trouw, L., Truedsson, L., Daha, M., Roos, A. and Seelen, M., (2018). Age and Sex-Associated Changes of Complement Activity and Complement Levels in a Healthy Caucasian Population. *Frontiers in Immunology*, 9.

Geiss, G., Bumgarner, R., Birditt, B., Dahl, T., Dowidar, N., Dunaway, D., Fell, H., Ferree, S., George, R., Grogan, T., James, J., Maysuria, M., Mitton, J., Oliveri, P., Osborn, J., Peng, T., Ratcliffe, A., Webster, P., Davidson, E., Hood, L. and Dimitrov, K., (2008). Direct multiplexed measurement of gene expression with color-coded probe pairs. *Nature Biotechnology*, 26(3), pp.317-325.

GeneCards - RPS6KA5 Gene (2021) | *KS6A5 Protein* | [online] Genecards.org. Available at: <https://www.genecards.org/cgi-bin/carddisp.pl?gene=RPS6KA5>

Gentili, C., Morelli, S. and de Boland, A., (2004). PTH and phospholipase A2 in the aging process of intestinal cells. *Journal of Cellular Biochemistry*, 93(2), pp.312-326.

Georgakopoulou, E., Tsimaratou, K., Evangelou, K., Fernandez, M., Zoumpourlis, V., Trougakos, I., Kletsas, D., Bartek, J., Serrano, M. and Gorgoulis, V. (2012). Specific lipofuscin staining as a novel biomarker to detect replicative and stress-induced senescence. A method applicable in cryo-preserved and archival tissues. *Aging*, 5(1), pp.37-50.

Giaimo, S. and d'Adda di Fagagna, F. (2012). Is cellular senescence an example of antagonistic pleiotropy?. *Aging Cell*, 11(3), pp.378-383.

Gilbert SF. Developmental Biology. 6th edition. Sunderland (MA): Sinauer Associates; (2000). Aging: The Biology of Senescence. Available from: https://www.ncbi.nlm.nih.gov/books/NBK10041/

Gire, V. and Dulić, V. (2015). Senescence from G2 arrest, revisited. *Cell Cycle*, 14(3), pp.297-304.

Glück, S., Guey, B., Gulen, M., Wolter, K., Kang, T., Schmacke, N., Bridgeman, A., Rehwinkel, J., Zender, L. and Ablasser, A., (2017). Innate immune sensing of cytosolic chromatin fragments through cGAS promotes senescence. *Nature Cell Biology*, 19(9), pp.1061-1070.

Gonzalez-Hunt, C., Wadhwa, M. and Sanders, L. (2018). DNA damage by oxidative stress: Measurement strategies for two genomes. *Current Opinion in Toxicology*, 7, pp.87-94.

González-Hunt, C., Wadhwa, M. and Sanders, L. (2018). DNA damage by oxidative stress: Measurement strategies for two genomes. *Current Opinion in Toxicology*, 7, pp.87-94.

Gonzalez-Meljem, J.M., Apps, J.R., Fraser, H.C. and Martinez-Barbera, J.P. (2018) Paracrine roles of cellular senescence in promoting tumourigenesis. *British Journal of Cancer* 118, pp.1283–1288.

González-Gualda, E., Pàez-Ribes, M., Lozano-Torres, B., Macias, D., Wilson, J., González-López, C., Ou, H., Mirón-Barroso, S., Zhang, Z., Lérida-Viso, A., Blandez, J., Bernardos, A., Sancenón, F., Rovira, M., Fruk, L., Martins, C., Serrano, M., Doherty, G., Martínez-Máñez, R. and Muñoz-Espín, D., (2020). Galacto-conjugation of Navitoclax as an efficient strategy to increase senolytic specificity and reduce platelet toxicity. *Aging Cell*, 19(4).

Gorgoulis, V. and Halazonetis, T. (2010). Oncogene-induced senescence: the bright and dark side of the response. *Current Opinion in Cell Biology*, 22(6), pp.816-827.

Gourgolis, V.G & Konstantinos, E. (2016) Sudan Black B, The specific histochemical stain for Lipofuscin: A Novel method to detect senescent cells. *Methods Molecular Biology.* pp111-119

Green, L., Njoku, V., Mund, J., Case, J., Yoder, M., Murphy, M. and Clauss, M., (2016). Endogenous Transmembrane TNF-Alpha Protects Against Premature Senescence in Endothelial Colony Forming Cells. *Circulation Research*, 118(10), pp.1512-1524.

Gu, X., Boldrup, L., Coates, P., Fahraeus, R., Nylander, E., Loizou, C., Olofsson, K., Norberg-Spaak, L., Gärskog, O. and Nylander, K., (2016). Epigenetic

regulation of OAS2 shows disease-specific DNA methylation profiles at individual CpG sites. *Scientific Reports*, 6(1).

Hahn, H., Kim, K., An, I., Ahn, K. and Han, H., (2017). Protective effects of rosmarinic acid against hydrogen peroxide-induced cellular senescence and the inflammatory response in normal human dermal fibroblasts. *Molecular Medicine Reports*, 16(6), pp.9763-9769.

Harley, C.B., Futcher, A.B., & Greider, C.W. (1990) Telomeres shorten during aging of human fibroblasts. *Nature* 345 pp.458-460

Harman, D. (1992). Free radical theory of aging. *Mutation Research/DNAging*, 275(3-6), pp.257-266.

Harrison, D., Strong, R., Sharp, Z., Nelson, J., Astle, C., Flurkey, K., Nadon, N., Wilkinson, J., Frenkel, K., Carter, C., Pahor, M., Javors, M., Fernandez, E. and Miller, R., (2009). Rapamycin fed late in life extends lifespan in genetically heterogeneous mice. *Nature*, 460(7253), pp.392-395.

Hassona, Y., Cirillo, N., Heesom, K., Parkinson, E. and Prime, S., (2014). Senescent cancer-associated fibroblasts secrete active MMP-2 that promotes keratinocyte dis-cohesion and invasion. *British Journal of Cancer*, 111(6), pp.1230-1237.

Hayflick, L. (1965). The limited in vitro lifetime of human diploid cell strains. *Experimental Cell Research*, 37(3), pp.614-636.

Hayflick, L. and Moorhead, P. (1961). The serial cultivation of human diploid cell strains. *Experimental Cell Research*, 25(3), pp.585-621.

Hernandez-Segura, A., Nehme, J. and Demaria, M. (2018). Hallmarks of Cellular Senescence. *Trends in Cell Biology*, 28(6), pp.436-453.

Herranz, N. and Gil, J., (2018). Mechanisms and functions of cellular senescence. *Journal of Clinical Investigation*, 128(4), pp.1238-1246.

Hewitt, G., Jurk, D., Marques, F., Correia-Melo, C., Hardy, T., Gackowska, A., Anderson, R., Taschuk, M., Mann, J. and Passos, J. (2012). Telomeres are favoured targets of a persistent DNA damage response in ageing and stress-induced senescence. *Nature Communications*, 3(1).

Hewitt, G., von Zglinicki, T. and Passos, J., (2013). Cell Sorting of Young and Senescent Cells. *Methods in Molecular Biology*, pp.31-47.

Hickson, L., Langhi Prata, L., Bobart, S., Evans, T., Giorgadze, N., Hashmi, S., Herrmann, S., Jensen, M., Jia, Q., Jordan, K., Kellogg, T., Khosla, S., Koerber, D., Lagnado, A., Lawson, D., LeBrasseur, N., Lerman, L., McDonald, K., McKenzie, T., Passos, J., Pignolo, R., Pirtskhalava, T., Saadiq, I., Schaefer, K., Textor, S., Victorelli, S., Volkman, T., Xue, A., Wentworth, M., Wissler Gerdes, E., Zhu, Y., Tchkonia, T. and Kirkland, J., (2019). Senolytics decrease senescent cells in humans: Preliminary report from a clinical trial of Dasatinib plus Quercetin in individuals with diabetic kidney disease. *EBioMedicine*, 47, pp.446-456.

Hinkal, G., Gatza, C., Parikh, N. and Donehower, L., (2009). Altered senescence, apoptosis, and DNA damage response in a mutant p53 model of accelerated aging. *Mechanisms of Ageing and Development*, 130(4), pp.262-271.

Hockenbery, D., Oltvai, Z., Yin, X., Milliman, C. and Korsmeyer, S., (1993). Bcl-2 functions in an antioxidant pathway to prevent apoptosis. *Cell*, 75(2), pp.241-251.

Hofmann, J., Zhao, X., De Cecco, M., Peterson, A., Pagliaroli, L., Manivannan, J., Hubbard, G., Ikeno, Y., Zhang, Y., Feng, B., Li, X., Serre, T., Qi, W., Van Remmen, H., Miller, R., Bath, K., de Cabo, R., Xu, H., Neretti, N. and Sedivy, J., (2015). Reduced Expression of MYC Increases Longevity and Enhances Healthspan. *Cell*, 160(3), pp.477-488.

Holbrook, J., Lara-Reyna, S., Jarosz-Griffiths, H. and McDermott, M., (2019). Tumour necrosis factor signalling in health and disease. *F1000Research*, 8, p.111.

Hong, W., Mo, F., Zhang, Z., Huang, M. and Wei, X., (2020). Nicotinamide Mononucleotide: A Promising Molecule for Therapy of Diverse Diseases by Targeting NAD+ Metabolism. *Frontiers in Cell and Developmental Biology*, 8.
Hsu, C., Altschuler, S. and Wu, L., 2019. Patterns of Early p21 Dynamics Determine Proliferation-Senescence Cell Fate after Chemotherapy. *Cell*, 178(2), pp.361-373.

Huang DW, Sherman BT, Lempicki RA. (2009) Bioinformatics enrichment tools: paths toward the comprehensive functional analysis of large gene lists. *Nucleic Acids Res;37(1):1-13.*

Huang DW, Sherman BT, Lempicki RA. (2009) Systematic and integrative analysis of large gene lists using DAVID Bioinformatics Resources. *Nature Protoc;*4(1):44-57

Huang, T. and Rivera-Pérez, J. (2014). Senescence-associated β-galactosidase activity marks the visceral endoderm of mouse embryos but is not indicative of senescence. *genesis*, 52(4), pp.300-308.

Hydbring, P. and Larsson, L., (2010). Cdk2: a key regulator of the senescence control function of Myc. *Aging*, 2(4), pp.244-250.

Imaizumi, N., Monnier, Y., Hegi, M., Mirimanoff, R. and Rüegg, C., (2010). Radiotherapy Suppresses Angiogenesis in Mice through TGF-βRI/ALK5-Dependent Inhibition of Endothelial Cell Sprouting. *PLoS ONE*, 5(6), p.e11084
.
Islam, M., Ali, E., Uddin, S., Shaw, S., Islam, M., Ahmed, M., Chandra Shill, M., Karmakar, U., Yarla, N., Khan, I., Billah, M., Pieczynska, M., Zengin, G., Malainer, C., Nicoletti, F., Gulei, D., Berindan-Neagoe, I., Apostolov, A., Banach, M., Yeung, A., El-Demerdash, A., Xiao, J., Dey, P., Yele, S., Jóźwik, A., Strzałkowska, N., Marchewka, J., Rengasamy, K., Horbańczuk, J., Kamal, M., Mubarak, M., Mishra, S., Shilpi, J. and Atanasov, A., (2018). Phytol: A review of biomedical activities. *Food and Chemical Toxicology*, 121, pp.82-94.

Jackson, S. and Bartek, J. (2009). The DNA-damage response in human biology and disease. *Nature*, 461(7267), pp.1071-1078.

Jamshidi, N. and Cohen, M., (2017). The Clinical Efficacy and Safety of Tulsi in Humans: A Systematic Review of the Literature. *Evidence-Based Complementary and Alternative Medicine*, pp.1-13.

Janeway CA Jr, Travers P, Walport M, et al. (2001) Immunobiology: The Immune System in Health and Disease - The complement system and innate immunity. 5th edition. New York: Garland Science.Available from: https://www.ncbi.nlm.nih.gov/books/NBK27100/

Jeong, S., (2018). Inhibitory effect of phytol on cellular senescence. *Biomedical Dermatology*, 2(1).

Jiang, J., Zhao, W., Tang, Q., Wang, B., Li, X. and Feng, Z., (2019). Over expression of amphiregulin promoted malignant progression in gastric cancer. *Pathology - Research and Practice*, 215(10), p.152576.

Jing, H. and Lee, S., (2014). NF-κB in Cellular Senescence and Cancer Treatment. *Molecules and Cells*, 37(3), pp.189-195.

Jingwen, B., Yaochen, L. and Guojun, Z. (2017). Cell cycle regulation and anticancer drug discovery. *Cancer Biology & Medicine*, 14(4), p.348.

Jose, G., Raghavankutty, M. and Kurup, G., (2019). Attenuation of hydrogenperoxide-induced oxidative damages in L929 fibroblast cells by sulfated polysaccharides isolated from the edible marine algae Padina tetrastromatica. *Journal of Bioactive and Compatible Polymers*, 34(2), pp.150-162.

Justice, J., Nambiar, A., Tchkonia, T., LeBrasseur, N., Pascual, R., Hashmi, S., et al. (2019). Senolytics in idiopathic pulmonary fibrosis: results from a first-in-human, open-label, pilot study. *EBioMedicine* 40, 554–563.

Kaiser, F., Kaufmann, S. and Zerrahn, J., (2004). IIGP, a member of the IFN inducible and microbial defense mediating 47 kDa GTPase family, interacts with the microtubule binding protein hook3. *Journal of Cell Science*, 117(9), pp.1747-1756.

Kale, J., Osterlund, E. and Andrews, D., (2017). BCL-2 family proteins: changing partners in the dance towards death. *Cell Death & Differentiation*, 25(1), pp.65-80.

Kalra, E., (2003). Nutraceutical-definition and introduction. *AAPS PharmSci*, 5(3), pp.27-28.

Kandhaya-Pillai, R., Miro-Mur, F., Alijotas-Reig, J., Tchkonia, T., Kirkland, J. and Schwartz, S., (2017). TNFα-senescence initiates a STAT-dependent positive feedback loop, leading to a sustained interferon signature, DNA damage, and cytokine secretion. *Aging*, 9(11), pp.2411-2435.

Kaur, A., Macip, S. and Stover, C., (2020). An Appraisal on the Value of Using Nutraceutical Based Senolytics and Senostatics in Aging. *Frontiers in Cell and Developmental Biology*, 8.

Khan, M. and Gasser, S., (2016). Generating Primary Fibroblast Cultures from Mouse Ear and Tail Tissues. *Journal of Visualized Experiments*, (107).

Kim, E., Moon, S., Kim, D., Zhang, X. and Kim, J., (2018). CXCL1 induces senescence of cancer-associated fibroblasts via autocrine loops in oral squamous cell carcinoma. *PLOS ONE*, 13(1), p.e0188847.

Kim, H., 2016. Protective Effect of Garlic on Cellular Senescence in UVB-Exposed HaCaT Human Keratinocytes. *Nutrients*, 8(8), p.464.

Kim, K., Kang, K., Seu, Y., Baek, S. and Kim, J., (2009). Interferon-γ induces cellular senescence through p53-dependent DNA damage signaling in human endothelial cells. *Mechanisms of Ageing and Development*, 130(3), pp.179-188.

Kim, S., Park, J., Lee, M., Park, J., Park, S. and Han, J., (2008). Selective COX-2 inhibitors modulate cellular senescence in human dermal fibroblasts in a catalytic activity-independent manner. *Mechanisms of Ageing and Development*, 129(12), pp.706-713.

Kim, Y., Lee, C. and Shin, M., (2019). Downregulation of activin-signaling gene expression in passaged normal human dermal fibroblasts. *Biomedical Reports*. 12(1), pp.17-22.

Kirkwood, T. and Cremer, T. (1982). Cytogerontology since 1881: A reappraisal of August Weismann and a review of modern progress. *Human Genetics*, 60(2), pp.101-121.

Kirschner, K., Rattanavirotkul, N., Quince, M. and Chandra, T., (2020). Functional heterogeneity in senescence. *Biochemical Society Transactions*, 48(3), pp.765-773.

Kiyoshima, T., Enoki, N., Kobayashi, I., Sakai, T., Nagata, K., Wada, H., Fujiwara, H., Ookuma, Y. and Sakai, H., (2012). Oxidative stress caused by a low concentration of hydrogen peroxide induces senescence-like changes in mouse gingival fibroblasts. *International Journal of Molecular Medicine*, 30(5), pp.1007-1012.

Ko, A., Han, S., Choi, C., Cho, H., Lee, M., Kim, S., Song, J., Hong, K., Lee, H., Hewitt, S., Chung, J. and Song, J. (2018). Oncogene-induced senescence mediated by c-Myc requires USP10 dependent deubiquitination and stabilization of p14ARF. *Cell Death & Differentiation*, 25(6), pp.1050-1062.

Krishnamurthy, J., Torrice, C., Ramsey, M., Kovalev, G., Al-Regaiey, K., Su, L. and Sharpless, N., 2004. Ink4a/Arf expression is a biomarker of aging. *Journal of Clinical Investigation*, 114(9), pp.1299-1307.

Krizhanovsky, V., Yon, M., Dickins, R., Hearn, S., Simon, J., Miething, C., Yee, H., Zender, L. and Lowe, S., (2008). Senescence of Activated Stellate Cells Limits Liver Fibrosis. *Cell*, 134(4), pp.657-667.

Kucheryavenko, O., Nelson, G., von Zglinicki, T., Korolchuk, V. and Carroll, B., (2019). The mTORC1-autophagy pathway is a target for senescent cell elimination. *Biogerontology*, 20(3), pp.331-335.

Kuilman, T., Michaloglou, C., Vredeveld, L., Douma, S., van Doorn, R., Desmet, C., Aarden, L., Mooi, W. and Peeper, D., (2008). Oncogene-Induced Senescence

Relayed by an Interleukin-Dependent Inflammatory Network. *Cell*, 133(6), pp.1019-1031.

Laberge, R., Awad, P., Campisi, J. and Desprez, P. (2011). Epithelial-Mesenchymal Transition Induced by Senescent Fibroblasts. *Cancer Microenvironment*, 5(1), pp.39-44.

Lawson, L. and Hunsaker, S., (2018). Allicin Bioavailability and Bioequivalence from Garlic Supplements and Garlic Foods. *Nutrients*, 10(7), p.812.

Lee, B., Han, J., Im, J., Morrone, A., Johung, K., Goodwin, E., Kleijer, W., DiMaio, D. and Hwang, E. (2006). Senescence-associated β-galactosidase is lysosomal β-galactosidase. *Aging Cell*, 5(2), pp.187-195.

Lesina, M., Wörmann, S., Morton, J., Diakopoulos, K., Korneeva, O., Wimmer, M., Einwächter, H., Sperveslage, J., Demir, I., Kehl, T., Saur, D., Sipos, B., Heikenwälder, M., Steiner, J., Wang, T., Sansom, O., Schmid, R. and Algül, H., (2016). RelA regulates CXCL1/CXCR2-dependent oncogene-induced senescence in murine Kras-driven pancreatic carcinogenesis. *Journal of Clinical Investigation*, 126(8), pp.2919-2932.

Li, M., You, L., Xue, J. and Lu, Y., (2018). Ionizing Radiation-Induced Cellular Senescence in Normal, Non-transformed Cells and the Involved DNA Damage Response: A Mini Review. *Frontiers in Pharmacology*, 9.

Li, P., Gan, Y., Xu, Y., Song, L., Wang, L., Ouyang, B., Zhang, C. and Zhou, Q., (2017). The inflammatory cytokine TNF-α promotes the premature senescence of rat nucleus pulposus cells via the PI3K/Akt signaling pathway. *Scientific Reports*, 7(1).

Liesenfeld, O., Parvanova, I., Zerrahn, J., Han, S., Heinrich, F., Muñoz, M., Kaiser, F., Aebischer, T., Buch, T., Waisman, A., Reichmann, G., Utermöhlen, O., von Stebut, E., von Loewenich, F., Bogdan, C., Specht, S., Saeftel, M., Hoerauf, A., Mota, M., Könen-Waisman, S., Kaufmann, S. and Howard, J., (2011). The IFN-γ-Inducible GTPase, Irga6, Protects Mice against Toxoplasma gondii but Not against Plasmodium berghei and Some Other Intracellular Pathogens. *PLoS ONE*, 6(6), p.e20568.

Lin, A., Barradas, M., Stone, J., van Aelst, L., Serrano, M. and Lowe, S., (1998). Premature senescence involving p53 and p16 is activated in response to constitutive MEK/MAPK mitogenic signaling. *Genes & Development*, 12(19), pp.3008-3019.

Lin, I., Chang, J., Hua, K., Huang, W., Hsu, M. and Chen, Y., (2018). Skeletal muscle in aged mice reveals extensive transformation of muscle gene expression. *BMC Genetics*, 19(1).

Lin, X., Liu, Y., Liu, M., Hu, H., Pan, Y., Fan, X., Hu, X. and Zou, W., (2017). Inhibition of Hydrogen Peroxide-Induced Human Umbilical Vein Endothelial Cells Aging by Allicin Depends on Sirtuin1 Activation. *Medical Science Monitor*, 23, pp.563-570.

List, E., Jensen, E., Kowalski, J., Buchman, M., Berryman, D. and Kopchick, J., (2016). Diet-induced weight loss is sufficient to reduce senescent cell number in white adipose tissue of weight-cycled mice. *Nutrition and Healthy Aging*, 4(1), pp.95-99.

Liu, Y., Cai, Y., Liu, L., Wu, Y. and Xiong, X., (2018). Crucial biological functions of CCL7 in cancer. *PeerJ*, 6, p.e4928.

Liu, Y., You, M., Shen, J., Xu, Y., Li, L., Wang, D. and Yang, Y., (2019). Allicin Reversed the Process of Frailty in Aging Male Fischer 344 Rats With Osteoporosis. *The Journals of Gerontology: Series A*, 75(5), pp.821-825.

López-Otín, C., Blasco, M., Partridge, L., Serrano, M. and Kroemer, G. (2013). The Hallmarks of Aging. *Cell*, 153(6), pp.1194-1217.

Mah, L., El-Osta, A. and Karagiannis, T. (2010). γH2AX as a molecular marker of aging and disease. *Epigenetics*, 5(2), pp.129-136.

Makpol, S., Abdul Rahim, N., Kien Hui, C. and Wan Ngah, W., (2012). Inhibition of Mitochondrial CytochromecRelease and Suppression of Caspases by Gamma-Tocotrienol Prevent Apoptosis and Delay Aging in Stress-Induced Premature Senescence of Skin Fibroblasts. *Oxidative Medicine and Cellular Longevity*, 2012, pp.1-13.

Manaharan, T., Thirugnanasampandan, R., Jayakumar, R., Ramya, G., Ramnath, G. and Kanthimathi, M., 2014. Antimetastatic and Anti-Inflammatory Potentials of Essential Oil from Edible Ocimum sanctum Leaves. *The Scientific World Journal*, 2014, pp.1-5.

Mao, Z., Ke, Z., Gorbunova, V., & Seluanov, A. (2012). Replicatively senescent cells are arrested in G1 and G2 phases. *Aging*, *4*(6), 431–435.

Marechal, A. and Zou, L., (2013). DNA Damage Sensing by the ATM and ATR Kinases. *Cold Spring Harbor Perspectives in Biology*, 5(9), pp.a012716-a012716.

Martin-Montalvo, A., Mercken, E., Mitchell, S., Palacios, H., Mote, P., Scheibye-Knudsen, M., Gomes, A., Ward, T., Minor, R., Blouin, M., Schwab, M., Pollak, M., Zhang, Y., Yu, Y., Becker, K., Bohr, V., Ingram, D., Sinclair, D., Wolf, N., Spindler, S., Bernier, M. and de Cabo, R., (2013). Metformin improves healthspan and lifespan in mice. *Nature Communications*, 4(1).

Medeiros Tavares Marques, J., Cornélio, D., Nogueira Silbiger, V., Ducati Luchessi, A., de Souza, S. and Batistuzzo de Medeiros, S., (2017). Identification of new genes associated to senescent and tumorigenic phenotypes in mesenchymal stem cells. *Scientific Reports*, 7(1).

Meyer, P., Maity, P., Burkovski, A., Schwab, J., Müssel, C., Singh, K., Ferreira, F., Krug, L., Maier, H., Wlaschek, M., Wirth, T., Kestler, H. and Scharffetter-Kochanek, K., (2017). A model of the onset of the senescence associated secretory phenotype after DNA damage induced senescence. *PLOS Computational Biology*, 13(12), p.e1005741.
Mijit, M., Caracciolo, V., Melillo, A., Amicarelli, F. and Giordano, A., (2020). Role of p53 in the Regulation of Cellular Senescence. *Biomolecules*, 10(3), p.420.

Mikuła-Pietrasik, J., Niklas, A., Uruski, P., Tykarski, A. and Książek, K., (2019). Mechanisms and significance of therapy-induced and spontaneous senescence of cancer cells. *Cellular and Molecular Life Sciences*, 77(2), pp.213-229.

Mirzayans, R. and Murray, D., (2020). Do TUNEL and Other Apoptosis Assays Detect Cell Death in Preclinical Studies?. *International Journal of Molecular Sciences*, 21(23), p.9090.

Mirzayans, R., Andrais, B. and Murray, D., (2017). Impact of Premature Senescence on Radiosensitivity Measured by High Throughput Cell-Based Assays. *International Journal of Molecular Sciences*, 18(7), p.1460.

Mirzayans, R., Andrais, B., Hansen, G. and Murray, D., (2012). Role ofp16INK4Ain Replicative Senescence and DNA Damage-Induced Premature Senescence in p53-Deficient Human Cells. *Biochemistry Research International*, 2012, pp.1-8.

Mohan Kumar, K., Harsha, M., Kagathur, S. and Amberkar, V., (2020). Effect of Ocimum sanctum extract on leukemic cell lines:A preliminary in-vitro study. *Journal of Oral and Maxillofacial Pathology*, 24(1), p.93.

Moiseeva, O., Deschênes-Simard, X., St-Germain, E., Igelmann, S., Huot, G., Cadar, A., et al. (2013). Metformin inhibits the senescence-associated secretory phenotype by interfering with IKK/NF-κB activation. *Aging Cell* 12, 489–498.

Mombach, J., Bugs, C. and Chaouiya, C., (2014). Modelling the onset of senescence at the G1/S cell cycle checkpoint. *BMC Genomics*, 15(Suppl 7).

Moon, K.C, Lee, H.S, Son, S.T., Lee, J.S., Dhong, E.S., Jeong, S.H., & Han, S.K. (2019). Effects of Granulocyte Macrophage colony stimulating factor on neuronal senescence in UV irradiated skin. *Journal of Craniofacial Surgery* 30(3), pp.930-935.

Morpheus, https://software.broadinstitute.org/morpheus

Mullani, N., Porozhan, Y., Costallat, M., Batsché, E., Goodhardt, M., Cenci, G., Mann, C. and Muchardt, C., (2019). Reduced RNA turnover as a driver of cellular senescence. *Life Science Alliance*, 4(3)

Muraki, K., Nyhan, K., Han, L. and Murnane, J. (2012). Mechanisms of telomere loss and their consequences for chromosome instability. *Frontiers in Oncology*, 2.

Nadeem, M., Imran, M., Aslam Gondal, T., Imran, A., Shahbaz, M., Muhammad Amir, R., Wasim Sajid, M., Batool Qaisrani, T., Atif, M., Hussain, G., Salehi, B., Adrian Ostrander, E., Martorell, M., Sharifi-Rad, J., C. Cho, W. and Martins, N., (2019). Therapeutic Potential of Rosmarinic Acid: A Comprehensive Review. *Applied Sciences*, 9(15), p.3139.

Nakamoto, M., Kunimura, K., Suzuki, J. and Kodera, Y., (2019). Antimicrobial properties of hydrophobic compounds in garlic: Allicin, vinyldithiin, ajoene and diallyl polysulfides (Review). *Experimental and Therapeutic Medicine*. 19(2), pp.1550-1553.

Naseri, M., Mahdavi, M., Davoodi, J., Tackallou, S., Goudarzvand, M. and Neishabouri, S., (2015). Up regulation of Bax and down regulation of Bcl2 during 3-NC mediated apoptosis in human cancer cells. *Cancer Cell International*, 15(1).

Neurohr, G., Terry, R., Lengefeld, J., Bonney, M., Brittingham, G., Moretto, F., Miettinen, T., Vaites, L., Soares, L., Paulo, J., Harper, J., Buratowski, S., Manalis, S., van Werven, F., Holt, L. and Amon, A., (2019). Excessive Cell Growth Causes Cytoplasm Dilution And Contributes to Senescence. *Cell*, 176(5), pp.1083-1097.e18.

Nishiyama, N., Moriguchi, T. and Saito, H., (1997). Beneficial effects of aged garlic extract on learning and memory impairment in the senescence-accelerated mouse. *Experimental Gerontology*, 32(1-2), pp.149-160.

Noren Hooten, N. and Evans, M., (2017). Techniques to Induce and Quantify Cellular Senescence. *Journal of Visualized Experiments*, (123).

Ogrodnik, M., Evans, S., Fielder, E., Victorelli, S., Kruger, P., Salmonowicz, H., Weigand, B., Patel, A., Pirtskhalava, T., Inman, C., Johnson, K., Dickinson, S., Rocha, A., Schafer, M., Zhu, Y., Allison, D., Zglinicki, T., LeBrasseur, N., Tchkonia, T., Neretti, N., Passos, J., Kirkland, J. and Jurk, D., (2021). Whole-body senescent cell clearance alleviates age-related brain inflammation and cognitive impairment in mice. *Aging Cell*, 20(2).

Ohgo, S., Hasegawa, S., Hasebe, Y., Mizutani, H., Nakata, S. and Akamatsu, H., (2015). Senescent dermal fibroblasts enhance stem cell migration through CCL2/CCR2 axis. *Experimental Dermatology*, 24(7), pp.552-554.

Ohgo, S., Hasegawa, S., Hasebe, Y., Mizutani, H., Nakata, S. and Akamatsu, H., (2015). Senescent dermal fibroblasts enhance stem cell migration through CCL2/CCR2 axis. *Experimental Dermatology*, 24(7), pp.552-554.

Ortiz-Montero, P., Londoño-Vallejo, A. and Vernot, J., (2017). Senescence-associated IL-6 and IL-8 cytokines induce a self- and cross-reinforced senescence/inflammatory milieu strengthening tumorigenic capabilities in the MCF-7 breast cancer cell line. *Cell Communication and Signaling*, 15(1):17.

Osuala, K. and Sloane, B., 2021. *Many Roles of CCL20: Emphasis on Breast Cancer*. [online] PubMed. Available at: <https://pubmed.ncbi.nlm.nih.gov/27631019/> [Accessed 24 February 2021].

Pan, H., Wang, X., Huang, W., Dai, Y., Yang, M., Liang, H., Wu, X., Zhang, L., Huang, W., Yuan, L., Wu, Y., Wang, Y., Liao, L., Huang, J. and Guan, J., (2020). Interferon-Induced Protein 44 Correlated With Immune Infiltration Serves as a Potential Prognostic Indicator in Head and Neck Squamous Cell Carcinoma. *Frontiers in Oncology*, 10.

Panchal P, Parvez N (2019) Phytochemical analysis of medicinal herb (*ocimum sanctum*). Int J Nanomater Nanotechnol Nanomed 5(2): 008-011.

Pandey R, Gupta S, Shukla V, Tandon S, Shukla V. (2013) Antiaging, antistress and ROS scavenging activity of crude extract of Ocimum sanctum (L.) in Caenorhabditis elegans (Maupas, 1900). *Indian J Exp Biol*. Jul;51(7), pp515-521.

Papismadov, N., Gal, H. and Krizhanovsky, V., (2017). The anti-aging promise of p21. *Cell Cycle*, 16(21), pp.1997-1998.

Parasuraman, S., Balamurugan, S., Christapher, P., Petchi, R., Yeng, W., Sujithra, J. and Vijaya, C., (2015). Evaluation of Antidiabetic and Antihyperlipidemic Effects of Hydroalcoholic Extract of Leaves of Ocimum tenuiflorum (Lamiaceae) and Prediction of Biological Activity of its Phytoconstituents. *Pharmacognosy Research*, 7(2), p.156.

Park, H. and Kim, S., (2021). Endothelial cell senescence: A machine learning-based meta-analysis of transcriptomic studies. *Ageing Research Reviews*, 65, p.101213.

Park, J., Lee, N., Lim, H., Ji, S., Kim, Y., Jang, W., Kim, D., Kang, S., Yun, J., Ha, J., Kim, H., Lee, D., Baek, S. and Kwon, S., (2020). Pharmacological inhibition of mTOR attenuates replicative cell senescence and improves cellular function via regulating the STAT3-PIM1 axis in human cardiac progenitor cells. *Experimental & Molecular Medicine*, 52(4), pp.615-628.

Park, J.H., Lee, N.K., Lim, H.J. *et al.* (2020).Pharmacological inhibition of mTOR attenuates replicative cell senescence and improves cellular function via regulating the STAT3-PIM1 axis in human cardiac progenitor cells. *Exp Mol Med* 52**,** pp.615–628.

Park, Y. M., Anderson, R. L., Spitz, D. R., & Hahn, G. M. (1992). Hypoxia and resistance to hydrogen peroxide confer resistance to tumor necrosis factor in murine L929 cells. *Radiation research*, *131*(2), pp.162–168.

Parry, A. and Narita, M. (2016). Old cells, new tricks: chromatin structure in senescence. *Mammalian Genome*, 27(7-8), pp.320-331.

Pawelec, G. (2018). Age and immunity: What is "immunosenescence"?. *Experimental Gerontology*, 105, pp.4-9.

Pidugu, V., Pidugu, H., Wu, M., Liu, C. and Lee, T., (2019). Emerging Functions of Human IFIT Proteins in Cancer. *Frontiers in Molecular Biosciences*, 6.

Pizzino, G., Irrera, N., Cucinotta, M., Pallio, G., Mannino, F., Arcoraci, V., Squadrito, F., Altavilla, D. and Bitto, A., (2017). Oxidative Stress: Harms and Benefits for Human Health. *Oxidative Medicine and Cellular Longevity*, pp.1-13.
Plesca, D., Mazumder, S. and Almasan, A., 2008. Chapter 6 DNA Damage Response and Apoptosis. *Methods in Enzymology*, pp.107-122.

Pommer, M., Kuphal, S. and Bosserhoff, A., (2021). Amphiregulin Regulates Melanocytic Senescence. *Cells*, 10(2), p.326.

Ponnusam, Y., Louis, T., Madhavachandran, V., Kumar, S., Thoprani, N., Hamblin, M. R., & Lakshmanan, S. (2015). Antioxidant Activity of The Ancient Herb, Holy Basil in CCl_4-Induced Liver Injury in Rats. *Ayurvedic*, *2*(2), 34–38.

Prasad, K., Laxdal, V., Yu, M. and Raney, B., (1995). Antioxidant activity of allicin, an active principle in garlic. *Molecular and Cellular Biochemistry*, 148(2), pp.183-189.

Purcell, M., Kruger, A. and Tainsky, M., (2014). Gene expression profiling of replicative and induced senescence. *Cell Cycle*, 13(24), pp.3927-3937

Puzianowska-Kuźnicka, M., Owczarz, M., Wieczorowska-Tobis, K., Nadrowski, P., Chudek, J., Slusarczyk, P., Skalska, A., Jonas, M., Franek, E. and Mossakowska, M., (2016). Interleukin-6 and C-reactive protein, successful aging, and mortality: the PolSenior study. *Immunity & Ageing*, 13(1).

Qiu, X., Guo, H., Yang, J., Ji, Y., Wu, C. and Chen, X., (2018). Down-regulation of guanylate binding protein 1 causes mitochondrial dysfunction and cellular senescence in macrophages. *Scientific Reports*, 8(1).

Rahman, K., (2003). Garlic and aging: new insights into an old remedy. *Ageing Research Reviews*, 2(1), pp.39-56.

Rashid, K., Sundar, I., Gerloff, J., Li, D. and Rahman, I., (2018). Lung cellular senescence is independent of aging in a mouse model of COPD/emphysema. *Scientific Reports*, 8(1).

Rhinn, M., Ritschka, B. and Keyes, W., (2019). Cellular senescence in development, regeneration and disease. *Development*, 146(20).

Ribeiro, F., de Oliveira, M., Singh, S., Sakthivel, T., Neal, C., Seal, S., Ueda-Nakamura, T., Lautenschlager, S. and Nakamura, C., (2020). Ceria Nanoparticles Decrease UVA-Induced Fibroblast Death Through Cell Redox Regulation Leading to Cell Survival, Migration and Proliferation. *Frontiers in Bioengineering and Biotechnology*, 8.

Ricciotti, E. and FitzGerald, G., (2011). Prostaglandins and Inflammation. *Arteriosclerosis, Thrombosis, and Vascular Biology*, 31(5), pp.986-1000.

Riss T, Niles A, Moravec R, Karassina, N & Vidugiriene, J. (2004). The Assay Guidance Manual – Cytotoxicity Assays: In vitro Methods to measure Dead cells. Available from: https://www.ncbi.nlm.nih.gov/books/NBK540958/

Rivard, A., Andres, V. and Principe, N., (2000). Age-dependent increase in c-fos activity and cyclin A expression in vascular smooth muscle cells A potential link between aging, smooth muscle cell proliferation and atherosclerosis. *Cardiovascular Research*, 45(4), pp.1026-1034.

Rodier, F. and Campisi, J. (2011). Four faces of cellular senescence. *The Journal of Cell Biology*, 192(4), pp.547-556.

Rodier, F., Coppé, J., Patil, C., Hoeijmakers, W., Muñoz, D., Raza, S., Freund, A., Campeau, E., Davalos, A. and Campisi, J., (2009). Persistent DNA damage signalling triggers senescence-associated inflammatory cytokine secretion. *Nature Cell Biology*, 11(8), pp.973-979.

Rogińska, D., Kawa, M., Pius-Sadowska, E., Lejkowska, R., Łuczkowska, K., Wiszniewska, B., Kaarniranta, K., Paterno, J., Schmidt, C., Machaliński, B. and Machalińska, A., (2017). Depletion of the Third Complement Component Ameliorates Age-Dependent Oxidative Stress and Positively Modulates Autophagic Activity in Aged Retinas in a Mouse Model. *Oxidative Medicine and Cellular Longevity*, 2017, pp.1-17.

Rolt, A., Nair, A. and Cox, L., (2019). Optimisation of a screening platform for determining IL-6 inflammatory signalling in the senescence-associated secretory phenotype (SASP). *Biogerontology*, 20(3), pp.359-371.

Rosas-González, V., Téllez-Bañuelos, M., Hernández-Flores, G., Bravo-Cuellar, A., Aguilar-Lemarroy, A., Jave-Suárez, L., Haramati, J., Solorzano-Ibarra, F. and Ortiz-Lazareno, P., (2020). Differential effects of alliin and allicin on apoptosis and senescence in luminal A and triple-negative breast cancer: Caspase, ΔΨm, and pro-apoptotic gene involvement. *Fundamental & Clinical Pharmacology*, 34(6), pp.671-686.

Rose-John, S., Winthrop, K. and Calabrese, L., (2017). The role of IL-6 in host defence against infections: immunobiology and clinical implications. *Nature Reviews Rheumatology*, 13(7), pp.399-409.

Ruhland, M., Coussens, L. and Stewart, S. (2016). Senescence and cancer: An evolving inflammatory paradox. *Biochimica et Biophysica Acta (BBA) - Reviews on Cancer*, 1865(1), pp.14-22.

Salam, N., Rane, S., Das, R., Faulkner, M., Gund, R., Kandpal, U., Lewis, V., Mattoo, H., Prabhu, S., Ranganathan, V., Durdik, J., George, A., Rath, S. & Bal, V. (2013) T cell ageing: effects of age on development, survival & function. *Indian J Med Res*. 138(5) pp.595-608.

Salic, A. and Mitchison, T., (2008). A chemical method for fast and sensitive detection of DNA synthesis in vivo. *Proceedings of the National Academy of Sciences*, 105(7), pp.2415-2420.

Salminen, A., Kauppinen, A. & Kaarniranta, K. (2012). Emerging role of NF-KB signalling in the induction of senescence-associated secretory phenotype (SASP). *Cellular Signalling.* 24(4). pp835-845.

Salmon, T., Evert, B., Song, B. and Doetsch, P. (2004). Biological consequences of oxidative stress-induced DNA damage in Saccharomyces cerevisiae. *Nucleic Acids Research*, 32(12), pp.3712-3723.

Samaraweera, L., Adomako, A., Rodriguez-Gabin, A., and McDaid, H. (2017). A novel indication for panobinostat as a senolytic drug in NSCLC and HNSCC. *Sci. Rep.* 7:1900.

Santos, C., Salvadori, M., Mota, V., Costa, L., de Almeida, A., de Oliveira, G., Costa, J., de Sousa, D., de Freitas, R. and de Almeida, R., (2013). Antinociceptive and Antioxidant Activities of Phytol In Vivo and In Vitro Models. *Neuroscience Journal*, 2013, pp.1-9.

Sathya, S., Shanmuganathan, B., Saranya, S., Vaidevi, S., Ruckmani, K. and Pandima Devi, K., (2017). Phytol-loaded PLGA nanoparticle as a modulator of Alzheimer's toxic Aβ peptide aggregation and fibrillation associated with impaired neuronal cell function. *Artificial Cells, Nanomedicine, and Biotechnology*, pp.1-12.

Sawant, K., Poluri, K., Dutta, A., Sepuru, K., Troshkina, A., Garofalo, R. and Rajarathnam, K., (2016). Chemokine CXCL1 mediated neutrophil recruitment: Role of glycosaminoglycan interactions. *Scientific Reports*, 6(1).

Schäfer, G. and Kaschula, C., (2014). The Immunomodulation and Anti-Inflammatory Effects of Garlic Organosulfur Compounds in Cancer Chemoprevention. *Anti-Cancer Agents in Medicinal Chemistry*, 14(2), pp.233-240.

Schwab, N., Grenier, K. and Hazrati, L., (2019). DNA repair deficiency and senescence in concussed professional athletes involved in contact sports. *Acta Neuropathologica Communications*, 7(1).

Serrano, M & Munoz-Espin, D. (2014) Cellular Senescence: from physiology to pathology. *Nature Reviews Molecular Cell Biology* volume 15, pages 482–496

Serrano, M., Lin, A., McCurrach, M., Beach, D. and Lowe, S. (1997). Oncogenic ras Provokes Premature Cell Senescence Associated with Accumulation of p53 and p16INK4a. *Cell*, 88(5), pp.593-602.

Seshadri, T. and Campisi, J., (1990). Repression of c-fos transcription and an altered genetic program in senescent human fibroblasts. *Science*, 247(4939), pp.205-209.

Severino, J., Allen, R., Balin, S., Balin, A. and Cristofalo, V., (2000). Is β-Galactosidase Staining a Marker of Senescence in Vitro and in Vivo?. *Experimental Cell Research*, 257(1), pp.162-171.

Shammas, M. (2011). Telomeres, lifestyle, cancer, and aging. *Current Opinion in Clinical Nutrition and Metabolic Care*, 14(1), pp.28-34.

Sheikh, F., Lyon, R. and Chen, J., 2015. Functions of myosin light chain-2 (MYL2) in cardiac muscle and disease. *Gene*, 569(1), pp.14-20.

Shi, Q., Colodner, K., Matousek, S., Merry, K., Hong, S., Kenison, J., Frost, J., Le, K., Li, S., Dodart, J., Caldarone, B., Stevens, B. and Lemere, C., (2015). Complement C3-Deficient Mice Fail to Display Age-Related Hippocampal Decline. *Journal of Neuroscience*, 35(38), pp.13029-13042.

Shimi, T., Butin-Israeli, V., Adam, S., Hamanaka, R., Goldman, A., Lucas, C., Shumaker, D., Kosak, S., Chandel, N. and Goldman, R., (2011). The role of nuclear lamin B1 in cell proliferation and senescence. *Genes & Development*, 25(24), pp.2579-2593.

Short, S., Fielder, E., Miwa, S., and von Zglinicki, T. (2019). Senolytics and senostatics as adjuvant tumour therapy. *EBioMedicine* 41, 683–692

Sidler, C., Kovalchuk, O. and Kovalchuk, I. (2017). Epigenetic Regulation of Cellular Senescence and Aging. *Frontiers in Genetics*, 8.

Silva, R., Sousa, F., Damasceno, S., Carvalho, N., Silva, V., Oliveira, F., Sousa, D., Aragão, K., Barbosa, A., Freitas, R. and Medeiros, J., (2013). Phytol, a diterpene alcohol, inhibits the inflammatory response by reducing cytokine production and oxidative stress. *Fundamental & Clinical Pharmacology*, 28(4), pp.455-464.

Singh, D. and Chaudhuri, P., (2018). A review on phytochemical and pharmacological properties of Holy basil (Ocimum sanctum L.). *Industrial Crops and Products*, 118, pp.367-382.

Soares-Silva, M., Diniz, F., Gomes, G. and Bahia, D., (2016). The Mitogen-Activated Protein Kinase (MAPK) Pathway: Role in Immune Evasion by Trypanosomatids. *Frontiers in Microbiology*, 7.

Sodagam, L., Lewinska, A., Kwasniewicz, E., Kokhanovska, S., Wnuk, M., Siems, K. and Rattan, S., (2019). Phytochemicals Rosmarinic Acid, Ampelopsin, and Amorfrutin-A Can Modulate Age-Related Phenotype of Serially Passaged Human Skin Fibroblasts in vitro. *Frontiers in Genetics*, 10.

Song, Y., Shen, H., Schenten, D., Shan, P., Lee, P. and Goldstein, D., (2012). Aging Enhances the Basal Production of IL-6 and CCL2 in Vascular Smooth Muscle Cells. *Arteriosclerosis, Thrombosis, and Vascular Biology*, 32(1), pp.103-109.

Stein, G., Drullinger, L., Soulard, A. and Dulić, V. (1999). Differential Roles for Cyclin-Dependent Kinase Inhibitors p21 and p16 in the Mechanisms of Senescence and Differentiation in Human Fibroblasts. *Molecular and Cellular Biology*, 19(3), pp.2109-2117.

Stewart, S.A., Ren, Q. & Faget, D.V. (2019) Unmasking senescence: context-dependent effects of SASP in cancer. *Nature Reviews Cancer* 19. pp439-453.

Storer, M., Mas, A., Robert-Monero, A., Pecoraro, M., Ortells, M.C., Giacomo, V., Yosef, R., Pilpel, N., Krizhanovsky, V., Sharpe, J., & Keyes, W.M. (2013). Senescence is a developmemtal mechanism that contributes to embryonic growth and patterning. *Cell.* 155, pp..1119-1130.

Studencka, M. and Schaber, J., (2017). Senoptosis: non-lethal DNA cleavage as a route to deep senescence. *Oncotarget*, 8(19), pp.30656-30671.

Subramanian, M., Chintalwar, G. and Chattopadhyay, S., (2005). Antioxidant and radioprotective properties of anOcimum sanctumpolysaccharide. *Redox Report*, 10(5), pp.257-264.

Sun, G., Zhang, S., Xie, Y., Zhang, Z. and Zhao, W., (2015). Gallic acid as a selective anticancer agent that induces apoptosis in SMMC-7721 human hepatocellular carcinoma cells. *Oncology Letters*, 11(1), pp.150-158.

Tang, H., Geng, A., Zhang, T, wang, C, Jiang., Y & Mao, Z. (2019). Single senescent cell sequencing reveals heterogeneity in senescent cells induced by telomere erosion. *Protein Cell* 10, pp.370–375

Tasdemir, N. and Lowe, S. (2013). Senescent cells spread the word: non-cell autonomous propagation of cellular senescence. *The EMBO Journal*, 32(14), pp.1975-1976.

Teo, Y., Rattanavirotkul, N., Olova, N., Salzano, A., Quintanilla, A., Tarrats, N., Kiourtis, C., Müller, M., Green, A., Adams, P., Acosta, J., Bird, T., Kirschner, K., Neretti, N. and Chandra, T., (2019). Notch Signaling Mediates Secondary Senescence. *Cell Reports*, 27(4), pp.997-1007.

Terman, A. and Brunk, U. (2004). Lipofuscin. *The International Journal of Biochemistry & Cell Biology*, 36(8), pp.1400-1404.

Terzi, M., Izmirli, M. and Gogebakan, B. (2016). The cell fate: senescence or quiescence. *Molecular Biology Reports*, 43(11), pp.1213-1220.

Tombor, B., Rundell, K. and Oltvai, Z., (2003). Bcl-2 promotes premature senescence induced by oncogenic Ras. *Biochemical and Biophysical Research Communications*, 303(3), pp.800-807.

Tominaga, K. and Suzuki, H., (2019). TGF-β Signaling in Cellular Senescence and Aging-Related Pathology. *International Journal of Molecular Sciences*, 20(20), pp.5002.

Toussaint, O., Royer, V., Salmon, M. and Remacle, J., (2002). Stress-induced premature senescence and tissue ageing. *Biochemical Pharmacology*, 64(5-6), pp.1007-1009.

Tsai, W., Chang, H., Yin, H., Huang, M., Agrawal, D. and Wen, H., (2020). The protective ability and cellular mechanism of Koelreuteria henryi Dummer flower extract against hydrogen peroxide-induced cellular oxidative damage. *Electronic Journal of Biotechnology*, 47, pp.89-99.

Tsai, W., Li, W., Yin, H., Yu, M. and Wen, H., (2012). Constructing liposomal nanovesicles of ginseng extract against hydrogen peroxide-induced oxidative damage to L929 cells. *Food Chemistry*, 132(2), pp.744-751.
Tzifi, F., Economopoulou, C., Gourgiotis, D., Ardavanis, A., Papageorgiou, S. and Scorilas, A., (2012). The Role of BCL2 Family of Apoptosis Regulator Proteins in Acute and Chronic Leukemias. *Advances in Hematology*, 2012, pp.1-15.

Uniprot.org. (2020). *Mmp2 - 72 Kda Type IV Collagenase Precursor - Mus Musculus (Mouse) - Mmp2 Gene & Protein*. [online] Available at: <https://www.uniprot.org/uniprot/P33434#P33434-2>

Valentine, M., Link, P., Herbert, J., Kamga Gninzeko, F., Schneck, M., Shankar, K., Nkwocha, J., Reynolds, A. and Heise, R., (2018). Inflammation and Monocyte Recruitment Due to Aging and Mechanical Stretch in Alveolar Epithelium are Inhibited by the Molecular Chaperone 4-Phenylbutyrate. *Cellular and Molecular Bioengineering*, 11(6), pp.495-508.

van Deursen, J. (2014). The role of senescent cells in ageing. *Nature*, 509(7501), pp.439-446.

Varela, E. and Blasco, M. (2010). 2009 Nobel Prize in Physiology or Medicine: telomeres and telomerase. *Oncogene*, 29(11), pp.1561-1565.

Vassilieva, I., Kosheverova, V., Vitte, M., Kamentseva, R., Shatrova, A., Tsupkina, N., Skvortsova, E., Borodkina, A., Tolkunova, E., Nikolsky, N. and Burova, E., (2020). Paracrine senescence of human endometrial mesenchymal stem cells: a role for the insulin-like growth factor binding protein 3. *Aging*, 12(2), pp.1987-2004.

Velazquez, F., Caputto, B. and Boussin, F., (2015). C-Fos importance for brain development. *Aging*, 7(12), pp.1028-1029.

von Kobbe, C., 2019. Targeting senescent cells: approaches, opportunities, challenges. *Aging*, 11(24), pp.12844-12861.

Wallis, R., Mizen, H. and Bishop, C., (2020). The bright and dark side of extracellular vesicles in the senescence-associated secretory phenotype. *Mechanisms of Ageing and Development*, 189, pp.111263.

Wang, D., Liu, Y., Zhang, R., Zhang, F., Sui, W., Chen, L., Zheng, R., Chen, X., Wen, F., Ouyang, H. and Ji, J., (2016). Apoptotic transition of senescent cells accompanied with mitochondrial hyper-function. *Oncotarget*, 7(19), pp.28286-28300.

Wang, F., Liu, Q., Wang, L., Zhang, Q. and Hua, Z., (2011). The Molecular Mechanism of Rosmarinic Acid Extending the Lifespan of Caenorhabditis elegans. *Applied Mechanics and Materials*, 140, pp.469-472.

Wang, R., Yu, Z., Sunchu, B., Shoaf, J., Dang, I., Zhao, S., et al. (2017). Rapamycin inhibits the secretory phenotype of senescent cells by a Nrf2-independent mechanism. *Aging Cell* 16, pp.564–574.

Wang, Z., Wei, D. and Xiao, H., (2013). Methods of Cellular Senescence Induction Using Oxidative Stress. *Methods in Molecular Biology*, pp.135-144.

Wiley, C. and Campisi, J. (2016). From Ancient Pathways to Aging Cells—Connecting Metabolism and Cellular Senescence. *Cell Metabolism*, 23(6), pp.1013-1021.

Wiley, C., Velarde, M., Lecot, P., Liu, S., Sarnoski, E., Freund, A., Shirakawa, K., Lim, H., Davis, S., Ramanathan, A., Gerencser, A., Verdin, E. and Campisi, J. (2016). Mitochondrial Dysfunction Induces Senescence with a Distinct Secretory Phenotype. *Cell Metabolism*, 23(2), pp.303-314.

Williams, C., Mann, M. and DuBois, R., (1999). The role of cyclooxygenases in inflammation, cancer, and development. *Oncogene*, 18(55), pp.7908-7916.

Wilson, V. and Jones, P. (1983). DNA methylation decreases in aging but not in immortal cells. *Science*, 220(4601), pp.1055-1057.

Winkelstein, J., (1973). Opsonins: Their function, identity, and clinical significance. *The Journal of Pediatrics*, 82(5), pp.747-753.

Witowski, J.A. (1980) Dr Carrel's Immortal Cells. *Medical History*, 24 pp.129-142 Available online: https://www.ncbi.nlm.nih.gov/pmc/articles/PMC1082700/pdf/medhist00095-0007.pdf

Wu, X., Lin, L., Cui, J., Chen, Y., Yang, L. and Wan, J., (2020). Complement C3 deficiency ameliorates aging related changes in the kidney. *Life Sciences*, 260, pp.118370.

Xiang, M., Mo, L., Zhan, Y., Wen, H., Zhou, H. and Miao, W., (2019). P38-Mediated Cellular Senescence in Conjunctivochalasis Fibroblasts. *Investigative Opthalmology & Visual Science*, 60(14), pp.4643.

Xu, M., Pirtskhalava, T., Farr, J., Weigand, B., Palmer, A., Weivoda, M., Inman, C., Ogrodnik, M., Hachfeld, C., Fraser, D., Onken, J., Johnson, K., Verzosa, G., Langhi, L., Weigl, M., Giorgadze, N., LeBrasseur, N., Miller, J., Jurk, D., Singh, R., Allison, D., Ejima, K., Hubbard, G., Ikeno, Y., Cubro, H., Garovic, V., Hou, X., Weroha, S., Robbins, P., Niedernhofer, L., Khosla, S., Tchkonia, T. and Kirkland, J., (2018). Senolytics improve physical function and increase lifespan in old age. *Nature Medicine*, 24(8), pp.1246-1256.

Xu, Q., Long, Q., Zhu, D., Fu, D., Zhang, B., Han, L., Qian, M., Guo, J., Xu, J., Cao, L., Chin, Y., Coppé, J., Lam, E., Campisi, J. and Sun, Y., (2019). Targeting amphiregulin (AREG) derived from senescent stromal cells diminishes cancer resistance and averts programmed cell death 1 ligand (PD-L1)-mediated immunosuppression. *Aging Cell*, 18(6).

Yamagami, M., Otsuka, M., Kishikawa, T., Sekiba, K., Seimiya, T., Tanaka, E., Suzuki, T., Ishibashi, R., Ohno, M. and Koike, K., (2018). ISGF3 with reduced phosphorylation is associated with constitutive expression of interferon-induced genes in aging cells. *npj Aging and Mechanisms of Disease*, 4(1).

Yamane, M., Sato, S., Shimizu, E., Shibata, S., Hayano, M., Yaguchi, T., Kamijuku, H., Ogawa, M., Suzuki, T., Mukai, S., Shimmura, S., Okano, H., Takeuchi, T., Kawakami, Y., Ogawa, Y. and Tsubota, K., (2020). Senescence-associated secretory phenotype promotes chronic ocular graft-vs-host disease in mice and humans. *The FASEB Journal*, 34(8), pp.10778-10800.

Yamani, H., Pang, E., Mantri, N. and Deighton, M., (2016). Antimicrobial Activity of Tulsi (Ocimum tenuiflorum) Essential Oil and Their Major Constituents against Three Species of Bacteria. *Frontiers in Microbiology*, 7.

Yang, N. and Hu, M., (2005). The limitations and validities of senescence associated-β-galactosidase activity as an aging marker for human foreskin fibroblast Hs68 cells. *Experimental Gerontology*, 40(10), pp.813-819.

Yang, Z., Du, J., Zhu, J., Chen, S., Yu, L., Deng, X., Zhang, X., Sheng, H., Yang, L., Lu, X., Lin, D., Yin, B. and Lin, J., (2020). Allicin Inhibits Proliferation by Decreasing IL-6 and IFN-β in HCMV-Infected Glioma Cells. *Cancer Management and Research*, Volume 12, pp.7305-7317.

Yao, G. (2014). Modelling mammalian cellular quiescence. *Interface Focus*, 4(3), pp.20130074-20130074.

Ye, C., Zhang, X., Wan, J., Chang, L., Hu, W., Bing, Z., Zhang, S., Li, J., He, J., Wang, J. and Zhou, G., (2013). Radiation-induced cellular senescence results from a slippage of long-term G2 arrested cells into G1phase. *Cell Cycle*, 12(9), pp.1424-1432.

Yosef, R., Pilpel, N., Papismadov, N., Gal, H., Ovadya, Y., Vadai, E., Miller, S., Porat, Z., Ben-Dor, S. and Krizhanovsky, V., (2017). p21 maintains senescent cell viability under persistent DNA damage response by restraining JNK and caspase signaling. *The EMBO Journal*, 36(15), pp.2280-2295.

Yosef, R., Pilpel, N., Papismadov, N., Gal, H., Ovadya, Y., Vadai, E., Miller, S., Porat, Z., Ben-Dor, S. and Krizhanovsky, V., (2017). p21 maintains senescent cell viability under persistent DNA damage response by restraining JNK and caspase signaling. *The EMBO Journal*, 36(15), pp.2280-2295.

Yosef, R., Pilpel, N., Tokarsky-Amiel, R., Biran, A., Ovadya, Y., Cohen, S., et al. (2016). Directed elimination of senescent cells by inhibition of BCL-W and BCL-XL. *Nat. Commun.* 7:11190.

Yu, J.H, Liu, C.Y, Zheng, G.B, Zhang, L., Yan, M.H, Zhang, W.Y., Meng, X.Y. and Yu, X.F. (2013). Pseudolaric Acid B Induced Cell Cycle Arrest, Autophagy and Senescence in Murine Fibrosarcoma L929 Cell. *International Journal of Medical Sciences*, 10(6), pp.707-718.

Yu, Q., Katlinskaya, Y., Carbone, C., Zhao, B., Katlinski, K., Zheng, H., Guha, M., Li, N., Chen, Q., Yang, T., Lengner, C., Greenberg, R., Johnson, F. and Fuchs, S., (2015). DNA-Damage-Induced Type I Interferon Promotes Senescence and Inhibits Stem Cell Function. *Cell Reports*, 11(5), pp.785-797.

Yu, T., Pang, J., Wu, K., Chen, M., Chen, C. and Tsai, W., (2013). Aging is associated with increased activities of matrix metalloproteinase-2 and -9 in tenocytes. *BMC Musculoskeletal Disorders*, 14(1).

Zaiss, D., Gause, W., Osborne, L. and Artis, D., (2015). Emerging Functions of Amphiregulin in Orchestrating Immunity, Inflammation, and Tissue Repair. *Immunity*, 42(2), pp.216-226.

Zdanov, S., Bernard, D., Debacqchainiaux, F., Martien, S., Gosselin, K., Vercamer, C., Chelli, F., Toussaint, O. and Abbadie, C., (2007). Normal or stress-induced fibroblast senescence involves COX-2 activity. *Experimental Cell Research*, 313(14), pp.3046-3056.

Zerrahn, J., Schaible, U., Brinkmann, V., Guhlich, U. and Kaufmann, S., (2002). The IFN-Inducible Golgi- and Endoplasmic Reticulum- Associated 47-kDa GTPase IIGP Is Transiently Expressed During Listeriosis. *The Journal of Immunology*, 168(7), pp.3428-3436.

Zhang, Q. and Yang, D., (2018). Allicin suppresses the migration and invasion in cervical cancer cells mainly by inhibiting NRF2. *Experimental and Therapeutic Medicine*,. 17(3), pp.1523-1528.

Zhang, Q., Lin, L. and Ye, W., (2018). Techniques for extraction and isolation of natural products: a comprehensive review. *Chinese Medicine*, 13(1).

Zhu, L., Chen, S. and Chen, Y., (2011). Unraveling the biological functions of Smad7 with mouse models. *Cell & Bioscience*, 1(1), pp.44.

Zhu, Y., Tchkonia, T., Pirtskhalava, T., Gower, A., Ding, H., Giorgadze, N., Palmer, A., Ikeno, Y., Hubbard, G., Lenburg, M., O'Hara, S., LaRusso, N., Miller,

J., Roos, C., Verzosa, G., LeBrasseur, N., Wren, J., Farr, J., Khosla, S., Stout, M., McGowan, S., Fuhrmann-Stroissnigg, H., Gurkar, A., Zhao, J., Colangelo, D., Dorronsoro, A., Ling, Y., Barghouthy, A., Navarro, D., Sano, T., Robbins, P., Niedernhofer, L. and Kirkland, J., (2015). The Achilles' heel of senescent cells: from transcriptome to senolytic drugs. *Aging Cell*, 14(4), pp.644-658.